Mechanisms of salt frost scaling on portland cement-bound materials: studies and hypothesis

Lindmark, Sture

1998

LUND UNIVERSITY
LUND INSTITUTE OF TECHNOLOGY
Division of Building Materials

Mechanisms of Salt Frost Scaling of Portland Cement-bound Materials: Studies and Hypothesis

Sture Lindmark

Report TVBM 1017

Lund 1998

LUND UNIVERSITY, LUND
Lund Institute of Technology
Division of Building Materials

MECHANISMS OF SALT FROST SCALING OF PORTLAND CEMENT-BOUND MATERIALS: STUDIES AND HYPOTHESIS

Sture Lindmark

Report TVBM 1017
Lund 1998

Keywords:

Cement
Concrete
Durability
Deterioration
Freeze-Thaw
Frost
Salt
Mechanism
ChIoride
Diffusion
Adsorption

ISRN LUTVDG/TVBM--98/l017--SE(I-266)
ISSN 0348-7911 TVBM
ISBN 91-628-3285-9

Lund Institute of Technology
Division of Building Materials
P.O. Box 118, SE-221 00 Lund
Sweden
Telephone: +464622274 15
Telefax: +46 46 222 44 27
E-mail: postmaster@byggtek.lth.se
Internet: ldc.lu.se/lthbml/index.htm

Printed in Lund: BTJ Tryck AB, 1998

Errata

to 'Mechanisms of Salt Frost Scaling of Portland Cement-bound Materials', TVBM-1017
Sture Lindmark, Building Materials, Lund Institute of Technology, 1998

Place in the text	Text	Should be
List of symbols	Content of non-hydrated cement per unit volume	Content of non-hydrated cement per unit volume of hardened paste
List of symbols, line 31	of hardened paste	(omitted)
p. 38, text to figure 2.3.3.		Reprinted from [B l 1986] with permission from Elsevier Science (Missing text)
p. 48, line 3	[S 1986]	[B l 1986]
p. 49, figure 2.4.2	Eq.2.5.41	Eq.2.4.39
p. 78	(Decimals not significant.)	(omitted)
p. 110, figure 4.1.2		Reference should be [Sd 1988]
p. 128	eq. (2.4.2)	eq. (4.2.2)
p. 132	[Pil 19xx]	[Pil 1996]
p. 146	The cement was a low alkali Portland cement with 5% limestone filler produced by Cementa AB, ..	The cement was a low alkali Portland cement produced by Cementa AB, ..
p. 169, figure 5.2.22, y-axis label	Transport coefficient D	Transport coefficient $D^* 10^{12}$
p. 185, 5th line	...the laboratory tests section of this paper,...	section 7.1
p. 228, line 4	... one specimen tested in the 1%...	...one specimen pre-stored in the 1%...
p. 239, figure 7.2.2, x-label	Time [min]	Time [hours]
p. 261	D 1966 ...Green%Co Ltd	D !966 ...Green&Co Ltd
p. 262	F 1996 ...."The required Air Content in Content"	F 1996 ...."The required Air Content in Concrete"
p. 263	M 1987 ....Painetr	M 1987 ...Painter
p. 266	W 1970 Winslow, Diamond 1970: (fig 2.1)	W 1970 Winslow, D N, Diamond, S: "A Mercury Porosimetry Study of the Evolution of Porosity in Portland Cement Paste", J. Materials 5, 1970

ABSTRACT

Concrete surfaces are often severely deteriorated when simultaneously exposed to a de-icing solution and sub-freezing temperatures. Typically, the surface is flaked off. In severe cases, concrete reinforcement is uncovered and the structure's strength is reduced. Because the mechanisms causing such deterioration are unknown, the concrete quality required in a given construction cannot be predicted and service life cannot be reliably estimated. Instead, concrete qualities are tested before use under standardised test methods. Typically, one surface of a concrete specimen is subjected to a salt solution and the specimen is frozen and thawed repeatedly, usually once a day, with the solution continuously present on the specimen surface. Such test methods, however, cannot be properly designed unless the mechanisms causing deterioration are known. It has been the aim of this work to contribute to the knowledge of those mechanisms.

From the literature, which primarily reports results obtained with traditional test methods, the following generalisations may be made. Surface deterioration reaches a maximum for moderate concentrations of de-icer in the outer solution. The de-icer need not be a salt. Scaling increases with decreasing minimum temperature in the frost cycle, at least for intermediate concrete qualities. In the absence of an outer solution, no scaling occurs. Scaling is worse, the higher the w/c ratio of the cement paste.

A hypothesis regarding the mechanism causing salt frost scaling is described. It is assumed that deterioration is due to osmotic micro ice body growth, as has been previously proposed by Powers and Helmuth [P 1953] for frost deterioration of moisture-isolated specimens of cement-bound materials. In moisture-isolated specimens, this ice body growth stops when the micro structure is drained to a certain extent. In a specimen exposed to salt frost attack, however, an outer liquid phase will be present on the specimen surface (as long as temperature is above the eutecticum for the actual de-icer solution). When micro ice bodies just beneath the specimen surface begin to grow, thereby draining the surrounding pore system, the outer liquid is sucked into the pore system, thereby eliminating the drainage required for micro ice body growth to stop. In a zone close to the material surface in which the liquid from outside may be transported to the growing ice bodies at a high enough rate, micro ice bodies will thus be able to grow much more than in a moisture-isolated specimen. The specimen surface will therefore be destroyed.

Predictions are made concerning the dependence of scaling and moisture uptake on minimum temperature, cooling rate, presence of de-icing agent and microstructure, and these are compared to results reported in the literature and also to experiments carried out as part of this research. The predictions were fulfilled. It therefore seems reasonable that the major mechanism causing salt frost scaling is the one described.

Results are reported from a study of chloride ion penetration into hardened Portland cement paste over short periods, 0.5 - 3 hours. A simple relation, based on the Kozeny-Carman equation, between the transport coefficients and the porosity and specific surface of the material is presented.

A study of the differential sorption enthalpy and differential sorption entropy was carried out using a sorption calorimeter recently developed by Wadsö and Wadsö [W 1997, W 1996]. The results cover the range 0-95% relative humidity at +25°C. Desorption isotherms were determined at 5° and 18°C by drying samples over saturated salt solutions. Freezing calorimetry tests were conducted on the same materials. The results from the room temperature experiments were used to calculate what heat flow rates were to be expected during the melting phase of the freezing calorimetry tests. These calculated heat flow rates were compared to those actually obtained. There are differences between the

calculated and the measured heat flows during melting which are difficult to explain. It is hypothesised that these differences are due to unintentional carbonation of the samples used for determination of the desorption isotherms. The results still indicate that ice formation takes place mainly through successive drying of the micro pores.

Preface

The research work described here was carried out at the Division of Building Materials, Lund Institute of Technology, under the supervision of Professor Göran Fagerlund. I thank him for introducing me to this interesting field and for giving me the practical and financial opportunities to carry out this work. It has been a great privilege to have been able to work on a single topic, free from financial and other distractions.

I am deeply indebted to Professor Bengt Jönsson, Department of Physical Chemistry 1, Lund University, to whom I express my sincere gratitude for his patience and commitment through all the long hours of discussion we have had. Any knowledge I may have acquired in the fields of physical chemistry and thermodynamics is attributable to him. (Any errors on these topics in this report are, of course, mine alone.)

I thank all the staff at our Division for their help during this work. I would especially like to mention Mr. Stefan Backe, whose patience was sorely tested during the many reconstructions of the laboratory equipment in the initial years of my research, and Lars Wadsö, PhD, who presently divides his time between our Division and the Department of Thermochemistry, Lund University, for his help and encouragement with the work on sorption calorimetry reported in Chapter 3.

Many people outside our department have helped me in one way or another. I express my sincere gratitude to all of them: Professor Erik J Sellevold, The Norwegian Institute of Technology, Trondheim; Sven Knutsson, Associate Professor, Soil Mechanics and Foundation Engineering, Luleå University; Staffan Hansen, Senior Lecturer, Inorganic Chemistry 2, Lund Institute of Technology; Natalia Markova, Postgraduate student, Dept. of Thermochemistry, Lund University; Kjell Jarring, PhD, Astra Draco AB, Lund; Thomas Carlsson, Licentiate in Engineering, previously of this Division, presently of the Royal Institute of Technology, Department of Built Environment, Materials Technology, Gävle, Johan Larsson, MSc, Scancem Research AB, Slite.

I would also like to thank my mother-in-law, Professor Bodil Jönsson, for the many discussions on general aspects of research work that we have had, and my sister, Kerstin, for her invaluable help with the English language in the papers I wrote in the course of this work. For the excellent help with revision of the present text, however, my sincere thanks are addressed to Anna-Karin and Greg Batcheller. (Since I had to do some changes in the text after Anna-Karin and Greg had revised it, they are though not responsible for any linguistic deficiencies.)

The financial support provided by the Swedish Research Council for Engineering Sciences and by the Consortium for Research on High Performance Concrete, which consisted of BFR (The Swedish Council for Building Research), NUTEK (The Swedish Board of Technical Development), Cementa AB, Elkem Materials A/S, Euroc Beton, NCC, SKANSKA and Strängbetong, is gratefully acknowledged.

Finally, I thank my wife, Ulrika, for her support and for her patience, especially during the writing of this report.

Lund, November 1998

Sture Lindmark

CONTENTS

List of symbols and abbreviations

Symbols

μ	Chemical potential	J/mole
α	Coefficient of thermal contraction	K^{-1}
α	Degree of hydration	–
a	Internal area per unit volume	m^2/m^3
a	Intermolecular distance	m
B	Permeability	s
c	Concentration	–
c	Salt concentration	% b.w.
C	Chloride ion concentration	mg/l, mg/mm^3
C,c	Mass of cement	kg
C_v	Content of non-hydrated cement per unit volume of hardened paste	kg/m^3
D	Chloride ion transport coefficient	m^2/s
D	Coefficient of self diffusion	m^2/s
δ_v	Moisture transport coefficient	m^2/s
ϕ	Relative vapour pressure	–
ϕ_1	Relative vapour pressure at completion of first monolayer of adsorbate	–
G	Gibbs energy	J/mole
g_v	Moisture flow rate	$kg/m^2/s$
H	Enthalpy	J/mole
$\Delta_{ads}H$	Enthalpy of adsorption	J/mole
$\Delta_{fus}H$	Heat of fusion	J/mole
KC	Kozeny-Carman Pore structure parameter	m
k	Correction coefficient	–
k	Boltzmann's constant	J/K
L	Air volume	m^3
m	Mass	kg
n	Amount of a substance	mole
n_{sol}	Amount of a solute	mole
n_{solv}	Amount of a solvent	mole
p	Pozzolana	kg
P, p	Pressure	Pa
P, p	Porosity	–
ρ	Density	kg/m^3
R	Gas constant	J/K/mole
r	Radius	m
R.H.	Relative humidity	–
S	Degree of water saturation	–
S	Entropy	J/K/mole
S_w	Pore wall area per unit volume of solid phase	m^2/m^3
s	Mass of silica fume	kg
$\sigma_{l\text{-}s}$	Interface free energy of a surface liquid-solid	J/m^2
$\sigma_{l\text{-}v}$	Surface free energy of a surface liquid-vapour	J/m^2

$\sigma_{v\text{-}s}$	Surface free energy of a surface vapour-solid	J/m^2
T	Temperature	K
θ	Temperature	°C
u	Moisture content	g/g
v	Growth velocity	m/s
v	Humidity by volume	kg/m^3
V	Volume	m^3
V_{ads}	Volume of adsorbate	cm^3
w/c	Water cement ratio, defined in eq. (2.1)	–
W_0	Mixing water	kg
X	Mole fraction	–

Indici:

0	reference state
m	molar
a	air
w	water
i	ice
sol	solution
i	initial value
f	final value
fus	fusion

Abbreviations

SFS	Salt Frost Scaling
HCP	Hardened Cement Paste (Portland cement unless otherwise stated)
b.w.	by weight

1 INTRODUCTION

Background

Anyone who has ever put a bottle of beer in the freezer to cool and forgotten about it will be familiar with the phenomenon of frost destruction. In such a simple case, it is the volumetric expansion accompanying the transformation of water into ice that causes destruction. Even though the precise mechanisms causing destruction may be somewhat different, the same phenomenon occurs in all materials which are capable of containing moisture, whether it be in cracks, *e.g.* in rocks, or in pores that are a natural part of the structure of the material, such as in brick or concrete. This kind of destruction destroys the material over its entire volume so that, for instance, its modulus of elasticity is drastically decreased. In severe cases, this destruction may be seen in the form of cracks on the surfaces of the material. This kind of frost destruction is often referred to as Inner Frost Attack. The present report though deals with a type of frost attack that primarily affects the surfaces of porous materials.

Ever since the use of de-icing chemicals for removing ice from roads became common in the 1930s and 1940s, it has been well known that the combination of de-icing chemicals and frost causes serious degradation of concrete structures. Other examples of structures where this combined effect of salt and frost causes severe damage and high costs of repair are airfields and marine constructions, such as harbours and bridges.

The combined effect of salt and frost, which is often referred to as Salt-Frost Attack or De-icer Frost Attack, mainly affects the surfaces of a construction. Flaking and spalling are the common signs. The serious consequence is obvious: when spalling and flaking have finally destroyed the entire concrete cover, the adhesion of the reinforcement to the concrete is reduced, resulting in serious loss of structural strength. In climates where salt frost attack is possible, service life estimations based on reinforcement corrosion may become completely irrelevant, since the estimated time for the initiation and propagation of reinforcement corrosion may be overtaken by the time required for the entire concrete cover to spall off.

In serious cases, this can spell the end of the service life of the structure. In less serious cases, costly repair will be necessary. Although the exact figures are uncertain, it may be safely estimated that the costs of repair of Swedish road bridges is some 50 million SEK annually (estimated from figures presented in 1987 by the Swedish Road Directorate). The costs for airfields, harbours, and other structures must be added to this figure.

In order to prevent or at least reduce as far as possible this destruction of concrete structures, many countries have established various methods for testing concrete with respect to salt frost resistance before using it in real applications. A short review of three often used test methods is given in General Appendix 1 (SS 13 72 44, CDF, ASTM C672). In most such test methods, a concrete specimen is subjected to a salt solution on a single surface and then the specimen and the salt solution are repeatedly frozen and thawed. These test methods share a common intention of simulating concrete in its real use. It is an often-discussed topic whether the test methods presently used are truly well-designed for this purpose. For example, a temperature cycle ranging from room temperature to some -20°C is usually used and its length is often limited to one day or even less. It is quite clear that such frost cycles seldom, if ever, occur in nature. Neither does it seem likely that concrete in nature would, during such repeated freezing, be

continuously covered with a 3% NaCl solution - a circumstance frequently prescribed in test methods.

Since the test methods do not simulate real-life exposure, we cannot know whether the results are truly relevant, *i.e.* we cannot know for certain that the test methods can be used to distinguish concretes that are durable in nature from those that are not. Unfortunately, it is not possible to simulate real-life exposure in a laboratory test method. We need some kind of accelerated and well-defined test which produces results that may be used to predict the real-life performance of a concrete.

Aim of the present work

It is impossible to design such a test unless the major mechanisms responsible for breakdown are known. Since the first reports of studies of salt frost scaling were published by Arnfelt [A 1943] and Verbeck and Klieger [V 1957], various hypotheses regarding the mechanism causing this degradation have been proposed. A topic of special interest has been the observation that scaling tends to reach a maximum when the concentration of de-icer (*e.g.* some salt) in the solution applied to the specimen surface is rather moderate, *e.g.* some 2-4% by weight in the case of sodium chloride. However, none of the proposed hypotheses has been recognised as fully satisfactory.

As a result of this lack of knowledge and of the need for a relevant standard test method, a RILEM Committee, chaired by professor Setzer of the Univerity of Essen, Germany, was established in 1990 and took on the task of trying to solve these problems. At the same time, outside the realm of this committee, mainly in the Nordic countries and in the United States and Canada, a number of investigations, primarily under laboratory conditions but also field studies, were undertaken and published. A great deal of information regarding the characteristic phenomena of salt frost deterioration has been made available.

At about the same time, professor Göran Fagerlund offered me a chance to work as a postgraduate student at the Division of Building Materials, Lund Institute of Technology. The task was to clarify the (major) mechanism(s) causing salt frost-induced degradation of concrete and other brittle, porous materials. It was also anticipated that if a major mechanism could be identified, a relevant test method would be developed.

In this report, a mechanism is described which I believe may be the major mechanism causing salt frost deterioration. This mechanism is based on the same kind of ice formation, osmotic ice body growth, as has been recognised to be the cause of soil heaving in cold regions and which has also been put forward as one of the major mechanisms of inner frost deterioration of concrete. By considering the physical principles of osmotic ice body growth in porous media and the special conditions of moisture accessibility associated with the exposure of concrete to a salt solution during freezing, it has been possible to explain many of the phenomena reported from studies of salt frost deterioration of concrete. In that regard, the results published by many other researchers has played a significant role.

Limitations of the present work

The experimental work was carried out entirely in the laboratory. The reason for this was the need for good control of all those parameters which may affect the final result of any type of frost deterioration experiment. Thus, no field studies have been carried out.

Furthermore, the work has been restricted to Portland cement-bound materials. One characteristic property of such materials is their brittleness. This means that when estimating, in a first approximation, the amounts of ice and ice pressure required to cause

destruction in the materials, the possibility of the material yielding under stress need not be considered.

This work has focused on freezing-related phenomena. Purely salt-dependent mechanisms have been excluded, partly because a review of the literature showed that without freezing no scaling will occur, and partly because salt frost scaling also appears when the salt is substituted by some non-salt de-icing chemical, such as ethanol.

Organisation of the report

A review of the major constituents involved in salt frost destruction of Portland cement-bound materials - the material itself, the water and the ice - is set out in chapter 2. Since it has been shown that the de-icer need not be a salt, no special attention is devoted to salts. In addition, there is a short review of the basic thermodynamics involved in frost destruction.

Results from a study of some of the properties of the liquid held in the pores of Portland cement-based materials are contained in chapter 3.

Chapter 4 reviews the literature on phenomena observed in connection with salt frost resistance of Portland cement-bound materials and that on previously proposed mechanisms for explaining some of these phenomena.

Some of my own, preliminary laboratory experiments are described in chapter 5. The first part of the chapter presents results from a study of the importance of salt concentrations, distribution of salts and frost cycle used. A study of the salt frost resistance of high performance concrete is also presented. In the next part, results are presented from a study of the penetration of chloride ions into pure Portland cement paste. The purpose of this study was to examine how far into the material surface chloride ions might reach during the approximately 3 hours (in a normal test method) which elapse from the application of a salt solution to the surface of a specimen until freezing begins. This was thought to be the best approximate estimation of the depth to which the chemical composition of the pore solution is affected by the outer salt solution during those hours. Furthermore, no similar study, *i.e.* one in which such short periods of exposure had been used, was known to the author to have been previously published. Therefore an experiment of this kind was thought to be a possible source of new information.

In chapter 6, a hypothesis regarding a major mechanism of salt frost scaling is presented. The basic mechanism is the well-known ability of an ice body, surrounded by moisture of higher vapour pressure than its own, to grow by consuming moisture from those surroundings. This mechanism is what causes soil heaving and has also been proposed as the major mechanism of inner frost destruction of concrete. Here, however, it is complemented by the importance of the outer brine, which remains liquid to temperatures far below the freezing point of the natural pore solution. The description of the mechanism is followed by some suggestions for ways of testing the relevance of the mechanism.

In chapter 7, two such studies are presented. The results do not contradict the hypothesis, but reveal other phenomena which are yet to be explained.

In chapter 8, some conclusions are drawn from the present work and the principles of a relevant test method are discussed.

2

MATERIALS AND BASIC THERMODYNAMICS

The aim of this chapter is to describe the relevant properties of the major materials (the hardened cement paste itself, the water, the ice and the de-icing chemicals) involved in salt frost scaling on Portland cement-based materials.

2.1 HARDENED (PORTLAND) CEMENT PASTE, HCP

Concrete and mortar are made up of a mix of cement paste and some aggregate (gravel and/or sand). Provided a frost resistant aggregate quality is chosen, the question of whether the final concrete or mortar will be (salt) frost resistant is thus a question of whether the cement paste used in it has been made (salt) frost resistant. The present description therefore deals primarily with the properties of the hardened paste itself. Only those properties of the paste which are believed to be of concern to its frost resistance are dealt with.

This is only a very brief description of the properties of Portland cement. For more complete descriptions, the reader is referred to the literature, *e.g.* Taylor [Tr 1990], Roy [R 1985], and Powers and Brownyard [P 1948].

2.1.1 Composition and micro structure of Portland cement paste

Hardened Portland cement is a more or less porous material. The solid phase consists of a poorly crystalline calcium silicate hydrate (approximate composition $3CaO{\cdot}2SiO_2{\cdot}4H_2O$) and crystalline $Ca(OH)_2$. This calcium silicate hydrate, which constitutes 70-80% of the solid content of fully reacted Portland cement, is denoted C-S-H gel or cement gel and consists of particles of less than 1 µm in any dimension. Although its physical structure is still debated, it may, for present purposes, be described as an extremely fine porous solid with pores ranging up to 2 nm and a total porosity of 28%. Its specific surface, as measured with water, is 200-250 m²/g.

By mixing Portland cement with water, a slurry is obtained which is denoted as fresh cement paste. The reaction between cement and water, hydration, starts immediately and within a few hours the fresh mix stiffens. During hydration, water is chemically bound to the cement. In the presence of water, hydration continues until each unit of cement has reacted with a certain amount of water. The exact amount of this chemically bound water at complete hydration is determined by the cement composition. For ordinary Portland cements, it amounts to approximately 0.25 g of water per gram of cement. Based on this, the degree of hydration, α, which denotes how close hydration is to completion, is defined:

$$\alpha = \frac{W_n}{0.25C} \qquad (2.1.1)$$

in which W_n = weight of chemically bound water
C = weight of cement.

The volume of the reaction product, which is called the cement gel, is slightly more voluminous than the original cement grains. The cement grains thus swell to occupy some of the volume of the fresh paste which was originally water-filled. Depending on the ratio of mixing water to cement, the final, hardened paste will therefore be more or less porous. The total porosity consists of both gel porosity and pores which were not filled with reaction products. These pores are larger than the gel pores (typical width up to 1000 nm) and are named capillary pores. The amount of capillary pores is thus determined by the ratio of mixing water to cement and degree of hydration. The former is called water cement ratio and is defined:

$$w/c = \frac{W_0}{C} \qquad (2.1.2)$$

in which W_0 and C are the amounts of mixing water [kg] and cement [kg], respectively.

The total porosity of the hardened cement paste is calculated from the water cement ratio as :

$$P_{paste} = \frac{w/c - 0.19\alpha}{0.32 + w/c} \qquad (2.1.3)$$

in which P_{paste} = total porosity [l/l]
α = degree of hydration, eq. (2.1.1)
w/c = water cement ratio, eq. (2.1.2)
0.32 = specific volume of portland cement [l/kg]

That part of the total paste porosity which is due to the porosity of the gel is called gel porosity and is calculated:

$$P_{gel} = \frac{0.20\alpha}{0.32 + w/c} \qquad (2.1.4)$$

The capillary porosity is obtained by subtracting the gel porosity from the total porosity:

$$P_{cap} = \frac{w/c - 0.39\alpha}{0.32 + w/c} \qquad (2.1.5)$$

As hydration proceeds, the mixing water is consumed. When hydration proceeds in the absence of any moisture source, the mixing water will be consumed so that complete hydration ($\alpha = 1$) cannot be reached unless $w/c > 0.44$. When water is available, complete hydration may be reached if $w/c < 0.39$. For smaller w/c ratios, lack of space for the

reaction products will set a limit to the reaction. The ultimate degree of hydration for such pastes is:

$$\alpha_{max} = \frac{w/c}{0.39} \qquad w/c < 0.39 \qquad (2.1.6)$$

These equations, which are all from Powers and Brownyard [P 1948], give only the total porosities. The pore size distributions cannot be calculated, but need to be determined experimentally. Examples of such determinations are given in figure 2.1.1. The micro structure may also be characterised by a sorption isotherm. Examples of isotherms are given in chapter 3.

Pore liquid

The liquid in the pores of a non-leached HCP contains different dissolved ions, mainly K^+, Na^+, Ca^{2+} and OH^-. There are also small amounts of S, Al, Fe, Mg and Si. The pH value of the (non-disturbed) pore solution is approximately 13. An example of pore solution composition is given in chapter 3.

2.1.2 Physical properties

Strength

Hardened cement pastes of normal porosities have compressive strengths of 20-150 MPa. However, the tensile strength, which is the more relevant strength for estimating the effects of the pressures associated with ice formation in HCP, normally amounts to only approximately $1/10^{th}$ of the compressive strength. The pressures from the ice formation processes which are necessary to cause damage will, nevertheless, depend on geometrical conditions.

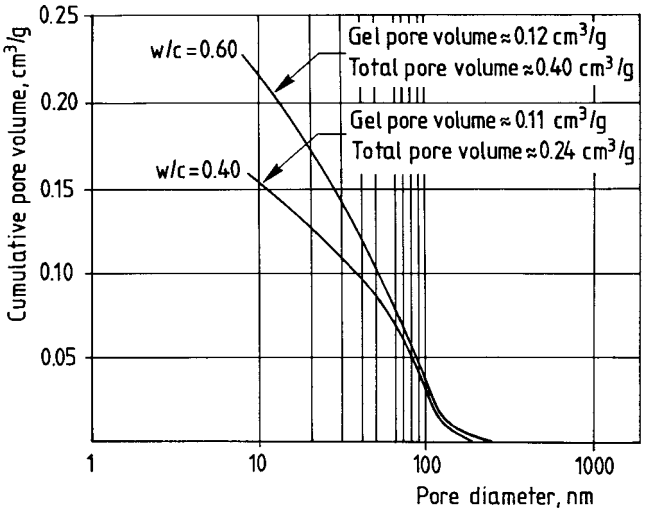

Figur 2.1.1: Pore size distribution obtained by mercury intrusion porosimetry. From [B 1982] after [W 1970]

Water permeability

As will be seen in later chapters, the pattern of ice formation in the pores of HCP may be greatly affected by the availability of moisture. The permeability to water transport is therefore of fundamental importance to the mechanisms of frost-induced deterioration of Portland cement-bound materials.

The coefficient of moisture transport in HCP is strongly dependent on the capillary porosity and the degree of water saturation. Hedenblad [H 1993] evaluated the vapour transport coefficient in cement paste from moisture content profiles obtained in specimens which had been exposed for a few years to different relative humidities on two sides so that one-dimensional steady moisture flow had been established. Using

$$g_v = -\delta_v \frac{dv}{dx} \qquad (2.1.7)$$

in which g_v is the moisture flow rate [kg/m²/s] and v is humidity by volume (in the pores) [kg/m^3], he found the transport coefficient δ_v [m²/s] to vary with R.H. as shown in figure 2.1.2. A reduction in R.H. obviously causes large reductions in the transport coefficient. Since the moisture content is related to R.H. by the sorption isotherm (see chapter 3), a reduction in moisture content causes large reductions in the moisture transport properties of HCP.

Powers *et al* [P 1954] measured the water permeability of cement paste in a water-saturated state by pressing water through specimens using external pressure. These authors found that the viscosity of water in HCP seems to depend on the channel radius and therefore preferred to use Darcy's law with the viscosity term included in the permeability coefficient, *i.e.* in the form:

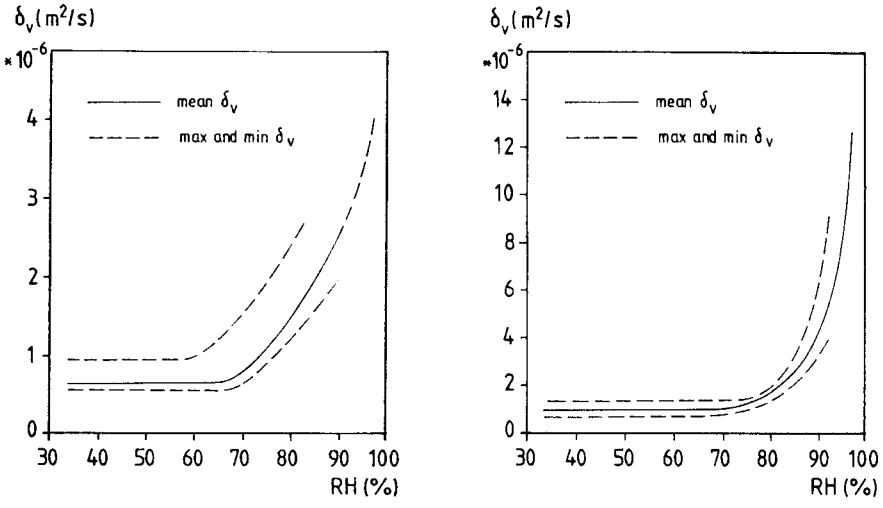

Figure 2.1.2: Coefficient of vapour transport in HCP as function of R.H.. w/c ratios: 0.50 (left) and 0.60. [H 1993].

$$g = B\frac{dP}{dx} \qquad (2.1.8)$$

in which g = the moisture flow rate [kg/m²/s]
B = the permeability coefficient [s]
dP/dX = the driving pressure gradient [Pa/m]

The relation of permeability to capillary porosity is plotted in figure 2.1.3.

2.1.3 Effects of drying, carbonation and leakage on the micro structure of hcp

As a result of the minute size of the pores and the presence of dissolved ions, water held in the pores of HCP will not have the properties of bulk water. A relevant example in this context is the freezing point depression of the pore water. Examples of this are shown in figure 2.3.4. (The dependence of freezing depression on pore size is treated in chapter 2.4.) The effect of micro structure on the freezing point depression of pore water has a large influence on the ability of the material to withstand frost attack because it determines, for example, how much water will be frozen in a sample at a given temperature.

As the micro structure may be affected over time by the environment in which a concrete is used, a few examples of known environmental effects are given below.

Drying

Powers *et al* [P 1954] showed that slow, stepwise drying of HCP to 70% R.H. increased its permeability to saturated water flow rate by a factor of 70. They explained that this was caused by walls of cement gel between larger capillary pores being destroyed by the drying process. The exact increase in permeability depends on the *w/c* ratio, degree of hydration, and extent of drying.

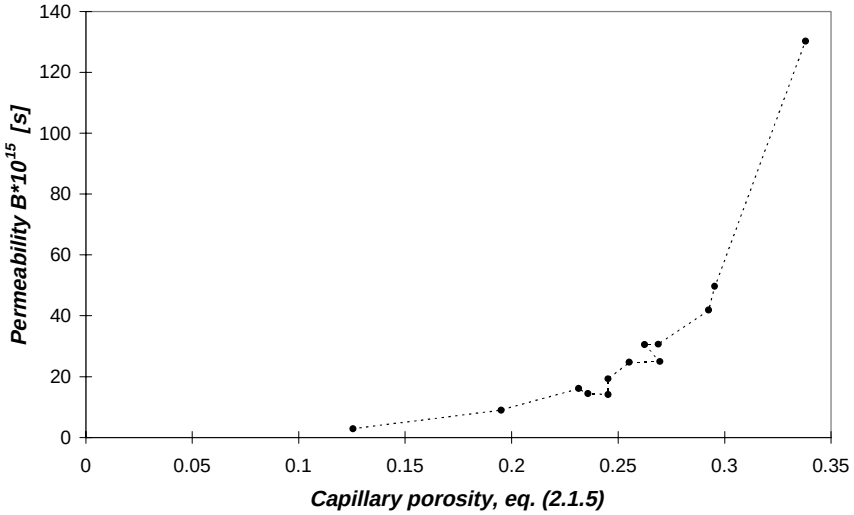

Figure 2.1.3: Water permeability vs. capillary porosity of cement paste. w/c ratios 0.46-0.71, $\alpha \approx 0.93$. Calculated from data in [P1954].

Thus the factor 70 reported by Powers *et al* may be significantly different under different conditions. Also, Sellevold and Bager [B2 1986] concluded, based on results from calorimetric freezing experiments, that the pore structure coarsens during drying.

Carbonation

According to the results obtained by Powers *et al*, permeability is reduced when capillary porosity is reduced. One example of a process that may change the capillary porosity is carbonation, *i.e.* the reaction of CO_2 with the $Ca(OH)_2$ present in the HCP. Matala [M1995] reports results from low temperature calorimetric investigations on both pure Portland cement pastes and pastes prepared from Portland cement with additions of granulated blast furnace slag (GBFS). Matala found that the pore structure is coarsened in both types of pastes, but that coarsening is less in pure Portland cement pastes than in the pastes containing GBFS. Total porosity, however, is decreased in both types of pastes. The net effect seems to be that carbonation increases the amount of freezable water in both types of pastes, although much more in pastes containing GBFS. With respect to mortar in particular (in contrast to pure pastes), the volume of very large capillary pores (>100 nm) increases much more in pastes containing GBFS than in pure Portland cement pastes.

Kropp [K 1986] presented results from studies on the effects of carbonation on the structure and other properties of HCP. From desorption isotherms determinations, it became clear that carbonation causes densification of cement pastes of pure Portland cement paste, figure 2.1.4.

Tumidajski and Chan [T 1996] found that chloride penetration into concrete produced with pure Portland cement decreases after 60 months' exposure to CO_2. This indicates a densification of the pore structure. The authors also found that for concrete produced with the same cement but with the addition of slag, the opposite was observed. Both these findings may be explained by the effects of carbonation on microstructure reported by Matala [M 1995] and by Kropp [K 1986].

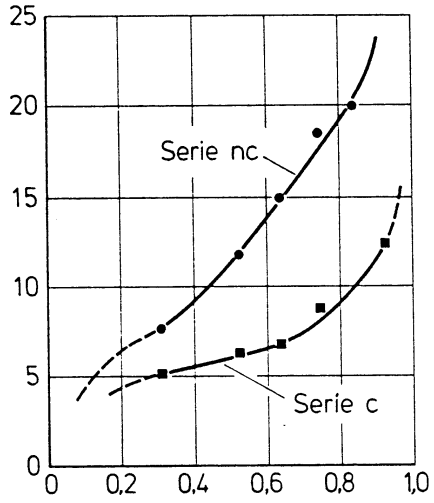

Figure 2.1.4: Effect of carbonation on desorption isotherm. Moisture content [% b.w.] vs. relative humidity. nc: non-carbonated, c: carbonated. HCP w/c ratio 0.50. [K 1986]

Leaching

Apart from pore size distribution, freezing point depression is also affected by the amount of dissolved ions in the pore liquid. Thus if the materials are subjected to leaching, as may be the case for instance in dam constructions, it is possible that the pore liquid, after a certain period of leaching, may become so diluted that at a given temperature more water will be freezable. Due to the relatively low amount of dissolved ions and the balance between reaction products in solid form and the amount of dissolved ions (which to some extent is maintained through the release of ions from the CSH gel), this is probably of minor importance.

2.1.4 The air void system

In order to make HCP frost resistant, an additive is used which, during the mixing of the concrete, forms a foam. The bubbles thus formed are preserved in the hardened paste. Provided these cavities remain air-filled, they provide space for the volumetric expansion which occurs when pore water freezes.

The extent to which such bubbles are able to protect the materials from frost deterioration is dependent on the total amount of air and on the distances across which water must be transported in order to relieve the pressure rises occurring during ice formation.

Assuming that the air bubbles are cubically arranged in the cement paste, Powers [P 1949] defined a spacing factor *a* which is half the maximum distance between cubically arranged spheres with a diameter equal to the mean diameter of all the air bubbles in unit volume of the paste. Powers derived the following relation between total air content, mean air bubble diameter and the spacing factor (the parameters are explained in figure 2.1.5):

$$a = \frac{D}{2}\left\{1.4\left(\frac{V_p}{L}+1\right)^{1/3}-1\right\} \qquad \textit{(provided } V_p/L>4.33) \qquad (2.1.9)$$

in which a = spacing factor [mm]
D = mean diameter of the bubbles [mm]
Vp = volume of paste [m^3/m^3]
L = volume of air [m^3/m^3]

Often, a third parameter, the specific surface α the air bubbles, *i.e.* the ratio of surface area to volume [mm^2/mm^3], is used to denote the fineness of the bubbles. At a given total air content, the spacing factor *a* will be smaller the smaller the bubbles.

The natural air content, *i.e.* air which is mixed into concrete without the use of any air entraining agents, amounts to approximately 2%. Normally, the required total air content for a concrete to be frost resistant ranges from 3-7% by volume. The relation between the various parameters describing the air pore system and frost resistance have been studied by many researchers. For concrete to be frost resistant, it has been reported that the spacing factor must be less than some 0.25 mm. Different researchers give different values.

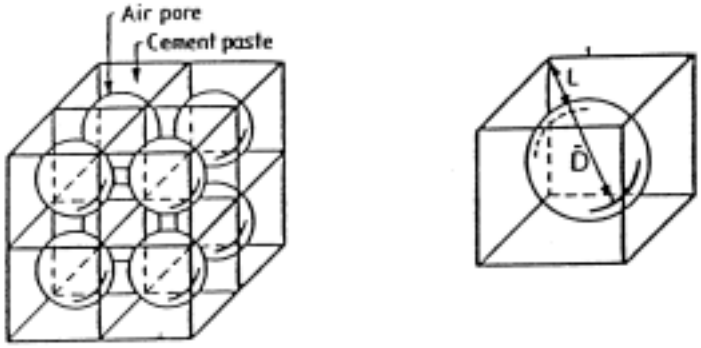

Figure 2.1.5: Illustration of parameters used in eq. 2.1.11

There are many reasons for this: Different researchers use different ways of testing for frost resistance, using different criteria for the definition of frost resistance. Sometimes the degree of saturation and the water filling of small air bubbles is considered, sometimes not. Sometimes the total air content is varied by the use of different amounts of one and the same air entraining agent and this is used to calculate different required spacing factors, while in fact it might be that it is the total air content that is decisive. Furthermore, the techniques for analysing air void systems are sensitive to small variations in preparation and imaging technique, possibly resulting in different researchers reporting different values for the characteristic parameters of identical air void systems.

2.1.5 Transition zone Aggregate – HCP

The thin transition zone between aggregate and HCP is known to be more porous than the HCP itself and therefore may contain water with only a small freezing point depression. It seems that little research has focused on the importance of this zone to the frost resistance of concrete.

2.2 WATER

The aim of this section is to briefly describe those properties of water which may have an effect on the frost resistance of hardened cement paste.

2.2.1 Density

The density of water varies with temperature, as set out in to figure 2.2.1. In the interval $243.15<T<293.15$, the density [kg/m^3] may be calculated as:

$$\rho = -3479.56 + 46.301T \ - 0.1591T^2 + 1.8171 \cdot 10^{-4} T^3 \qquad (2.2.1)$$

The molar volume thus is:

$$V_{m,l} = -3.4228 \cdot 10^{-12} T^3 + 2.9896 \cdot 10^{-9} T^2 - 8.6806 \cdot 10^{-7} T + 1.0182 \cdot 10^{-4} \qquad (2.2.2)$$

Density of water in the pores of HPC

Due to adsorption forces, the density of water contained in the pores of hardened Portland cement paste is higher than that of bulk water. The exact difference, though, is not known. Powers and Brownyard [P 1948] estimated the density of water held in the gel pores at 1.1 g/cm^3. This was later supported by results from Copeland *et al* [C 1960], who measured entropy changes of water during adsorption in HCP. Copeland *et al* [C 1956] derived an expression according to which the density of the loosely held capillary water is 1.01 g/cm^3.

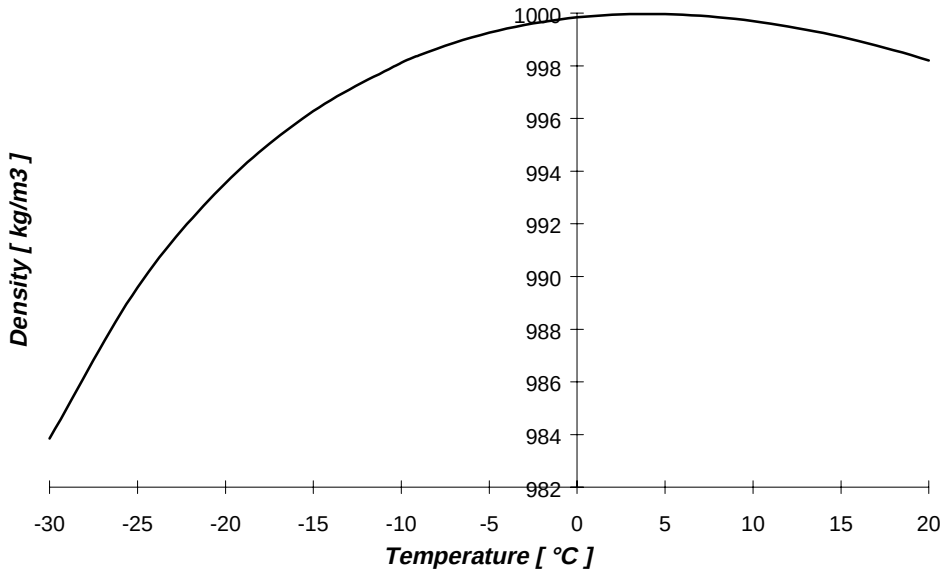

Figure 2.2.1: Variation of bulk water density with temperature at 1 atm. [H 1991]

Density of solutions of NaCl

The most common de-icing agent seems to be sodium chloride, NaCl. It may therefore be of interest to study the density of such solutions as a function of their NaCl concentration. Using data from [H 1990], the density of NaCl solutions at 20°C varies in accordance with:

$$\rho(c) = 7.2416c + 997.98 \qquad (2.2.3)$$

in which c is the concentration of NaCl in % by weight of the solution. This relation is valid up to c = 26% with an error of less than 1%.

2.2.2 Heat capacity, enthalpy and entropy

In the interval 267.15<T<293.15K (-6<θ<20°C) the heat capacity of water may be described by:

$$C_p = AT + B \qquad (2.2.4)$$

Expressing C_p in [J/mol/K], the best fit to data from [H 1990] is obtained with A = -0.05987 and B = 92.3687.

Changes in heat capacity due to adsorption

Heat capacity is changed when water is adsorbed in porous materials. Thus Braun and Drost-Hansen [B1976] measured the heat capacity of water adsorbed in different solid materials (porous glass, activated carbon, a zeolite and synthetic diamond powder) and concluded that heat capacity increases by about 25% compared to that of bulk water at +25°C independent of adsorbent. A compilation of literature-reported data regarding changes of C_p for water caused by adsorption is given by Etzler and Conners [E1990, E1991]. By measuring such changes for water adsorbed in different types of silica gel, the authors estimated the effect of the pore radius on C_p (figure 2.2.2).

Low [L 1979] reports changes in several of the properties of the adsorbed water, *e.g.* changes in its heat capacity when adsorbed in montmorillonite. According to Low, C_p increases by up to 12%, the increase being greater the lower the water content of the montmorillonite. Low, however, says nothing about the relative humidities at which these measurements were taken.

As a result of interaction with the pore walls, the enthalpy and entropy of adsorbed water is lower than that of bulk water. The simultaneous increase in heat capacity will also change the temperature dependence of the enthalpy and entropy of the adsorbed water from that of bulk water.

2.2.3 Surface free energy (Surface tension)

The surface free energy, or surface tension, of a surface liquid water-vapour varies with temperature and content of solutes in the liquid. An example of the latter, for NaCl, is given in figure 2.2.3. Other electrolytes, as well as sugar, qualitatively have the same effect, *i.e.* they all cause increases in surface tension. According to Shaw [Sw 1992], the reason is that the attractive forces between solute and solvent are stronger than those between the solvent molecules.

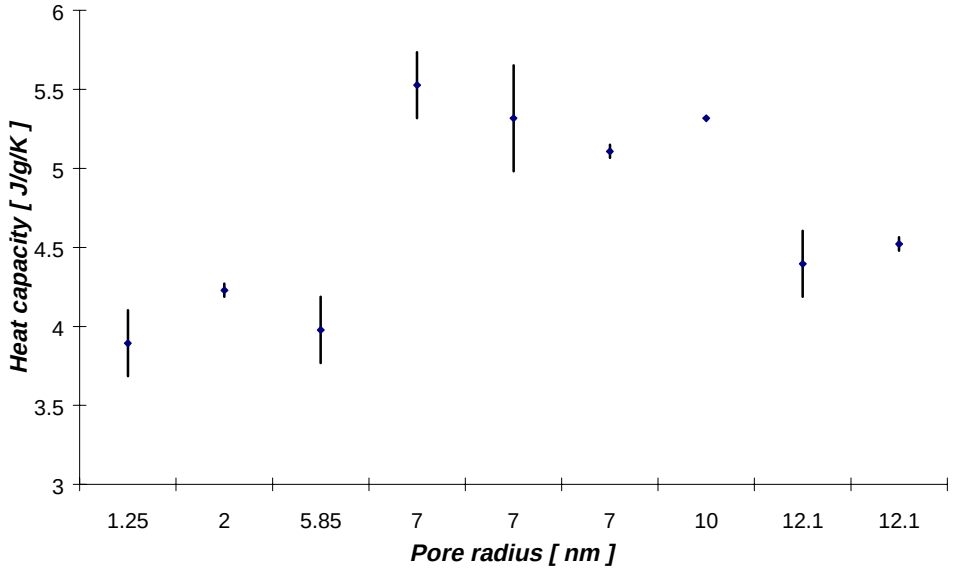

Figure 2.2.2: Variation of C_p with pore radius in silica gel at 25°C. Data from several authors, compiled by Etzler&Conners [E 1991].

The surface free energy is described as a function of the concentration of NaCl by:

$$\sigma_{l-v}(c)_{293K} = \frac{72.72 + 0.325c}{1000} \qquad (2.2.5)$$

in which $\sigma(c)$ is given in J/m² and the concentration of NaCl (c) is given in % by weight of the solution [H 1990]. Eq. (2.2.5) yields errors of less than 1% for c< 20%.

In the interval 265<T<298K (-8<θ<25°C), the temperature dependence of the surface free energy of a surface liquid water-vapour (fitted to data from [H 1990]) is given by:

$$\sigma_{l-v}(T) = -0.1484 \cdot 10^{-3} T + 0.11623 \qquad (2.2.6)$$

Surface tension is dependent on the curvature of the meniscus. According to Adamson [An 1990], this however does not cause any distinguishable effects until the radius of curvature is of the same order of magnitude as the molecular diameter. Adamson, referring to *Christenson* [*C 1985*], states that the LaPlace equation is valid for water for radii of curvature larger than 2 nm. The present report, therefore, does not deal with the effect of curvature itself on surface free energy.

2.2.4 Viscosity– effect of temperature, dissolved substances and adsorptive forces

There are different opinions as to whether it is saturated or non-saturated moisture flows that are dominant during the processes leading to frost deterioration. In any case, the mobility of the pore liquid is essential. This will be highly dependent on the viscosity of the pore solution. Therefore, a short description is given here of the dependence of viscosity on temperature, dissolved substances and adsorptive forces.

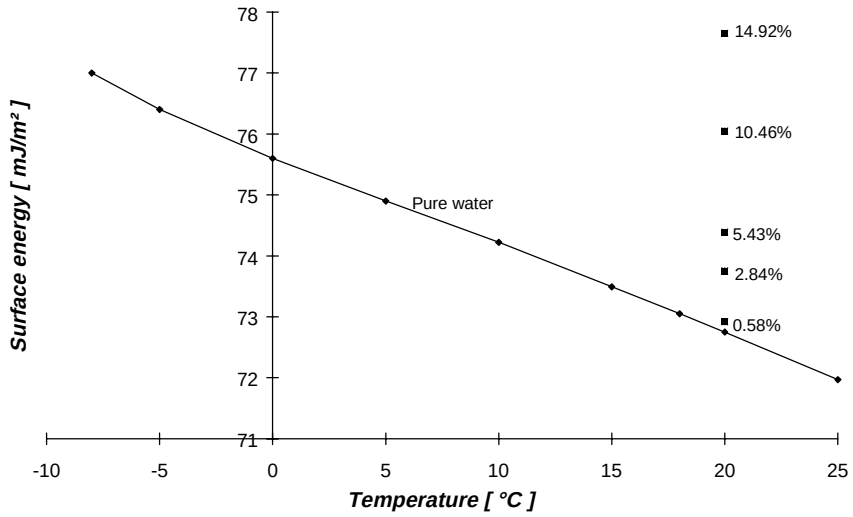

Figure 2.2.3: Variation of surface energy of pure, bulk water with temperature and effect of addition of sodium chloride (% b.w.). Data from [H 1990].

There are two ways of describing the state of mobility of a liquid, *viz*. its absolute viscosity and its kinematic viscosity, where the latter equals the former divided by the liquid density. The higher the viscosity, the higher the inner friction and thus the lower the mobility of the liquid.

Temperature

The absolute viscosity of water varies with temperature as shown in figure 2.2.4.

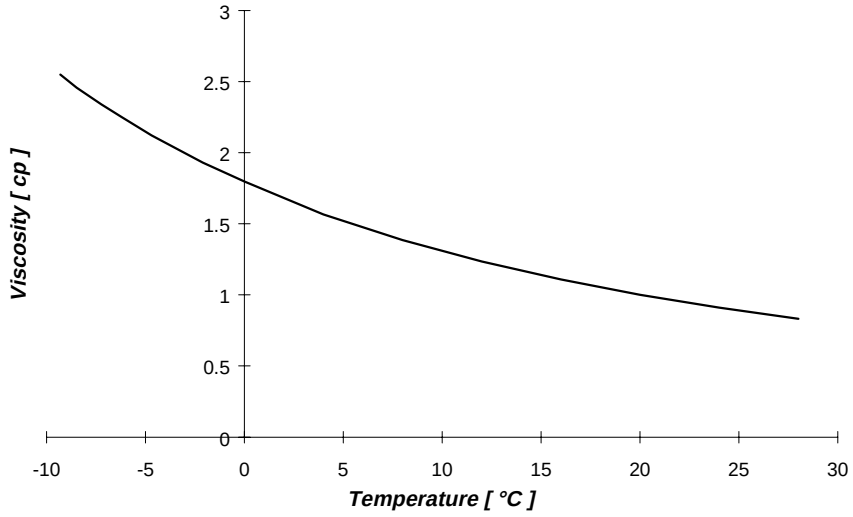

Figure 2.2.4: Dependence of absolute viscosity of pure water on temperature.

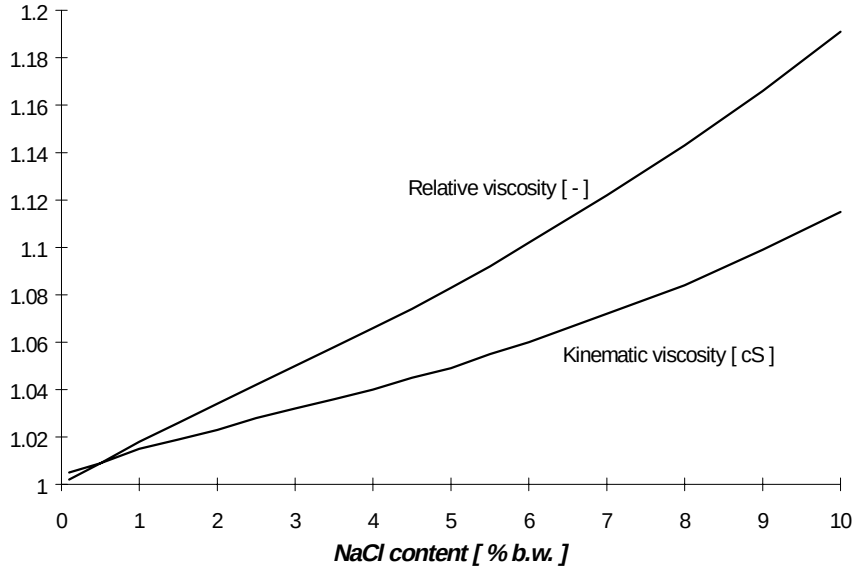

Figure 2.2.5: Dependence of kinematic (η/ρ) and relative viscosity (η/η_0) on sodium chloride content. η_0 =absolute viscosity of pure water at 20°C.

Dissolved substances

The effect of NaCl on the viscosity of water is shown in figure 2.2.5. It can be seen that the sodium chloride content causes only minor effects on viscosity. Furthermore, it can be seen that an increase in concentration causes an almost linear increase in viscosity.

One of the classic hypotheses regarding the mechanisms of frost deterioration of HCP states that deterioration is due to the hydraulic pressures which arise when water is pressed out of pores in which ice formation is taking place (chapter 4). As this hydraulic pressure is dependent on the viscosity of the liquid, it has been proposed that perhaps the more severe damage caused by salt frost scaling is attributable to the increase in viscosity caused by the de-icing chemical. As is shown in figure 2.2.5, however, the presence of NaCl causes only minor increases in viscosity (other de-icing chemicals act similarly). Furthermore, it can be seen that the increase is almost linearly related to concentration and thus the maximum damage obtained at rather low concentrations cannot be explained as due solely to a viscosity effect of the de-icing chemical.

Adsorption forces

On adsorption, water molecules become more strictly ordered than in bulk water and the mobility of the molecules is reduced. The water viscosity should thus be higher for water molecules subjected to adsorptive forces than for bulk water. Low [L 1979] reports measurements of the viscosity of water adsorbed in montmorillonite, figure 2.2.6. According to Low, the viscosity is almost unaffected by adsorptive forces when water is present in pores in which the distance between montmorillonite layers (the interlayer distance) exceeds 5 nm. In pores of shorter interlayer distances the viscosity increases so that at an interlayer distance of 3.5 nm it is approximately 10 % higher than that of bulk water, and at an interlayer distance of 1.5 nm it is approximately 80% higher. At even smaller interlayer distances, viscosity increases dramatically. Since montmorillonite resembles HCP in that it consists of silicon, aluminium and oxygen, it may be assumed that

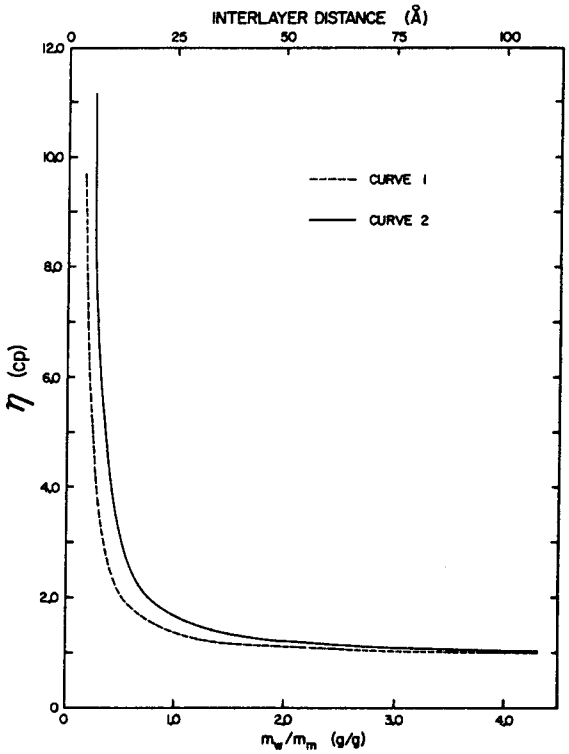

Figure 2.2.6: Dependence of the average viscosity of water on water content (and interlayer distance) in montmorillonite [L 1979].

the adsorptive forces are of similar character and therefore that the effect on viscosity should be similar in HCP. Powers *et al* [P 1954] also found that the viscosity of water seems to depend on the radius of the channel through which it is flowing, at least in HCP.

Since frost deterioration occurs only at high moisture contents, it may be assumed that most (but not all) of the water involved in the ice formation processes is subjected to such weak adsorptive forces that its viscosity is almost equal to that of bulk water.

2.3 ICE

This chapter briefly reviews those properties of ice which may be relevant to frost deterioration of HCP. A short review of studies on the appearance of ice in HCP-based materials is also given. Detailed descriptions of the structure of ice and its electrical and mechanical properties are given by Fletcher [F 1970] and by Hobbs [H 1974].

2.3.1 Types of ice and ice in porous silicious materials

Many different types of ice exist. In bulk, temperature and pressure decide which kind of ice is stable, figure 2.3.1. At ordinary temperatures and pressures, the stable form is hexagonal ice $I_{1,h}$. Anderson [A 1967] reviews several studies on the type of ice that forms in micro porous materials. According to Anderson, it is probable that ice which forms in silicate materials at temperatures above -80°C is normal ice $I_{1,h}$. (At lower temperatures, it may be that cubic ice, I_c, forms directly from vapour. Such ice nevertheless readily transforms into I_h when temperature rises.) Anderson stresses the need for further research.

Pearson and Derbyshire [P 1974], using NMR technique, studied ice formation in specimens of porous silica. Their results indicate that normal ice forms and that it forms within the pores. Pearson and Derbyshire also referred to *Barnes [B 1962]*, who had obtained similar results.

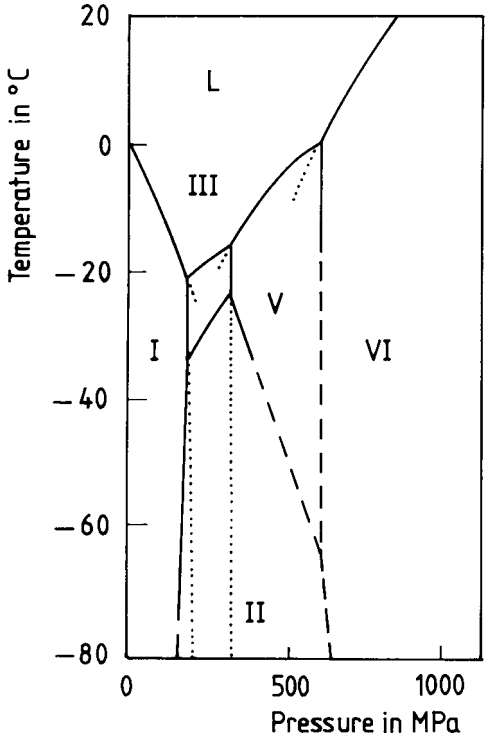

Figure 2.3.1: Phase diagram of ice. Roman numbers denote which type of ice is stable in each region. From [F 1970].

2.3.2 Nucleation

There are two types of nucleation. Ice nucleation may be homogeneous, in which case nucleation takes place in the liquid, *i.e.* the ice crystal is entirely surrounded by the liquid and an ice–liquid interface is created, or it may nucleate heterogeneously, *i.e.* it nucleates and grows on a foreign surface, *e.g.* a foreign particle or the surface of a pore wall.

The ice formation process is heavily dependent on the structure of the water. This structure is poorly known [D-H 1967], especially at large super-coolings, and Fletcher [F 1970], whose work forms the basis for much of this review, therefore limits his discussion on nucleation to temperatures close to 0°C. Since it is known that the structure of water changes significantly when water is adsorbed to solid surfaces, it follows that no detailed description of the nucleation processes in micro porous materials can be given. Helmuth [H 1960], however, states that from the large super-cooling of pore liquid (down to -15°C) which is often observed in HCP, it is obvious that there is no structure of the cement paste which facilitates heterogeneous nucleation.

Homogeneous nucleation creates a solid-liquid interface. This causes a rise in the free energy of the system which must be overcome by the loss of free energy due to the phase transition itself in order for nucleation to occur. The consequence is that a nucleus smaller than a certain size at a certain temperature is thermodynamically unstable and immediately melts. In chapter 2.4, the following expression for the critical radius of a spherical ice nucleus in super cooled bulk water as a function of temperature is derived:

$$r_s = \frac{2\sigma_{s-l} V_{m,s}}{0.0997T^2 - 76.4532T + 13444.483} \qquad (2.4.34)$$

in which T = temperature [K]
$V_{m,s}$ = molar volume of ice, m^3/mol
$\sigma_{l\text{-}s}$ = free energy of the interface liquid-solid, J/m^2

In order for an ice nucleus to be stable at -1°C, its radius must be larger than 59 nm (assuming $\sigma_{s-l} = 0.033$ J/m²). This requires that 26 million molecules adopt the appropriate structure simultaneously. This is very unlikely to occur and thus super-cooling occurs. At -30°C the required radius is 1.3 nm (using $\sigma_{s-l} = 0.025$ J/m²). This requires only 290 molecules and the probability for this nucleus to form is therefore much greater. In calorimetric freezing experiments on HCP, a peak in the heat flow rate is almost always observed close to -42°C (see below). The common interpretation is that a distinct amount of ice forms at this temperature. At this temperature, the radius of a stable ice nucleus is only 0.87 nm, corresponding to some 90 molecules. At -46°C, the requisite radius corresponds to approximately 12 molecules, which is approximately the smallest number of molecules required to form an ice crystal. Obviously, the use of ordinary thermodynamics must be questioned when applied in this way, but the calculation nevertheless shows that the probability of the formation of a stable ice nucleus increases rapidly with decreasing temperature. The ”freezing peak” observed at -40°– -45°C may simply be the result of homogeneous freezing of super-cooled water in pores in which it is isolated from ice in nearby pores so that it can not be nucleated by seeding from those pores. The absence of this peak during melting also supports this view (fig 2.3.3).

Fletcher states that homogeneous nucleation requires extremely pure water. In reality, there are usually foreign particles present on which heterogeneous nucleation can occur. This, according to Fletcher, would be the probable means of nucleation in porous media.

If the surface structure of the pore wall is well-suited to it, the free energy of the ice–pore wall interface may be even less than that of the liquid water–pore wall interface. This will facilitate ice nucleation. The required calculated critical radius of the ice nucleus then will be smaller than that calculated above. However, as stated above, Helmuth believed that HCP does not provide a surface structure that facilitates ice nucleation [H 1960]. Without further elaboration, Litvan even said that freezing of adsorbed supercooled water cannot be initiated by nucleation *in situ*, but that it needs to be redistributed (moved to coarser pores) before being transformed into ice [L 1973].

2.3.3 Growth

When a stable ice nucleus has formed, its subsequent growth will take place either through the freezing of remaining water in its surroundings or through sublimation of vapour. Independently, its growth will be limited either by the availability of molecules and the possibility of incorporating these into the ice structure, or by the possibility of dissipating the heat released on freezing. Fletcher [F 1970] splits the potentials of the growth process into one part concerning the transport of molecules to the crystal surface, and one part concerning the transition of molecules from the liquid to the solid phase, *i.e.* a pure interface process. Geometrically, this is done at a distance of one mean free path from the crystal surface, which corresponds to approximately one molecular diameter.

That part of the growth process which concerns the transport of molecules to the interface and the dissipation of heat is entirely dependent on the circumstances of each and every situation. Thus that part cannot be treated generally.

Simplifications can be made, however, to facilitate estimations of the rate of the pure interface process. This, according to Fletcher, is highly dependent on the surface of the crystal. For a crystal that is rough on a molecular scale, Fletcher derives the following equation for the rate of the interface process:

$$v \approx \frac{D\Delta S_v \Delta T}{kTn_s a} \qquad (2.3.1)$$

in which
v = growth velocity [m/s]
D = coefficient of self-diffusion in the liquid phase [m²/s]
ΔS_v = average entropy of fusion per unit volume of ice over the super cooling interval ΔT [J/K/m^3]
ΔT = super-cooling interval [K]
k = Boltzmann's constant [J/K]
T = Temperature [K]
n_s = concentration of molecules in the solid phase [m^{-3}]
a = intermolecular distance [m]

The super cooling interval $\Delta T = T_{fus}$-T. The term $\Delta S_v \Delta T$ represents the chemical potential difference between the phases. (It is equal to the denominator of eq. (2.4.34), but on a volumetric basis.)

Because $n_s = A/V_m$ and $kA = R$ (A = Avogadro's constant), equation (2.3.2) may be rewritten as:

$$v \approx \frac{DV_{m,s}\Delta S_v \Delta T}{RT\,a} \qquad (2.3.2)$$

Using $D \approx 2.26 \cdot 10^{-9}$ m²/s [A 1990], $V_{m,s} \approx 19.65 \cdot 10^{-6}$ m^3/mole, $a \approx 0.35$ nm, and using $\Delta S_v \approx (1.13\text{-}0.004\Delta T) \cdot 10^6$ J/m^3/K (according to Fletcher), one obtains:

$$v \approx 15.26 \cdot \frac{(1.13 - 0.004\Delta T)\Delta T}{T} \qquad (2.3.3)$$

A super-cooling interval of -0.5°C, *i.e.* depression of the freezing from 273.15 to 272.65K yields a growth velocity of 0.032 m/s. Similarly, a 5°C super-cooling yields a growth velocity of 0.32 m/s

Fletcher [F 1970], making reference to *Lindenmeyer&Chalmers [L 1966]* and *Pruppacher [P 1967a,b]*, says the presence of ionic solutes "…in concentrations up to 0.1 M do not greatly affect either the growth forms or crystallisation kinetics, though the actual crystallisation velocity at a given supercooling (relative to the equilibrium freezing point of the solution) may be changed by a factor of 2 or so. Higher solute concentrations tend to depress the crystallisation velocity more severely." By inserting the complete expressions for the chemical potentials (see chapter 2.4), it might thus be possible to use equation (2.3.2), at least as a rough approximation, even for calculating the rate of ice lens growth in porous media in which the chemical potentials depend on temperature, pressure and mole fractions.

When estimating growth velocity in real situations in which water and heat transport are also important, many possibilities arise. In the first place, the direction of heat transport relative to the phases (ice and water) determines whether the growth will be planar or dendritic. The latter will most probably be the case when ice grows into super-cooled water. When heat is withdrawn from the interface via the ice phase, the growth front will be planar. In such a case, the ice crystals may adopt different orientations relative to the surface. Fletcher [F 1970] and Hobbs [H 1974] have different opinions as to which orientation of the ice crystals will have the fastest growth. Both authors point to the many difficulties in determining equations for the growth rate. Considering the complex situations in the pore system of hardened cement paste, it seems impossible to predict the manner and rate of ice crystal growth.

Hobbs and Fletcher have both published compilations of studies done by many other researchers on the growth rate of ice crystals in super-cooled water. For a super-cooling ΔT (= T_{fus} - T, T_{fus} = true melting temperature) in the interval $10^{-4} < \Delta T < 10^2$, these results may be roughly described by the equation:

$$\log(v) = 1.75\log(\Delta T) - 0.75 \qquad (2.3.4)$$

in which v is the growth velocity [cm/s]. For super-coolings of 0.5 and 5°C, eq. (2.3.4) yields growth rates of 52 µm/s and 3 cm/s, respectively. The scatter between results from different researchers is however rather large, probably because of the differing circumstances under which the growth occurred (perfect/imperfect crystals in glass tubes, copper tubes or in bulk water and the variances in conditions for cooling accompanying these variations).

The equations fitted to experimental results thus yield lower growth velocities than the equation of Fletcher (eq. (2.3.2)). Indeed, Fletcher points out that values calculated by equation (2.3.1) constitute an upper limit of possible growth velocities.

Dendritic ice crystal growth may also occur in porous media if heat is more readily transported through the solid phase than through the liquid. The mechanisms of such growth are poorly known [F 1970] and because of the complexity of the conditions for heat transfer and water transport in porous media, it cannot be said what kind of ice growth, planar or dendritic, will take place.

2.3.4 Density

The most striking thing about the density of ice, is the well known fact that it is lower than that of water. According to X-ray investigations, the density of ice at 0°C is 916.4 kg/m^3 [F 1970]. As the density of water at the same temperature is 999.8395 kg/m^3, the phase transition brings about an expansion of 9.1%. This, of course, is the most apparent cause of frost damage. Also interesting is the dependence of density on temperature, see fig. 2.3.2. According to this figure, the thermal expansion of ice is approximately five times larger than that of hardened cement paste. This may lead to cracking during thawing, as will be further discussed in chapter 4.

The density of ice as a function of temperature may be estimated from the following equation:

$$\rho(T) = \frac{\rho(273.15)}{\left(1+\alpha(T-273.15)\right)^3} \qquad (2.3.5)$$

in which $\rho(T)$ = density at temperature T
$\rho(273.15)$ = density at T = 273.15K, 1 atm (916.4 kg/m^3)
α = coefficient of linear expansion

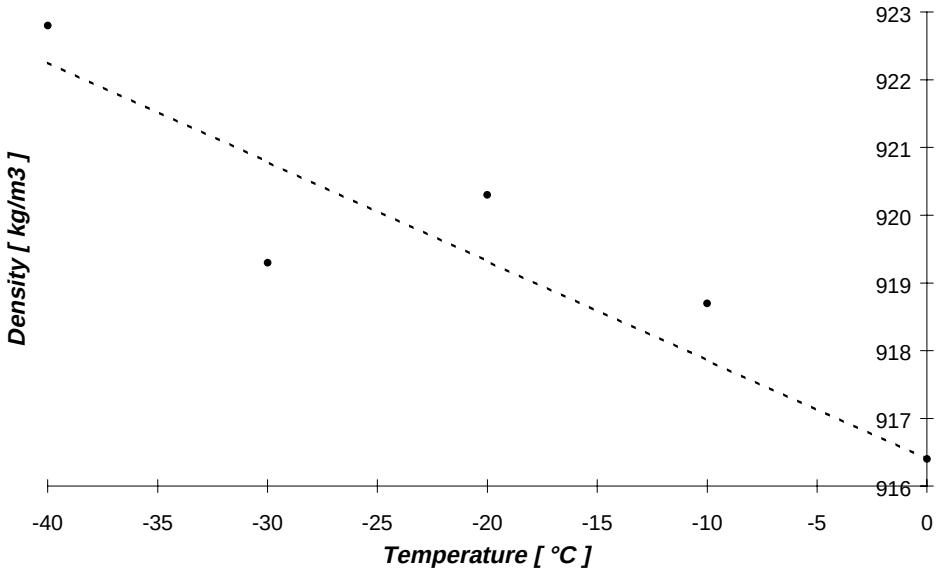

Figure 2.3.2: Density of ice. •: Data from [H 1974] and [F 1970] following from several authors. ---: Calculated, eq. (2.3.5).

The calculated densities shown in fig.2.3.2 were obtained with $\alpha = 53 \cdot 10^{-6}\ K^{-1}$.

From eq. (2.3.5), the molar volume of ice as a function of absolute temperature may be calculated from:

$$V_{m,s} = \frac{1}{53086.97 - 8.121T} \qquad (2.3.6)$$

2.3.5 Heat capacity

As for water, the heat capacity of ice may be expressed as:

$$C_p = AT + B \qquad (2.3.7)$$

Fitting to data from [H 1990], C_p of ice is obtained in J/mole with A = 0.1408 and B = -0.3268 (for the interval $241.15 < T < 273.15$K).

The entropy of ice at T = 273.15K is calculated (from $\Delta_{fus}H$ = 6010 J/mole) to be 41.366 J/K/mole. Calculation of the dependence of entropy on temperature is described in chapter 2.4.

2.3.6 Compressibility

The isothermal compressibility of a substance is defined:

$$\kappa_T = -\frac{1}{V}\left(\frac{\partial V}{\partial P}\right)_T \qquad (2.3.8)$$

in which V is the volume and P the pressure. For a small change of volume, from V_i to V_f, and for a constant κ_T, eq. (2.3.8) may be integrated to give the change in pressure:

$$\Delta P = -\frac{1}{\kappa_T}\ln\left(\frac{V_f}{V_i}\right) \qquad (2.3.9)$$

From the compilation by Hobbs [H 1974], the isothermal compressibility of ice in the temperature region $-20 < \theta < 0$ °C may be estimated to be approximately $250 \cdot 10^{-12}\ Pa^{-1}$. Thus, for a volume change so that $V_f / V_i = 0.99$, the pressure in a volume of ice is raised by some 40 MPa. Clearly, ice is capable of withstanding very high pressures, as compared to the tensile strength of cement paste, without being compressed. Furthermore, as will be seen in chapter 2.4, increasing the pressure lowers the melting point by about 1°C/10 MPa (when ice and liquid water are both exposed to the same pressure). Thus, the counter pressure which the pore walls of a hardened cement paste are able to exert, will be insufficient to stop the expansion of an ice lens when it gains water molecules.

2.3.7 Surface energy

The surface energy of an ice - liquid surface and its dependence on temperature has been studied by many different techniques. Hobbs and Ketcham estimated the value of the surface energy for the ice - liquid surface to be $\sigma_{l\text{-}s}$ = (33±3) mJ/m² and that of the ice - vapour surface to be $\sigma_{v\text{-}s}$ = (109±3) mJ/m² at 0°C (reported in [H 1974]). Hobbs also refers to *Mason* [M1952] and *McDonald* [*M1953*] who, according to Hobbs, found $85 < \sigma_{v\text{-}s} < 122$ mJ/m² (at 0°C) by calculating the number of hydrogen bonds which must be cut in order to create an ice surface. Several other researchers (referred to by both Hobbs and Fletcher), using different techniques, have made estimations of $\sigma_{l\text{-}s}$, and obtained values in the range $7<\sigma_{l\text{-}s}< 38$ mJ/m² (at approximately -40°C). Hobbs, by extrapolating the value of $\sigma_{v\text{-}l}$ to -40°C, calculates $\sigma_{l\text{-}s}$ = (25±3) mJ/m² at -40°C. Thus, the value of the surface energy $\sigma_{l\text{-}s}$ in J/m² at different temperatures may be estimated from:

$$\sigma_{l-s} = \frac{33 + 0.2\theta}{1000} \qquad (2.3.10\ a)$$

or

$$\sigma_{l-s} = \frac{0.2T - 21.63}{1000} \qquad (2.3.10\ b)$$

Alternative formulations have been expressed. For example, Hesstvedt [Ht 1964], by studying spontaneous freezing of small water droplets, found:

$$\sigma_{l-s} = 0.0305 \cdot \left\{1 - 0.0093(T_0 - T)\right\} \qquad (2.3.11)$$

Hesstvedt's equation thus gives values somewhat lower than those obtained from eq. (2.3.10).

The surface energy of ice as described here requires a continuum approach. For a single ice crystal, the surface free energy is different for different surfaces. However, when dealing with freezing phenomena related to frost resistance of hardened cement paste, the size of the ice lenses is large enough to make the continuum approach possible.

2.3.8 Effects of salts on the properties of ice

Pruppacher [P 1963] studied the effect of dissolved substances on homogenous nucleation and found that the structure of water was affected by the solutes such that a somewhat larger super-cooling normally occurred. This increase, though, was only 0-2K (depending on type of solute) and is thus of little practical importance.

Dissolved matter may also affect the structure of the growing ice. For example, the tendency towards dendritic growth into super-cooled liquid may be reduced as the concentration of dissolved matter increases in front of the growing ice and thus reduces the rate of growth at that particular front [F 1970].

2.3.9 Interaction with pore walls

As will be seen in chapter 2.4, the equilibrium between ice and water in micro porous media is affected by the interaction of the ice (and the water) with the pore walls. This interaction is reflected by the free energy of the interface separating the ice from its surroundings, which will be either remaining (adsorbed) water or the solid matrix itself. If the ice is formed within a large water volume in a pore so that it is entirely surrounded by water, the interface energy is that given by equations (2.3.10) and (2.3.11). If the ice is in direct contact with the pore wall, the interface free energy will be different.

In order to make any reasonably correct predictions of the process of ice formation in porous media, it is therefore necessary to know the extent of the interaction between the ice and its surroundings. Direct measurement of this interaction is, to the knowledge of the author, impossible. Therefore, some assumptions must be made. The simplest assumption is that there remains a layer of water between the ice and the pore wall so that the ice is completely surrounded by water and thus the interface energy is given by eqs. (2.3.10) and/or (2.3.11). It is a prerequisite, however, that the thickness of this remaining liquid water is such that there is no interaction between the ice and the matrix. The existence of such a "liquid-like layer" has been dealt with by many researchers. For example, Drost-Hansen [D-H 1967] comments on several indirect studies which indicate that such a liquid-like layer does exist. According to Hobbs [H 1974], Fletcher is "…the only worker who has tackled the difficult problem of trying to develop a quantitative theory of the surface structure of ice (and water)." Fletcher calculates that at temperatures in the interval $-6<\theta<0$°C there exists a liquid-like layer with a thickness of some 10-30 Å on ice. Hobbs says it has never been experimentally determined that such a layer exists and he also points to the difficulties in doing so, partly because of the very thin layer of water and partly because of its character, which is something in between that of ice and that of liquid water.

Hobbs also discusses results by several researchers which show that there is only a very small difference in the condensation coefficient (the probability that a molecule incident on a surface will be adsorbed, thermally equilibrated, and incorporated into the surface) between ice and water, which, according to Hobbs, may be interpreted as evidence of the existence of a liquid-like layer [H 1974].

Takagi [T 1990] calculated the thickness of a liquid-like layer on an ice sphere as a function of temperature and found that for temperatures in the interval $0>\theta>-20$°C and for ice spheres radii in the interval $1<r<100$nm, the thickness of the liquid-like layer is in the interval $0.1<\delta<1$nm, which is in fairly good agreement with that calculated by Fletcher.

Fagerlund [F 1973] calculated the thickness of the layer of water between an ice crystal and the pore wall. Fagerlund however uses an expression by *Wheeler [W 1955]*, which is intended for the calculation of the thickness of a layer of water adsorbed to the pore walls. For temperatures in the interval $0 > \theta > -20$°C, Fagerlund calculates the thickness δ of the adsorbed water to lie in the interval $0.9 < \delta < 1.5$nm. Thus the equation by Fagerlund yields thicker layers than that by Takagi.

The equations given by Fletcher, by Takagi and by Fagerlund are intended for situations other than the present. While Fletcher and Takagi model an ice layer exposed to air, Fagerlund uses a model in which water adsorbed on a pore wall is exposed to air. The actual situation however is that the contingent liquid-like layer is confined between the pore wall and an ice surface. In such a situation, the liquid water is subjected to forces both from the ice and from the pore wall. There are widely differing opinions on the distances across which such forces are felt by the water molecules. While some claim that

these surface forces range over only a few molecular layers, others say the surface forces are felt over distances corresponding to thousands of molecular layers. Anderson [A 1967] says, "…significant effects extend at least 50Å from the surface…", a value corresponding to approximately 15-20 molecular layers. Thus the thickness of a liquid-like layer between an ice crystal and the pore wall cannot be calculated with the equations given by Fletcher or by Takagi. Also the effect of the pore wall must be taken into account. From measurements on the rate of transport of glass spheres frozen into an ice volume, Hoekstra and Miller [H 1967] estimated the thickness of the liquid-like layer at approximately 50 Å at some -0.01°C. These authors refer to *Anderson and Hoekstra* [*A 1965*] who had found that the thickness of a liquid-like layer in clays does not exceed 5-10Å at -1°C.

It is difficult to say whether the thickness of a liquid-like layer confined between an ice body and the pore wall will be larger or smaller than the value mentioned above, since the water molecules will be subjected to attractive forces from two directions. In any case, it seems safe to conclude that a liquid-like layer in fact does exist. Such a layer may be of great importance to moisture movements in partly frozen materials.

The mechanical interaction of ice with pore walls was studied by Sellevold and Radjy [Sd 1976], who measured the modulus of elasticity of beams of porous Vycor glass at different temperature. They found that at -40°C, at which temperature at least 50% of the water content had frozen (according to the authors), the E-modulus had increased by only 11%, while at -160°, it had increased by more than 70%. Their explanation of the small increase at -40°C was that the ice forms in the centre of the pores and that the ice bodies are surrounded by water so that the ice–pore wall interaction is almost negligible. This implies that the interface free energy associated with ice formation is close to that of an ice - liquid water interface. For HCP, however, Sellevold and Radjy reported that phase transition of the capillary-held water produced an increase in the modulus of elasticity. Thus, ice does interact mechanically with the HCP matrix. However, one cannot say how this interaction affects the interface free energy associated with ice formation, since the mechanical interaction may be due to friction as well as to molecular interaction.

2.3.10 Ice formation in HCP

Due to the minute size of the pores in which water is held in hardened cement paste, the freezing point of the water will be depressed (see further chapter 2.4). The freezing process has been studied by several researchers, *e.g.* Vuorinen [V 1969], and Sellevold and co-workers [S 1980], [B 1980], [B1 1986], [B2 1986].

Figure 2.3.3 shows the apparent heat capacity as measured during cooling at 3.3 °C/h and heating at 4.1 °C/h [B1 1986]. The curves clearly show that super-cooling to -8°C readily occurs (even larger super-coolings have been reported, *e.g.* [P 1953]). There is also a large hysteresis between the freezing and melting processes. While the melting process is similar to what may be estimated from the moisture isotherms, the freezing process reveals three peaks in apparent heat capacity, most probably reflecting the fact that ice formation takes place in three separate temperature intervals. Bager and Sellevold explain this as caused by the presence of three concentrations of pore sizes. However, if this were the case, the melting curve ought also to show the same three peaks and the sorption isotherms would have at least two steep regions close to 60 and 80% R.H., respectively,

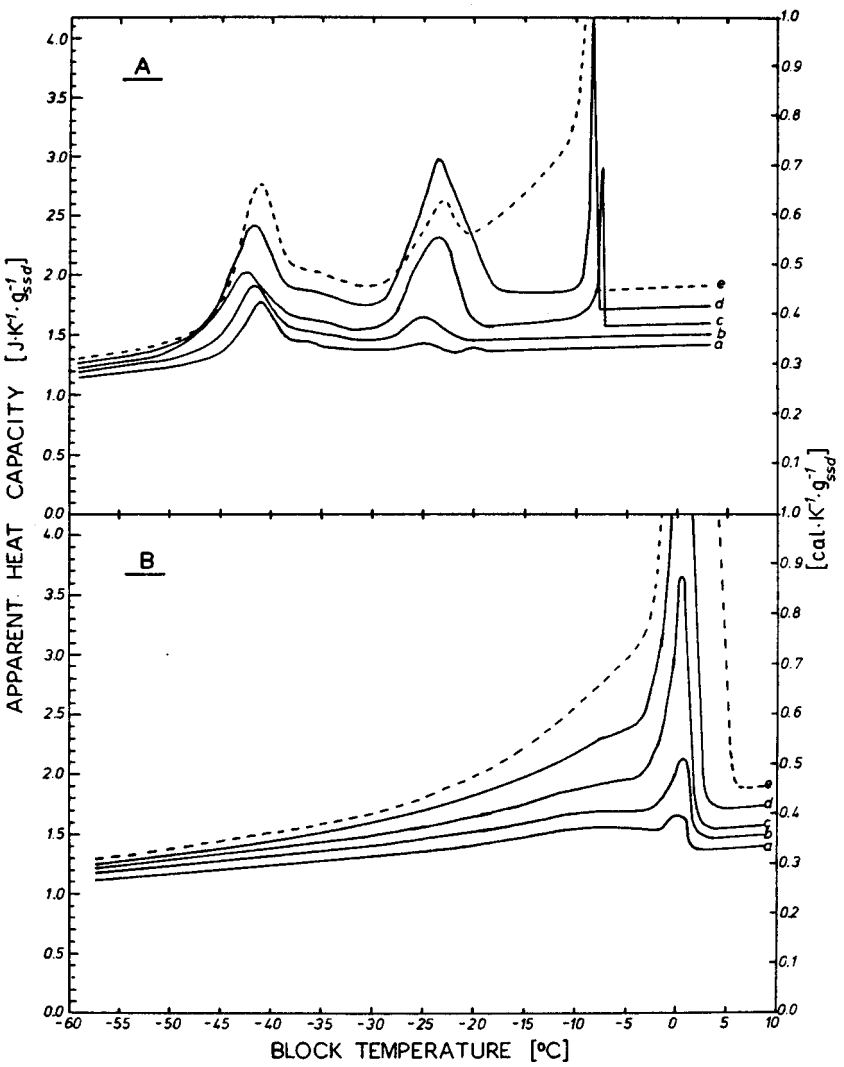

Figure 2.3.3: Apparent heat capacity during cooling (A) and heating (B) of water saturated never-dried hardened cement paste specimens. Curves represent w/c ratios 0.35, 0.40, 0.45, 0.50 and 0.60 (bottom to top). Reprinted from [B1 1986] with permission from Elsevier Science.

separated by more flat regions both at higher, lower and intermediate levels of relative humidity, since these are the humidities which correspond to freezing at approximately -40°C and -20°C. To the knowledge of the present author, no such sorption isotherms have been reported for HCP. (The third peak, the one appearing at -5° – -8°C, is probably mainly due to freezing of super-cooled moisture held in the largest pores, in which the true freezing point depression is almost negligible. Also freezing of water with a true freezing point depression of 5–10°C should be included in this peak.)

The lack of the described properties of the melting curve and the sorption isotherm indicate that the three peaks which appear during cooling are not caused by the presence of three concentrations in pore sizes. Instead, it may be due to freezing of locally supercooled water. This may be water that is effectively isolated by smaller pore necks from the more or less continuous ice phase, thus rendering nucleation by seeding impossible and leaving homogeneous nucleation the only possibility for continued ice formation. As

was shown above, the probability of formation of thermodynamically stable ice nuclei becomes quite high as temperature drops to -40° – -45°C. Indeed, there is a freezing peak in this interval. This explanation, *i.e.* the presence of narrow necks isolating freezable water from the continuous ice, is put forward by Bager and Sellevold in [B 1980].

The many results described in the literature, and those reported in chapter 3 of this report, clearly show that the freezing process is dependent on the previous moisture history of the material. It is also clear that freezing of water held in HCP is a matter of probability and that it is far from independent of temperature. In any truly good numerical simulations of freezing phenomena, all these facts must be considered.

2.4 BASIC THERMODYNAMICS OF ICE FORMATION AND ICE SPREADING

In anticipation of the discussion in chapter 4 on previously proposed mechanisms and of the hypotheses which are put forward in this report, a short review of the basic thermodynamics of ice formation and ice spreading in porous media is set out here. Most of the descriptions may be found in common textbooks on physical chemistry, *e.g.* [A 1990], [L1995], [An 1990], and [Sw 1992].

2.4.1 Criterion for the spontaneity of a process

For a process to be spontaneous, it is necessary that the net overall entropy change be positive, *i.e.* the sum of the changes of entropy of the system and of the surroundings must be positive ($dS_{sys}+dS_{surr}\geq 0$). The entropy change dS_{surr} of the surroundings equals the heat dq_{sys} released from the system divided by the temperature T of the surroundings. Thus, for a spontaneous change:

$$dS_{sys} + \frac{dq_{surr}}{T_{surr}} \geq 0 \qquad (2.4.1)$$

While the equality is valid for a reversible change, the inequality is valid for an irreversible one.

For a process in which heat is transferred from the system to its surroundings (which remain at constant temperature and pressure) and in which there is no work other than expansion work, $dq_{surr} = -dH_{sys}$. Because the Gibbs (free) energy of a system is defined:

$$G = H - TS \qquad (2.4.2)$$

it follows that, at constant temperature and pressure, the criterion for a process to be spontaneous (eq. (2.4.1)) may be expressed in terms of the Gibbs energy as:

$$dG_{sys}\Big|_{T,P} = dH_{sys} - TdS_{sys} \leq 0 \qquad (2.4.3)$$

As before, the equality is valid for a reversible change while the inequality is valid for an irreversible one.

2.4.2 Expressions for the chemical potential of ice and water in porous systems

Definition of chemical potential

The chemical potential of a substance *j* in a system may be defined as the change of the Gibbs energy of the entire system which an infinitesimal change in the amount n_j of substance *j* causes:

$$\mu_j = \left(\frac{\partial G}{\partial n_j} \right) \qquad (2.4.4)$$

The Gibbs energy of an entire system may then be expressed as:

$$G = \sum_j n_j \mu_j \qquad (2.4.5)$$

For a one-component, multi-phase system at internal equilibrium, a distribution of the component in the different phases is adopted so that the system's Gibbs energy comes to a minimum.

Chemical potential of pure substances in bulk

With an infinitesimal change in pressure and temperature, the Gibbs energy of a closed system (doing no non-expansion work) changes as follows:

$$dG = VdP - SdT \qquad (2.4.6)$$

For a pure substance, put on a molar scale, this leads to a change in chemical potential which is:

$$d\mu = \mu - \mu_0 = V_m dP - S_m dT \qquad (2.4.7)$$

For two separate systems to be in equilibrium, it is necessary that their Gibbs energies be equal. For two systems, each of which is a pure substance, this means that the chemical potentials of the two substances must be equal.

Effect of surface energy on the chemical potential of water

The free energy of a system is dependent on the free energies of the interfaces and surfaces that it comprises so that

$$G = G_0 + \sum \sigma_i A_i \qquad (2.4.8)$$

in which G_0 is the free energy of the bulk phases and A_i are the areas of the interfaces/surfaces of free energies σ_i. Thus when an interface area within a system changes, the free energy of the system changes. For example, water entering a narrow pore in a matrix of solid material causes a change in interface energies. Before entering, there is a matrix–air interface. Afterwards, there is a matrix–water interface. This change in free energy of the system is caused by the addition of water and thus, according to definition (2.4.4), the chemical potential of the water in the system is:

$$\mu = \mu_0 + \Delta\sigma \cdot dA_m \qquad (2.4.9)$$

with μ_0 the chemical potential in the bulk state, $\Delta\sigma$ the interface energy change and dA_m the change of interface area per mole of added water. The interface energy change is defined:

$$\Delta\sigma = \sigma_f - \sigma_i \qquad (2.4.10)$$

in which σ_f is the interface energy of the final interface and σ_i that of the initial one.

In capillary suction, the matrix–water interface energy is lower than that of the matrix–air interface. Uptake of water thus causes a decrease in the free energy of the system (bulk water + solid) and so the process is spontaneous.

In the case of a cylindrical pore of circular cross section (fig (2.4.1)), the term dA (omitting the area of the pore ends) is:

$$dA = 2\pi r dx \qquad (2.4.11)$$

in which r is the pore radius and dx is the depth of water penetration. dx is calculated from the volume of water that enters the pore:

$$dV = V_{m,l} dn_l = \pi \cdot r^2 dx \qquad (2.4.12)$$

with $V_{m,l}$ the molar volume of water and dn_l the change of water content. The change of interface area per mole of water that enters the pore, dA_m, thus becomes:

$$\frac{dA}{dn_l} = dA_m = \frac{2V_{m,l}}{r} \qquad (2.4.13)$$

The chemical potential of the water thus becomes:

$$\mu = \mu_0 + \Delta\sigma \frac{2V_{m,l}}{r} \qquad (2.4.14)$$

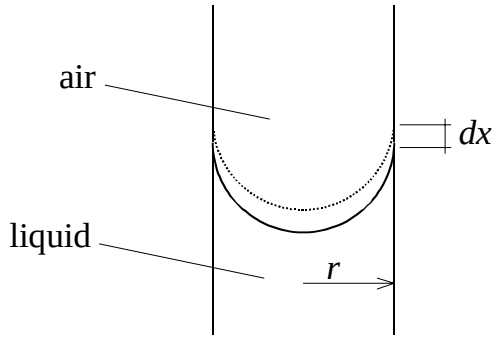

Figure 2.4.1: Water meniscus penetrating a distance dx into a cylinder of circular cross section. Illustration of parameters for eqs. (2.4.11-14).

If the pore is not of circular cross section, the factor *2/r* must be replaced by the hydraulic radius of the pore, *i.e.* the ratio of its circumference to its cross section area. (This has been used by Setzer [S 1993] in a calculation of the differences between freezing and melting in non-cylindrical pores, see below.)

Effect of dissolved substances on the chemical potential of water

For an ideal solution, in which the mole fraction of solvent is *X*, the chemical potential of the solvent is:

$$\mu = \mu_0 + RT\ln(X) \qquad (2.4.15)$$

where *R* is the gas constant and *T* the temperature. The mole fraction *X* is defined:

$$X_j = \frac{n_j}{n_{tot}} \qquad (2.4.16)$$

with n_j representing the number of molecules of the solvent in the solution and n_{tot} representing the total number of moles of molecules in the solution.

Eq. (2.4.15) is valid only for ideal solutions. However, for a solution of NaCl in water (up to a concentration of 15% b.w. (X_l = 0.90)) it yields only minor errors. Thus, at a concentration of 15 % b.w. the calculated freezing point is -9.8°C, while the true one is -10.9°C.

The complete expression for the chemical potential of water, when its temperature and pressure are changed by infinitesimal amounts *dT* and *dP* from their respective reference states and when it is present in a finely divided form and when a solute is added to it, thus becomes:

$$\mu = \mu_{0,l} - S_{m,l}dT_l + V_{m,l}dP_l + RT\ln(X_l) + \Delta\sigma_l \cdot dA_{m,l} \qquad (2.4.17)$$

in which index *l* denotes the liquid phase. The same kind of expression is valid for ice. In this report, however, ice will always be assumed to be pure ice and thus X_{ice}=1, which leads to:

$$\mu_s = \mu_{0,s} - S_{m,s}dT_s + V_{m,s}dP_s + \Delta\sigma_s \cdot dA_{m,s} \qquad (2.4.18)$$

in which index *s* denotes the solid phase.

2.4.3 Equilibrium

Equilibrium in bulk

At the triple point (273.16K, 6.11 mBar), ice and water are in equilibrium, *i.e.* their chemical potentials are equal. For infinitesimal changes in pressure and temperature, the change in chemical potential of each phase is:

$$d\mu = \mu - \mu_0 = -S_m dT + V_m dP \qquad (2.4.19)$$

If the changes in temperature and pressure occur so that the equilibrium is maintained, then:

$$d\mu_l = d\mu_s \qquad (2.4.20)$$

and thus:

$$-S_{m,l}dT + V_{m,l}dP = -S_{m,s}dT + V_{m,s}dP \qquad (2.4.21)$$

If temperature and pressure are both equal in both phases, this leads to:

$$\left(S_{m,s} - S_{m,l}\right)dT = \left(V_{m,s} - V_{m,l}\right)dP \qquad (2.4.22)$$

For a reversible change, the entropy change of the system is equal to its change of molar enthalpy divided by the temperature at which it occurs, so that:

$$S_{m,s} - S_{m,l} = \frac{-\Delta_{fus}H}{T} \qquad (2.4.23)$$

With the change of molar volume:

$$\Delta_{fus}V = V_{m,l} - V_{m,s} \qquad (2.4.24)$$

we get, finally:

$$\frac{dP}{dT} = \frac{\Delta_{fus}H}{T\Delta_{fus}V} \qquad (2.4.25)$$

This is the classic Clapeyron-equation, which describes the solid-liquid boundary in the phase diagram of water. For water, $\Delta_{fus}V$ is negative and thus dP/dT has a negative slope. From the values of temperature and pressure at the triple point (T_{trip} = 273.16, P_{trip} = 611 mBar), the temperature of fusion at atmospheric pressure is calculated from eq. (2.4.25) to be 273.15K (using ΔP = (101325-611) Pa, $\Delta_{fus}H \approx$ 6010 J/mol, $\Delta_{fus}V \approx -1.64 \cdot 10^{-6}$ m^3/mol).

Equilibrium between a small ice body and bulk water

The chemical potential of a small ice body is obtained from eq. (2.4.18) and that of bulk water is obtained from eq. (2.4.7). From these equations, it can be seen that the chemical potential of an ice body will exceed that of bulk water if its surface area is sufficiently large. Such an ice body will be unstable and will melt. Comparing the chemical potentials, we may find the temperature dependence of the size of a stable ice body in its own melt from:

$$-S_{m,s}dT_s + V_{m,s}dP_s + \sigma_{s-l} \cdot dA_{m,s} = -S_{m,l}dT + V_{m,l}dP_l \qquad (2.4.26)$$

Assuming the ice body to be spherical, the interface area changes with the number of moles of ice according to

$$dA_{m,s} = \frac{2V_{m,s}}{r_s} dn_s \qquad (2.4.27)$$

in which r_s is the radius of the ice sphere. The interface energy σ_{s-l} is that of an ice–water interface, which is approximately 0.033 J/m² (eq. (2.3.10)). Above, a Δ-sign was used to allow for changes in type of interface following the different processes. Here, the interface energy remains constant (only the interface area changes) and thus the Δ-sign is omitted.

Assuming the pressures remain atmospheric and the temperatures of the two phases to be equal, we find:

$$\sigma_{s-l} \frac{2V_{m,s}}{r_s} = (S_{m,s} - S_{m,l})dT \qquad (2.4.28)$$

The right hand side of eq. (2.4.28) has to be integrated (from the temperature of fusion in bulk to the actual temperature), taking the temperature dependence of the molar entropies into consideration. The entropy of a substance varies with temperature in accordance with:

$$S(T_f) = S(T_i) + \int_{T_i}^{T_f} \frac{C_p(T)}{T} dT \qquad (2.4.29)$$

The heat capacity may, within reasonable intervals, be expressed with an expression in the form:

$$C_p = AT + B \qquad (2.4.30)$$

(The coefficients A and B for water and ice are given in chapters 2.2 and 2.3, respectively). The solution to eq. (2.4.30) is thus:

$$S(T_f) = S(T_i) + A\left(T_f - T_i\right) + B\ln\left(\frac{T_f}{T_i}\right) \qquad (2.4.31)$$

and thus we find

$$\int_{T_i}^{T_f} S(T)dT = S(T_i)(T_f - T_i) + \frac{A}{2}\left(T_f - T_i\right)^2 + B\left\{\frac{T_f}{T_i}\left(\ln(\frac{T_f}{T_i}) - 1\right) + 1\right\} \qquad (2.4.32)$$

The difference in the right hand side of eq. (2.4.28) is evaluated by solving eq. (2.4.32) for both water and ice. For numerical calculations, this difference in chemical potential between the liquid and the solid phase may be obtained directly from:

$$\Delta(\Delta\mu) = \int_{Tref}^{T} (S_{m,s}(T) - S_{m,l}(T))dT = 0.0997T^2 - 76.4532T + 13444.483 \qquad (2.4.33)$$

which expression is directly fitted to values calculated from eq. (2.4.32). T_{ref} is the bulk melting temperature 273.15K. In the interval 231<T<273.14K the values obtained with eq. (2.4.33) differ from those obtained through the use of eq. (2.4.32) by less than 0.15%.

The temperature dependence of the size of a stable ice sphere of radius r_s is thus:

$$r_s = \frac{2\sigma_{s-l}V_{m,s}}{0.0997T^2 - 76.4532T + 13444.483} \qquad (2.4.34)$$

According to this equation, an ice sphere is not stable in bulk water at -10°C unless its radius is larger than 5.1 nm (using $\sigma_{s\text{-}l}$ = 0.030 J/m², $V_{m,s}$ = 19.65·10^{-6} m^3/mol).

For increased accuracy of the predicted relation between temperature and ice sphere radius, the temperature dependence of the molar volume of ice and the interface energy should be taken into consideration (eqs. (2.3.5) and(2.3.9)).

(More detailed information on the derivations of these expressions are found in Volmer [V 1939], Haynes [H 1968] and Defay *et al* [D 1966].)

Equilibrium between ice and aqueous solutions in porous systems

Equilibrium between ice and water is reached when their chemical potentials are equal. If both phases are spread out in a porous material and the water contains a solute, the equilibrium is found by equilibrating eqs. (2.4.17) and (2.4.18):

$$-S_{m,l}dT_l + V_{m,l}dP_l + RT_l \ln(X_l) + \Delta\sigma_l \cdot dA_{m,l} = -S_{m,s}dT_s + V_{m,s}dP_s + \Delta\sigma_s \cdot dA_{m,s} \qquad (2.4.35)$$

This expression may be used, for example, for calculating the temperature of fusion of ice in a narrow capillary or for calculating the pressure needed to avoid ice lens growth in a soil (soil heaving). A few applications of eq. (2.4.35) will demonstrate its implications.

Freezing of water held in narrow pores

First, eq. (2.4.35) is used for calculating the freezing point of water enclosed in a long, narrow pore of circular cross section of radius *r*. The surface energy terms are found from eq. (2.4.14). Eq. (2.4.35) thus takes the form:

$$-S_{m,l}dT_l + V_{m,l}dP_l + RT_l \ln(X_l) + \Delta\sigma_{l-m} \cdot \frac{2V_{m,l}}{r} = -S_{m,s}dT_s + V_{m,s}dP_s + \Delta\sigma_{s-m} \cdot \frac{2V_{m,s}}{r} \qquad (2.4.36)$$

in which $\Delta\sigma_{l\text{-}m}$ and $\Delta\sigma_{s\text{-}m}$ denote the surface free energy changes which occur when liquid and solid are spread over the surface of the matrix.

The difference in chemical potential between ice and water caused by the temperature change alone, $\Delta(\Delta\mu(T))$, is calculated:

$$\Delta\left(\Delta\mu(T)\right) = \int_{T^*}^{T} \left\{S_{m,s} - S_{m,l}\right\} dT \qquad (2.4.37)$$

in which T is the equilibrium temperature.

As set out above, the right hand side of eq. (2.4.37) is replaced by:

$$\Delta\left(\Delta\mu(T)\right) = 0.0997T^2 - 76.4532T + 13444.483 \qquad (2.4.38)$$

We can now use eq. (2.4.36) to do some calculations for specific situations. First we calculate the temperature of fusion for some pore radii under the assumptions that the liquid is pure water (X=1) and that the pressure of both water and ice remain unchanged, *i.e. dP = 0* (see below). Accordingly, the equilibrium temperature may be calculated from:

$$\frac{2}{r}\left(V_{m,s}\Delta\sigma_{s-m} - V_{m,l}\Delta\sigma_{l-m}\right) = 0.0997T^2 - 76.4532T + 13444.483 \qquad (2.4.39)$$

For this calculation, we need to know the surface energy changes when the liquid–matrix and solid–matrix interfaces change, respectively. As pointed out with regard to eq. (2.4.10), the actual changes are those in which, in the first case, a matrix–air interface is replaced by that of matrix–liquid and, in the latter case, a matrix–air interface is replaced by one of matrix–solid. Since the surface energy of the (dry) matrix is not known, a reasonable assumption must be made. This may be done by considering that when

freezing takes place not all the water freezes; even at temperatures of -45°C some layers of unfrozen water will still exist on the pore walls [*e.g.* B1 1986]. At higher temperatures more water will remain unfrozen and thus the solid–matrix interface may be assumed to have the same surface energy as that of solid–liquid. Similarly, when drying takes place, some adsorbed water will remain on the matrix surfaces and so the surface energy of the matrix–air interface may be assumed to be the same as that of liquid–air. These two assumptions are further justified when one considers that the moisture contents involved in freezing at temperatures above -40°C correspond to the moisture contents obtained at levels of relative humidity of 60% or higher. At such high R.H. there will definitely be some adsorbed water on the matrix surfaces. Thus the following assumptions are made:

$$\Delta\sigma_{l-m} = \sigma_{l-m} - \sigma_{a-m} = \sigma_{l-l} - \sigma_{a-l} \approx 0.1484 \cdot 10^{-3} T - 0.11623 \qquad (2.4.40)$$

$$\Delta\sigma_{s-m} = \sigma_{s-m} - \sigma_{a-m} = \sigma_{s-l} - \sigma_{a-l} \approx \frac{0.2T - 21.63}{1000} - (-.1484 \cdot 10^{-3} T + 0.11623)$$

$$= \frac{0.3484T - 137.86}{1000} \qquad (2.4.41)$$

where the temperature dependencies have been obtained from eqs. (2.2.9) and (2.3.9).

The radius *r* calculated from eq. (2.4.39) is the radius of a critical ice nucleus. The true *pore* radius is obtained when the thickness *t* of the non-freezable layers of water close to the pore wall are added to the calculated radius, *i.e.:*

$$r_{pore} = r + t \qquad (2.4.42)$$

The existence of such unfrozen layers is a prerequisite for the choices of surface energies which were made above. As discussed in section 2.3, the thickness of the unfrozen layer is not precisely known, either as a function of temperature or as a function of ice lens size. At -55°C, Bager and Sellevold [B1 1986] found that the amount of non-frozen water corresponded to a layer thickness approximately corresponding to 3 monolayers. The temperature dependence however was not discussed by these authors. Brun *et al* [B 1977] simply assumed the unfrozen layer to have a thickness of 8Å, independent of pore size and temperature. From the literature survey on liquid-like layers in section 2.3, it seems that only at very mild freezing point depressions will the liquid-like layer reach a thickness of more than about one nanometer. For simplicity, the liquid-like layer may be assumed to be 1 nm, independent of both temperature and radius.

Corresponding values of temperature of fusion and pore radius are shown in figure 2.4.2. For these calculations the values of the molar volumes were obtained from eqs. (2.2.2) and (2.3.6). For comparison, values obtained from measurements on alumina porous plugs and Vycor glass by Brun *et al* [B 1977] are also shown.

Also shown in figure 2.4.2 is the relation between temperature and freezing point of water in a slit-shaped pore. For such a pore shape, the factor 2/*r* in eq. (2.4.39) is replaced by 1/*r*. Setzer [S 1993] uses this difference to explain the hysteresis observed between freezing and melting of water held in the pores of HCP (*e.g.* figure 2.3.4). Setzer explains that even in a slit-shaped pore, the first ice nucleus is spherical (fig. 2.4.3),which

means that the water in a pore of given size freezes based on the upper curve of figure 2.4.2 (using 2/*r*). During melting however, according to Setzer, the temperature of fusion is determined by the lower curve (1/*r*) and thus there should be a true hysteresis between freezing and melting of water in a slit-shaped pore. As is seen in figure 2.4.2, the hysteresis amounts to several degrees for small pores. One may object that Setzer's explanation of the hysteresis between freezing and melting requires that ice nucleation is homogeneous in each individual pore, while it seems reasonable that in fact, to a large extent, ice spreads into smaller pores through successive seeding from ice in larger pores, as concluded by Bager and Sellevold [B1 1986]. If this is correct, ice formation and spreading into smaller pores will be controlled by seeding rather than nucleation *in situ* and thus the hydraulic radius of the ice is the same during melting as during freezing. Still though, since large super cooling has often been reported, indicating that the pore walls of HCP does not facilitate nucleation, it is possible that homogeneous ice formation does occur to such an extent that Setzer's explanation is relevant. Fagerlund [F 1974] considers the hysteresis between freezing and melting to be due to local super-cooling of pore water held in pores which are isolated from the (continuous) ice by pores in which water is held so rigidly to the pore walls that nucleation cannot take place in them (not even by seeding) until considerably lower temperatures are established. The same explanation is given by Bager and Sellevold [B1980].

Apart from the fact that the exact geometry of pores in real materials is unknown, one large source of error is the lack of knowledge of the actual surface energies. For example, the assumption that the surface energy of the liquid-like layer is the same as in bulk is likely to be wrong; dispersion forces will probably have some effect on all molecules in such a layer. However, it is the net changes as described by eqs. (2.4.40) and (2.4.41) which determine the freezing point depression and thus erroneous assumptions tend to cancel themselves out. One other way of dealing with this problem is by using the

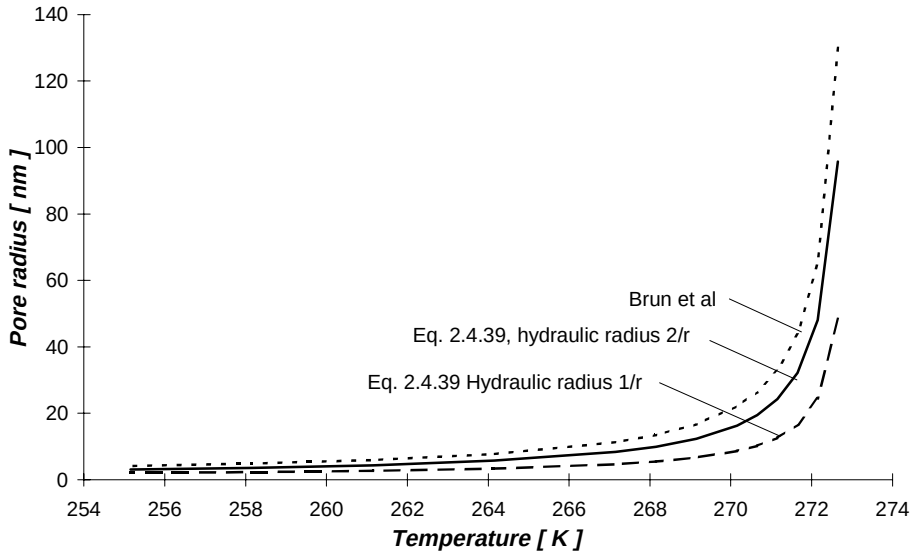

Figure 2.4.2: Calculated relation between temperature of fusion and pore radius for pores of different hydraulic radii. Thickness of remaining layer of unfrozen water assumed to be 1 nm. ---: Brun et al [B 1977]

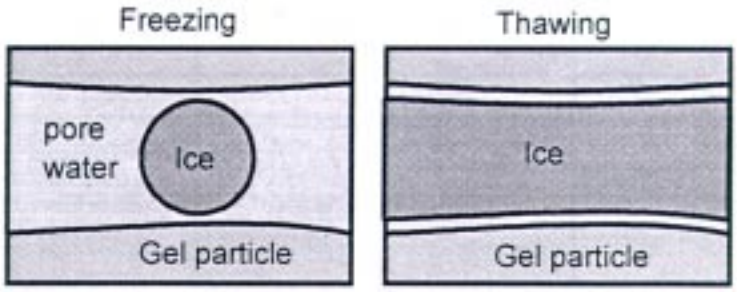

Figure 2.4.3: Illustration of different hydraulic radii of ice during freezing and melting, respectively. [S 1993].

differential enthalpies and entropies of adsorption instead of surface energies. In this way, the amount of freezable water can be calculated without relying on uncertain surface energy values. (This is further discussed in Chapter 3.) Still, as is seen from figure 2.4.2, the qualitative behaviour of eq. (2.4.39) is correct and thus we may use it for further studies of the equilibrium between ice and water in porous materials under different conditions.

Soil heaving

Equation (2.4.35) also may be used to calculate heaving pressures due to ice lens growth in soils. In such a case, an ice lens of a thickness of between a few centimetres and several meters grows at a depth below the earth surface by consuming water from the ground water level while cooling is provided from above. The pores are quite coarse and so the surface energy terms need not be dealt with. Because the size of the ice lens and the depth beneath the soil surface are large (meter scale), the temperature of the water close to the ice lens may be assumed to be equal to that of the lens, *i.e.* $dT_l = dT_s = T\text{-}T_0$. Eq. (2.4.35) then takes the following form:

$$V_{m,s}\left(P_s - P_0\right) = \Delta(\Delta\mu(T)) + V_{m,l}\left(P_l - P_0\right) + RT\ln(X_l) \qquad (2.4.43)$$

If the pore water is pure water (X=1), the only way of re-establishing equilibrium is by establishing a pressure difference between the ice and the water so that $P_l \neq P_s$. If the water remains at atmospheric pressure, *i.e.* there is no lack of water, a pressure of 3.5 MPa is needed in the ice in order to establish equilibrium at -3°C. (As long as this pressure difference is not established, the chemical potential of the ice is lower than that of the water and consequently the ice lens growth will continue, provided the heat flow is large enough to avoid temperature rises.)

If the pore solution contains some solute, the required ice pressure may be reduced. In the example above, the mole fraction of water in the pore solution would have to be X_l = 0.97 in order for equilibrium to be established with both phases remaining at atmospheric pressure. (In the case of the solute being NaCl, this corresponds to a concentration of 4.7% by weight.)

Adjacent pores of different sizes - pressures required for equilibrium

The next point of interest concerns the equilibrium between ice and water enclosed in pores of different size in a porous material. A model for this is shown in figure 2.4.4. An ice lens of spherical shape (radius r_s) is connected to a narrow and somewhat conically shaped pore of circular cross section. This latter pore is water-filled up to a point where its cross sectional radius is r_l. The appropriate expression for the equilibrium between the ice in the large pore and the liquid in the smaller one is

$$-S_{m,l}dT_l + V_{m,l}dP_l + RT_l \ln(X_l) + \Delta\sigma_{l-m} \cdot \frac{2V_{m,l}}{r_l} = -S_{m,s}dT_s + V_{m,s}dP_s + \Delta\sigma_{s-m} \cdot \frac{2V_{m,s}}{r_s} \qquad (2.4.44)$$

From this expression, the equilibrium ice lens pressure has been calculated and some of the results are shown in figure 2.4.5. The calculations were done with the values of the molar volumes and surface energies given above. In all calculations it was assumed that the (spherical) ice lens has a radius of 1μm.

As long as the ice lens can gain more moisture from its surroundings, it will not stop growing unless its pressure reaches the levels shown in figure 2.4.5. It is seen in this figure that the needed pressure easily rises to several MPa, which can be compared with the tensile strength of the matrix, which is normally in the range 2-7 MPa (for Portland cement-based materials).

Figure 2.4.5 also shows that the equilibrium pressure increases almost linearly with decreasing temperature, approximately 1.2MPa/K, independent of the water channel radius.

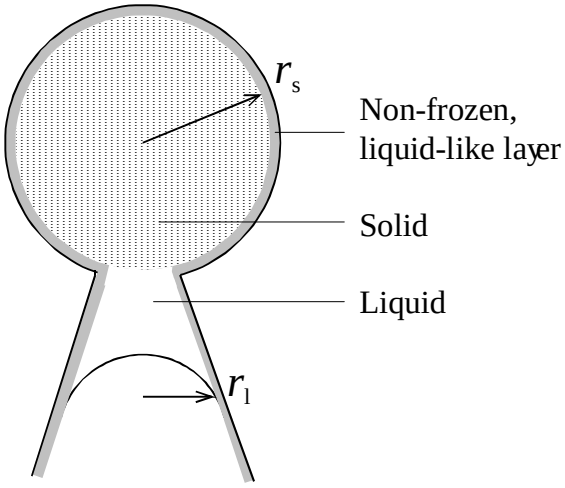

Figure 2.4.4: Pore model used for eq. (2.4.44).

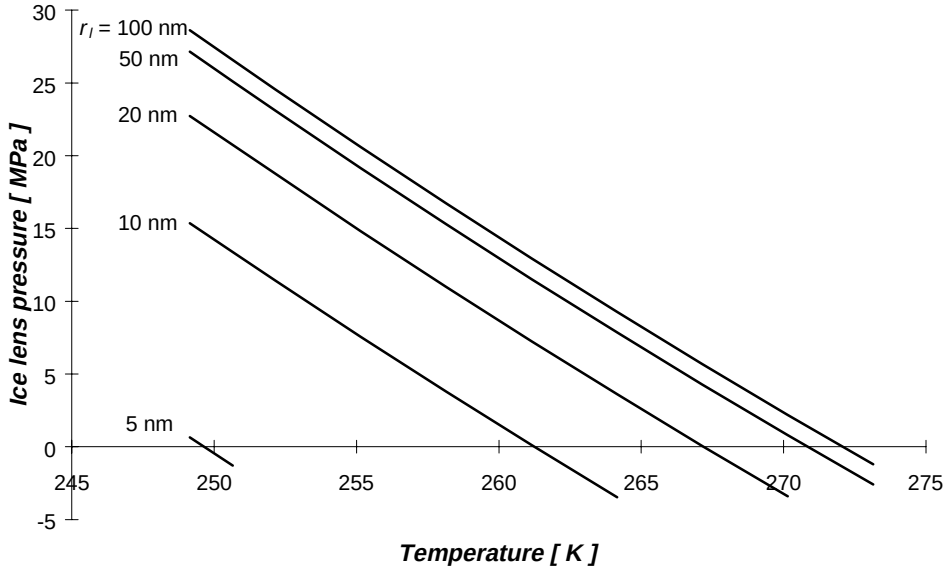

Figure 2.4.5: Temperature dependence of the ice lens pressure needed for equilibrium between a spherical ice lens of radius 1 µm and pure water enclosed in a narrow capillary of indicated radius (model in fig 2.4.4).

Of course, the size of the ice lens also affects the equilibrium pressure. Some calculated values of this are shown in figure 2.4.6. The uppermost line, for which the radius of the ice crystal is equal to that of the water-filled pore, crosses the abscissa at the temperature of fusion of this pore size (except for the effect of the omitted unfrozen water).

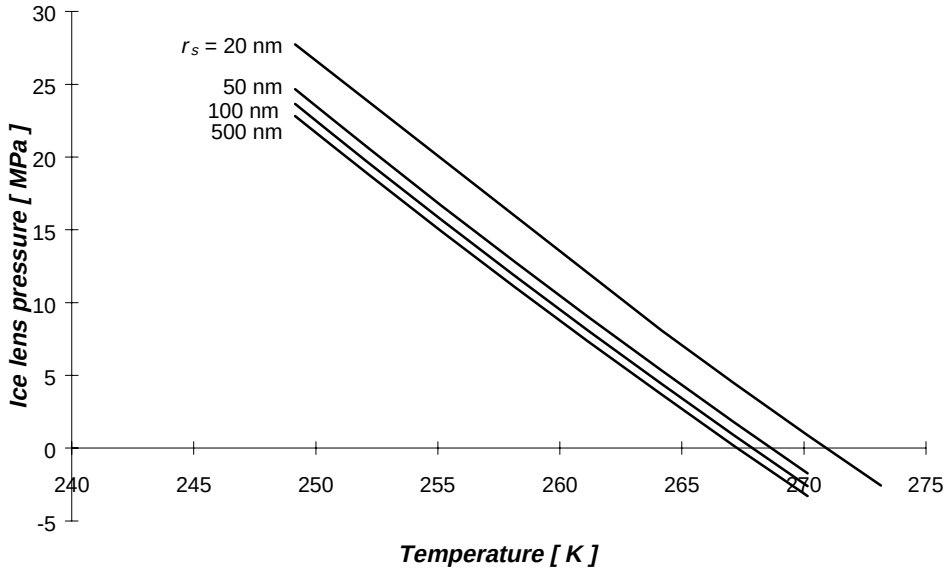

Figure 2.4.6: Temperature dependence of the ice lens pressure needed for equilibrium between water in a cylindrical pore of radius = 20 nm and a spherical ice lens of indicated radius (model in fig 2.4.4).

Defay *et al* [D 1966] assumes mechanical and physicochemical equilibrium between the ice and the water remaining in a porous system. From that standpoint, the pressure difference between the phases can be calculated from the interfacial tension and an assumption regarding the radius of curvature of the meniscus separating the two phases. In the equations given above, no such assumptions are made. However, at equilibrium, this rule must be obeyed. Thus the radius of *curvature* may be calculated:

$$r = \frac{2\sigma}{\Delta P} \qquad (2.4.45)$$

in which σ is the interface tension for the interface between the two phases (not towards the matrix!). Above, the pressure difference was calculated for a case in which the ice is in a coarse pore and the water is in a narrow one. We may now calculate the radius of curvature of the meniscus separating the phases. At 265 K and with a water channel radius equal to 20 nm and an ice body of radius 1 µm, the pressure difference at equilibrium was found to be 2.6 MPa (fig 2.4.4). With the solid–liquid interface energy = 0.031, eq. (2.4.45) yields a radius of curvature of 23.8 nm. This is larger than the radius of the water channel and thus the ice does not spread into the narrow channel (provided that the contact angle is ≈0°). This has been described by Everett [E 1961].

Effect of salts in pore water

If the pore water contains some solutes, the mole fraction of water is lowered (X_w<1) and so the chemical potential of the water is reduced. This immediately leads to a lower freezing temperature and so, at a given temperature, the reduction of the pressure on the liquid that was calculated in the preceding sections for equilibrium between pure ice and the solution, is reduced. In table 2.4.1 some calculated values are given. The pressure change in the last column of table 2.4.1 is simply the negative of the osmotic pressure of the salt solution at the two temperatures. Changing the ice lens radius does not affect the required pressure change.

2.4.4 Spreading of ice in the pore system

As will be dealt with in chapter 4, there has been some discussion of the spreading of ice in hardened cement paste. Some authors have concluded that ice spreads from larger to smaller pores as temperature is lowered, while others have ventured that the firstly formed ice lenses are able to consume moisture from the surrounding pores so quickly

Table 2.4.1: Comparison of required ice pressures for equilibrium with water or a 3% b.w. NaCl-solution (X_l = 0.981). Pore model as in figure 2.4.3. Spherical ice lens of radius 1µm.

Water channel radius [nm] and temperature [K]	Required ice lens pressure, pure water [MPa]	Required ice lens pressure, salt solution [MPa]	Change of required ice lens pressure [MPa]
25 nm, 255.15K	16.25	14.20	-2.04
100nm, 255.15K	20.59	18.55	-2.04
25nm, 267.15K	1.47	-0.67	-2.14
100nm, 267.15K	5.68	3.55	-2.14

that ice formation in those pores is rendered impossible. Doubtless, in reality, the nucleation itself (*i.e.* the annulment of super-cooling) also plays a major role.

The following is a brief illustration of a few of the possible ways in which ice spreading occurs in a pore system under varying conditions and of their limitations. Haynes [H 1968] contains a more complete and detailed description.

As was shown in section 2.4.3, the size of a stable ice body in bulk water is temperature dependent. In short, the area-to-volume ratio of the ice body has to be so low that the chemical potential of the ice does not exceed that of the surrounding water. Consequently, when an ice nucleus forms, it has to immediately reach such a size that it becomes stable. In a narrow pore, this may prevent ice formation at the bulk transition temperature, even if the pore is completely water saturated. This phenomenon, for the case of hardened Portland cement paste, has been described by Helmuth [H 1960].

When a water-saturated specimen of hardened cement paste (HCP) is cooled, the water contained in it becomes thermodynamically unstable when temperatures drop below 273.15 K. However, due to the size restrictions, stable ice can form only in the coarsest pores. For example, at 273.14 K, the required radius of an ice sphere is some 5 µm. Since the volume of pores of a size larger than 5 µm is exceedingly low in any well cast and well cured HCP (*e.g.* fig 2.1.1), almost no ice can remain stable at this temperature. (In reality, dissolved reaction products also serve to lower the freezing point of the solution held in HCP.)

For the following discussion, we need to distinguish between ice spreading in specimens with a fixed moisture content and ice spreading in specimens which are connected to a moisture source throughout the freezing process.

Ice spreading in a porous specimen of constant moisture content

After the first stable ice nucleii have formed in a water-saturated fine porous specimen, the remaining pore water may still be thermodynamically unstable. This means there is a large amount of potentially freezable water which, because of the size restrictions, cannot turn into ice *in situ*. In order to establish equilibrium between the remaining water and the existing ice, the vapour pressure of the remaining water must be reduced. This is achieved by reducing the degree of saturation of the pore system: water is transported out of zones where it was thermodynamically unstable (but where it was also prevented from freezing) into pores where ice is already present. There, phase transition occurs and the existing ice body grows. When the water content of the smaller pores is reduced, the chemical potential of the remaining water is reduced (due to the interaction between the remaining water and the pore wall). The transport of moisture to and the volume increase accompanying phase transition in the initially ice-containing pores, may lead to complete filling of these pores. This will increase the pressure on (and thus the chemical potential of) the ice. Both the changes in total interface energy that are due to loss of water and the increase of pressure on the ice act to even out the difference in thermodynamic state of the remaining water and the ice.

When temperature is further lowered, the chemical potential of the ice increases less than that of the water ($d\mu = -SdT$, $S_l > S_s$), and thus more water will be thermodynamically unstable. There are then two geometrically different possibilities for continued ice formation: Either continued ice formation will take place through transport of moisture from small pores to those coarse pores in which ice already exists, or ice will

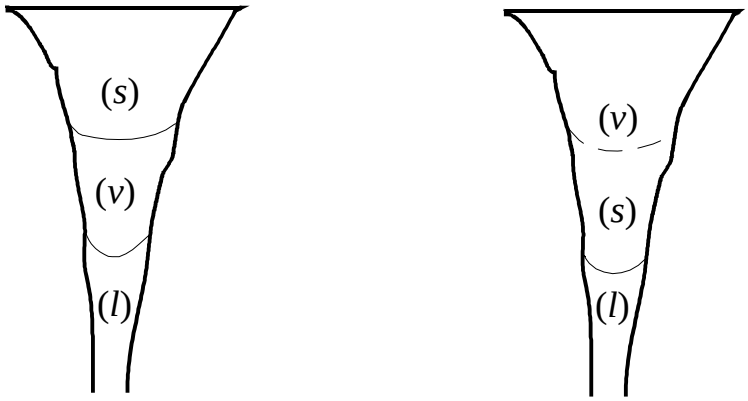

Figure 2.4.7: Illustration of different ice spreading patterns described in the text. Dashed line: Curvature of solid–vapour meniscus unknown. (Liquid-like layer of adsorbed water molecules have been omitted.)

form *in situ* in those of the smaller pores which are large enough to permit such ice formation. Which type of ice formation will take place is dependent on the pore geometry. The following is an effort to illustrate these two major possibilities. (In reality, it cannot be excluded that ice formation will be a mix of both types described here.)

The first type of continued ice formation (fig 2.4.7, left) means water in the smaller pores is replaced by moist air (which may previously have been present in the larger pores). When equilibrium is reached, an interface between the remaining adsorbed water and the vapour phase will exist. As this process proceeds, the ice-containing pore may become completely filled and the ice pressure will rise. When the pressure reaches a certain value, which will be dependent on temperature, pore sizes, and interface energies, the ice will penetrate into smaller pores. If the matrix tensile strength is too low, the matrix will be fractured before this ”spreading pressure” is established. If instead the largest pore is open to the surroundings, the process described will act to empty the pore system and no pressure increase will occur. This kind of ice formation has been described by Litvan [L 1972].

In the second case (fig. 2.4.7, right), ice spreads into smaller pores through *in situ* ice formation and no vapour–liquid interface is formed. As it is only the volume increase associated with phase transition which acts to fill the coarsest pore, in which initial nucleation took place, this pore will not be filled with ice as fast as in the first case. Depending on the initial degree of saturation, it may in fact not become filled at all.

Because the vapour–adsorbed water interface energy is most probably about twice as high as that of an ice–adsorbed water interface, the first case is probably unrealistic (fig 2.4.7 left). Instead, this argument predicts an ice formation pattern of type 2, *i.e.* continuous spreading of ice into smaller pores along with moisture flow from the small pores to the ice, so that the sum of the interface energies is minimised (fig 2.4.7, right). This means that the free energy of the interface ice–adsorbed, non-frozen water is such that the ice wets the pore walls. This view is supported by results reported by Sellevold and Radjy, who studied ice formation in beams of porous Vycor glass indirectly by measuring changes in elastic modulus that occur during freezing [Sd 1976]. The authors found smaller freezing point depressions than could be predicted under the assumption that the ice pressure remained atmospheric. They concluded, therefore, that the ice pressure had to be less than atmospheric and thus that the enthalpy and chemical potential of the ice would be less than that of bulk ice.

A calculation by way of example will illustrate the large difference in the changes of a system's Gibbs energy resulting from ice formation in the two ways described above. Suppose an ice body exists in the coarsest part of a porous system consisting of three distinctly different pore sizes, fig. 2.4.8. In figure 2.4.8-*A* equilibrium is established. Now suppose another small amount of ice is to be formed from the liquid in the finest pores. This may occur in such a way that the ice grows in the largest pore, which implies that vapour will be transported from the coarse pore to the middle pore, fig 2.4.8-*B*. This corresponds to the first case described above. The other alternative, in which the ice replaces the volume of water which is lost from the narrowest pore and also grows slightly in the coarsest pore (by the excess volume caused by phase transition), is shown in fig. 2.4.8-*C*.

The interface energy changes resulting from either of these two different modes of ice spreading when 1 mmoleof moisture transforms into ice, are calculated as follows:

$\underline{A \rightarrow B}$: Two interface changes occur: In the middle pore, water is replaced by vapour along a length of the pore corresponding to the volume of water lost. The area is calculated:

$$\Delta A = \frac{2\Delta V}{r}$$

1 mmolecorresponds approximately to $18 \cdot 10^{-9}$ m^3. Setting r = 20 nm thus yields an area of 1.8 m².

The interface energy changes from $\sigma_{l\text{-}m}$ to $\sigma_{v\text{-}m}$ (the negative of eq. (2.4.40)), which means the interface energy increases by approximately 0.075 J/m².

Meanwhile, the solid–vapour meniscus is moved upwards. The interface energy change here is approximately -0.043 J/m² (eq. (2.4.41)). As the molar volume of ice is larger than that of water, the volume change is approximately $19.7 \cdot 10^{-9}$. The area change in the 50 nm pore therefore is 0.79 m².

The total interface energy change is thus:

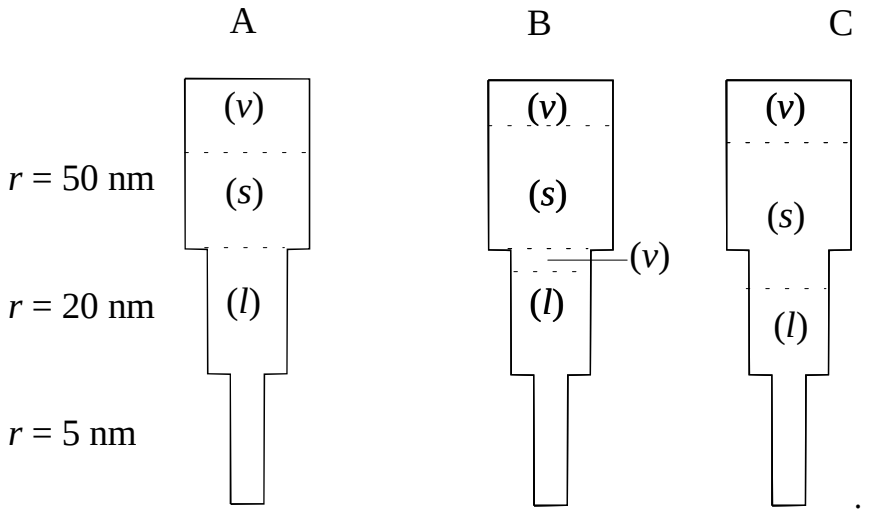

Figure 2.4.8: Different types of ice spreading (schematically). Curvatures of menisci unknown.

$$\sum \Delta(\sigma \cdot A) = 0.075 \cdot 1.8 - 0.043 \cdot 0.79 = 0.101 J \text{ J}$$

$\underline{A \rightarrow C}$: The liquid lost from the middle pore is entirely replaced by ice. The area is the same as calculated above, 1.8 m². The interface energy change is now approximately +0.033 J/m² (eq. 2.4.40). The upper meniscus is moved a distance corresponding to the volume increase caused by the phase transition, *i.e.* $(19.7\text{-}18)\cdot 10^{-6}$ m³/mol. For 1 mmoleand for a radius r = 50 nm, the interface area change thus is 0.068 m². The interface energy change is the same as above, -0.043 J/m². The total interface energy change for case *C* is thus:

$$\sum \Delta(\sigma \cdot A) = 0.033 \cdot 1.8 - 0.043 \cdot 0.068 = 0.056 \text{ J}$$

Obviously, the total interface energy increase is less for the process A–C than for A–B. Thus, the preferred ice formation pattern is the spreading of ice into smaller and smaller pores and, thus, no drainage will occur. If the described phase transition was to take place at a certain temperature, more heat would be lost from system *C* than from system *B* due to the smaller increase in total interface energy. This shows that the heat released on freezing (*e.g.* measured in calorimetric measurements) is dependent on the location of *both* menisci. As long as the ice–vapour meniscus is located in coarse pores, however, its importance to the amount of heat released is small. (This is an idealised description in that it assumes that a certain amount of water will freeze at a certain temperature, independent of the interface energy changes which occur. In reality, freezing of the same amount of water will take place at a higher temperature in the system in which smaller interface energy increases take place.)

This description is valid for a system in which there are no neck pores, *i.e.* narrow channels connecting wider pores. In pore systems without such neck pores, ice formation in small pores is readily seeded from ice bodies existing in larger pores and super cooling of water in smaller pores is unlikely. The following describes what might occur if there were such neck pores.

A system consisting of two wide pores connected by a narrow channel is shown in figure 2.4.9. The temperature is such that formation of a stable ice nucleus has just become possible in the largest pore (radius r_s). The rest of the pore system remains water saturated and the remaining water is thermodynamically unstable. Due to the size restrictions, however, ice cannot form in the other pores at this temperature. Thus, there will be a potential for transport of this water towards the ice in the largest pore, by which process the pore of radius r_l would be emptied. When the temperature at which it would have been possible for a stable ice nucleus to form in pore *B* is eventually reached, this pore may already be empty. Whether this will be so is dependent on the relative volumes of pores of radii r_l and r_s, the permeability to flow of water and the rate of temperature decrease.

The processes described above are very much dependent on the initial degree of saturation, the pore size distribution of the matrix and, not least, the extent to which super-cooling may occur. The exact sequence of events must be analysed for each individual situation.

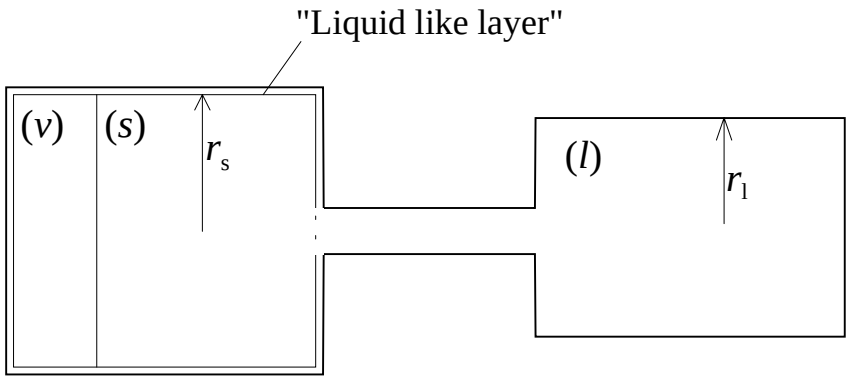

Figure 2.4.9: Ice in large pore connected to water in middle size pore via water in narrow pore. All pores have circular cross section. Shape of meniscus ice-water depends on conditions (dashed line).

Ice spreading in a porous specimen with access to a moisture source

In the case of a porous specimen connected to a source of liquid water, the ice formation pattern described above may change significantly. It was seen above that the total interface energy of the porous system increases when ice replaces water in a certain pore. Such a process will therefore be avoided whenever possible. Instead, the water in the small pores will tend to flow towards the ice in the coarser pores. In the case of a fixed moisture content, this brings about a reduction of the chemical potential of the remaining water and thus the process may be stopped. However, if the system is in contact with a moisture source so that the moisture flowing from the narrow pores towards the coarser ones is continuously replaced, the chemical potential of the moisture remaining in the narrow pores will remain unchanged. As before, because of size restrictions, ice cannot nucleate *in situ* in these pores. Instead, the ice body in the coarsest pore will grow. This kind of ice formation is called micro ice-lens growth (or osmotic ice-lens growth) and will continue until the ice completely fills its pore and thereby starts exerting a pressure on the pore walls. Thereafter, either the matrix will be fractured or such high pressure will develop that the ice will spread into the small pore, since that, despite the increase in interface energy, increases the system's free energy less than if the ice pressure were to continue to increase.

These statements may all be derived from the equations set out in section 2.4.3. The statement that ice will spread into the smaller pores when its pressure exceeds a certain value has been outlined by Everett [E 1961], who showed that the pressure difference between ice and remaining water required for ice to spread into a cylindrical pore of circular cross section is:

$$\Delta P = \frac{2\Delta\sigma}{r}$$

in which $\Delta\sigma$ (= $s_{s\text{-}m}$ - $s_{l\text{-}m}$ (≈0.033 J/m²)) is the interface energy change when ice replaces water in the narrow pore and r is the radius of the narrow pore.

This kind of ice formation is what causes frost heaving in soils. The phenomenon is called macro ice-lens formation. In such a case, an ice lens situated in between the soil

surface and the ground water level gains moisture from the ground water while heat flows towards the soil surface.

When the withdrawn heat and the moisture flowing to the ice lens balance each other (so that the heat released on freezing is constantly withdrawn), the ice lens growth mechanism described above reaches a state of dynamic equilibrium. The solid–liquid meniscus then does not move. If cooling is too intense (too much heat is withdrawn compared to the maximum possible moisture flow), temperature will be lowered and ice formation will spread into smaller pores.

3

STUDY OF SOME THERMODYNAMIC PROPERTIES OF PORE WATER AND ITS FREEZING IN PORTLAND CEMENT-BOUND MATERIALS

The heat flow rate from a micro mortar specimen subjected to thawing at +3K/h were calculated from adsorption and desorption isotherms determined at room temperature and compared to heat flow rates actually obtained during cooling and melting of specimens of the same materials The intention was to study whether ice forms through successive drying of the pore system or if it spreads into the pore system. The calculation was carried out under the assumption that the ice has bulk ice properties, which is to say that the ice forms only in the very coarse pores of the pore system and thus through successive drying of the pore system.

The calculated heat flow rates are lower than those actually measured. This may be because the enthalpy of the ice is lower than assumed (possibly indicating that ice actually forms within the pores), or it may be because the thermodynamic state of the pore water cannot be calculated from the temperature as presumed in this text, or, finally, it may be because the desorption isotherms used in the calculations were erroneously determined. These different possibilities are shortly discussed.

3.1 Introduction

The freezing of water adsorbed in fine porous materials is dependent on the thermodynamic state of the adsorbed water. The temperature dependence of the freezing process may be estimated by using a pore model and a pore size distribution together with assumptions about reasonable interface energy changes and pressure changes (similar to what was described in chapter 2.5). However, because of all these assumptions, the outcome of such an estimation may be highly questionable. An alternative way of describing the freezing process is to measure the relevant properties of the capillary-held water and then compare its free energy, as a function of temperature, to that of ice. (This only requires that some assumption be made concerning the state of the ice.) Freezing will take place when the free energy of the ice is lower than that of the capillary water.

In this chapter, results from such a study are described. The thermodynamic state of the pore water was determined using a twin double microcalorimeter, recently developed by Professor Ingemar Wadsö, Division of Thermochemistry, Lund University, and by Dr. Lars Wadsö, of our own division. With this calorimeter, the heat of adsorption and the adsorption isotherm are determined simultaneously (at +25°C in this study). The data obtained are well in accordance with data found in the literature. Also, the desorption isotherm (at +5 and +18°C) was determined, although using a simpler technique. Since the adsorption and desorption isotherms were obtained by different techniques, they were not straightforwardly comparable. In order to overcome this drawback, an attempt was made to determine the isotherms using a sorption balance. Unfortunately, during the time this apparatus was at my disposal, no successful measurements were accomplished.

The heat flow rates during freezing and melting were determined with a scanning calorimeter (Calvet type, produced by Setaram, France).

3.2 Materials

Materials

Three micro mortars of *w/c* 0.40, 0.50 and 0.65 were cast. The term "micro mortar" is used to denote that the grain size of the sand used in these mortars was an extremely finely divided quartzite flour. A sieve analysis, supplied by the producer, Fyleverken IMB AB, Sjöbo, Sweden, is given in Table 3.1. According to the producer, the sand is 99% SiO_2, and the remainder is Al_2O_3, Fe_2O_3 and TiO_2. The glow loss is 0.2%. The density of SiO_2 varies from 2635 to 2660 kg/m^3 [H 1990]. Thus, from its chemical composition, the sand compact density is estimated to be 2650 kg/m^3. The complete mortar compositions are given in Table 3.2.

Specimen preparation

Casting, drilling and cutting

The specimens were cast in a steel form (230·200·950 mm^3) and both table and poker vibrated for 5-10 minutes in order to avoid as far as possible any compaction pores. After casting, a tight plexiglass lid was put onto the steel form (with a rubber gasket). A small amount of water was poured onto the specimen surface in the air gap between the cast surface and the lid.

The *w/c* 0.65 and 0.50 were demoulded on the day after casting while the 0.40 was demoulded three days after casting (the water coverage on the cast surface was maintained at all times). The blocks were then water stored another night.

Cylindrical specimens, 20 from each block, with a diameter of 64 mm, were drilled out of the blocks perpendicular to the direction of casting. These cylinders were drilled in two rows, figure 3.1. The outermost 20 mm of the block in each direction were not used.

These cylinders were cut with a diamond saw so that 4 discs of a thickness of 25 mm and one of 35 mm were obtained from each core (again, the outermost 20 mm were not used).

From the cast material remaining between the drilled holes, cores of a diameter of approximately 12 mm were drilled for subsequent calorimetric experiments. (The diameter varied depending on the material quality. In materials of high strength the thin drill vibrates and thus produces thinner cylinders than when drilling in materials of low strength.)

Pre-storage

All drilled out specimens were stored in lime water (under a lid) until testing began. For the sorption studies, 10 discs (ϕ64·25mm) of each quality were used. These were taken up after 5 months in the storage bath. Density and porosity were determined by the Archimedes principle. Thus the specimens were weighed, dried at 105°C for 3 days (tests had shown that no weight changes would occur after 48 hours), evacuated in a vacuum and water saturated. The specimens were weighed under water and in air and densities and porosities were calculated as described in Appendix 3.1. Average data on density and porosity are given in table 3.3. After this determination, all specimens were continuously stored under water until testing, and also during crushing (see below).

Crushing

The specimens were crushed and sieved under water by Scancem Research AB, Slite, Sweden. The materials were divided into two different fractions. The first was intended for the desorption isotherm determination and comprised grains in the interval 0.25 – 1.5 mm. The second was intended for the calorimetric experiments and consisted of grains with a mean diameter of approximately 50 µm. The grain size distributions for these materials was determined by Scancem Research AB and the results are shown in Appendix 3.2 to this chapter.

Table 3.1: Sieve analysis of the sand used.

Sieve opening [mm]	
0.20 - 0.18	0 %
0.18 - 0.15	0 %
0.15 - 0.10	0.1 %
0.10 - 0.074	0.3 %
0.074 - 0.05	2.6 %
0.05 - 0.045	3.5 %
< 0.045	93.5 %
Total:	100

Table 3.2: Mortar mix compositions.

w/c ratio	0.40	0.50	0.65
Cement* [kg/m^3]	1050	840	646.2
Water [kg/m^3]	420	420	420
Sand [kg/m^3]	653.7	830.3	993.4

*The cement was the Swedish "Anläggnings cement" described in General Appendix 2.

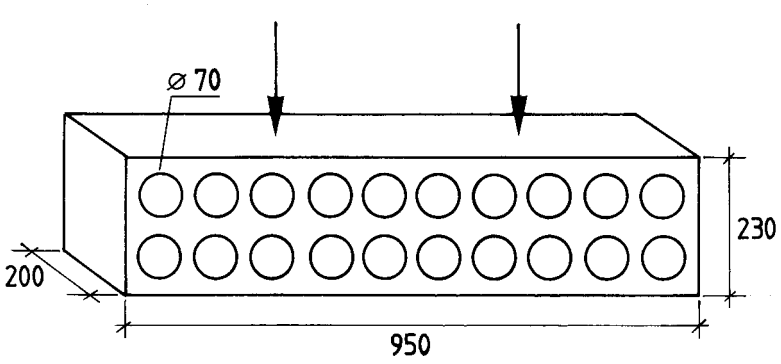

Figure 3.1: Cores were drilled out perpendicular to the direction of casting (indicated by arrows).

Table 3.3: Density and porosity data. Mean values and standard deviation (in parenthesis) from 10 samples of each quality. Calculations described in Appendix 3.1.

Material	Density [g/cm^3]	Porosity [% b.vol.]	Max. moisture content [% b.w.]
w/c 0.40	1.859 (0.01)	28.62 (0.245)	15.4
w/c 0.50	1.796 (0.01)	31.16 (0.181)	17.3
w/c 0.65	1.701 (0.01)	34.88 (0.187)	20.5

It is clear that the median grain size of the crushed materials is similar to the grain size of the sand used. However, since the sand content of the cast materials is rather low (25 – 37% by volume) and since it can be seen from the grain size distribution curves that some 50% of the crushed material consists of grains in the interval 50 - 200 μm, I do not think any of the results obtained are substantially affected by the properties of the sand.

Degrees of hydration

Degrees of hydration were determined on specimens from the same batches as were used for determining moisture transport coefficients. These specimens were taken out of the storage water 5 months after casting, *i.e.* at the same time as the sorption isotherm specimens. After determination of porosity and density (including drying at 105°C) these specimens were conditioned (by two subsequent dryings) to various moisture contents (in the interval $0.95<S<1.0$) and stored in plastic bags for another 10 weeks. After the test on moisture transport coefficients, the degrees of hydration were determined on two specimens of each quality by ignition at 1050°C. The results are given in table 3.4. It is assumed that the degrees of hydration of these samples are fairly equal to those of the samples used for the isotherms.

Table 3.4. Approximate degrees of hydration.

Material	Degree of hydration
w/c 0.40, sample 1	0.721
w/c 0.40, sample 2	0.723
w/c 0.50, sample 1	0.767
w/c 0.50, sample 2	0.769
w/c 0.65, sample 1	0.789
w/c 0.65, sample 2	0.793

Table 3.5: Results from analysis of the chemical composition of the pore solution [mM]

Material	Ca^{+}	K^{+}	Na^{+}	S^{-2}	Al^{+3}	Fe	Mg^{+2}	Si	OH^{-}
w/c 0.40	1.5	130	28	1.5	0.02	0.03	<0.1	0.97	150
w/c 0.50	7	54	13	0.2	0.01	<0.01	<0.1	0.14	85
w/c 0.65	17	19	6	0.1	<0.1	<0.01	<0.1	0.13	65

Note: Standard deviation/Mean value <0.1, according to the analyst, Scancem Research

Chemistry of the pore solution

In conjunction with the crushing, an analysis of the chemical composition of the pore solution was carried out by Scancem Research AB. The results are given in table 3.5. After crushing, the grains were stored in a lime water volume about three times as large as the material volume. The true composition of the pore solution in the samples used for the isotherm determinations must thus have differed slightly from the values given in table 3.5.

According to table 3.5, the mole fraction of water in the pore solution is approximately 0.995 for the 0.40 quality and higher for the others.

3.3 Determination of desorption isotherms

Method

The desorption isotherms were determined in our own laboratory. Samples of the water-saturated crushed material (grain size 0.25–1.5 mm) were allowed to dry in different climates until equilibrium was attained. The sample size was some 20 g (dry weight).

This was done for 10 levels of relative humidity at two temperatures, +5° and +18°C. The different climates were obtained by preparing saturated aqueous solutions of different salts and placing them in a plastic box with a tight lid. The salts used and the expected levels of R.H. are given in table 3.6. Soda lime was used as a CO_2 absorbent in the boxes in order to minimise carbonation of the samples. The principle test set-up is shown in figure 3.2.

The R.H. levels were checked with a dew point meter (Protimeter, England) and the CO_2 concentration was measured with hand-held equipment produced by Svenska Termoinstrument, Sweden. The former results are given in Appendix 3.3 to this chapter.

Because of the scatter in the measurements taken with the dew point meter, both in the calibration and in the boxes, it was not possible to determine exactly what relative humidity had been obtained in the boxes. The dew point meter therefore was used only to check that the levels of R.H. were reasonably correct (*i.e.* to check for leakage, etc). In the results, the expected value of relative humidity in each box has been used. From the measurements taken it seems reasonable that the R.H. levels are correct to within 1.5 % R.H.

Table 3.6. Salts used to produce different levels of R.H. and the expected levels [%]. [G 1977]

Temp	LiCl	$C_2H_3KO_2$	$MgCl_2$	KI_3	NaCl	KBr	KCl	$Sr(NO_3)_2$	KNO_3	K_2SO_4
18°C	11.3	23.4	33.2	70.3	75.5	82.0	85.4	87.6	94.9	97.7
4.8°C	11.3	23.4	37	73.3	76.8	85.1	87.7	92.4	96.3	98.5

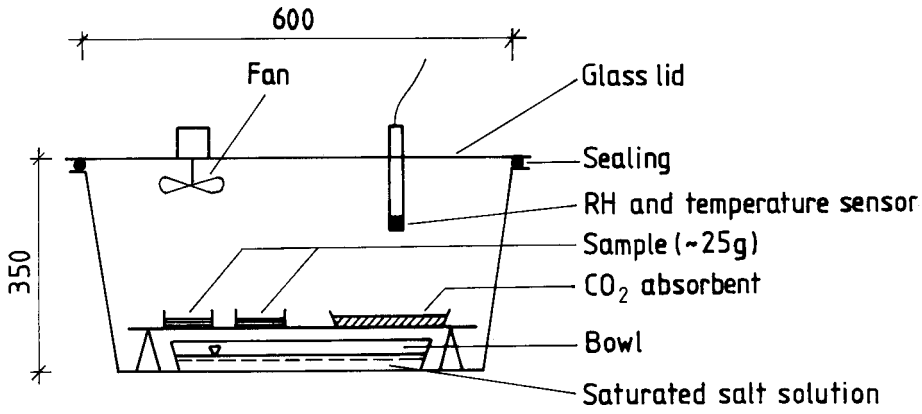

Figure 3.2: Climate box for determination of desorption isotherm.

As for the CO_2 concentration, the measured values varied. At the beginning of the test, the measured level in the boxes was some 25±10 ppm and by the end it had risen to lie in the interval of 70-100 ppm. Direct measurement in the atmosphere normally gave values in the interval of 600-1000 ppm. Thus, some carbonation probably had occurred, especially for samples at intermediate levels of R.H. The extent of carbonation was, however, not measured.

The samples were kept in the boxes for 13-14 weeks, *i.e.* some 90-100 days. Since it was desirable not to open the boxes because this would increase the CO_2 concentration and disturb the R.H. level, the drying process was checked in a parallel box (R.H. 94%) on one individual specimen. The weight of this sample as a function of time is shown in figure 3.3. From this it seems that drying had stopped after some 40 days. In fact, the final weight is slightly higher than the one taken at 36 days. This may be due to carbonation since no carbon dioxide absorbent was used in this box.

According to Nilsson [N 1977], *Grudemo* [*G 1976*] reported that a drying time of half a year was required in order to reach equilibrium in 1 mm thick discs of C_3S paste of *w/c* ratio 0.50 at an age of 5.8 years. For diffusion processes in which the moisture diffusion coefficient does not vary, drying time decreases with the square of the hydraulic radius. The hydraulic radius of Grudemo's discs is 0.5 mm. Assuming the grains in this study to be spherical, their hydraulic radii vary from 0.08 to 0.5 mm. Since the grains are not perfectly spherical, these values should actually be even smaller. Furthermore, the degree of hydration was probably higher in Grudemo's specimens than in the present ones. Based on these considerations and the experimental results in figure 3.3, it seems reasonable that equilibrium had been reached at the time drying was interrupted.

Results

The desorption isotherms obtained at +5°C and +18°C, are shown in figures 3.4 and 3.5. The complete set of data is given in Appendix 3.4. From this, it can be seen that the measured degree of hydration exceeds 1.0 for some samples. Obviously this cannot be correct and is probably attributable to too short drying at 105°C. By modifying the

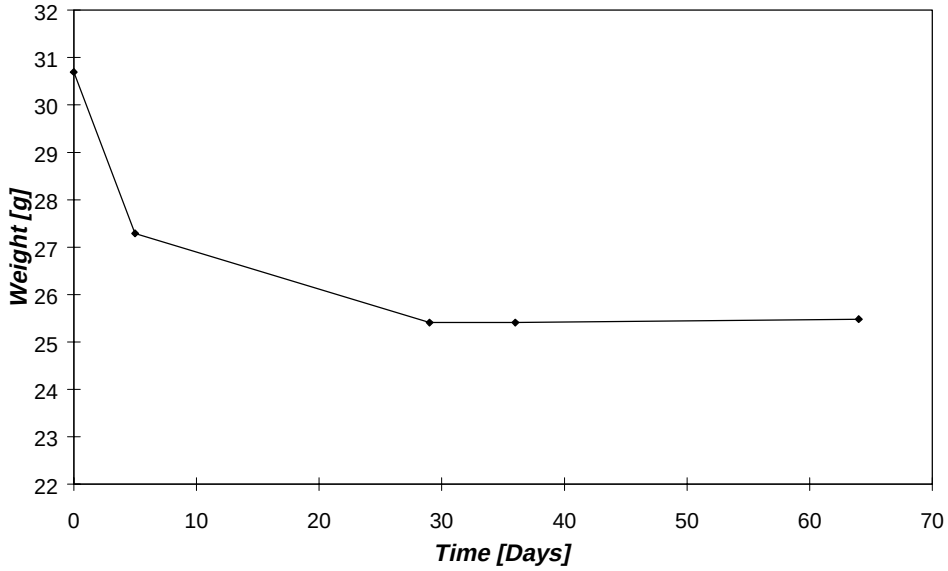

Figure 3.3: Weight of duplicate sample during desorption in 94% R.H., 21°C vs. time.

measured dry weights so that more reasonable degrees of hydration are obtained, the desorption isotherms in figures 3.6 and 3.7 are obtained. In these figures, the weights have been adjusted to yield degrees of hydration of approximately 0.73, 0.79 and 0.80. These values are based on the values shown in table 3.4.

For the isotherm obtained at +18°C these modifications seem to yield a small improvement. For the 5°-isotherm, though, the modification yields larger scatter.

In some cases, the moisture contents obtained at 87.6% R.H. seem to be erroneous as compared to the other values. These values therefore have been omitted in the calculations of ice formation described in section 3.7.

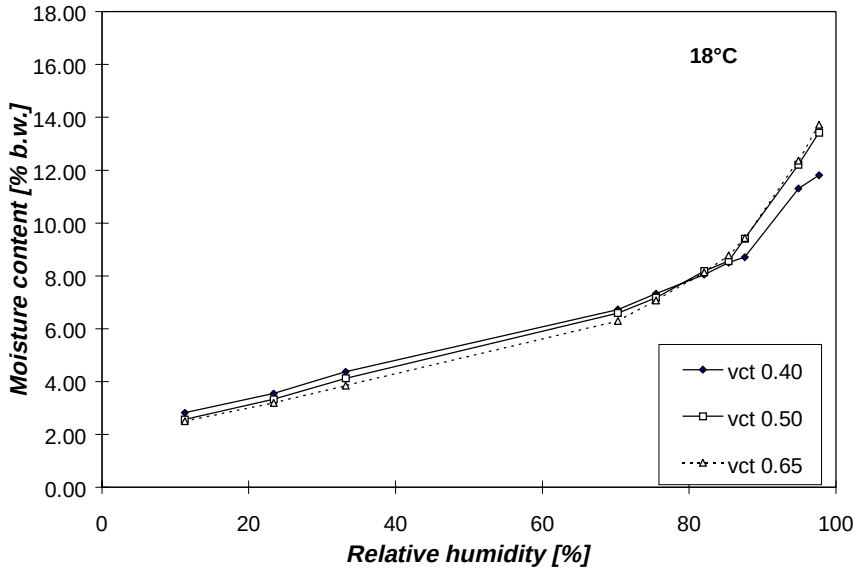

Figure 3.4: Desorption isotherms obtained at 18°C.

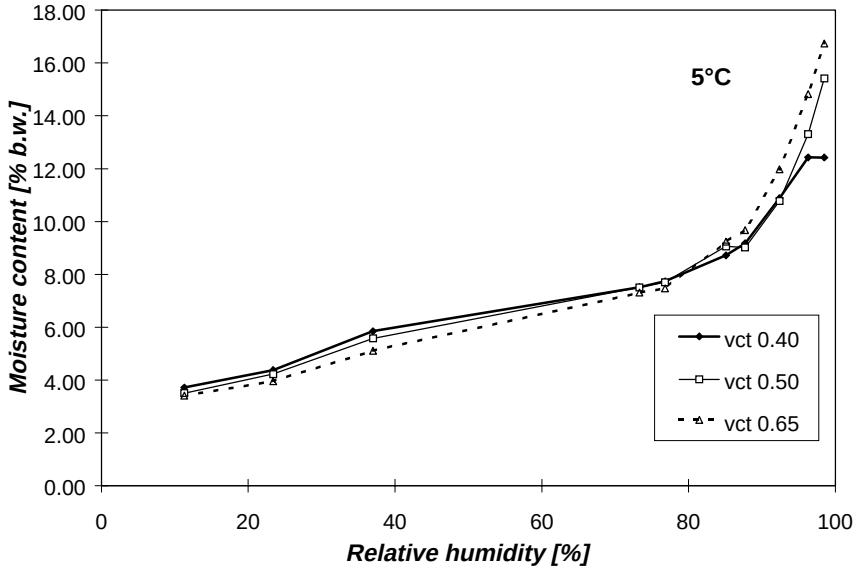

Figure 3.5: Desorption isotherms obtained at 5°C.

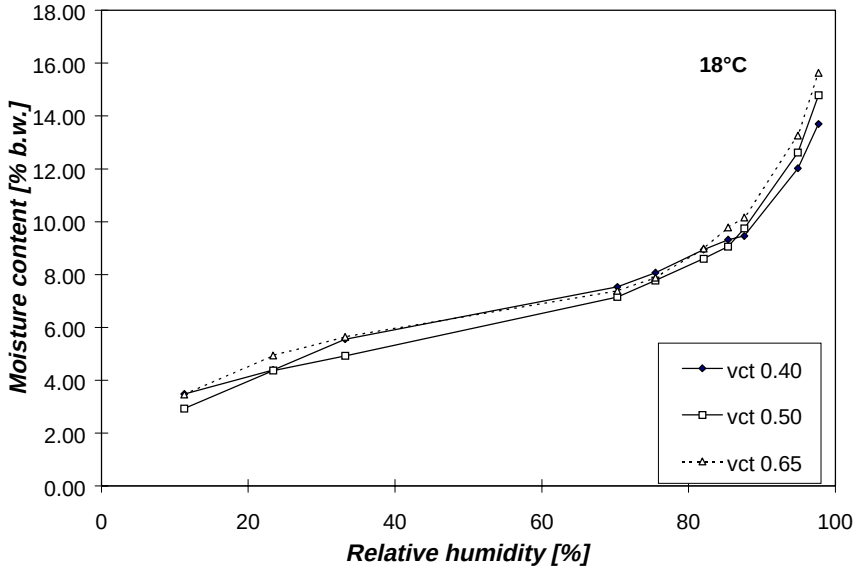

Figure 3.6: Desorption isotherms obtained at 18°C, modified weights (described in the text).

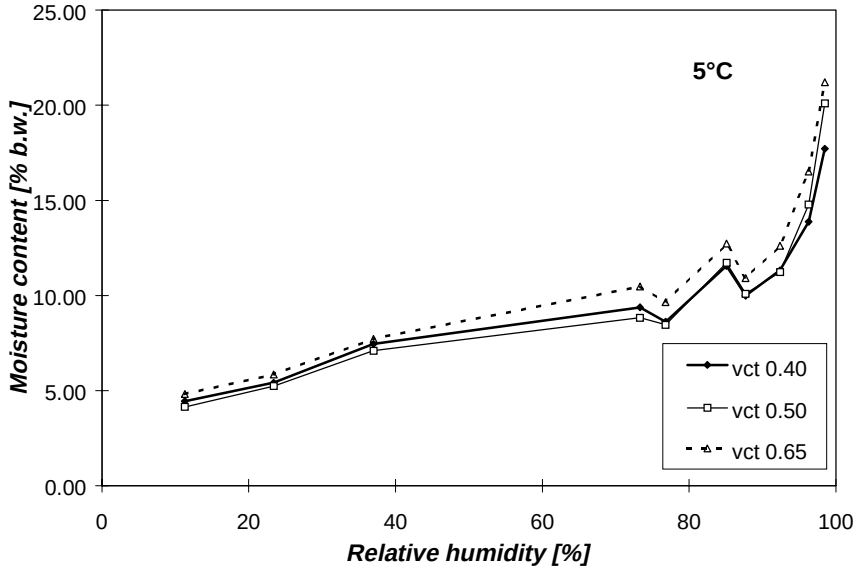

Figure 3.7: Desorption isotherms obtained at 5°C, modified weights (described in the text).

Discussion

From the figures, it seems that the isotherms are almost independent of *w/c* ratio. This is because the dry densities of the *entire specimens* are used for calculating the moisture content. When the moisture content is calculated as the ratio of mass of moisture to mass of cement, curves like those of Nilsson [N 1977] are obtained, which show a clear dependence of moisture content on *w/c* ratio, figure 3.8. It can be seen that at 70-80 % R.H., the moisture contents measured in the present study are even lower than those

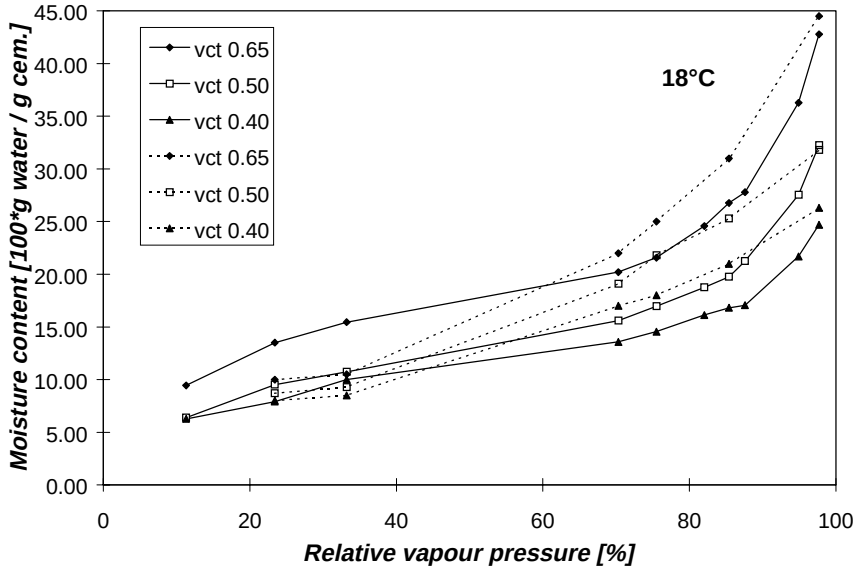

Figure 3.8: Isotherms for micro mortars at +18°C. Moisture content related to mass of cement. Weights modified as described in the text. Dashed lines: Expected values, calculated from [N 1977].

calculated from Nilsson's report. Because Nilsson says this is the level of relative humidity at which drying is the slowest, this may be taken as further evidence that the drying time was long enough to reach equilibrium. It may however be that some carbonation had occurred, despite the use of a CO_2 absorbent. This would serve to reduce the moisture content at any given R.H., figure 2.1.3.

The reason why the moisture content of the 0.65 specimens is higher at low relative humidities than expected (based on Nilsson's report) is unknown.

3.4 Adsorption isotherm and differential enthalpy of adsorption

Method

The apparatus used for this determination is a twin calorimeter developed at the Division of Thermochemistry, Lund University, and the Division of Building Materials, Lund Institute of Technology. It has been described by Wadsö and Wadsö in [W 1996] and [W 1997]. It consists of two calorimetric chambers. In one of these, a vapour evaporates and in the other the vapour is adsorbed by a sample. The two chambers are connected via a tube. As vapour is adsorbed by the sample, the vapour pressure in the sorption chamber will increase to near saturation. The flow rate is governed by diffusion through the tube between the vessels. From the thermal power measured in the vaporisation calorimeter it is possible to evaluate the sorption isotherm, and using information from both calorimeters the heat of sorption may be calculated as a function of equilibrium vapour pressure. The technique involves the assumption that the sorption processes take place at essentially equilibrium conditions. This, Wadsö and Wadsö say, is justified since in most cases the rate of sorption is low during measurement. (Description from [W 1997].) The calorimeter has been used for determining the adsorption isotherm

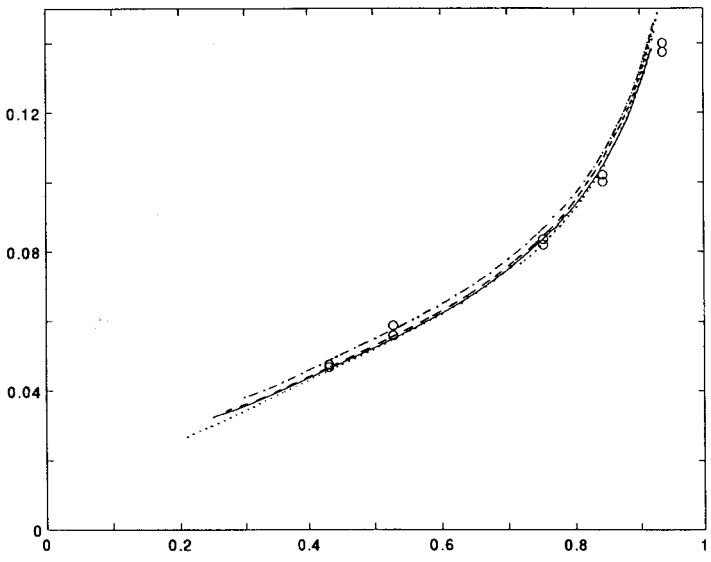

*Fig 3.9: Cotton wool isotherms obtained with the present sorption calorimeter (dashed lines, specimen sizes 19-47 mg) and results from conventional weighing experiments conducted on duplicate samples (*o*),[W 1996].*

of cotton wool and the results agree well with results obtained by other methods, figure 3.9.

The design of the calorimeter necessitates starting the measurement at a low relative humidity and thus only adsorption isotherms may be determined. The sample must be finely divided in order to avoid problems of diffusion within the material pores. The fineness of the present samples is shown in Appendix 3.2. The mean diameter of the grains, as obtained by laser diffraction, is some 50 µm.

Samples

The materials and the crushing technique were described above. The samples were dried in a vacuum at 298 K before testing. In order to avoid carbonation, the samples were kept in nitrogen gas during weighing and insertion into the calorimeter cell.

Results

The results, adsorption isotherms and graphs of differential enthalpy of adsorption versus both moisture content and relative vapour pressure, are shown in figures 3.10-3.18. All measurements were taken at 298.15 K.

The differential enthalpy of adsorption is calculated:

$$\Delta_{ads} H = H_{sorbed} - H_{bulk} = \frac{dQ}{dn} \qquad (3.1)$$

in which *dQ* is the heat released on adsorption of *dn* moles of moisture. This shows how the enthalpy of a system containing a certain amount of water changes when an infinitely small amount of water is added to it. Normally, such changes are assigned to the adsorbate and thus it is said that it is the enthalpy of the water that changes.

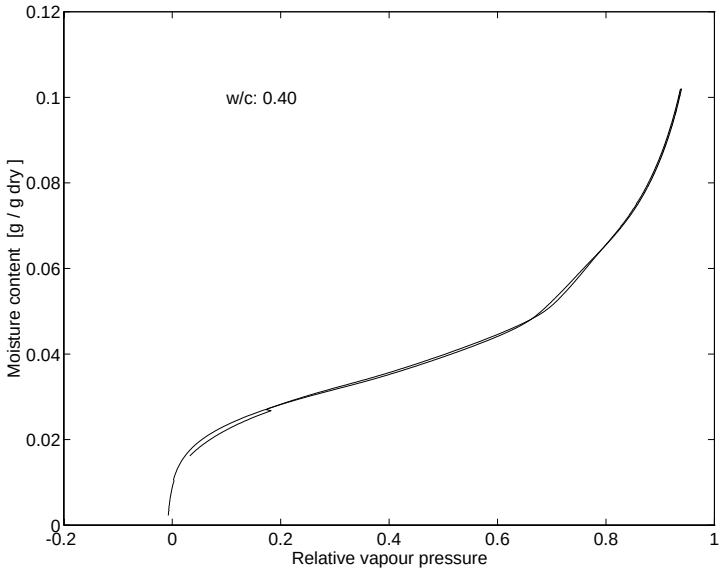

Figure 3.10: Adsorption isotherm for micro mortar of w/c ratio 0.40.

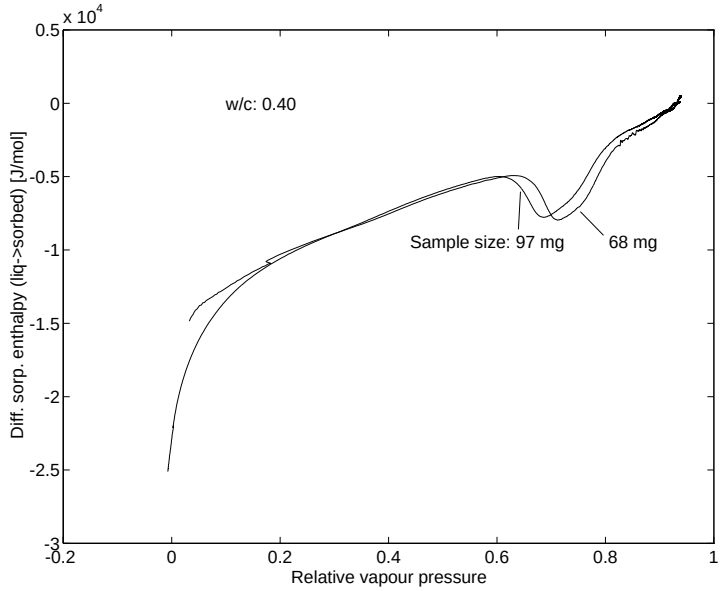

Figure 3.11: Differential sorption enthalpy for micro mortar of w/c ratio 0.40.

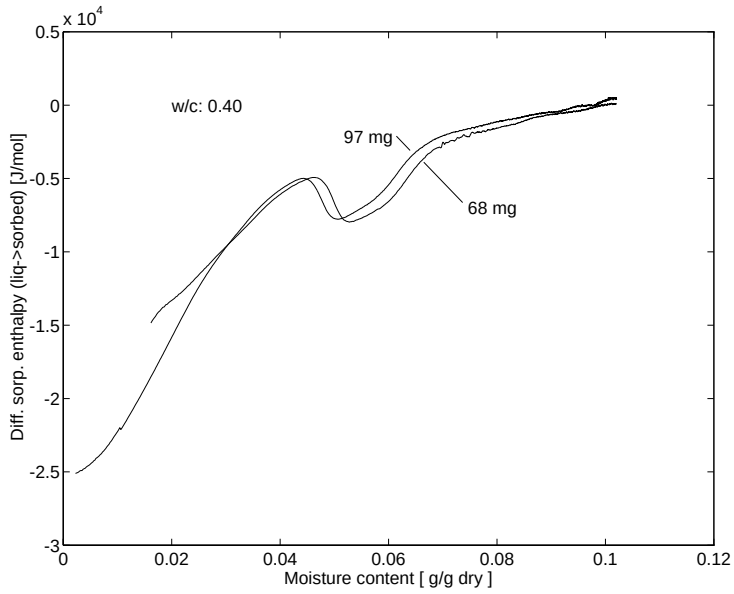

Figure 3.12: Differential sorption entropy for micro mortar of w/c ratio 0.40.

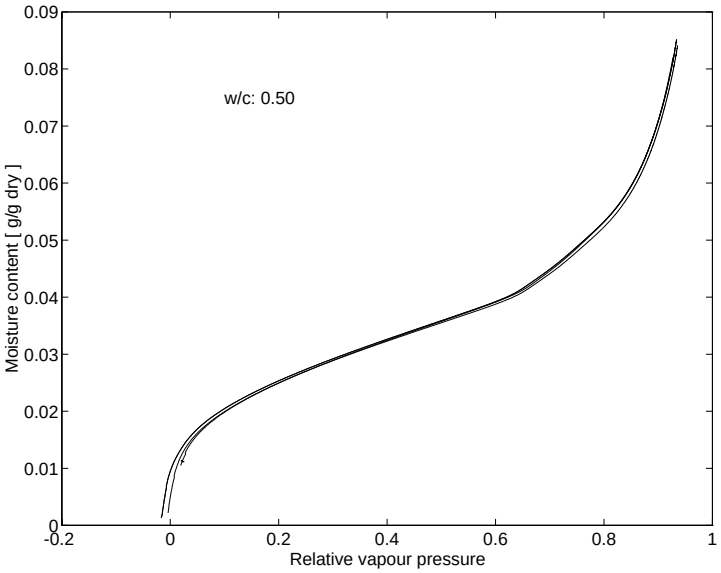

Figure 3.13: Adsorption isotherm for micro mortar of w/c ratio 0.50.

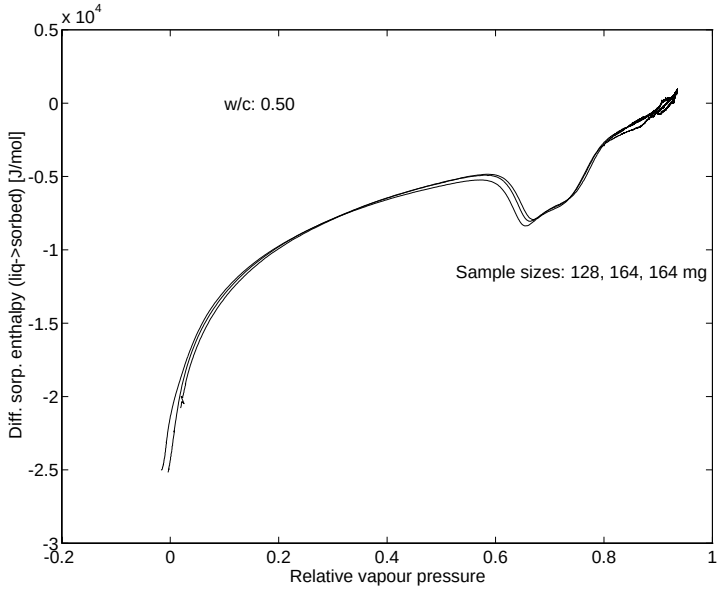

Figure 3.14: Differential sorption enthalpy for micro mortar of w/c ratio 0.50.

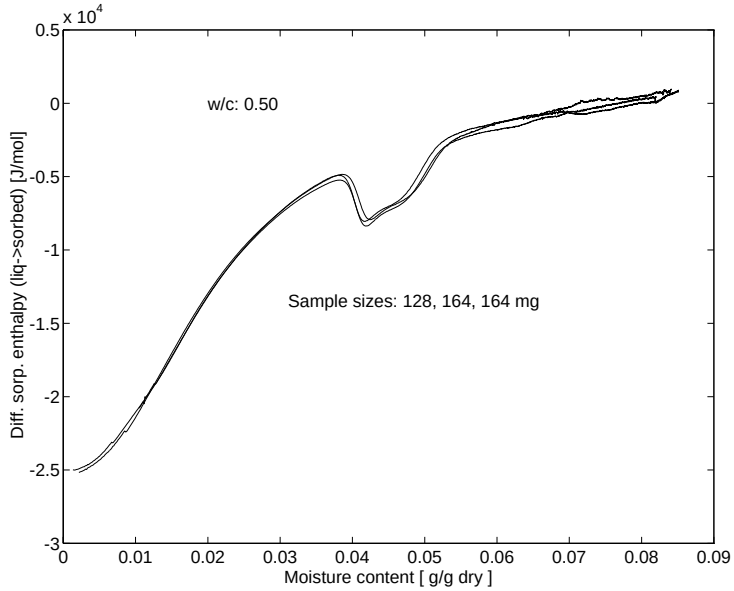

Figure 3.15: Differential sorption entropy for micro mortar of w/c ratio 0.50.

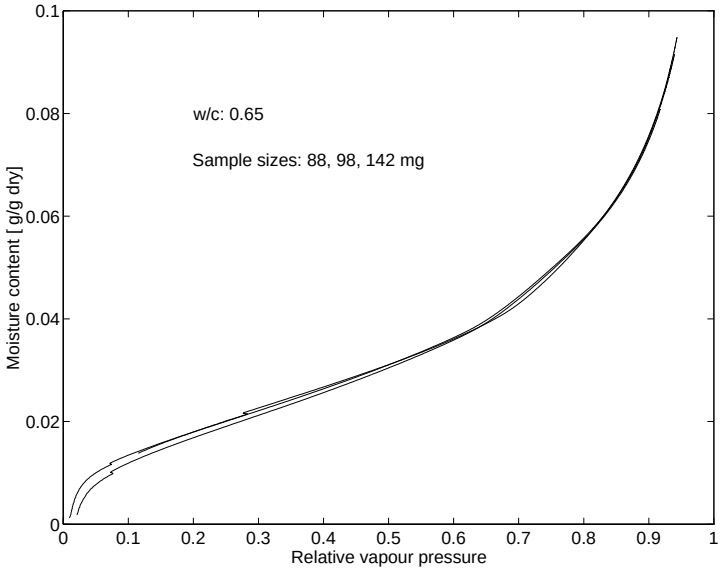

Figure 3.16: Adsorption isotherm for micro mortar of w/c ratio 0.65.

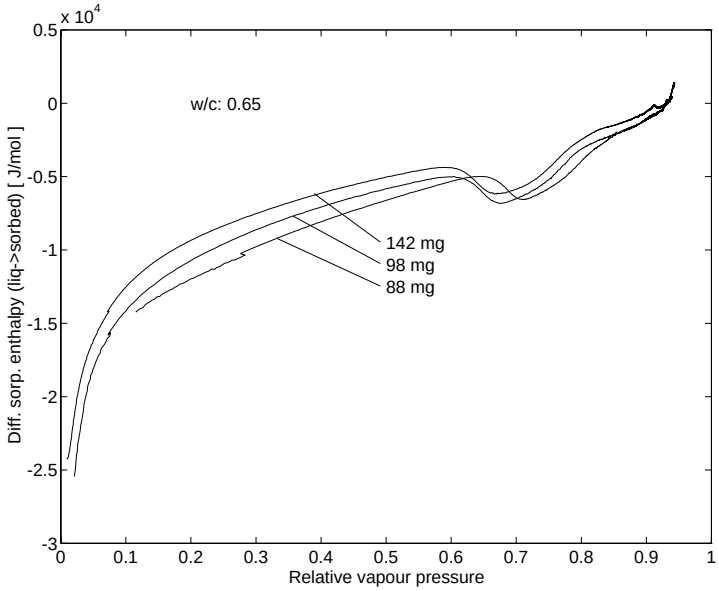

Figure 3.17: Differential sorption enthalpy for micro mortar of w/c ratio 0.65.

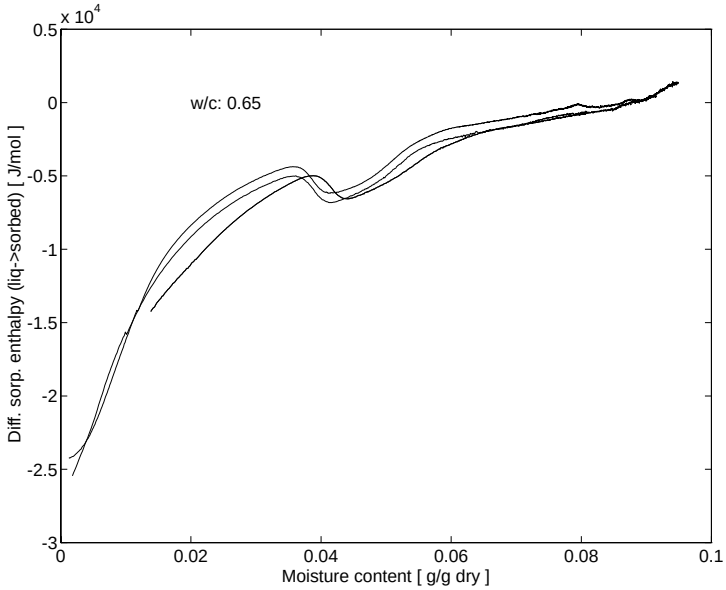

Figure 3.18: Differential sorption entropy for micro mortar of w/c ratio 0.65.

In some figures, it can be seen that the relative vapour pressure initially falls below 0%. This is due to poor initial stability of the thermal powers. For instance, the thermal power in the two calorimeter chambers may be disturbed at the moment water is introduced into the evaporation cell.

The results for differential sorption enthalpy become fuzzier and fuzzier as the vapour pressure saturation approaches saturation. It even seems that the differential adsorption enthalpy approaches positive values as saturation is reached. The fuzziness is because the

thermal powers decrease and tend to zero. Since the enthalpy of sorption is calculated from the ratio between these two, the calculated value becomes very sensitive to small changes in any one of these two values. Furthermore, at this level, any errors in the determination of calibration coefficients become important. The final value certainly must be positive, since the pore solution contains some naturally occurring dissolved ions. The absolute value however is small – tenths of Joules per mole. The final registered values are therefore mainly due to calibration errors.

It is clear from the figures that the adsorption isotherm is insensitive to sample size. This indicates that diffusion inside the grains has not had any appreciable effect on the processes. The reason for the scatter in the plots of differential enthalpy is unknown.

The "dips" occurring in the plots of differential enthalpy of adsorption at approximately 60% R.H. are discussed below.

In figures 3.19-3.21, the adsorption isotherms obtained by the calorimetric method are compared to the desorption isotherms described above. At low levels of relative humidity (R.H.≈0.30), the moisture content during desorption is approximately twice the moisture content during adsorption. This is in accord with the results from Nilsson.

Discussion

The validity of the data obtained may be checked by comparing it with data reported by other researchers. Here, two such comparisons are made: one dealing with the specific area and the other with the enthalpy of adsorption of the water adsorbed in the first monolayer.

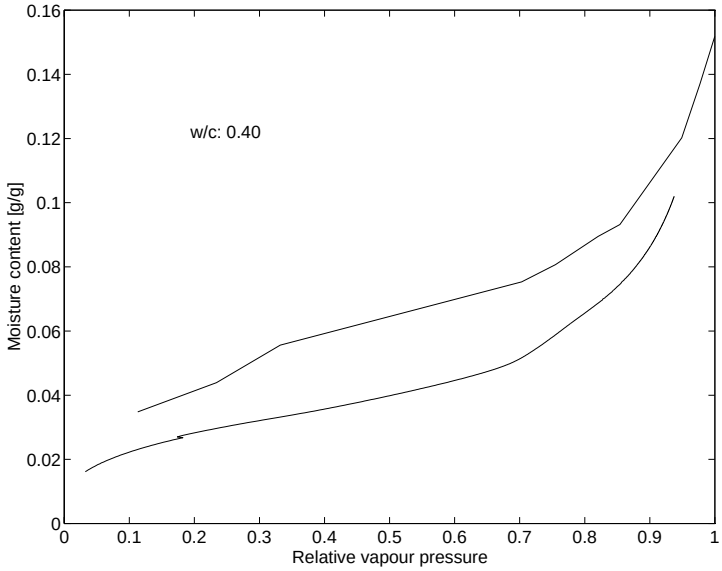

Figure 3.19: Comparison between desorption (upper curves) and adsorption isotherms obtained by different techniques. Micro mortar, w/c ratio 0.40. Moisture content at $(p/p_s)=1$ determined by vacuum saturation.

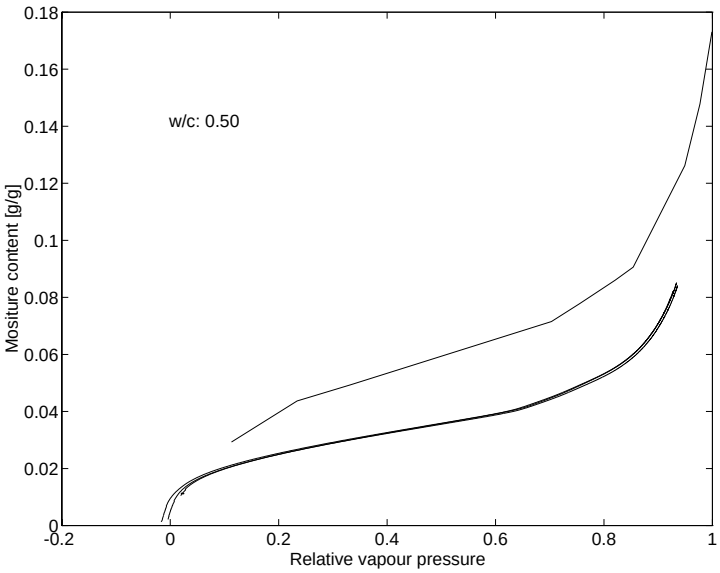

Figure 3.20: Comparison between desorption (upper curves) and adsorption isotherms obtained by different techniques. Micro mortar, w/c ratio 0.50. Moisture content at (p/p_s)=1 determined by vacuum saturation.

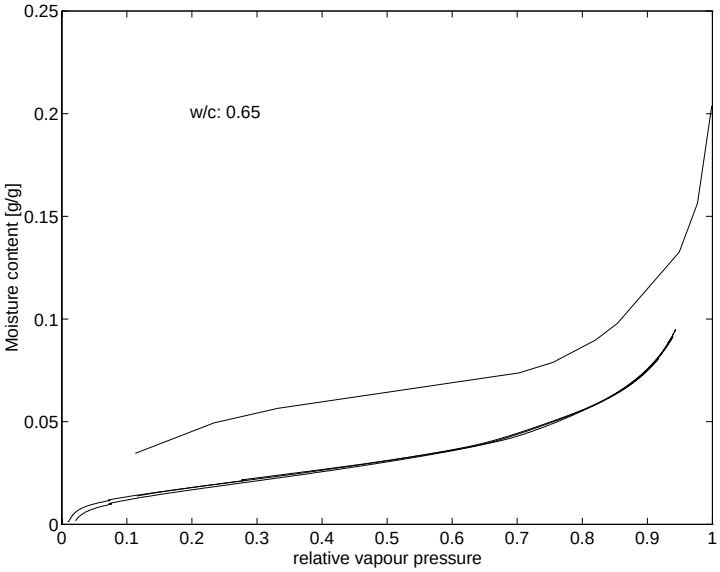

Figure 3.21: Comparison between desorption (upper curves) and adsorption isotherms obtained by different techniques. Micro mortar, w/c ratio 0.65. Moisture content at (p/p_s)=1 determined by vacuum saturation.

Comparison of specific area

The specific surfaces of the materials were determined from a BET plot, table 3.7. The slopes of the factor 1/(Vads(f-1)) vs p/p_s are shown in figure 3.22. It can be seen that the slope varies slightly with the level of relative vapour pressure. Thus, the specific surfaces were calculated by stepwise refinement of the R.H.-interval in which the slopes were

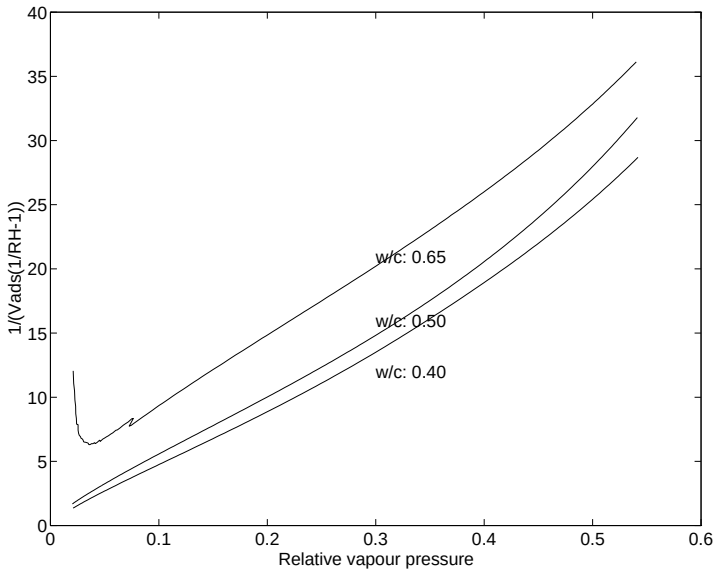

Figure 3.22: BET parameter 1/(V_{ads}(1/ϕ-1)) vs. relative vapour pressure.

determined, so that, finally, the R.H. level corresponding to one monolayer, $R.H._1$, is in the middle of an interval $R.H._1-3<R.H.<R.H._1+3$ (R.H. in %). It was assumed that the area covered by the first monolayer is $3.57 \cdot 10^3$ m²/g of adsorbed water, *i.e.* that the density of the adsorbate is the same as that of bulk water.

It can be further seen that the BET plot is not valid above certain relative vapour pressures. This limit varies with material type and is approximately 0.22, 0.25, and 0.35 for the *w/c* ratios 0.40, 0.50 and 0.65, respectively.

Assuming the specific area is entirely due to the cement paste, the specific area of the hardened paste may be calculated to be and 132, 144, and 142 m²/g for *w/c* 0.40, 0.50 and 0.65, respectively (using the values of table 3.7, the mix proportions (table 3.1), the density data of table 3.3, and the degrees of hydration of table 3.4. Decimals not significant.).

Powers and Brownyard [P 1948] related the specific area to the amount of hydrated water and found:

Table 3.7: Specific surface [m²/g] and relative vapour pressure at which one monolayer is completed.

Material	Sample 1	Sample 2	Sample 3	Mean specific surface m²/g	Monolayer capacity [g/g dry material]
0.40	86.8 m²/g, 11.6%	86.6 m²/g, 13.3%	(not tested)	86.7	0.024
0.50	78.7 m²/g, 13.8%	78.9 m²/g, 13.0%	79.0 m²/g, 14.1% (51%)	78.9	0.022
0.65	62.1 m²/g, 21.3%	63.4 m²/g, 19.6%	61.5 m²/g, 18.3% (52%)	62.3	0.017

$$S = 892 \cdot W_n \qquad (3.2)$$

in which S is the specific area [m²/g dry, hardened paste] and W_n is the amount of non-evaporable water [g/g dry, hardened paste]. (Equation (3.2) is dependent on cement type, but serves as a good comparison.) Based on tables 3.1 and 3.4 (from which the amount of chemically-bound water is obtained), this yields specific areas of 136, 143 and 147 m²/g of pure paste. This good conformity indicates that the adsorption isotherms shown in figures 3.10, 3.13 and 3.16 are correctly determined at least in the area of low relative humidities. Since the processes are slower at higher relative humidities, the requirement of a quasi-equilibrium process is better fulfilled the higher the R.H. and thus it may be assumed that the entire adsorption isotherm is correct.

Comparison of enthalpy of adsorption

The second comparison refers to the average heat of adsorption of the water held in the first monolayer. Powers and Brownyard, who assumed one complete layer was formed before any molecules were held in a second layer, found values of 20 000 – 23 000 J/mole of water [P 1948, p 576]. Ahlgren [A 1972] measured the heat of adsorption for the amount of water corresponding to one monolayer and reported values of approximately 7000±300 J/mole of water adsorbed in the first monolayer. Ahlgren however said the values were "somewhat uncertain". The corresponding values for the present measurements are obtained by integrating the differential enthalpy of adsorption with respect to the amount of adsorbed moisture from the start of sorption (0% R.H.) until one monolayer is completed (R.H. level according to columns 2-4 of table 3.7). On doing this (graphically) in figures 3.11, 3.14 and 3.17 (using the data of table 3.7), values of 18000, 20000 and 21000 J/mole are obtained for *w/c* 0.65, 0.50 and 0.40, respectively. The agreement with the values reported by Powers and Brownyard is fully satisfactory.

Anomalous differential adsorption enthalpy at 60-80% R.H.?

A striking peculiarity in the plots of differential heat of adsorption is the "dip" appearing at a relative vapour pressure of approximately 60% (magnification in figure 3.24A). This may be caused either by re-solution of naturally occurring ions in the pore solution (which were left behind in the preceding drying), or it may be caused by the destruction of interfaces between adsorbed water–vapour as adsorption proceeds, *i.e.* it may reflect capillary condensation.

Such destruction of interfaces is illustrated in figure 3.23. In figure 3.23A, one complete monolayer is adsorbed on the pore walls of a porous material. In figure 3.23B, the second one is completed. It can be seen that the adsorbate - vapour interface has been eliminated over a length dl. In a pore of circular cross section and in which the distance between the firstly adsorbed monolayers is $2r$, the area destroyed is $2\pi r dl$. When this interface destruction occurs for the first time, a large area is destroyed and thus a large amount of heat is liberated. As adsorption proceeds, adsorption takes place on pore walls which are increasingly far apart and thus the area destroyed per mole of added water decreases. The shape of the dip will thus reflect the pore size distribution.

The following example calculation (concerning the *w/c* ratio 0.50 material) illustrates the reasonableness of the assumption that the "dips" are due to the described interface elimination. It is seen in figure 3.24A that the dip appears at 59% relative vapour pressure and that its minimum occurs at 67% relative vapour pressure. In figure 3.24B, it is seen

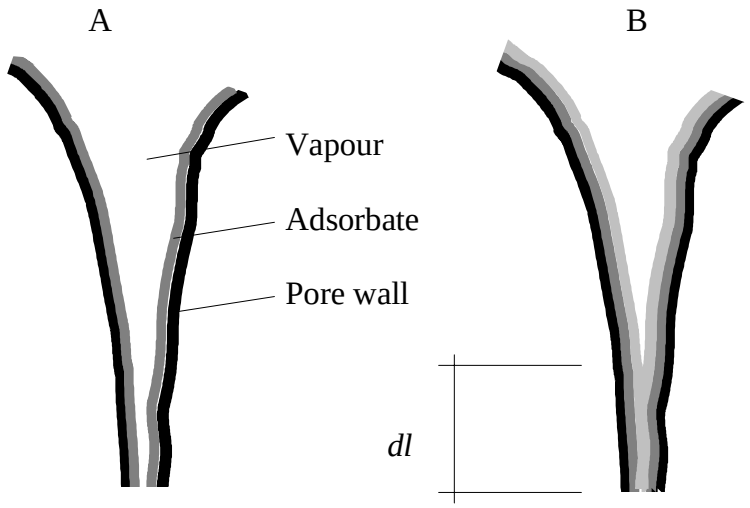

Figure 3.23: Different stages of adsorption. Interface elimination along a distance dl.

that this corresponds to moisture contents of approximately 38.6 and 42.6 mg/g dry sample. This corresponds to 1.76 and 1.93 times the monolayer capacity, respectively, indicating that destruction of interfaces commences even while the second layer of molecules is being built up. During adsorption from 59 to 67% R.H., the area in the dip, as shaded in figure 3.24C, corresponds to 0.38 J/g of sample. This amount thus is released as the moisture content increases from 2.14mmole/g to 2.36 mmole/g, *i.e.* by an amount of 0.22 mmole/g.

It is difficult to estimate how large an area is destroyed by this uptake (depending on the shape of the pores which are filled). Using the entire internal surface of the specimen certainly produces an overestimation of the destroyed area, since the adsorbed amount of water, 0.16 mmole, can destroy interfaces only in pores where capillary condensation is just about to take place. Accordingly, only the area of these pores should be used. For this estimation, a pore model must be used. Assuming the pores are of equal shape, the radii of the pores may be calculated from the Kelvin equation. This has been done in figure 3.25 for the *w/c* = 0.50 material both under the assumption that the pores are cylinders of circular cross section and under the assumption that they are slits of width 2*r*. When summing either of these two curves, it turns out that the ratio of calculated total area to measured internal area is about 2.5 when assuming circular cross sections and about 1.25 for the slit model. Thus, the slit model will be used here. (The areas calculated, summed and shown in figure 3.25. were calculated from the adsorption isotherm obtained at +25° using $V_{m,l}$ =18.068 m^3/mole, $\sigma_{l\text{-}v}$ = 0.07197 J/m^2 and Area = Volume/radius for a slit shaped pore, Area = 2·Volume/radius for a cylindrical pore of circular cross section.)

Powers and Brownyard [P 1948] measured adsorption isotherms after equilibrium had been reached and reported that capillary condensation begins at ϕ = 0.45 (although the amount of adsorbed moisture corresponds only to some 1.5-2 monolayers).

Due to kinetics, it seems reasonable that in the dynamic measurement carried out here, it may be that the capillary condensation is delayed so that it does not show until $\phi > 0.45$

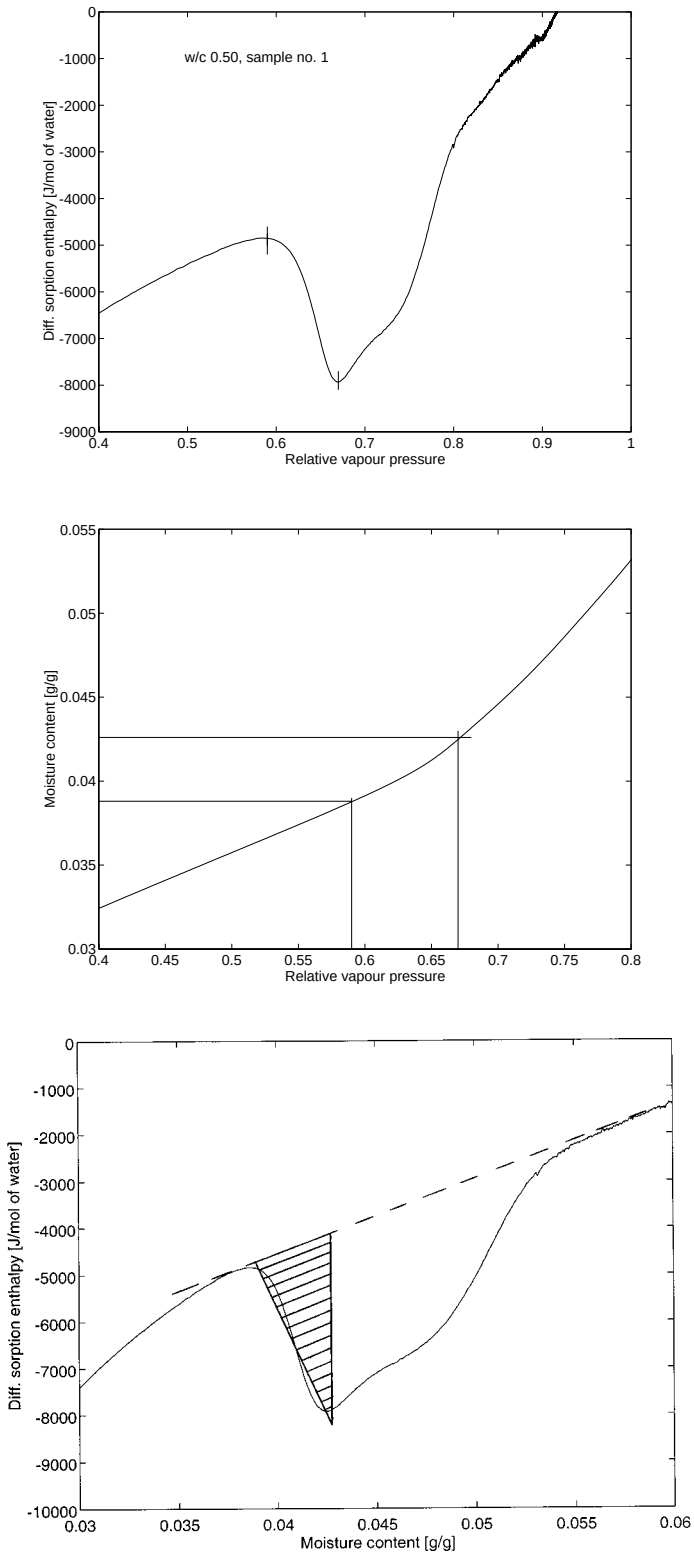

Figure 3.24: A(uppermost): Magnification of ”dip” in figure 3.14. B (middle): Magnification of adsorption isotherm in figure 3.13. C: Illustration for calculation of amount of heat released due to assumed interface elimination.

is reached. As an approximation, we assume that when the dip appears, capillary condensation appears simultaneously in pores of radii corresponding to $\phi > 0.50$ (the beginning of capillary condensation is weakly marked as a deflection point at approximately this R.H. level in figures 3.10, 3.13 and 3.16). According to the slit model, the pore wall area of the pores of radii corresponding to the interval $0.50 \leq \phi \leq 0.67$ is 3.31 m². The surface energy of the destroyed interface is thus 0.38/3.31 = 0.115 J/m². This seems quite reasonable, since the surface energy of an adsorbed layer of water with a thickness corresponding to 1-2 molecular layers reasonably is somewhat higher than that of a bulk water–vapour surface (≈72 mJ/m²). (Had the lower limit $\phi = 0.45$ been used, the area would have been 4.44 m² and the corresponding interface energy 86 mJ/m².)

It can also be seen in the plots of differential sorption enthalpy that the dip vanishes at a level of relative humidity of some 80%. This is probably because the surface area destroyed per mole of added water decreases rapidly with increasing relative humidity and also because the surface energy of the destroyed surface decreases.

Although there are many uncertainties in the above calculations, I believe it is safe to conclude that the dip is attributable to capillary condensation phenomena.

3.5 Calculated differential entropies of adsorption

An entropy change takes place in each amount of water that is adsorbed. The size of the change varies with the relative vapour pressure at which the water is adsorbed. This is the differential adsorption entropy. Together with the differential adsorption enthalpy, it describes the change in Gibbs energy of the water and thus may be used together with the desorption isotherm to calculate the amounts of ice which may form at a certain temperature.

The differential adsorption entropy is calculated:

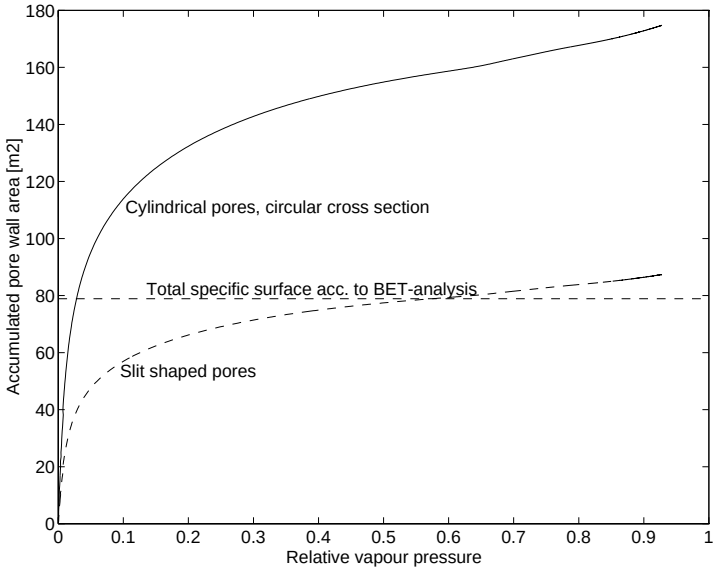

Figure 3.25: Distribution of pore wall area on pores of radius corresponding to the relative vapour pressure according to the Kelvin equation. 1 g of dry material w/c 0.50.

$$\Delta_{ads} S = \frac{\Delta_{ads} H - \Delta_{ads} G}{T} \qquad (3.3)$$

in which $\Delta_{ads}G$ is the change in molar Gibbs energy of the water when going from bulk to the adsorbed phase. This change is determined from the relative vapour pressure:

$$\Delta_{ads} G = G_{sorb} - G_{bulk} = RT \ln(\frac{p}{p_{s,T}}) \qquad (3.4)$$

in which p is the vapour pressure and indices s and T denote saturation and temperature, respectively.

Calculated values of $\Delta_{ads}S$ versus moisture content and versus relative vapour pressure are shown in figures 3.26-28. (The "dips" occurring at 60% R.H. are a direct consequence of the corresponding "dips" in the plots of $\Delta_{ads}H$.)

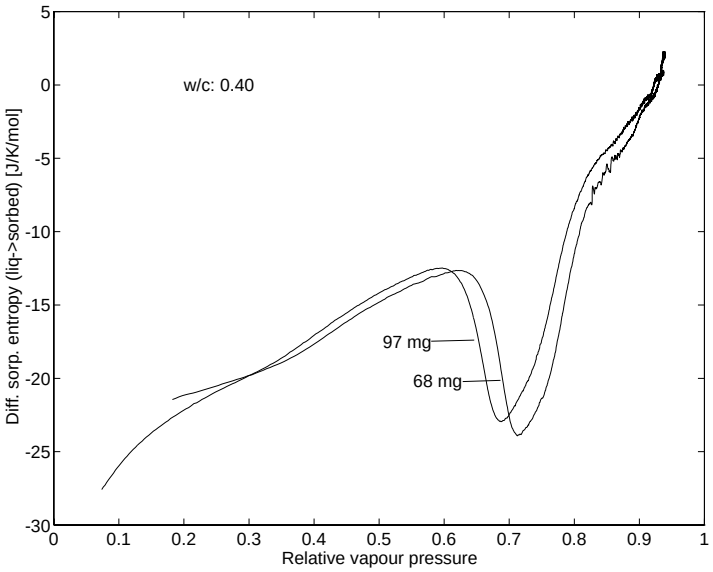

Figure 3.26: Calculated differential sorption entropy for micro mortar of w/c ratio 0.40.

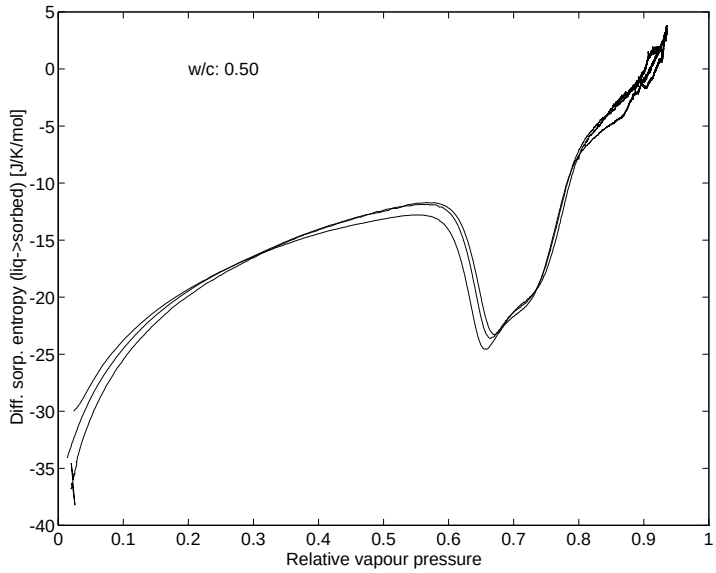

Figure 3.27: Calculated differential sorption entropy for micro mortar of w/c ratio 0.50.

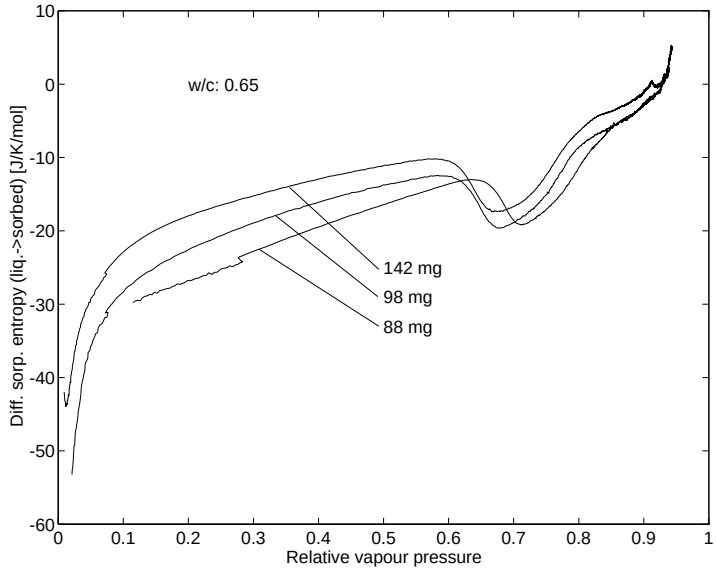

Figure 3.28: Calculated differential sorption entropy for micro mortar of w/c ratio 0.65.

3.6 Calorimetric freezing experiments

Method

These measurements were done using a Calvet-type calorimeter operating between +20 and -60°C (produced by Setaram, France). The samples measured approximately $\phi 12 \cdot 60$ mm. The samples had been dried and vacuum impregnated with water along with the other samples used in this study (*i.e.* on the same occasions). The samples were wrapped in aluminium foil in order to minimise evaporation and to bridge the air gap between the sample and the wall of the calorimeter container. (The specimen container has an inner diameter of 15 mm, leaving a gap of approximately 1-2 mm between the specimen and the container wall, which delays heat transport.)

The samples were weighed before and after the calorimetric experiments. The degree of hydration was determined for each specimen after the freezing test. The values are given in table 3.8. In this table it can be seen that the moisture contents at full saturation differ from those given in table 3.3. This probably reflects the presence of compaction pores, which will hold large amounts of water. The wet densities given in the 5th column of table 3.8 have been corrected for this by assuming the density of the solid phase to be the same in these specimens as in those reported in table 3.3.

Results

The results are shown in figures 3.29, 3.30 and 3.31. These curves have not been corrected for the heat flow from the calorimeter itself. (A small amount of silicon oil was present in the reference cell during the experiments but had been removed before the baseline was registered. This silicon oil had been used in earlier experiments, for which it had been chosen because of its stability over a large temperature range. Since no strange heat flow phenomena were observed in previous experiments on the silicon oil itself, it is believed that the presence of the silicon oil during the experiments reported here has had only negligible effect.)

All curves show that final melting takes place at approximately +2°C to +4°C. Because of the amount of naturally occurring dissolved ions in the pore solution, one would expect final melting to take place at approximately -1°C. This error is due to the time lag between temperature registrations and heat flux registrations, which are attributable to the design of the calorimeter and cannot be completely avoided. It must therefore be understood that the measured heat flow rates should be displaced towards lower temperatures by some 3-5°C.

The error might be reduced by using the Tian equation. Since the Tian equation is intended for a non-scanning mode of calorimeter operation, however, it cannot compensate for the time lag caused by the scanning mode used here. In the present measurements, the Tian equation lowers the final melting point by no more than approximately 0.5°C. Accordingly, it has not been used here.

Discussion

It can be seen that super-cooling to approximately -8°C occurs in all specimens tested. It can also be seen that the peak occurring at -23°C in figure 2.3.3 is absent in these figures. At -42°C though, there are peaks similar to those reported by Bager and Sellevold [B1 1986], fig 2.3.3. This peak is absent during thawing in all figures

Table 3.8: Data for specimens used in calorimetric freezing experiments. (Wet weights were taken immediately before and after the calorimeter test.)

Material	Wet weight (before/after) [g]	Dry weight [g] (105°C, 2 days)	Moisture cont. [% b.w.]	Adj. Wet density [kg/m^3]	Degree of hydration
w/c 0.40-1	14.454 / 14.449	12.439	16.20	2128	0.775
w/c 0.50-1	15.088 / 15.083	12.690	18.90	2078	0.750
w/c 0.65-2	18.464 / 18.458	15.240	21.15	2038	0.807

presented here. This hysteresis is probably the result of local super-cooling. (If it were due to the effect of the different shapes of the freezing/melting ice body as described by Setzer [S 1993], water that freezes at -42°C would melt at -24°C (eq. (2.4.41) and, assuming the hydraulic radii differ by a factor of 2, there would thus be a peak in the melting curve at this temperature. For a pore to cause a freezing point depression of 42°C, its radius is calculated to be less than 1 nm (eq. (2.4.41)). The use of ordinary thermodynamics as described in chapter 2.4 is probably insufficient for a precise description of the thermodynamic state of water or ice contained in such a pore.)

The absence of the peak during freezing at -23°C is probably due to these specimens having been dried at 105°C for two days, a process which may have caused opening of the entrances into pores in which water may remain super-cooled unless nucleated by seeding from ice in nearby pores. (Such an effect on the pore structure was discussed both in [B 1980] and [B2 1986].) The final freezing at -42°C and the absence of any peak at this temperature during melting shows that the drying process does not lead to changes in the pore structure nor to corresponding ice formation processes that completely eliminate local super-cooling.

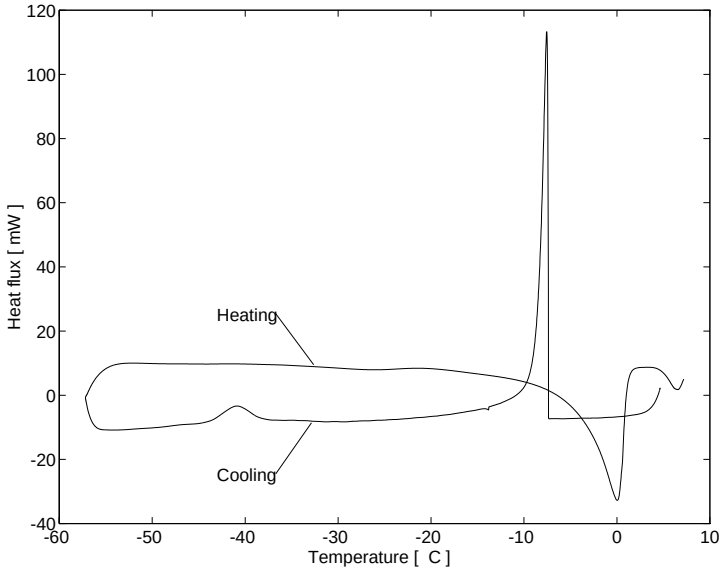

Figure 3.29: Entire freezing and melting event, w/c 0.40. Large super-cooling and typical peak at -40°C during freezing.

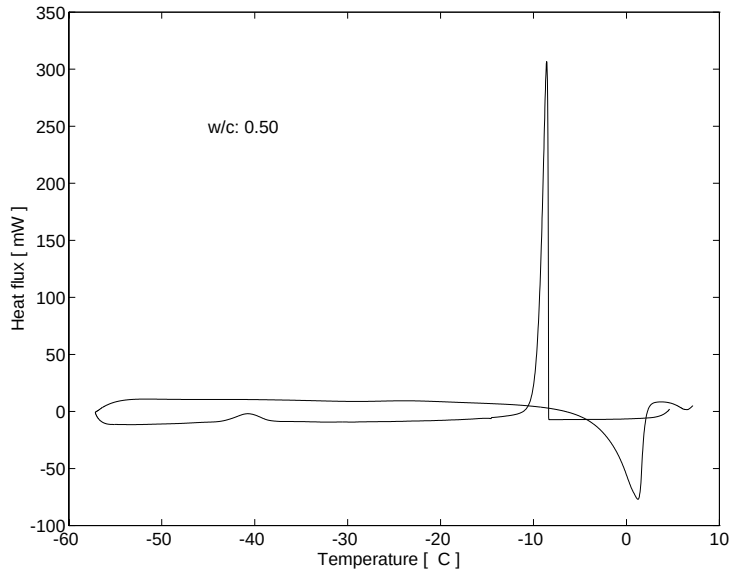

Figure 3.30: Entire freezing and melting event, w/c 0.50. Large super-cooling and freezing peak at -40°C during freeing.

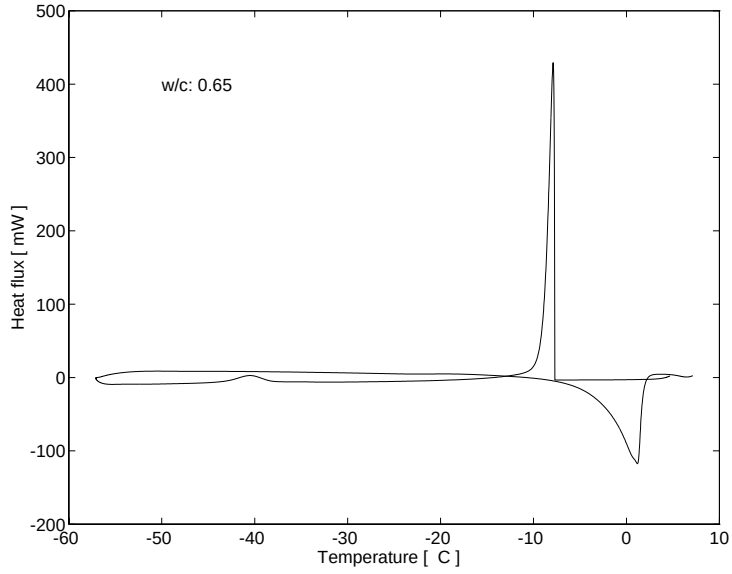

Figure 3.31: Entire freezing and melting curve, w/c 0.65. Large super-cooling and freezing peak at -40°C during freezing.

3.7 Calculation of amount of ice formed at different temperatures from the enthalpies and entropies of adsorption

Purpose of the calculation

With the data now at hand, it should be possible to calculate the level of free energy of the pore liquid as a function of temperature and moisture content. By comparing this to the free energy of ice, the amount of ice formed at any given temperature and the heat released on freezing may be calculated. Furthermore, the output of the calculation may provide some information concerning the ice formation process. This, however, requires some assumptions as to the state of the ice which forms. Assuming the properties of the moisture are well described by our data, the result of this calculation will provide insights into the true state of the ice formed.

In this section, the calculation is carried out under the assumptions that:

1. the ice which forms in the pore system has bulk ice properties (thus surface energy effects and pressure effects are assumed to be negligible),
2. the sorption enthalpy and sorption entropy are temperature independent,
3. the free energy of water in one pore is not affected by freezing of any other water volumes (*e.g.* by hydraulic pressures occurring as a result of ice formation. The possible effects resulting from changes in the pore water pressure are included in the $\Delta_{ads}H$ values), and
4. redistribution of dissolved matter need not be taken into account.

The assumption that the surface energy of the ice is negligible implies that ice either forms in large cavities and/or outside the specimen and/or that its interaction with the pore walls (or the moisture adsorbed on the pore walls) is negligible. If ice *does* in fact spread into the pores and interact significantly with the pore walls (or the adsorbed moisture), the surface energy changes will not be as large as if water is drained out of the pores and replaced with air. If this is what actually does occur, then ice will form at somewhat higher temperatures than those calculated from the assumptions made above and the heat released will probably be higher, since the interface energy of the new ice - pore wall interface will probably be less than that of a pore wall - air interface (see section 2.4).

Calculation

Bulk ice and bulk water are in equilibrium at T = 273.15 K and P = 101325 Pa. If either the temperature or the pressure changes ($dT = T\text{-}T_0$, $dP = P\text{-}P_0$, where T_0 and P_0 are 273.15K and 101325 Pa, respectively), the change in free energy of each phase is given by:

$$dG_s = V_s dP_s - S_s dT_s \qquad (3.5a)$$

$$dG_l = V_l dP_l - S_l dT_l \qquad (3.5b)$$

For water adsorbed in a porous adsorbent, the adsorption forces also act to lower the free energy of the water. Thus the free energy G_{sorb} of the adsorbed moisture is:

$$G_{sorb} = G_{0,l} + \Delta_{ads} G \qquad (3.6)$$

in which $G_{0,l}$ is the free energy of the bulk liquid in the reference state. By assuming the adsorption enthalpy and the adsorption entropy to be temperature independent, the term $\Delta_{ads}G$ as a function of the water content is obtained from the results above as:

$$\Delta_{ads} G(u) = \Delta_{ads} H(u) - T\Delta_{ads} S(u) \qquad (3.7)$$

in which u denotes water content [g/g]. Since the effects of pressure changes in the water are assumed to be incorporated in $\Delta_{ads}H$ (from above), the free energy of the adsorbed water as a function of temperature and moisture content is thus obtained from:

$$G_{sorb}(T,u) = G_{0,l} - \int_{T_0}^{T} S_l(T)dT - T\Delta_{ads} S(u) + \Delta_{ads} H(u) \qquad (3.8)$$

The terms $\Delta_{ads}H(u)$ and $\Delta_{ads}S(u)$ are obtained from the measurements taken at 298.15 K. By relating the differential sorption enthalpy to the relative vapour pressure (not to moisture content), the equations describing this relation become almost independent of material quality: For relative humidities in excess of 0.8, this may be done with a straight line as shown for *w/c* 0.50 in figure 3.32. In fitting this curve, it was assumed that the differential sorption enthalpy is 0 at 100% relative vapour pressure and also that the dip is a superimposed "peak" on a true curve describing the adsorption phenomena. However, a cautious approach should be taken and the straight lines cannot uncritically be used for relative vapour pressures below 0.8. For calculations on ice formation at temperatures above -20°C, this is good enough, since this is the temperature at which the vapour pressure of ice is approximately 80% of that of liquid water. The following fitted equations are obtained:

$$w/c\ 0.40: \quad \Delta_{ads} H = 12100(\phi - 1) \qquad (3.9a)$$
$$w/c\ 0.50: \quad \Delta_{ads} H = 10800(\phi - 1) \qquad (3.9b)$$
$$w/c\ 0.65: \quad \Delta_{ads} H = 11800(\phi - 1) \qquad (3.9c)$$

Considering the uncertainties in the measured values and the curve fit, we may set:

$$\Delta_{ads} H = 11600(\phi - 1) \qquad (3.9)$$

independent of material quality. The sorption entropy is then calculated from ϕ and $\Delta_{ads}H$ according to equations (3.2) and (3.3).

In the present calculation the relation to moisture content is achieved by feeding the computer with values from the desorption isotherms (*i.e.* the relation of u to ϕ).
Since the bulk water entropy is temperature dependent, the terms $-SdT$ in equation (3.5) must be integrated over the temperature change $\Delta T = T_f - T_0$. It was shown in chapter 2.4 that the solution to the integration of the term $-S(T)dT$ over the temperature interval ΔT is:

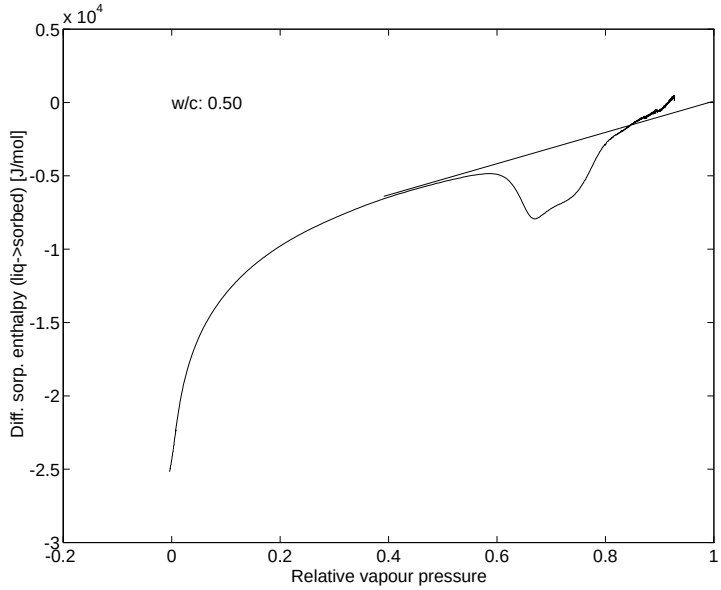

Figure 3.32: Straight line fit for eq. (3.9)

$$\int_{T_i}^{T_f} S(T)dT = S(T_i)(T_f - T_i) + \frac{A}{2}\left(T_f - T_i\right)^2 + B\left\{\frac{T_f}{T_i}\left(\ln(\frac{T_f}{T_i}) - 1\right) + 1\right\} \qquad (2.4.32)$$

(The constants *A* and *B* for ice and water were given in chapters 2.2 and 2.3.)

The free energy of bulk ice is calculated from equation (3.5a), using $dP = 0$ and equation (2.4.32) for the temperature dependent changes.

The desorption isotherm is discreted into steps of 1% R.H (solid line in figure 3.34). The amount of water in each such interval of relative humidity is calculated and its free energy as a function of temperature is determined from the equations given above. The freezing temperature of each such water volume is determined by numerically finding the temperature at which the free energy of the adsorbed water is equal to that of the ice.

Provided that the process is reversible, the heat of fusion is calculated from the enthalpy change as

$$\Delta_{fus}H = T\left(S_l(T) - S_s(T)\right) \qquad (3.10)$$

in which $S_l(T) = S_{l,bulk}(T) + \Delta_{ads}S$. The calculated heat of fusion is shown in figure 3.33. Because of the way the equation for the sorption enthalpy was derived (eq (3.9), limited to 80%<R.H.<100%), it most probably is not valid at temperatures lower than 253K (at which temperature the vapour pressure of ice is approximately 80% of that of super cooled water).

With the described calculations, it is possible to calculate the amount of ice which forms at a given temperature and how much heat is released when this amount of ice forms. The measured heat flow rates cannot however be used to calculate how much ice

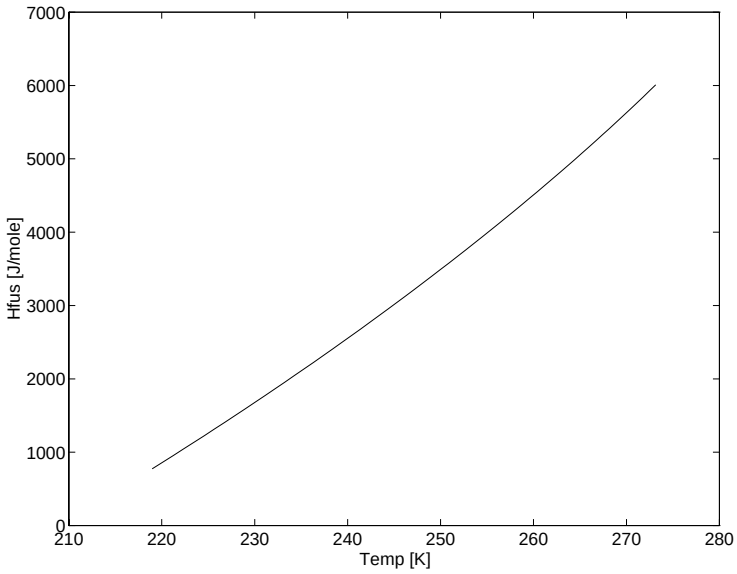

Figure 3.33: Heat of fusion for pore water as calculated from eq (3.9). See text for remarks on possible errors.

actually does form, since the true heat of fusion is not known. Therefore, the calculated extent of ice formation was used to simulate the heat flow rate from a sample of the same size as those used in the tests. Only the heat flow rate measured during melting was used, since the super-cooling phenomena which occur during cooling could not be simulated. The desorption isotherm was used to relate water content to R.H.

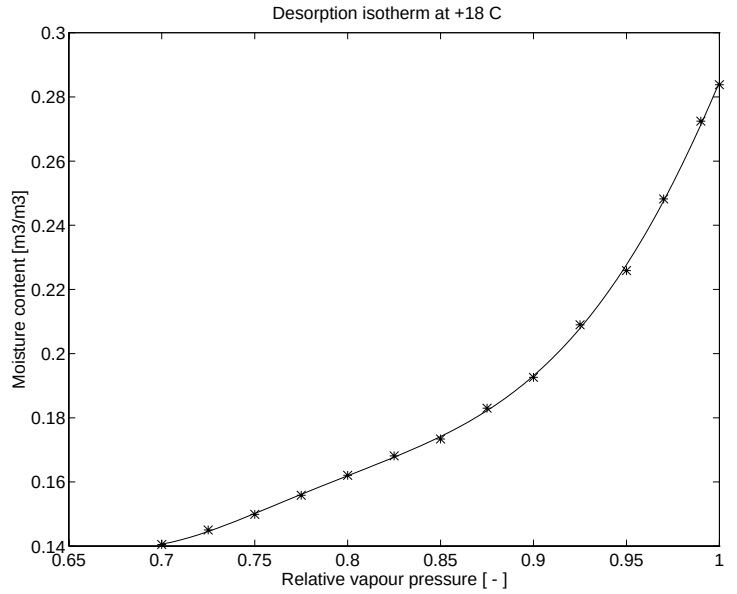

*Figure 3.34: Desorption isotherm used for calculation of amount of freezable water in micro mortar of w/c ratio 0.40. *: Interpolated values from figure 3.6, – : Finer interpolation used for the calculation. Desorption data at 87.6%/18°C omitted due to experimental uncertainties. In the calculations, the moisture content at 100% R.H. was set to 296.7 kg/m3 (described in text).*

Comparing tables 3.8 and 3.3, it can be seen that the moisture content of the samples used for freezing tests was higher than the maximum moisture content of the samples used for determining desorption isotherms. This may be due to the presence of water in large (compaction?) pores in the freeze test samples or to the presence of some water on their outer surfaces, although the latter seems far-fetched. Such water will be freezable almost without any freezing point depression and thus will affect the calculated heat flow rates at temperatures close to 0°C. These anomalies were dealt with by simply increasing the maximum water content in the desorption isotherms used for the ice formation calculation to that corresponding to the moisture content measured in the actual samples. For samples of *w/c* ratio 0.40 this brings about an increase from 283.8 kg/m^3 to 296.7 kg/m^3, for those of *w/c* ratio 0.50 an increase from 310.7 kg/m^3 to 330.3 kg/m^3 and for specimens of *w/c* ratio 0.65 it brings about an increase from 347.1 kg/m^3 to 355.9 kg/m^3. The wet densities were correspondingly changed (as shown in table 3.8).

The effects caused by the small differences in degree of hydration (table 3.4 and table 3.8) were not taken into consideration. The degree of hydration of the 0.40 sample is higher than that of the specimens used for determining the desorption isotherm. This means the material tested in the freezing experiments is more finely porous than the material used for determining the desorption isotherm. Thus there will be less freezable water at high temperatures and more freezable water at low temperatures than what could be expected from the desorption isotherm. Similarly, the degree of hydration of the 0.50 sample is less than that of the samples used for determining the desorption isotherm. Thus, this sample will show more freezable water at high temperatures and less freezable water at low temperatures than what might be expected from the desorption isotherm. The effects, though, are believed to be small.

Results

The calculated and measured heat flow rates are shown in figures 3.35-3.37. Because the freezing curve is distorted by super-cooling phenomena, the measured curves, to which the calculated heat flow rates are compared, are the melting curves. The measured and the calculated curves were fitted to each other at temperatures above ±0°C, because this is where we know the specimen composition and where we also know that no ice formation is taking place. (This fit was necessary because the heat capacity of the dry micro mortar was not known.)

The comparisons between calculated and measured heat flow rates are complicated because of the time lag between the registered (block) temperature and the heat flow rate from the sample in the low temperature calorimeter. As described above, there is no way to fully adjust for this delay. The measured heat flow rate should thus be displaced towards lower temperatures so that the final registered melting point becomes equal to the true final melting point, which is probably approximately -1°C due to dissolved ions. Because the registered final melting point varies between approximately +2° and +4°C, the heat flow signal should be displaced approximately 3–5°C towards lower temperatures. It can be seen that such a displacement would make all measured heat flows higher than the calculated ones at any given temperature.

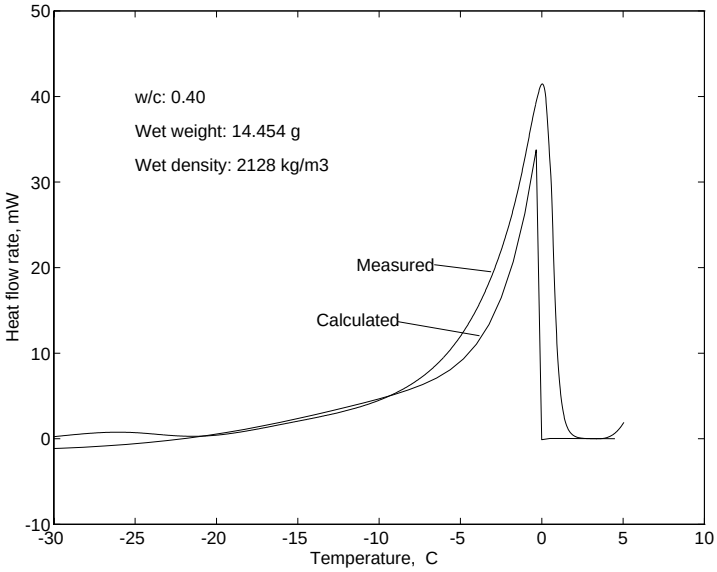

Figure 3.35: Measured and calculated heat flow rates vs. temperature during melting of a w/c ratio 0.40 specimen at a heating rate of 3 K/h.

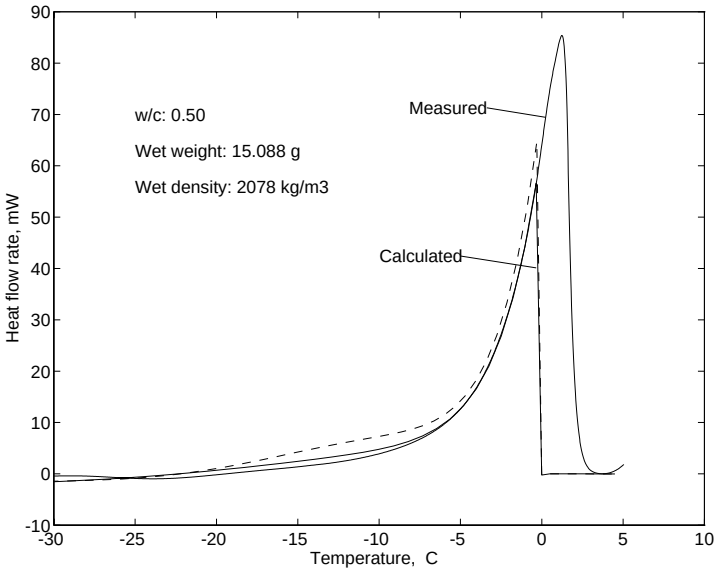

Figure 3.36: Measured and calculated heat flow rates vs. temperature during melting of a w/c ratio 0.50 specimen at a heating rate of 3 K/h. Dashed line: Calculated heat flow rate obtained by setting C=6000 in eq. (3.9).

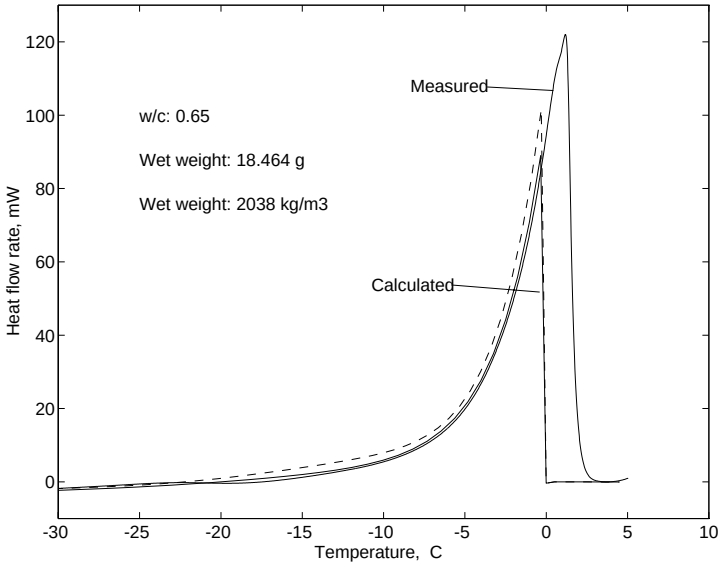

Figure 3.37: Measured and calculated heat flow rates vs. temperature during melting of a w/c ratio 0.65 specimen at a heating rate of 3 K/h. Dashed line: Calculated heat flow rate obtained by setting C=6000 in eq. (3.9).

The fraction of ice (in moles) to initial water content (in moles) as a function of temperature is shown in figure 3.38 for the material of *w/c* ratio 0.50. Le Sage de Fontenay and Sellevold [S 1980] reported corresponding fractions of frozen water of 20% for never-dried paste of *w/c* ratio 0.40 and 57 % for never-dried paste of *w/c* ratio 0.70 (at -55°C). Later, Bager and Sellevold [B2 1986] reported that drying to a relative humidity of 10-20% would increase the fraction of ice formed by approximately 50% for a Portland cement paste of *w/c* ratio 0.60. Based on this, and because the materials used here had been dried at 105°C for two days, the results shown in figure 3.38 were expected to be approximately 70% at -50°C instead of the 45% shown.

Discussion

The measured maximum heat flows exceed the calculated maximum heat flows by 24%, 52% and 37% for the materials of *w/c* ratios 0.40, 0.50 and 0.65, respectively. By displacing the measured curves towards lower temperatures, as described above, it can be seen that these relative errors increase with decreasing temperature.

There are three conceivable reasons for the occurrence of these errors:

- it may be incorrect to describe the free energy of the pore liquid using equation (3.9), or
- some of the assumptions on which the calculation is based may be wrong, or
- there may be something wrong with the materials.

First, it may be that the differential enthalpy and entropy as described by eq.(3.9) cannot be used, *i.e.* the thermodynamic state of the water, as a function of moisture content and temperature, may not be as well-known as is generally presumed. I therefore tested how the calculated heat flow is affected by the coefficient *C* in equation (3.9). In

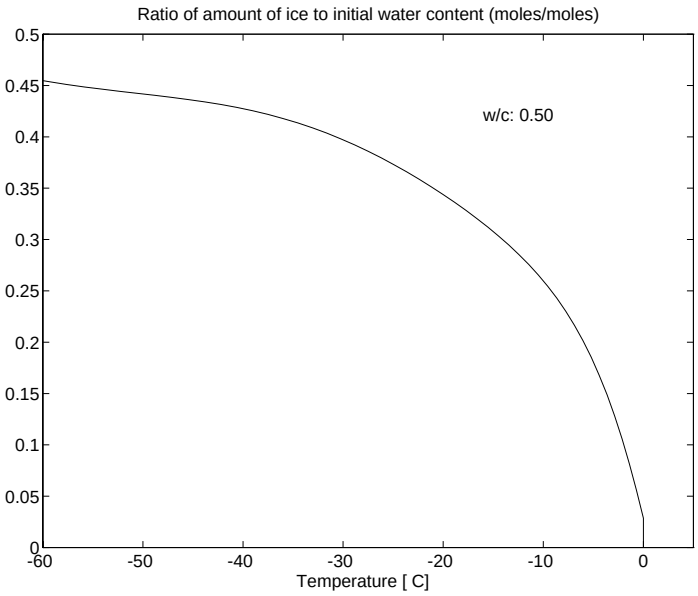

Figure 3.38: Relative amount of ice (moles) to initial water content (moles) for the w/c ratio 0.50 mortar.

the above calculations, the value for *C* was 11600. In the test calculation an arbitrarily chosen value of 6000 was used, *i.e. C* is almost halved. This change makes the calculated heat flow become larger (dashed lines in figures 3.36 and 3.37). However, it can be seen in these figures that this large change in the coefficient changes the calculated heat flow by only a small fraction and thus the disagreement between measured and calculated heat flows can not be explained by an error in the coefficient *C*. On decreasing *C* further, so that the calculated heat flow rates become correct close to 0°C, those calculated for lower temperatures become negative, which is definitely unrealistic. (A larger value of *C* results in a decreased calculated heat flow.) The conclusion is that the discrepancy between calculated and measured heat flows is not due to an erroneously chosen value for the coefficient *C*.

It might be that one or more of the assumptions on which the calculation is based may be wrong. The assumptions were:

1. The ice which forms in the pore system has bulk ice properties (thus surface energy effects and pressure effects are assumed to be negligible).
2. The sorption enthalpy and sorption entropy are temperature independent.
3. The free energy of water in one pore is not affected by freezing of any other water volumes (*e.g.* by hydraulic pressures occurring as a result of ice formation. The possible effects resulting from changes in the pore water pressure are included in the $\Delta_{ads}H$ values).
4. Redistribution of dissolved matter need not be taken into account.

Because any redistribution of dissolved matter occurring during freezing should also occur during drying at room temperature, assumption no. 4 should be correct.

Assumption no. 3: Since the measured heat flow rates are higher than the calculated ones, either the enthalpy of the ice is lower than assumed or that of the water is higher than assumed. However, if the enthalpy of the water is increased due to ice formation,

which was not taken into account in the calculation, it would have to be due to the preceding ice formation and, thus, the net effect will be zero. Such pressure changes therefore cannot explain the discrepancy between measured and calculated heat flow rates. Instead, it might be that the enthalpy of the ice is less than assumed. This in turn may be due to interface energy effects and is commented on further below.

Assumption no.2 may be questioned on basis of the studies of heat capacity of adsorbed water which were described in chapter 2.2. Several researchers have found that the heat capacity of adsorbed water is higher than that of bulk water. This means the entropy of the adsorbed water will change more with temperature than would be calculated from eq. (2.4.32) using the values for *A* and *B* given in chapter 2.2. Thus the sorption entropy will increase with decreasing temperature. This will cause phase transitions to be displaced towards lower temperatures, a result which would make the calculated heat flows even more erroneous.

Assumption no.1: Raising the calculated heat flow rates to the level of those measured requires more energy to be released from the system when ice forms than would follow from the above assumptions. This would be the case if either the ice which forms were under reduced pressure (as compared to bulk ice) or if the ice were to spread into the small pores to reduce the interface free energy which would result if the entire freezing process occurred as a drying out process, *i.e.* effectively emptying the pores (as described in chapter 2.5). Since the pressure on the ice cannot be reduced more than 100 kPa, which would change its enthalpy by some 2 J/mole, this is probably not the reason why the measured heat flow rates are higher than those calculated.

If it is assumed that the enthalpy change measured during adsorption is entirely due to interface energy changes, the increase in free energy of a porous system caused by the removal of water will be approximately 0.075 J per m² of drained pore wall area. If it is assumed that the enthalpy change measured during adsorption is entirely due to this interface energy change and if it is assumed that, during freezing, ice replaces lost water (rather than accumulating in large cavities), then the change in interface free energy will be some 0.042 J/m², rather than the 0.075 J/m² mentioned above (see chapter 2 for values on interface free energy changes). Only these 0.042 J/m² will be lost to the surroundings and registered in the calorimeter, *i.e.* only approximately half the interface energy change occurring during drying. Thus, larger amounts of heat will be released from the system during freezing. This change also causes displacement of ice formation towards higher temperatures. It also means the error will be larger (per mole of water) the smaller the pore in which freezing takes place, thus explaining to some extent the above described finding that the discrepancy between measured and calculated heat flows increases with decreasing temperature.

However, this change may be conveniently taken into the calculations by reducing the coefficient *C* in eq. (3.9) to approximately half the value used above. In fact, this modification was studied above and was found not to be large enough to explain the discrepancy between measured and calculated heat flow rates. This discrepancy thus cannot be due solely to a different pattern of ice spreading.

The discrepancy might be due to material properties. Although the freezing calorimeter specimens were solid cylinders which had been exposed to the atmosphere only during drying at 105°C, the specimens used for determining the desorption isotherms were exposed to air for some 90 days and, although the content of CO_2 in that air had been reduced, it was not completely removed. This may have caused some carbonation of the grains. In this kind of material, carbonation will cause a denser pore

structure, and the desorption isotherm will be displaced towards lower moisture contents at constant levels of relative humidity (figure 2.1.4). In fact, it was seen in figure 3.8 that the desorption isotherms measured for these materials predict less moisture content as compared to the isotherms reported by Nilsson, a fact which indicates that significant carbonation might have occurred. The consequence of this is that the amount of freezable water at a given temperature is underestimated in the calculations and this in turn results in too low calculated heat flow rates, as compared to the measured ones.

In figure 3.8, it can be seen, in the vicinity of 90% R.H., that the isotherms reported by Nilsson predict moisture contents approximately 15-20% higher than those measured here. The discrepancies between the calculated and the measured heat flows are larger than this and thus cannot be explained as being due solely to this carbonation effect, except possibly for the *w/c* ratio 0.40 quality. However, when the effects of carbonation are added to the effects due to the different interface energy changes, as described above, the total changes become large enough to explain the obtained results.

Obviously, there are many uncertainties involved in this discussion. Still, the results may be explained if it is assumed that the true moisture content of the freezing calorimeter samples is similar to those predicted from the isotherms reported by Nilsson *and* that ice formation takes place through the successive replacement of water by ice, *i.e.* ice formation takes place within the pores. The latter also seems reasonable because these samples had been dried and re-saturated with water, a process which is likely to affect the pore structure in such a way that ice formation is more easily initiated through seeding, which thus reduces the likelihood of super-cooling and thereby reduces the tendency towards freeze-drying (as described in chapter 2.4). The effect on pore structure of pre-drying and the changes in the ice formation process that it causes were described by Bager and Sellevold in [B2 1986]. Sellevold and Radjy [Sd 1976] had previously concluded that ice probably forms within the pores.

3.8 Conclusions

Some characteristics of the moisture adsorbed in samples of 3 different micro mortars were examined by sorption calorimetry at +25°C, determination of desorption isotherms at +18°C and +5°C, and by freezing calorimetry. The intention was to use the data from room temperature measurements to calculate the amount of ice formed at each temperature during freezing.

- The results from the sorption calorimeter, which was developed by Prof. Ingemar Wadsö and Dr. Lars Wadsö and which has never before been used on this type of material, were checked against literature data with the conclusion that the sorption calorimeter produces accurate and reproducible adsorption isotherms. The measured heats of adsorption seem to be somewhat less reliable.
- A BET calculation was used to calculate specific surfaces of the materials. A calculation based on the adsorption isotherm showed that a slit pore model is better than a pore model employing cylindrical pores of circular cross section in that it produces a total pore wall area closer to that determined by the BET technique.
- Differential adsorption enthalpy and differential sorption entropy were determined as functions of the relative vapour pressure during adsorption. Simple equations were determined to describe differential adsorption enthalpy as a function of relative vapour pressure.

- It was assumed that differential adsorption enthalpy and differential adsorption entropy may be used together with the desorption isotherm to calculate ice formation as a function of temperature. The calculated heat flows were considerably lower than those actually measured. It might be that this is due partly to imprecisely determined desorption isotherms, and partly to a different type of ice formation process than was assumed for the calculation. If this is true, it shows that ice forms within the pores and thus replaces the frozen water *in situ* in these materials.

Appendix 3.1

CALCULATION OF DENSITY, POROSITY AND NATURAL DEGREE OF SATURATION

Definitions:

$Q_{w,a}$ = **w**et weight in **a**ir
$Q_{d,a}$ = **d**ry weight in **a**ir
$Q'_{s,w}$ = **s**aturated weight in **w**ater, as measured
$Q'_{s,a}$ = **s**aturated weight in **a**ir, as measured

$Q_{s,w}$ = **s**aturated weight in **w**ater, corrected value
$Q_{s,a}$ = **s**aturated weight in **a**ir, corrected value

S_0 = degree of water saturation after prestorage (= "natural" degree of saturation)

$\rho_{w,i}$ = density of water used for impregnation
$\rho_{w,w}$ = density of water used in weighings

Correction of measured pore volume for unsatisfactory vacuum:

V_a = volume of air in "water-saturated" specimen
V_w = volume of water in "water-saturated" specimen
V_p = true pore volume
p_1 = minimum air pressure in vacuum chamber
p_2 = air pressure used for impregnation

Basically,

$$V_p = V_w + V_a$$

in which

$$V_w = \frac{Q_{s,a} - Q_{d,a}}{\rho_{w,i}}$$

According to the gas law,

$$V_a = V_p \cdot \frac{p_1}{p_2}$$

and thus

$$V_p = V_w + V_p \cdot \frac{p_1}{p_2}$$

which yields

$$V_p = \frac{V_w}{1 - \frac{p_1}{p_2}}$$

Correction of measured weights

$$Q_{s,w} = Q'_{s,w} + \left(V_p - V_w\right) \cdot \rho_w$$

$$Q_{s,a} = Q'_{s,a} + V_p \cdot \rho_w$$

Calculating correct data:

$$V = \frac{Q_{s,a} - Q_{s,w}}{\rho_{w,w}}$$

$$\rho = \frac{Q_{d,a}}{V}$$

$$P = \frac{V_p}{V}$$

$$S_0 = \frac{V_w}{V_p} = \frac{Q_{w,a} - Q_{d,a}}{\rho_{w,i} \cdot V_p}$$

Appendix 3.2

GRAIN SIZE DISTRIBUTION

The grain size distribution of the crushed materials used for adsorption calorimeter experiments were determined by laser diffraction at Scancem Research.

Grain size distribution for samples of w/c ratio 0.40

CILAS **Granulometer HR 850** 145

Sample : 0.40 Result number 1

Suspension fluid : etanol
Dispersing agent :
Ultrasonic mixer time : 60 s
Comments :

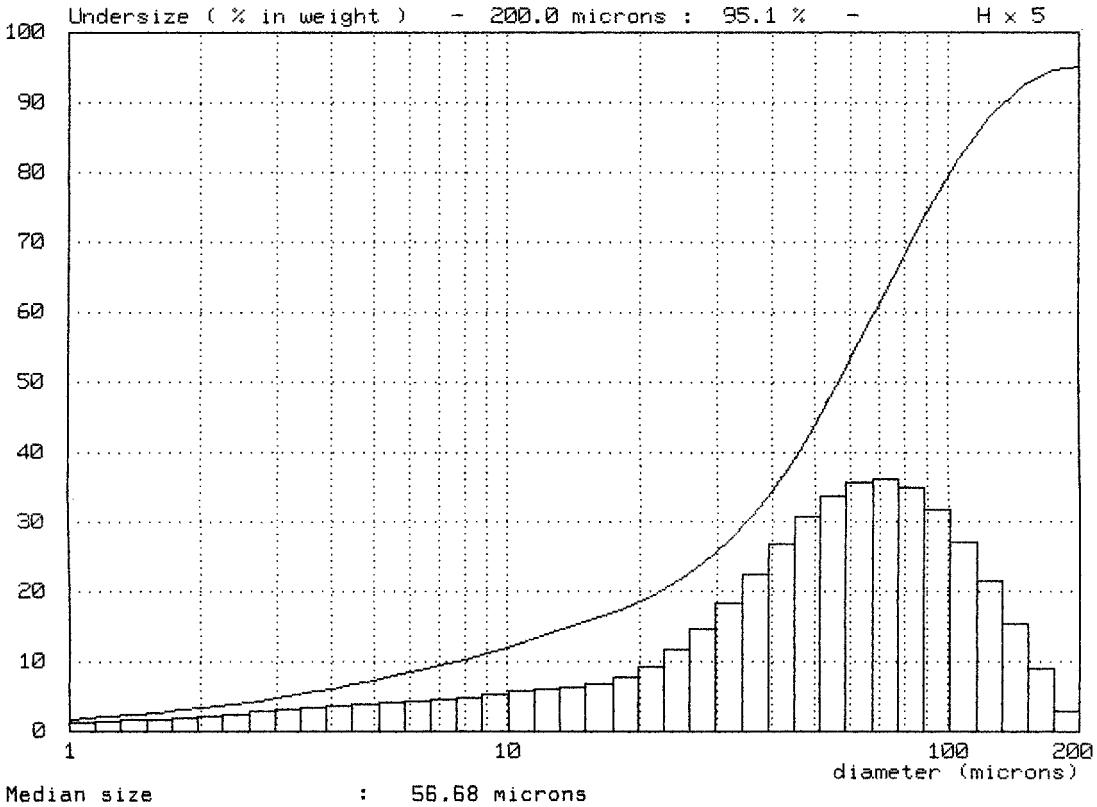

Median size : 56.68 microns

200 < Concentration < 400 : 202

D	1.0	1.2	1.4	1.6	1.8	2.0	2.2	2.6	3.0	3.5
%	1.7	2.0	2.4	2.7	3.0	3.3	3.6	4.2	4.8	5.5
D	4.0	4.5	5.0	5.5	6.3	7.0	8.0	9.0	10.0	12.0
%	6.1	6.7	7.3	7.9	8.7	9.3	10.2	11.1	11.9	13.5
D	15.0	18.0	20.0	22.0	25.0	28.0	32.0	36.0	40.0	45.0
%	15.6	17.4	18.6	19.8	21.8	24.0	27.2	30.7	34.4	39.1
D	50.0	56.0	63.0	75.0	90.0	106.0	125.0	150.0	175.0	200.0
%	43.8	49.4	55.5	64.9	74.4	82.0	88.2	92.7	94.6	95.1

Measurement performed by : mr
company : Scancem Research AB at : 0
on : 06/11/98 08:51:45

Grain size distribution for samples of w/c ratio 0.50

CILAS **Granulometer HR 850** 145

Sample : 0.5 Result number 4

Suspension fluid : etanol
Dispersing agent :
Ultrasonic mixer time : 60 s
Comments :

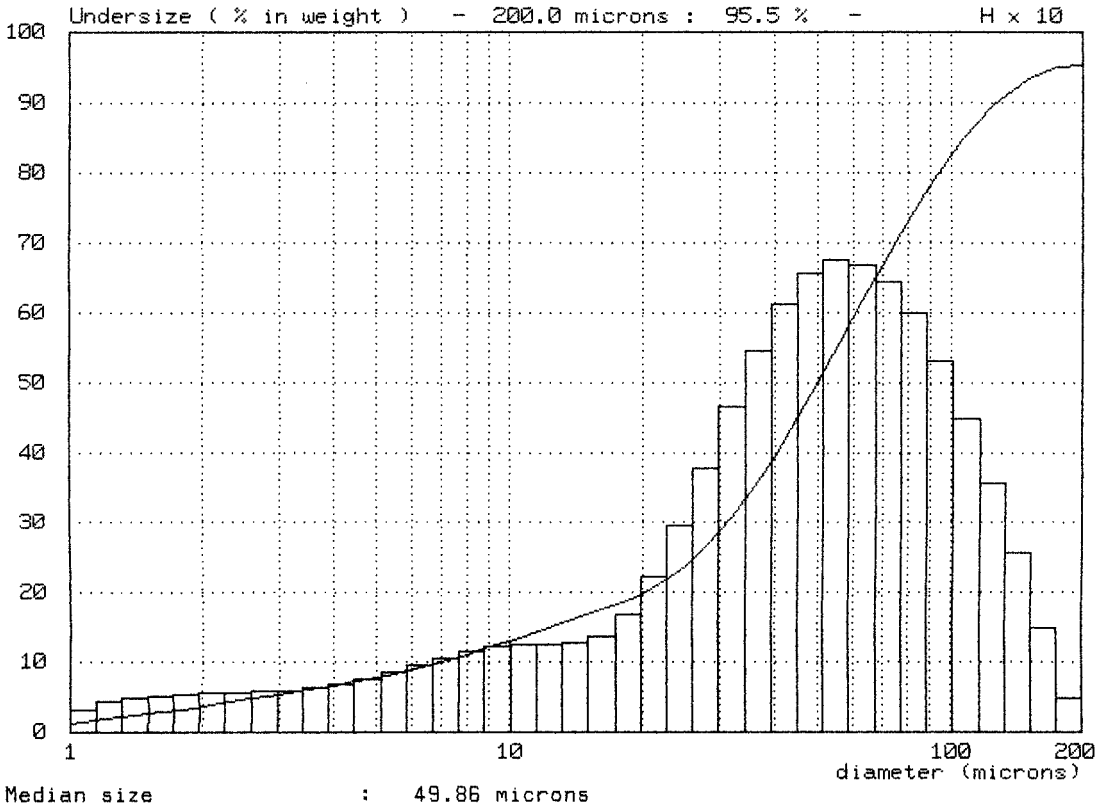

Median size : 49.86 microns

200 < Concentration < 400 : 155

D	1.0	1.2	1.4	1.6	1.8	2.0	2.2	2.6	3.0	3.5
%	1.2	1.8	2.3	2.8	3.2	3.6	4.0	4.7	5.3	5.9
D	4.0	4.5	5.0	5.5	6.3	7.0	8.0	9.0	10.0	12.0
%	6.6	7.1	7.7	8.3	9.2	10.0	11.0	12.0	13.0	14.6
D	15.0	18.0	20.0	22.0	25.0	28.0	32.0	36.0	40.0	45.0
%	16.7	18.4	19.7	21.2	23.7	26.5	30.7	35.1	39.6	45.0
D	50.0	56.0	63.0	75.0	90.0	106.0	125.0	150.0	175.0	200.0
%	50.1	55.8	61.7	70.2	78.4	84.7	89.7	93.5	95.1	95.5

Measurement performed by : mr
company : Scancem Research AB at : 0
on : 06/11/98 09:58:50

Grain size distribution for samples of w/c ratio 0.65

CILAS **Granulometer HR 850** 145

Sample : 0.65 Result number 3

Suspension fluid : etanol
Dispersing agent :
Ultrasonic mixer time : 60 s
Comments :

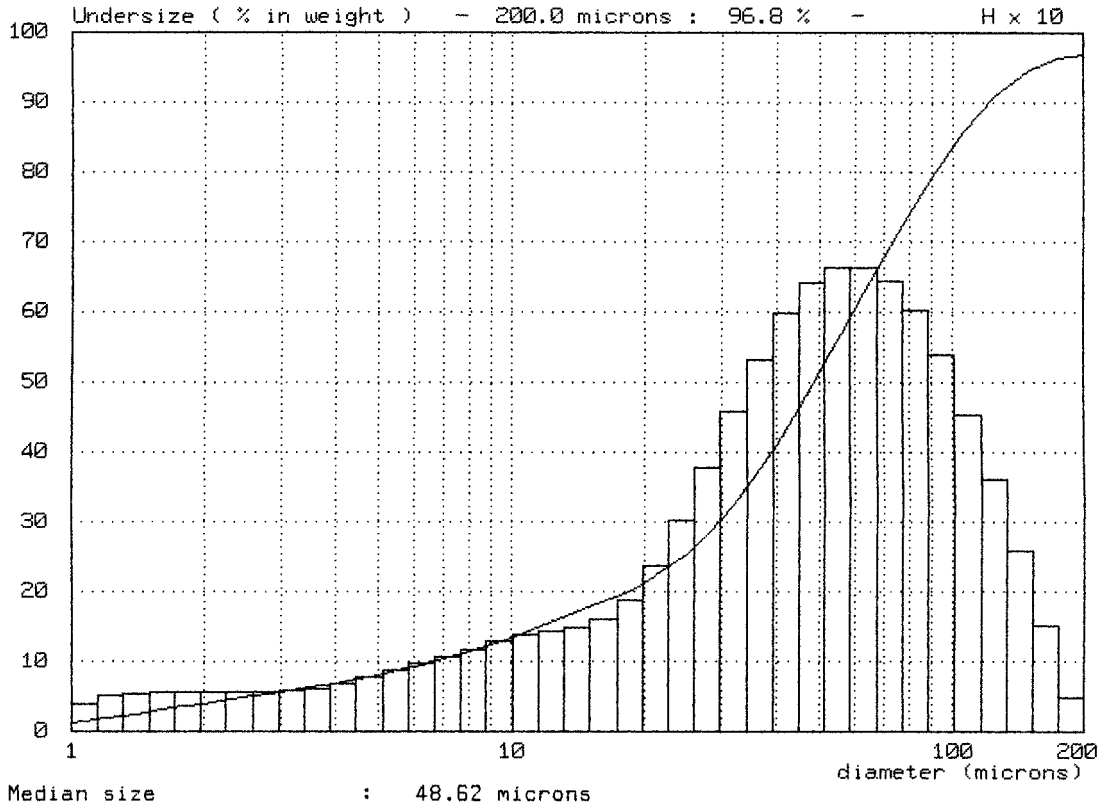

Median size : 48.62 microns

200 < Concentration < 400 : 207

D	1.0	1.2	1.4	1.6	1.8	2.0	2.2	2.6	3.0	3.5
%	1.2	1.9	2.5	3.0	3.5	3.9	4.3	5.0	5.6	6.3
D	4.0	4.5	5.0	5.5	6.3	7.0	8.0	9.0	10.0	12.0
%	6.9	7.4	8.0	8.6	9.5	10.3	11.4	12.4	13.4	15.3
D	15.0	18.0	20.0	22.0	25.0	28.0	32.0	36.0	40.0	45.0
%	17.7	19.8	21.3	22.8	25.4	28.3	32.4	36.7	41.1	46.3
D	50.0	56.0	63.0	75.0	90.0	106.0	125.0	150.0	175.0	200.0
%	51.3	56.9	62.7	71.2	79.4	85.8	90.9	94.7	96.3	96.8

Measurement performed by : mr
company : Scancem Research AB at : 0
on : 06/11/98 09:47:55

Appendix 3.3

DATA FROM R.H. MEASUREMENTS DURING DETERMINATION OF DESORPTION ISOTHERMS

Relative humidities were measured with dew-point meter (Protimeter, England). Measurements were taken after the dew-point meter had been installed in the boxes for some 3-8 hours. The random fluctuations amount to 0.5-1% R.H.According to the calibration, measured values (as reported here) are typically 1% R.H. too high. Due to uncertainties in the calibration procedure, though, the measured values have not been used for evaluation of desoroption isotherms (see text).

	LiCl		$C_2H_3KO_2$		$MgCl_2$		KI_3		NaCl	NaCl
Temp :	**5**	**18**	**5**	**18**	**5**	**18**	**5**	**18**	**5**	**18**
Exp. R.H:	**11.3**	**11.3**	**23.4**	**23.4**	**33.6**	**33.2**	**73.3**	**70.3**	**75.7**	**75.5**
980214	14.0%/5.2°									
980215	15.1%/5.3°									
980304										
980305										
980306										
980309										
980310										
980311										
980312										
980313	11.1%/6°									
980313	11.2%/6°									
980316			23.1/4.9°							
980317							72/4.4°			
980401									78.5%/4.2°	
980402									78.7%/4.2°	
980403									77.6%/4.2°	
980406									78.5%/4.1°	
980407					36.6%/4.2°					
980408					36.9%/4.2°					
980409					36.3%/4.2°					
980410					34.7%/4.3°					
980414							72.2/4.1°			
980417										
980420										
980422										
980423										
980511										
980515				24.3%/19.2°						
980515										
980518								69.2%/18.4°		
980518										76.3%/18.1°
980519										
980520						31.5%/20.5°				
980521										

	KBr		KCl		$Sr(NO_3)_2$		KNO_3		K_2SO_4	
Temp:	**5**	**18**	**5**	**18**	**5**	**18**	**5**	**18**	**5**	**18**
Exp. R.H.	**85.1**	**82**	**87.7**	**85.4**	**92.4**	**87.6**	**96.3**	**94.9**	**98.5**	**97.7**
980214										
980215										
980304									95.90%	
980305									97.3%/4.5°	
980306									96.6%/4.5°	
980309									97.3%/4.5°	
980310	84.4%/4.4°									
980311	85.0%/4.4°									
980312	84.4%/4.5°									
980313										
980313										
980316										
980317										
980401										
980402										
980403										
980406										
980407										
980408										
980409										
980410										
980414										
980417					96.6%/4.1°					
980420			88.7%/4.1°							
980422					91.20%					
980423							93.6%/4.1°			
980511			85.40%							
980515										
980515		82%/17.9°C								
980518										
980518										
980519										97%/18.1°
980520										
980521				85.9%/18°						

Appendix 3.4

WEIGHT DATA FROM DETERMINATION OF DESORPTION ISOTHERMS

Climate room: 18°C

Salt	Material	Crucible	Moist spec. incl. crucible	Dry spec. incl. cruc.	Ignited spec. incl. cruc.	Dry weight [g]	Moisture cont. [g]	Moisture cont. [%bw]	c/(c+b)	Cement cont. [g]	Wn [g]	Degree of hydration, α
LiCl	0.4	74.826	96.489	95.894	93.664	21.068	0.595	2.82	0.616	11.610	2.23	0.768
	0.5	75.119	100.596	99.958	97.678	24.839	0.638	2.57	0.503	11.345	2.28	0.804
	0.65	75.903	102.069	101.43	99.366	25.527	0.639	2.50	0.394	9.247	2.064	0.893
K-acetat	0.4	76.465	102.453	101.562	98.87	25.097	0.891	3.55	0.616	13.808	2.692	0.780
	0.5	77.009	97.33	96.675	94.757	19.666	0.655	3.33	0.503	8.925	1.918	0.860
	0.65	79.593	102.744	102.026	100.059	22.433	0.718	3.20	0.394	8.066	1.967	0.975
MgCl2	0.4	69.962	91.567	90.662	88.379	20.7	0.905	4.37	0.616	11.350	2.283	0.805
	0.5	69.552	103.572	102.224	99.104	32.672	1.348	4.13	0.503	14.862	3.12	0.840
	0.65	73.768	92.05	91.373	89.82	17.605	0.677	3.85	0.394	6.326	1.553	0.982
KI3	0.4	73.974	96.116	94.72	92.503	20.746	1.396	6.73	0.616	11.419	2.217	0.777
	0.5	75.936	97.746	96.397	94.486	20.461	1.349	6.59	0.503	9.329	1.911	0.819
	0.65	76.76	97.963	96.707	95.076	19.947	1.256	6.30	0.394	7.218	1.631	0.904
NaCl	0.4	72.778	90.893	89.656	87.863	16.878	1.237	7.33	0.616	9.297	1.793	0.771
	0.5	78.725	97.417	96.165	94.532	17.44	1.252	7.18	0.503	7.949	1.633	0.822
	0.65	74.594	95.958	94.547	92.962	19.953	1.411	7.07	0.394	7.239	1.585	0.876
KBr	0.4	74.933	99.998	98.131	95.63	23.198	1.867	8.05	0.616	12.756	2.501	0.784
	0.5	74.902	104.233	102.015	99.519	27.113	2.218	8.18	0.503	12.380	2.496	0.806
	0.65	76.576	99.042	97.351	95.698	20.775	1.691	8.14	0.394	7.536	1.653	0.877
KCl	0.4	74.877	98.379	96.537	94.22	21.66	1.842	8.50	0.616	11.921	2.317	0.777
	0.5	75.14	105.895	103.469	100.841	28.329	2.426	8.56	0.503	12.925	2.628	0.813
	0.65	77.216	100.748	98.849	97.099	21.633	1.899	8.78	0.394	7.836	1.75	0.893

Salt	Material	Crucible	Moist spec. incl. crucible	Dry spec. incl. cruc.	Ignited spec. incl. cruc.	Dry weight [g]	Moisture cont. [g]	Moisture cont. [%bw]	c/(c+b)	Cement cont. [g]	Wn [g]	Degree of hydration, α
Sr(NO3)2	0.4	75.001	95.49	93.848	91.842	18.847	1.642	8.71	0.616	10.379	2.006	0.773
	0.5	71.201	97.917	95.619	93.389	24.418	2.298	9.41	0.503	11.158	2.23	0.799
	0.65	74.505	98.783	96.691	94.947	22.186	2.092	9.43	0.394	8.056	1.744	0.866
KNO3	0.4	74.518	92.377	90.563	88.86	16.045	1.814	11.31	0.616	8.839	1.703	0.771
	0.5	76.211	102.828	99.932	97.751	23.721	2.896	12.21	0.503	10.832	2.181	0.805
	0.65	84.379	104.344	102.148	100.729	17.769	2.196	12.36	0.394	6.444	1.419	0.881
K2SO4	0.4	78.245	101.377	98.934	96.551	20.689	2.443	11.81	0.616	11.282	2.383	0.845
	0.5	105.502	135.102	131.6	129.007	26.098	3.502	13.42	0.503	11.821	2.593	0.877
	0.65	105.692	130.026	127.089	125.209	21.397	2.937	13.73	0.394	7.692	1.88	0.978

c/(c+b)=ratio of cement to total weight after ignition

		Moisture content [% b.w.]			Degree of hydration		
	R.H.	w/c 0.40	w/c 0.50	w/c 0.65	w/c 0.40	w/c 0.50	w/c 0.65
LiCl	11.3	2.82	2.57	2.50	0.768	0.804	0.893
$C_2H_3KO_2$	23.4	3.55	3.33	3.20	0.780	0.860	0.975
$MgCl_2$	33.2	4.37	4.13	3.85	0.805	0.840	0.982
KI_3	70.3	6.73	6.59	6.30	0.777	0.819	0.904
NaCl	75.5	7.33	7.18	7.07	0.771	0.822	0.876
KBr	82.05	8.05	8.18	8.14	0.784	0.806	0.877
KCl	85.4	8.50	8.56	8.78	0.777	0.813	0.893
$Sr(NO_3)_2$	87.6	8.71	9.41	9.43	0.773	0.799	0.866
KNO_3	94.9	11.31	12.21	12.36	0.771	0.805	0.881
K_2SO_4	97.7	11.81	13.42	13.73	0.845	0.877	0.978

Climate room: 5°C

Salt	Material	Crucible [g]	Most spec. incl. crucible [g]	Dry spec. (105°C) incl. cruc. [g]	Ignited spec. incl. cruc. [g]	Specimen dry weight	Moisture cont. [g]	Moisture cont. [%bw]	c/(c+b)	Cement content	Wn [g]	Degree of hydration
LiCl	0.4	73.762	112.667	111.273	107.283	37.511	1.394	3.72	0.6163	20.65899	3.99	0.772545
	0.5	74.983	107.412	106.313	103.371	31.33	1.099	3.51	0.5029	14.27633	2.942	0.824302
	0.65	71.203	100.203	99.247	96.873	28.044	0.956	3.41	0.3941	10.11655	2.374	0.93866
K-acetat	0.4	74.87	106.021	104.714	101.461	29.844	1.307	4.38	0.6163	16.38803	3.253	0.793994
	0.5	69.529	102.112	100.791	97.758	31.262	1.321	4.23	0.5029	14.19636	3.033	0.854585
	0.65	75.13	97.376	96.529	94.626	21.399	0.847	3.96	0.3941	7.683374	1.903	0.990711
MgCl2	0.4	76.986	107.99	106.277	102.96	29.291	1.713	5.85	0.6163	16.00778	3.317	0.828847
	0.5	84.355	119.124	117.287	113.949	32.932	1.837	5.58	0.5029	14.88282	3.338	0.897142
	0.65	74.561	99.336	98.131	95.901	23.57	1.205	5.11	0.3941	8.410094	2.23	1.06063
KI3	0.4	74.917	102.463	100.537	97.58	25.62	1.926	7.52	0.6163	13.96721	2.957	0.846841
	0.5	69.932	107.325	104.712	101.255	34.78	2.613	7.51	0.5029	15.75234	3.457	0.877838
	0.65	76.573	100.92	99.261	97.02	22.688	1.659	7.31	0.3941	8.058163	2.241	1.112412
NaCl	0.4	77.195	112.947	110.378	106.817	33.183	2.569	7.74	0.6163	18.25604	3.561	0.780235
	0.5	74.861	115.017	112.145	108.613	37.284	2.872	7.70	0.5029	16.97388	3.532	0.832338
	0.65	75.886	104.152	102.186	99.801	26.3	1.966	7.48	0.3941	9.424902	2.385	1.012212
KBr	0.4	75.095	99.56	97.597	94.83	22.502	1.963	8.72	0.6163	12.16268	2.767	0.909997
	0.5	74.801	107.606	104.88	101.566	30.079	2.726	9.06	0.5029	13.46012	3.314	0.984835
	0.65	78.682	101.31	99.396	97.303	20.714	1.914	9.24	0.3941	7.338536	2.093	1.140827
KCl	0.4	79.571	117.672	114.47	110.748	34.899	3.202	9.18	0.6163	19.21439	3.722	0.774836
	0.5	78.225	104.048	101.912	99.602	23.687	2.136	9.02	0.5029	10.75049	2.31	0.859495
	0.65	72.748	104.792	101.965	99.547	29.217	2.827	9.68	0.3941	10.56149	2.418	0.91578

Salt	Material	Crucible [g]	Most spec. incl. crucible [g]	Dry spec. (105°C) incl. cruc. [g]	Ignited spec. incl. cruc. [g]	Specimen dry weight	Moisture cont. [g]	Moisture cont. [%bw]	c/(c+b)	Cement content	Wn [g]	Degree of hydration
Sr(NO3)2	0.4	74.483	107.643	104.388	101.286	29.905	3.255	10.88	0.6163	16.51869	3.102	0.751149
	0.5	74.512	103.918	101.058	98.612	26.546	2.86	10.77	0.5029	12.11989	2.446	0.807268
	0.65	76.22	104.441	101.423	99.464	25.203	3.018	11.97	0.3941	9.16046	1.959	0.855416
KNO3	0.4	74.001	112.155	107.938	104.145	33.937	4.217	12.43	0.6163	18.57775	3.793	0.816676
	0.5	75.919	107.51	103.799	101.001	27.88	3.711	13.31	0.5029	12.61374	2.798	0.887287
	0.65	76.744	110.335	105.998	103.487	29.254	4.337	14.83	0.3941	10.53942	2.511	0.952994
K2SO4	0.4	76.445	100.125	97.508	94.543	21.063	2.617	12.42	0.6163	11.1538	2.965	1.063315
	0.5	105.476	137.762	133.45	129.982	27.974	4.312	15.41	0.5029	12.32407	3.468	1.125602
	0.65	105.671	135.487	131.211	128.487	25.54	4.276	16.74	0.3941	8.991786	2.724	1.211773

c/(c+b)=ratio of cement to total weight after ignition

		Moisture content [% b.w.]			Degree of hydration		
	R.H.	w/c 0.40	w/c 0.50	w/c 0.65	w/c 0.40	w/c 0.50	w/c 0.65
LiCl	11.3	3.72	3.51	3.41	0.773	0.824	0.939
$C_2H_3KO_2$	**23.4**	4.38	4.23	3.96	0.794	0.855	0.991
$MgCl_2$	37	5.85	5.58	5.11	0.829	0.897	1.061
KI_3	73.3	7.52	7.51	7.31	0.847	0.878	1.112
NaCl	76.8	7.74	7.70	7.48	0.780	0.832	1.012
KBr	85.1	8.72	9.06	9.24	0.910	0.985	1.141
KCl	87.7	9.18	9.02	9.68	0.775	0.859	0.916
$Sr(NO_3)_2$	92.4	10.88	10.77	11.97	0.751	0.807	0.855
KNO_3	96.3	12.43	13.31	14.83	0.817	0.887	0.953
K_2SO_4	98.5	12.42	15.41	16.74	1.063	1.126	1.212

4

LITERATURE STUDY

This chapter is intended to give an overview of the published literature on observed phenomena and the proposed explanations for these phenomena. Although the report deals mainly with salt frost scaling, this chapter also deals with the mechanisms of pure frost attack. This is necessary since many of the basic phenomena are the same.

Observed phenomena are reviewed in section 4.1 and an overview of proposed mechanisms is contained in section 4.2.

4.1 PHENOMENA OBSERVED IN LABORATORY SALT FROST SCALING TESTS

The objective of this section is to present some of the characteristics of salt frost scaling reported in the literature as a basis for the discussion of the mechanism proposed in chapter 6.

4.1.1 Classical studies

There are two articles which may be said to mark the start of research in the field of salt frost resistance (SFS) of cement-bound materials. These articles, in which very similar tests and similar results are reported, were written by Arnfelt [A 1943] and by Verbeck and Klieger [V 1957]. While these two articles are treated here in some detail, later reports are only briefly described in order to keep this compilation concise.

Arnfelt froze cubes completely submerged in different aqueous solutions (sodium chloride, barium chloride, potassium ferrocyanide, potassium ferricyanide, ethyl alcohol and urea) at -25°C for 12 hours and let them thaw in air at +20°C for 12 hours. Arnfelt chose these salts because of their wide differences in electrical charges and because it was foreseen they would not affect the concretes chemically. The solutions were prepared so that equal freezing point depressions were obtained. Arnfelt also tested roof bricks and sandstone. It turned out that, independent of the type of solution, the concretes were most deteriorated when frozen in intermediately concentrated solutions (freezing point depressions 1.5°C). The bricks and sandstones however were more deteriorated the purer the solutions. (It should be noted that the exact testing procedure for the latter materials is not described in Arnfelt's paper. It can only be assumed that it was similar to that of the concretes.)

Arnfelt concluded that, because the pure water caused less scaling than the intermediately concentrated solutions, the results could not be caused by simple volumetric expansion due to ice formation. Neither were the results attributable to chemical attack, since the solutions had been chosen because of their limited effect on concrete. Arnfelt believed the mechanism was of physico-chemical nature. But because of the different results for concrete on the one hand and sandstone and roof bricks on the other, Arnfelt refrained from proposing any explanation of the active mechanism.

Later, Verbeck and Klieger [V 1957] reported similar tests and similar results, although they used a frost cycle in which the freezing consisted of 18 h at -29°C and 6 h at +21°C and only applied the solution to the specimens' upper surfaces. Verbeck and Klieger used calcium chloride, sodium chloride, ethyl alcohol and urea. Some of their results are shown in figure 4.1.1. With calcium chloride, the deterioration was very severe at high concentrations. This, however, was due to chemical attack. Apart from this, their results are in accord with those of Arnfelt: intermediately concentrated solutions produce the most severe scaling and the qualitative behaviour is the same irrespective of the type of solute. Verbeck and Klieger also tested 3 different test procedures: In the first, they froze the specimens with pure water on the surface and then applied a solution immediately onto the ice before thawing. In the second procedure, they both froze and thawed the specimens with the salt solution applied on the surface. Finally, in the third procedure, specimens were frozen in a damp condition (*i.e.* without any liquid on the surface) and they then poured the different solutions onto the surface

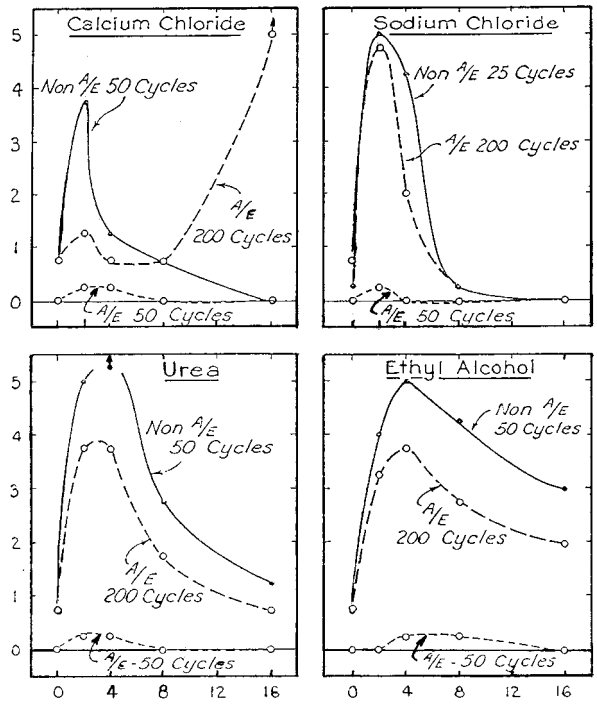

Figure 4.1.1: Results from Verbeck and Klieger [V 1957]. Visual damage rating: 0: Intact, 5: Severe scaling. A/E: Air entrained concrete.

before thawing. The results showed that procedure 2 was worse than procedure 1 and also that almost no scaling occurred when the third procedure was used. It is the opinion of the author that this implies that outer moisture is necessary for scaling to occur.

4.1.2 Repeatedly observed phenomena

In this section, different but repeatedly observed phenomena will be treated one by one. This is intended to facilitate the subsequent discussion of the mechanism proposed in chapter 6. Only phenomena connected with surface scaling are dealt with. As regards effects on resistance to inner frost deterioration, only those phenomena which are believed also to be common to surface scaling are discussed. In the tests referred to below, test methods have varied. Unless otherwise stated, the methods used have been either the Swedish SS 13 72 44, the German CDF or a method substantially similar to either of these. Thus, in order not to obscure the results reported, no details concerning test methods are given. Only where significantly different test methods have been used are details given.

Other compilations may be found in [P 1994], [Md 1994] and [Md 1995].

A: Water uptake during salt frost scaling tests

It has been observed several times that the water content of salt frost scaling specimens increases during the test, *e.g.* Browne & Cady [B1975], Fagerlund [F 1991], Setzer [S 1993] and Jacobsen [J 1995], who reported water uptake on several occasions. Setzer explains that the increased water uptake may be due to a ”pumping effect” which in turn is due to a combination of the freezing/melting hysteresis for pore water and the larger volumetric thermal expansion of water as compared to ice. Such a ”pumping

effect" was also proposed by Geiker and Thaulow [G 1996]. As will be seen in section 7.1, however, the thermally induced volume change of water does not explain the large observed moisture uptake.

B: Importance of outer liquid

Verbeck and Klieger found that when samples were frozen damp only, *i.e.* with no liquid present on the surface, there was no scaling. Studer [Sr 1993] also states that no scaling arises when the salt solution is missing (or is replaced by pure water). No further studies of this have been reported, but it has been observed several times that when the outer solution is accidentally missing, *e.g.* due to leakage, scaling ceases (consistent with our own experience). Also, in ordinary tests of frost resistance on moisture-isolated specimens, surface scaling almost never occurs.

C: Outer salt concentration

The "pessimum" concentration, *i.e.* the relatively weak concentration causing maximum deterioration, observed by Arnfelt and by Verbeck and Klieger, was later studied by Sellevold [Sd 1988]. Sellevold studied concretes with *w/c* ratios ranging from 0.27 to 0.55, with and without additional silica fume (7-10% b.w. of cement). The fresh-mix air content was some 6%. Sellevold's results indicate that there is a maximum in scaling for salt concentrations close to 3%, figure 4.1.2. However, scaling is also severe for higher concentrations. Due to inhomogeneous concretes, there was a large spread in the results and Sellevold therefore said it could not be concluded that the "pessimum" is a reality for normal concrete (*w/c* 0.55). However, for intermediate high-strength concrete (*w/c* = 0.36 and *s/(c+s)* = 0.10, *s* = silica fume), Sellevold found that there is *no* such optimum. For concrete of even lower *w/c* ratio, scaling is often almost non-existent and this too was found by Sellevold for concrete of *w/c* = 0.27 with silica fume (*s/(c+s)* = 0.10).

The present author has obtained results with *w/c* = 0.40 which show that an outer concentration of 3% is clearly worse than either 0% or 6%. For *w/c* = 0.35 with 5% silica fume and *w/c* = 0.30 with 10% silica fume (*s/c* = 0.10) it was shown that scaling was independent of outer concentration. With an outer concentration of 0%, however, scaling was non-existent. (See Chapter 5.1)

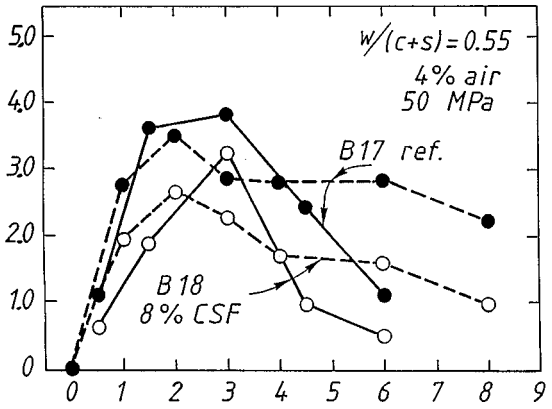

Figure 4.1.2: Scaling [kg/m²] vs. concentration of NaCl [% b.w.] in solution applied to the tested surface [Sd 1988].

D: Inner salt concentration

Snyder [Sy 1965] found that specimens in which the pore solution contained approximately 3% NaCl would scale much more slowly than those containing pure water, irrespective of whether the outer solution was a 3% NaCl solution or pure water. He also tried specimens in which there was a gradient in de-icer concentration from the surface inwards. The gradients were obtained by soaking the samples in a 3% NaCl solution for various periods of time, from 1 to 12 days. It turned out that a soaking time of one or two days would cause almost twice as much scaling as no soaking at all. Soaking for three days or more however resulted in considerably less scaling than no soaking at all. From this, Snyder concluded that a concentration gradient was needed for scaling to occur.

Petersson [P 1984] tested mortar prisms that had been stored in different NaCl solutions (0, 0.2, 0.5, 1.5, 3, 4.5, 6 and 12%) by immersing them to half their height in either pure water or a 3% NaCl solution. Specimens tested in the latter solution scaled very much more than those tested in water (by a factor of approximately 200). It is of interest in Petersson's results that specimens tested in the 3% solution tended to show larger scaling the less salt there was inside them. From this it seems that salt in the pore system has a protective action.

Sellevold [Sd 1988] ran tests according to the Swedish Standard SS 13 72 44 and found that the most severe scaling was obtained when the pore solution was free from salt.

The present author has studied the effect of inner salt concentration on concrete of *w/c* ratio 0.40 with maximum aggregate size 8 mm (chapter 5.1). The inner concentrations were obtained by soaking the specimens in NaCl solutions of 0, 3 and 6% for some 6 months before testing. For specimens tested with solutions of 3 or 6% on the surface, there is a tendency for scaling to increase with increasing inner salt concentration. This tendency, however, is not consistent and the scatter is rather large. Specimens tested with pure water on the surface show the same trend somewhat more consistently.

E: Minimum Temperature

Sellevold [Sd 1988] found that a minimum temperature of -10° resulted in less deterioration than did -20°C.

Studer [Sr 1993] found that the severity of the temperature cycles can best be characterised by the minimum temperature reached in the outer salt solution (Studer tested temperatures in the interval $-7°>\theta>-22°C$). Studer, however, says the relation is strongly non-linear, the effect being more pronounced at levels close to -18°C than at a level of -13°C.

Petersson [P 1994] ran similar tests and found that scaling increased with decreasing minimum temperature for concretes of intermediate quality. For high and low quality concretes, however, the minimum temperature did not significantly affect the results. In contrast to Studer, Petersson found that the influence was larger at the higher temperatures. In one series (out of five) Petersson found that a temperature of -27°C would cause less scaling than -24°C and, in another, even less than -18°C. No explanation was given for this observation. It may be noted, however, that -24°C always caused the most severe deterioration.

Finally, the present author studied the effect of minimum temperature (chapter 5.1). While it seems clear that -7°C causes only slight scaling, the difference between -14°C and -22°C is not unambiguous.

F: Rate of Cooling

Sellevold [Sd 1988] found no large effect of cooling rate. Although, from the figures in his report, it seems that scaling decreases with increased cooling rate. However, since the duration of the time at minimum temperature was also varied at the same time, it is impossible to say which factor is the more important.

Studer [Sr 1993] found no influence of either duration of the frost cycle or freezing rate. The latter however was varied in a narrow interval (-2.0°/h – -3.4°/h, measured in the outer solution) and therefore should have a very limited effect, probably disguised by other effects.

Jacobsen [J 1995], using the German CDF method, ran controlled tests on three non air-entrained concretes and one air-entrained. He managed to obtain cooling rates of 2.8, 4.9 and 12°C/h (measured in the outer solution). Since the minimum temperature was -18°C, the total time in the frozen condition varied widely. To deal with this, Jacobsen also ran tests in which the cooling rate was kept constant but the time at -18°C was varied, to facilitate comparison with the other freeze-thaw cycles. Jacobsen found that scaling was increased by reducing the rate of cooling and by increasing the time at minimum temperature. He also found that reducing the cooling rate (still using a minimum temperature of -18°C) caused larger weight losses than extending the time at the minimum temperature when this had been reached by fast cooling. The air-entrained concrete was of high quality and was not affected by changes in the freeze-thaw cycle.

G: Duration of frost cycle

Studer [Sr 1993] found no influence of the duration of the frost cycle. As mentioned above, Jacobsen [J 1995] found that an increased duration resulted in increased scaling.

H: Importance of freezing

It has been proposed that, to some extent, frost deterioration may be due to the thermal incompatibility between the cement paste itself and the aggregate. To test this, Sellevold *et al* [Sd 1993] temperature cycled concrete of *w/c* ratio 0.30 in the interval +5°C to +27°C. It was found that thermal incompatibility is not a major cause of deterioration in frost resistance tests.

I: Material quality

Generally, concretes of high water/cement ratio show very low resistance to salt frost attack. This seems natural, since an increased water/cement ratio will lead to a larger capillary porosity and thus to an increased amount of freezable water at each and every temperature. Because of this dependence on capillary porosity, it has been hypothesised that concrete of very low water/cement ratio might be salt frost resistant even without the use of an air-entraining agent. Indeed, on testing for SFS resistance with various test methods similar to the Swedish Standard SS 13 72 44, it was found that concrete of ”very good” SFS resistance may be produced by using a low *w/c* ratio, preferably less than 0.35 (Sellevold [Sd 1988], Jacobsen [J 1995], Sörensen [Sn 1983], Lindmark [Lk 1991]). Other researchers, using modified versions of the ASTM C-666 (in which a specimen is entirely submerged in water or some de-icer solution), have reported both good and poor SFS resistance for such high quality concretes (Saucier [Sc 1984], Penttala [P 1989], Okada *et al* [O 1981], Malhotra *et al* [M 1987], Foy et al [F 1988]).

In addition to a low water/cement ratio, a dense micro structure may also be obtained by carbonation, [M 1995], [Sk 1997], [K 1986]. Thus Petersson [P 1995] published results from field studies which showed that the salt frost resistance of concrete specimens exposed in the field had improved as compared to measurements taken on the newly cast concretes. When the field-exposed specimens were tested under the SS 13 72 44 method after their top layer had been cut off, the improvement in salt frost scaling obtained during the field exposure was lost. This improvement may be due to densification of the top-most layer of the specimen due to carbonation, although Petersson refrained from saying so at the time.

Although it seems that frost and salt frost induced deterioration is governed by a mainly physical mechanism, the chemical composition of the cement also has an influence. For example, Stark and Ludwig investigated the frost and salt frost resistance of concretes of w/c = 0.50 with cements with C_3A contents of 0, 2, 4…12% and found that for non air-entrained concretes, the frost resistance (CWF method, *i.e.* a scaling test in pure water) increased with increasing C_3A content. In the tests for SFS resistance, the authors used the CDF method and concretes with some 5% air. This time, the scaling resistance was observed to decrease with increasing C_3A content. The latter observation is in accord with experience from Swedish cements, which shows that a cement of low C_3A normally produces concrete of better SFS resistance, *e.g.* Malmström [M 1990]. Stark and Ludwig hypothesised that in the case of pure water frost attack, the decreased resistance may be due to a frost-induced transformation of AFm phase into Aft, but stressed that further investigation is needed.

Finally, Sellevold [Sd 1988] emphasised that SFS resistance is very sensitive to inhomogeneities and showed that the SFS resistance of any individual specimen may be strongly dependent on its position in the casting mould from which it was cut.

J: Relation of scaling to characteristics of the air void system

The air void system in a hardened concrete is characterised by its total volume, its specific surface or its spacing factor, *i.e.* a calculated mean half distance between the void boundaries (shortly described in section 2.1). One difficulty in relating the salt frost scaling resistance of concrete to any of these parameters is their close relationship. Thus, if one single air-entraining agent is used for studying the effect of the Powers spacing factor, it may be that when increasing the dosage (in order to obtain shorter spacing) the entire air content is also increased. And it may well be that it is the effect of entire air content rather than spacing itself that determines the SFS resistance. As for the specific surface of the air void system, one should not expect an air void system of very high specific surface to produce SFS resistant concrete if, at the same time, the entire air content is too low. Thus, we may be unable to obtain a correlation between SFS resistance and a single air void parameter. The only way of obtaining reliable results is by using different types of air-entraining agents to produce different types of air void systems in a matrix of non-varying composition. Unfortunately, it seems very little research has been done which takes this into account. Furthermore, the technique of calculating the values of the characteristic parameters may be dubious. Carlsson [C 1995] has shown that calculated values of the Powers spacing factor (and specific surface) for very different air void size distributions may produce identical values, thus indicating identical properties with regard to frost resistance.

The concept of a critical spacing factor was introduced by Powers as early as 1949. He stressed then the fact that the permissible spacing factor is dependent on the type of frost resistance test to which the material is subjected. Furthermore, since the determination of the air void system parameters involves several difficult steps in the laboratory work and since these parameters may also vary considerably within individual specimens, the precision of such determinations should not be overrated.

Several tests have shown that proper air-entrainment will make cement-bound materials resistant to salt frost attack, *e.g. [Bl 1977]*, [K 1981], [B 1979], [P 1989]. From these studies, it seems that an air void system of higher quality is required when concrete is subjected to combined salt and frost attack than when it is frozen in a moisture isolated state. Thus the critical spacing factor in connection with pure frost attack has been reported to be some 0.25 mm ([P 1949] and [I 1970]) while that required for salt frost resistance seems to be some 0.18-0.20 mm [B 1979],*[Bl 1977]*. Expressed in terms of total air content, the requirement for resistance to pure frost attack usually is some 2-3% while the requirement for salt frost resistance may be more than 4.5%.

There are, however, also several investigations which show poor correlation between salt scaling resistance on the one hand and either air content, spacing factor or specific surface of the air void system on the other hand. For example, Janssen and Snyder [J 1993] studied 8 different concretes (all with $w/(c+p)$ = 0.45 and with varying amounts of fly ash and ground blast furnace slag) by using the standard ASTM C666 (modified by substituting pure water for a 3% NaCl solution) and found no correlation between either air content, Powers spacing factor or Philleo factor P90 (a different technique for determining the characteristics of an air void system) with either mass loss after full test or number of cycles to reach 5% mass loss. The best correlation seems to have been that between air content and number of cycles needed to reach 5% mass loss, figure 4.1.3. An increased air content seems to improve scaling resistance. However, this seeming correlation is largely attributable to the two concretes with air content of approximately 3%.

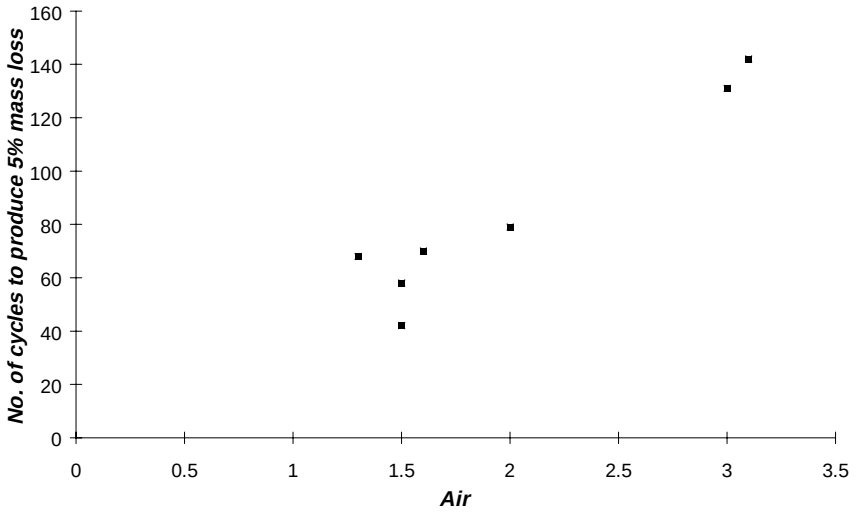

Fig 4.1.3: Relation between air content in the hardened concrete (linear traverse) and number of cycles required for a 5% mass loss in a modified ASTM C666 procedure (with 3% NaCl solution). W/c 0.45, different amounts and types of mineral admixtures. Janssen and Snyder [J 1993].

Another example is obtained from Setzer [S 1993], figures 4.1.4 and 4.1.5. In these figures, the acceptance criterion, as defined in the CDF test method (1500 g/m²), has been marked. From these figures, no distinct relation can be found between either air content or spacing factor and scaling.

Fagerlund, too, studied the effects of the air void parameters on SFS resistance with similar results [F 1993]. Fagerlund, using a single air-entraining agent, found a linear relation between the Powers spacing factor and SFS resistance, but, as Fagerlund pointed out, this may be due to the fact that only one parameter, air content, was varied.

Malmström [M 1990] used concretes of *w/c* = 0.46 with two different cements (C_3A contents of 8.5% and 1.8%, respectively) and varying amounts of two different air-entraining agents (vinsol resin and a type of synthetic tenside) and found a poor correlation between spacing factor and SFS resistance (SS 13 72 44). The correlation between total air content and SFS resistance was, however, rather good, irrespective of type of air-entraining agent. Instead, it was shown that the type of cement has a large influence. Whether this is due to the chemical composition of the cement *per se* or to its interaction with the air-entraining agents is impossible to say. It was shown that the specific surface of the air void systems was higher in the concretes produced with cements of high C_3A (7% and 17% for vinsol resin and tenside, respectively).

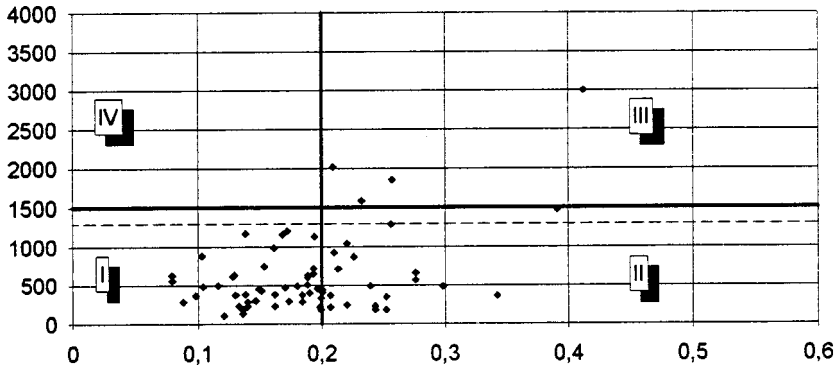

Figure 4.1.4: Dependence of scaling on spacing factor. "Critical" spacing factor marked at 0.2mm. CDF test method. Concrete qualities not specified. [S 1993].

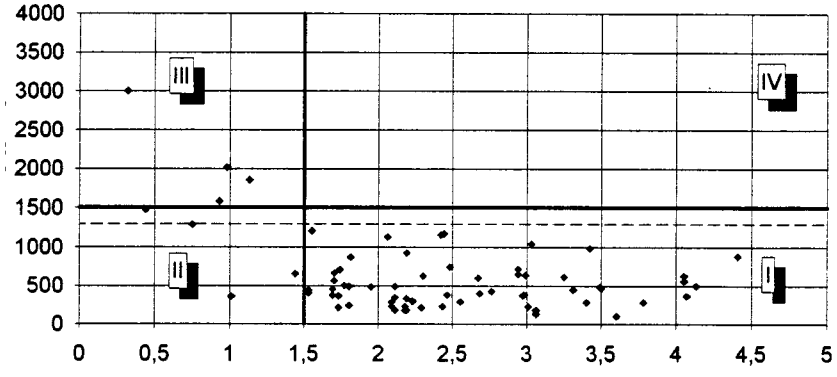

Figure 4.1.5: Dependence of scaling on volume of entrained air voids of diameter <300µm. "Critical" volume 1.5% marked. CDF test method. Concrete qualities not specified. [S 1993]

Stark and Ludwig report a lack of correlation between the air void system parameters and the salt frost scaling resistance of concrete made with large amounts of granulated blast furnace slag [Sk 1997]. They report that in concretes rich in GBFS not only calcite but also vaterite and aragonite form due to carbonation. According to these authors, the latter are unstable in the presence of an NaCl solution and readily dissolve during freeze-thaw testing. As a result, "…badly crystalline calcite is formed in situ which will quickly scale off under frost attack.". The authors give no explanation as to why this badly crystalline calcite would be scaled off so easily. Neither was it shown that the dissolution of these reaction products in the absence of freezing would cause any damage.

4.1.3 Other observations

Stark and Ludwig [Sk 1994] reported results according to which scaling on a *w/c* ratio 0.60 concrete, when tested by the CF method (similar to the CDF method but without any salt), increases with increasing water hardness. Thus, at a total hardness of 27°dH, a concrete containing pure Portland cement scaled off 0.490 kg/m² after 28 freeze/thaw cycles, while the same concrete tested in distilled water scaled only 0.2 kg/m². For a similar concrete with GBFS added to it, the corresponding results were 1.50 kg/m² and 0.41 kg/m², respectively.

Petersson has reported results from tests on concrete containing silica fume which, after a number of freeze/thaw cycles during which the concrete showed good resistance to salt frost attack, suddenly disintegrates very rapidly, figure 4.1.6 [P 1995]. These concretes were prepared without the use of any air-entraining agent. The water cement ratios were 0.35 and 0.40 and the addition of silica fume was 5% of the cement weight. Peterson refers to *Lagerblad and Utkin [L 1993]* who have proposed that this might be due to alkali silica reactions which in turn would be due to poor dispersion of the silica fume. Peterson, however, claims this cannot be the reason in this case because the silica fume was added in slurry form.

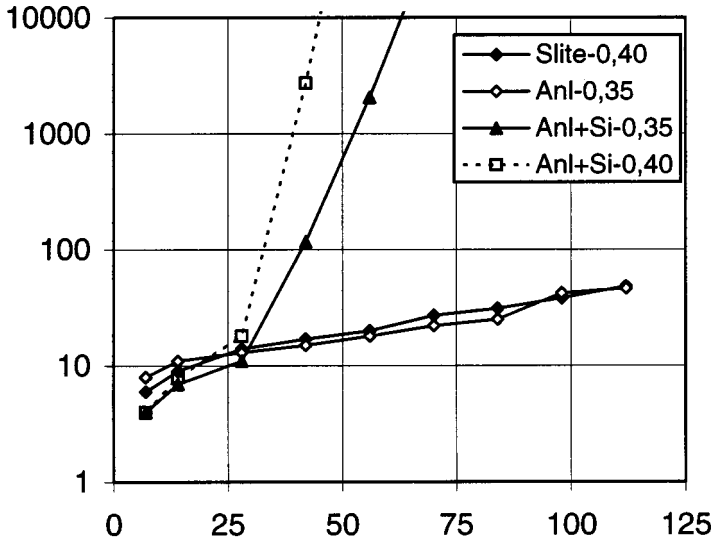

Figure 4.1.6: Accumulated scaling [g/m²] vs. number of frost cycles. Concretes with and without silica fume. No air entrainment. Cement type and w/c *ratios indicated. Anl: Cement type described in General Appendix 2. Slite: Standard Portland cement. 5% silica fume b.w. of cement.Test method SS 13 72 44. [P 1995]*

4.1.4 Purely salt-induced deterioration

Although the studies reported by Arnfelt [A 1943] and Verbeck and Klieger [V 1957] show that the de-icing agent in the outer solution need not be a salt, the pure chemical effect of salts has also been studied in connection with studies of the problem of salt frost scaling.

The most obvious way in which salts cause deterioration of HCP would seem to be crystallisation, *e.g.* [B 1987], [N 1991], [Y 1997]. Crystallisation, however, demands that the salt solution becomes over-saturated by, for instance, drying. Since the pore system of a concrete specimen subjected to any of the standardised salt frost scaling tests remains almost completely water-saturated throughout the test, it seems far-fetched that crystallisation would be responsible for any of the damage observed in such tests.

While NaCl has been shown to be non-harmful to HCP ([P 1991], [P 1984], [St 1997]), some salts, *e.g.* calcium chloride, calcium magnesium acetate and calcium acetate, do in fact deteriorate HCP-based materials very severely, *e.g.* [P 1991]. Depending on its concentration, the $CaCl_2$ adopts different compositions with various amounts of crystal water, and it therefore may cause extensive swelling. It is most detrimental when present in moderate concentrations [P 1991].

4.1.5 Conclusions

From the above compilation, it seems safe to make the following seven conclusions:

1. Surface scaling almost never appears in the absence of an outer solution which to some extent remains liquid at temperatures lower than the normal freezing point of the pore solution of HCP. It may even be noted that in the two reports in which scaling is reported when the outer solution was pure water, either that outer water was rich in naturally occurring ions [Sk 1994] or the specimen surface had been exposed to a salt solution prior to testing so that the pore system did contain some salt [Sy 1965].
2. Portland cement-bound materials with proper air void systems are able to withstand combined salt and frost attack, at least in laboratory tests.
3. The chemical composition of the de-icing agent seems to be of no importance.
4. Without actual freezing temperatures, no scaling occurs.
5. Use of a lower minimum temperature will produce more scaling, at least for minimum temperatures in the interval $0°C > \theta > -20°C$.
6. Coarse porous materials are more sensitive to salt frost attack than dense materials.
7. Purely chemical mechanisms are of little importance in comparison to physical mechanisms.

4.2 PREVIOUSLY PROPOSED MECHANISMS

This section describes various mechanisms of both pure frost attack and combined salt and frost attack which have been proposed previously. As will be seen, much work in this field has taken place on materials other than cement-bound materials. I think it is instructive to study these other materials as well, since the similarities and differences in behaviour under frost attack in relation to pore structure may have something to say about the mechanism of salt frost attack in cement-bound materials.

My intention is to describe not only the various proposed mechanisms but also the chronological order of the development of the research. For the sake of clarity, therefore, a summary is set out at the end of this chapter.

Other reviews of previously proposed mechanisms are given by Marchand *et al* [Md 1994], Marchand *et al* [Md 1995], Pigeon [Pn 1994].

4.2.1 Frost attack without salts

The simplest mechanism of frost deterioration is often referred to as the ”closed container mechanism”. It draws on the simple fact that the specific volume of ice is larger than that of water and, thus, if a non-permeable container contains more than a certain amount of water, ice formation will cause large pressures increases. Since the specific volume of ice is 9% larger than that of water, pressures will develop if initially more than 91.7% of the container volume was filled with water. Provided the container cannot yield under pressure, the pressure rise due to ice formation may be calculated from the Clapeyron equation, eq. (2.4.25). From this equation, it can be calculated that for ice and water to exist in equilibrium at a certain temperature below the normal bulk melting temperature (273.15K), a pressure increase of approximately 10 MPa/K is required. Thus, even at -1°C the pressure will be some 10 MPa, a pressure high enough to damage normal, porous, brittle building materials. This mechanism is obviously very closely related to the degree of saturation of a porous material. By determining the critical degrees of saturation of porous materials, it should be possible to clarify the mechanisms of frost deterioration and much work has been carried out in this field. Some of that work is reviewed below in a separate section.

Taber [T 1930] investigated the mechanisms of frost-induced heaving in soils. Taber found that in the cold end of a uni-directionally cooled cylindrical soil specimen, ice lenses were able to grow by consuming water from the warmer parts of the specimen and that the resulting ice lenses were able to exert considerable pressures. He also found that the pressure was exerted in the direction of growth of the ice lenses, which was parallel to the direction of the heat flow rate. This kind of ice formation is thus dependent on the presence of thermodynamically unstable water. The ice lens growth rate is determined by the difference in chemical potential between the ice and the water and is therefore referred to as osmotic ice lens growth.

Taber also pointed out the importance of distinguishing between soils frozen as open systems and those frozen as closed systems. In the latter type, the specimen did not have access to any moisture from outside. In such systems, in which there was also a temperature gradient, shrinkage occurred in the warm end of the specimens, because of the drainage that occurred in that end in favour of the ice formation in the cold end. In the

field of frost attack on cement-bound materials, a specimen frozen as a closed system is often referred to as being frozen under conditions of ”moisture isolation”.

Finally, Taber found that in clays frozen as closed systems, some 6-7% of the moisture content would not freeze. Taber thought this was due to surface-related phenomena.

In 1944, Collins [C 1944] published results from field investigations on frost-induced damage in concrete pavements in England. The concretes in question were of very low quality (high, and coarse porosity) and the winter of 1942, which was when the concretes were cast, had been extremely severe with very long periods of temperatures below freezing. Collins assumed that the primary mechanism had been the same as that described by Taber.

In 1945, Powers [P 1945] presented an hypothesis on the mechanism of frost deterioration of concrete. Powers had noted that, although concrete often contains enough air, even after long periods of storage under water, for it to be able to accommodate the volume increase caused by freezing, it would still not be frost resistant, *i.e.* although it seemed to be less than critically saturated, it would still fail. Powers therefore proposed that the major cause of disintegration was not the ice pressure itself, since this would consequently not need to develop, but rather the hydraulic pressures that would arise during ice formation when water was expelled from the pore in which freezing took place. Powers also did some calculations for a one-dimensional case to show the possible orders of magnitude of the hydraulic pressures. The results showed that the thickness of the saturated zone in front of the freezing front needed to be 0.25 inches (6mm) to produce hydraulic pressures high enough to damage the concrete. Powers thought such a depth of saturation would be entirely possible under laboratory conditions. This hypothesis has since been referred to as the ”Hydraulic pressure hypothesis”.

Powers also discussed the results of Collins, and thought that the mechanism proposed by Taber could not be responsible for damage observed in concrete, since the permeability of concrete would be so low as to make concrete freeze like a ”closed system”, *i.e.* one in which water movement is so restricted that lenses cannot form (under conditions of normal rates of cooling). Powers admits that the mechanism might be active ”when the rate of cooling is exceedingly slow”. Powers also realised that this kind of mechanism might be active on a submicroscopic level, so that ice formed in the capillaries might receive water from the surrounding walls of cement gel. Nevertheless, he did not think such a mechanism could explain why it had been observed that air-entrainment would make the concrete virtually immune to frost attack, or why damage seemed to increase with increased rate of cooling.

The hydraulic pressure hypothesis was immediately taken up by Terzaghi *et al* [T 1945] and by Collins [C 1945]. Terzaghi *et al* carried out more detailed calculations and found it unlikely that concrete, under natural conditions, would be saturated to such a depth as to render significant the mechanism proposed by Powers. Collins thought the Powers hypothesis might be valid in certain situations, but also insisted that the ice lens growth mechanism would still be active in many situations, especially for pavements. Collins pointed out that ice lenses had in fact been observed in concrete pavements in the field and that these lenses had been too large to have been formed from the water that may have been initially present in the concrete.

In his reply, Powers remarked that both his own and the calculation done by Terzaghi *et al* had been oversimplified in that it had been assumed that all freezable water in a unit volume of concrete freezes simultaneously. When taking into account that water freezes gradually and that permeability will be reduced as the pores are blocked with ice, Powers

concluded that it might be that disintegration eventually occurs, *i.e.* at low enough temperatures, due to static pressure. The discussions, both that of Terzaghi *et al* and that of Powers, were speculative and more laboratory data were needed for further progress.

In 1949, Powers presented [P 1949] further experimental results and, by applying the hydraulic pressure hypothesis, he showed that the measured air void characteristics in frost resistant specimens was in good agreement with what was expected from a calculation using a simple geometrical model. Powers used a model in which the air voids were all of the same size and cubically arranged. The maximum distance for water transport then equals half the maximum distance between such voids and can be calculated from the equation:

$$a = \frac{D}{2}\left\{1.4\left(\frac{V_p}{L}+1\right)^{1/3}-1\right\} \qquad \textit{when} \quad \frac{V_p}{L} \geq 4.33 \qquad \textit{(2.1.9)}$$

in which D is the diameter of an air void of the same specific surface as the entire air pore system, V_p is the volume of cement paste and L is the volume of air voids. The distance a is called the Powers spacing factor.

From material data on permeability (not compensated for ice formation) and amounts of ice formed (although simplified), Powers calculated permissible spacing factors of 0.2–0.7 mm for cement pastes of *w/c* in the range 0.32 to 0.62. Powers refers to Gonnerman [*G 1944*] who had found concrete to be frost resistant when the air content exceeded 3% b.v. By assuming values for the air void characteristics, for the permeability and for the amount of ice formed, Powers estimated the spacing factors of these concretes to have been approximately 0.25 mm. Powers considered the calculated values to be ”remarkably close” to those obtained from ”direct measurement” and regarded this agreement as strong support for the hydraulic pressure hypothesis. From his paper, it seems that the ”direct measurements” are the values for air content of frost resistant concrete obtained from Gonnerman together with the assumptions made by Powers. Obviously, therefore, the comparison is uncertain. Furthermore, contrary to his original suggestion, Powers used the permeability of hardened cement paste as measured at room temperature after correcting for the temperature dependence of the water viscosity. Powers justified this by stating that freezing takes place in the capillaries, not in the gel pores, and he claimed that the capillaries are isolated cavities in the gel. Thus, said Powers, the overall permeability should not be dependent on the amount of ice formed. This may be so, but because water will have to be expelled through the gel pores, it is the permeability of the gel that should be the limiting factor. This would alter the values of the permeabilities that Powers used for his calculation by a factor 5-50. Thus it seems that the permissible spacing should be considerably smaller than what was calculated by Powers and therefore that the validity of the proposed mechanism may be doubted. (This opinion is further strengthened when the temperature dependence of the viscosity of water is considered, figure 2.2.6.).

Another possible objection is that if hydraulic pressure is what causes expansion of specimens during cooling, then the expansion should diminish if cooling, and thus ice formation, is stopped. To my knowledge, no such observations have ever been made. This may possibly be explained by the simple fact that if the hydraulic pressures have been able to cause expansion of the specimen, it may have been damaged to an extent

that it cannot return to its original dimensions. Furthermore, if permeability is not affected by ice formation (as assumed by Powers), it seems likely that the most intense hydraulic pressures should develop when super-cooling is annulled and thus that significant damage should already be occurring at temperatures slightly below 0°C. In contrast to this, sudden *reversible* expansions appearing at the moment when freezing begins (a few degrees below 0°C) have been observed by many researchers studying dilation, *e.g.* Powers and Helmuth [P 1953], Fagerlund [F 1972], Kaufmann [K 1997] (in fact, such expansions are seen even in figure 4.2.2 at -2°C.) Such reversible expansions can hardly be explained by any phenomenon but hydraulic pressures, but at the same time they reveal that not even the hydraulic pressures generated by the heaving of super-cooling are large enough to cause damage, at least not in a pore system which is not clogged by ice.

These doubts may be strong evidence for another hypothesis later proposed by Powers and Helmuth [P 1953]. They had observed that specimens of non air-entrained pastes would expand during cooling and keep expanding during periods of constant sub-zero temperature, while specimens of air-entrained paste would contract. These observations were impossible to explain using the hydraulic pressure hypothesis. The fact that expansion would continue during periods of constant temperature was especially contradictory to the hypothesis. In actual fact, however, in Powers' figure showing the most striking example of expansion during times of constant temperature, figure 4.2.1, one might object that expansion (and probably freezing too) did not begin before -19° was reached, which in turn is an indication of strong super-cooling (which is quite likely to occur at this high cooling rate, appr. 30°C), and thus that part of the subsequent expansion may be due to delayed ice formation.

Powers and Helmuth explained the observations by a mechanism subsequently referred to as osmotic micro ice body growth. According to this hypothesis, freezing begins in some of the larger pores (and also in entrained air voids if there is water present in them). When cooling proceeds, the unfrozen water in the smaller pores will gain more free energy than the ice already formed, which will create a potential difference which will in turn cause moisture to move out of the small pores into the large ones where it

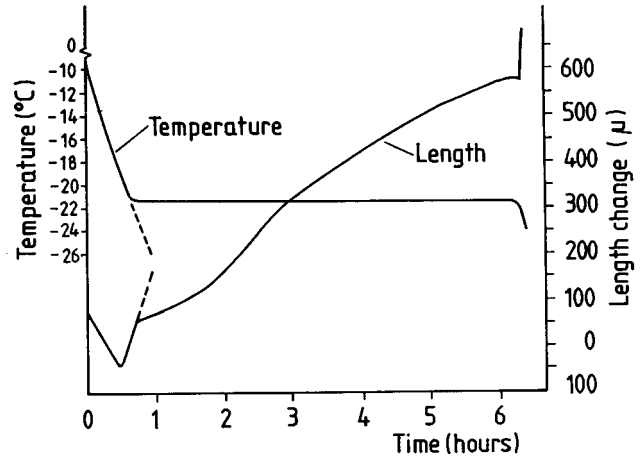

Figure 4.2.1: Example of expansion during a period of constant temperature. "Relatively dense paste", no air voids. [P 1953].

will freeze onto the existing ice bodies. This mechanism thus uses the same basic principles as that proposed by Taber on a sub-microscopic level. Such a mechanism, together with either the hydraulic pressures or the even simpler idea of over-saturated *in-situ* freezing (”closed container”), would explain all the observed phenomena. Powers and Helmuth claim that the expansions observed in air-free pastes when freezing commences or when cooling is resumed after a period of constant temperature, is due to hydraulic pressure. This, however, need not be true: it may well be that these expansions are also due to osmotic ice lens growth (provided the heat flow rate is not too high in relation to the water permeability), or to simple static ice pressure resulting from local over-saturation.

In passing, it should also be noted that Powers and Helmuth demonstrated the crucial importance of the spacing factor by presenting expansion curves together with the respective spacing factors, fig 4.2.2, and claimed that the expansions were due to too large spacing factors. However, the different air void systems of the tested materials had been obtained by using different amounts of air-entraining agents, thus the total air void volume also varied (but was not shown). For this reason, it cannot be said whether it is the short transport distances or the increased volume of air that is the determining factor.

Helmuth [H 1960] studied freezing phenomena in hardened Portland cement paste by studying dilation during cooling to sub-freezing temperatures. His findings support his hypothesis that ice forms dendritically in super-cooled water in the capillaries. (Helmuth had also found that super-cooling readily occurred down to -15°C and thus concluded that ”There is apparently no feature of the structure of the paste which can serve as a nucleation site for ice formation higher than this.”) He also found that ”…the expansion

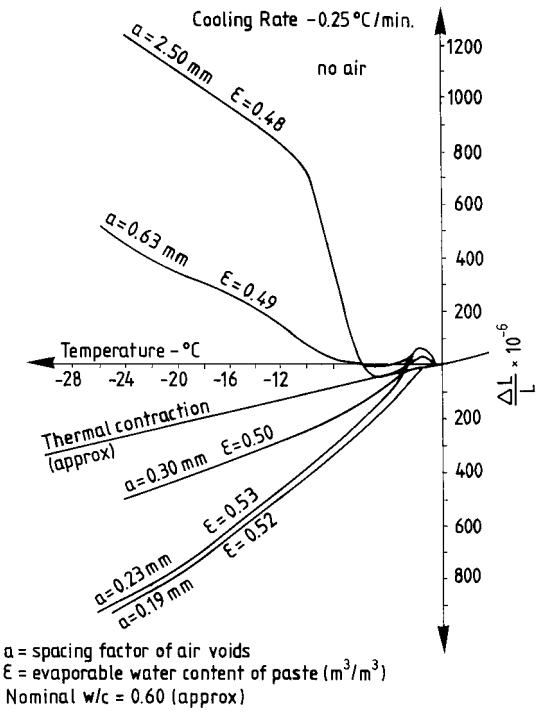

Figure 4.2.2: Effect of air entrainment on expansions of paste specimens during cooling. [P 1953]

rate during the initial freeze is rather small even though the rate of ice formation, as indicated by the rapid rise in specimen temperature, is much greater than during the subsequent progressive expansion". This indicates that the hydraulic pressure theory cannot explain damage caused by freezing, at least if it is assumed that permeability remains unchanged during freezing. These findings obviously contradict the hydraulic pressure hypothesis.

Some 25 years after the hydraulic pressure hypothesis had been developed and tested, more data were at hand and Powers [P 1975] wrote, "It became evident that most of the effects of freezing in cement pastes were due to the movement of unfrozen water to the freezing sites…" This conclusion was partly based on the work of Helmuth [H 1960], in which it had been shown that slightly desiccated pastes would initially shrink during cooling and would start expanding only after some critical temperature level was reached.

Everett [E 1961] described the thermodynamics of frost damage in porous materials and showed that, when at equal temperatures, super-cooled water and ice (each having the properties of their respective phases in bulk) must be separated by a meniscus with a radius of curvature small enough to produce the pressure difference between the phases which may be calculated from the Clapeyron equation (or estimated from the phase diagram). Everett's resulting equation reads:

$$r = \frac{2\sigma}{\Delta P}$$

in which σ is the energy of an interface separating liquid water from ice, r is the radius of curvature and ΔP is the pressure difference. Presuming the ice – pore wall contact angle to be 0°, Everett states that ice does not spread from a large pore into a small one if the radius of curvature of the meniscus separating the phases is larger than the radius of the small one. Thus before ice may spread from a large pore into a narrow pore of radius 10 nm, the pressure in the ice must be some 6 MPa.

Haynes [H 1964] carried out calculations based on the thermodynamics described by Everett and found that this "capillary effect" might to some extent be responsible for frost damage, although he doubted whether freezing in porous solids follows an equilibrium path, which is a requirement for the calculations to give correct values. Haynes, however, stressed the fact that the existence of this mechanism is undeniable.

Haynes also criticises the hydraulic pressure hypothesis put forward by Powers by claiming that an "approximate calculation" shows that the forces needed for disruption may be produced only under "exceptionally severe freezing conditions and with pores of less than 10^{-6} cm radius". Still, he recognises its ability to correctly predict that susceptibility to frost damage increases as the pore size of the medium decreases and as the freezing rate increases. (He nevertheless gives no examples of such observations.)

Dunn and Hudec *[D 1965]* studied frost deterioration of rock and proposed another mechanism of frost deterioration. (The description given here reflects that given by Cady [C 1969]). According to Cady, Dunn and Hudec had found that "smaller percentages of water of the contained water froze in unsound rocks than in sound rocks. In several instances, no freezing at all was detected in unsound rocks, and when freezing did occur in those rocks it was very gradual. Sound rocks, on the other hand, invariably displayed some freezing, and it usually occurred as a single pulse." Another observation was that water adsorbed at 100% relative humidity was not freezable! (Cady states this without

further comment.) They also found that unsound rocks tend to have large quantities of water taken up at relative humidities less than 45%. Dunn's and Hudec's explanation of these observations was that ”the major mechanism in the frost destruction of rock is a temperature-dependent volume change of adsorbed or ″ordered″ water contained in intergranular ″force spaces″ ” (in the words of Cady).

Criticising the fact that Dunn's and Hudec's investigations were limited to one type of aggregate only (clay-bearing dolomitic limestone), Cady undertook further investigations of the proposed mechanism. Using ”nine aggregates of widely varying mineralogical composition” he found that the hydraulic pressure hypothesis explained most of his observations, but also that the mechanism proposed by Dunn and Hudec was active.

In my opinion, unsoundness of water containing small amounts of freezable water may be explained if at the same time these materials were close to saturation. If they were, then only a very small amount of ice formation is needed in order to create very high pressures (see above regarding closed container). The fact that samples showing large amounts of freezable water were not destroyed may be explained in the same way, if it is assumed that the pore systems of these samples were not over-critically saturated. Since data on the degree of saturation is not available, it cannot be said whether these explanations are reasonable. The observation that materials that were sensitive to frost attack tended to contain large amounts of water adsorbed at relative humidities less than 45% may also be explained as being due to micro ice lens formation. This possibility was foreseen by Powers and Helmuth as early as 1953 [P 1953] and was also later pointed out by Hallet *et al* [H 1991].

Helmuth [H 1961] studied volume changes due to phenomena similar to those described by Cady in cement-based materials. Helmuth, however, did not mention that the temperature dependent re-location of water could possibly cause damage to the materials. On the contrary, he pointed to the fact that, in specimens (without entrained air) saturated at room temperature, some air-filled spaces would result from the initial cooling from room temperature during a frost resistance test, and that this would allow some ice to form without causing disruptive pressures. (These moisture movements would be due, according to Helmuth, to the lower entropy of water held in narrow pores as compared to that in coarser pores. When temperature is lowered, this causes a gradient in the level of free energy which tends to push water from coarser to finer pores.)

Helmuth proposes an equation for the effect of a temperature change on the degree of saturation of the capillary pores for a specimen cooled in air from +25° to ±0°C°. According to this equation, the degree of saturation may be reduced from 1.0 to 0.94 (independent of cement paste quality). Suppose the capillaries make up half the total porosity, then the overall degree of saturation may be reduced from unity to 0.97. Such a reduction would definitely have a large influence on frost resistance. Since the size of the capillaries vary over a wide range and since the described phenomenon is due to surface forces, Helmuth argues that the emptying effect of the temperature change would be larger in the large capillaries and smaller in the smaller ones. This in turn, he says, might render impossible *in-situ* freezing in the larger ones. Helmuth also has experimental results which show that this is true for pastes of *w/c* above 0.6. In pastes of lower *w/c*, though, expansions appear at the same temperature as in pastes in which the capillary pores have remained completely saturated.

Beaudoin and MacInnis [B 1974] ran dilation tests on $25 \cdot 25 \cdot 150$ mm^3 prisms of hardened Portland cement paste containing fly ash. Some specimens were saturated with water, while others were saturated with benzene, a liquid which contracts on

solidification. The specimens were then cooled at a rate of 2.5°C/h to -18°C. Despite the contraction on freezing, samples saturated with benzene expanded for some 40 minutes after nucleation had been initiated (at approximately +7°C). After the 40 minute period, the specimens contracted more than what could be expected from pure thermal effects. The authors thought there were three super-imposed effects causing this dilation: "…contraction due to migration from small pores or interlayer regions, dilation resulting from physical pressure of crystals due to boundary constraint and dilation due to hydraulic pressure." The authors explained it was mainly the hydraulic pressures arising as a result of migration of unfrozen benzene from small pores into those where nucleation had occurred that was the cause of expansion. It seems strange that this kind of flow, which is to be compared with a suction, should be able to cause expansive hydraulic pressures. On the other hand, it is also perplexing that in a closed system, relocation of the liquid from the small pores into larger ones, accompanied by volumetric contraction of the liquid, would cause expansion.

Litvan [L 1972] reported results from experiments on freezing of porous glass and cement paste. He concluded that moisture starts moving from the small pores out to the surface (or into large cavities) when temperature drops below 0° (*i.e.* even *before* any freezing has occurred), where it later freezes (*i.e.* at temperatures significantly below 0°C). He claims that damage results when the distance for the water migration is too large and/or when the amount of water which has to leave the small pores is too large. "The implication is that expansion occurs if the water concentration is much higher than the equilibrium value at the prevailing relative humidity." Litvan, however, does not explain exactly why expansion occurs because of a high water content.

An interesting aspect of Litvan's results is that it was possible to cool a 3.2 mm thick sample of *w/c* 0.7 in a state of full saturation at a cooling rate of 2.5°C/h without any expansion occurring above -40°C. At this low temperature expansion did occur, but it seems that no permanent dilation was obtained. In the interval $-20<\theta<0$°C, the sample contracted on cooling and expanded, reversibly, on heating. This behaviour may be explained if one assumes that ice did form on the sample surfaces and that moisture subsequently migrated out to this ice shell and then, later on as it melted on heating, migrated back into the pores. From his D.T.A. measurements, however, it seems that the expansion obtained at -40°C is not accompanied by freezing, *i.e.* there are no peaks on the D.T.A. curve. Litvan gives no explanation for this phenomenon. Whether it is due to ice formation (although invisible on the D.T.A.-curve) or some other phenomenon (like the ordered-water hypothesis of Dunn and Hudec) is impossible to say.

Considering that Litvan used very thin samples (1.25 and 3.2 mm thickness), his observations may be explained by the micro ice lens segregation hypothesis proposed by Powers and Helmuth. For example, the shrinkage of fully saturated 3.2 mm thick samples of *w/c* ratio 0.70 indicates a critical thickness of more than 3.2 mm for this kind of material. (The term critical thickness is explained below.) From geometrical calculations by Fagerlund [F 1986], this corresponds to a Powers spacing factor of approximately 0.7 mm. This is in good agreement with Powers' original calculations, but is larger than values normally reported as critical, including values reported by Powers and Helmuth [P 1953], [I 1970], [C 1963].

Litvan [L 1980] realised that unfrozen water in small pores may diffuse to nearby ice bodies and claimed that damage is due to the tensions caused by the moisture content gradients which develop when part of a specimen is dried. The fact that drying above 0°C

does not cause similar damage is explained by Litvan as due to the fact that drying at room temperature is rarely as fast as it often is during freezing.

Litvan says that when a specimen is cooled, its content of unstable water increases and at the same time, the rate of transport is decreased. According to Litvan, this results in formation of a non-crystalline, amorphous solid (ice). Litvan does not explain why this kind of ice forms, neither does he explain what led to his conclusion that it is not ordinary ice.

Hallet *et al* [H 1991] studied segregation ice growth in Berea sandstone and found, using a technique based on acoustic emissions, that the same phenomenon as described by Taber regarding soils, is also active in stone, although on a microscopic scale and provided the stone is frozen with access to moisture (*i.e.* as an open system). They found that the fracture activity was most intense at temperatures lower than the initial freezing temperature, typically at -3 – -6°C. They also found that too low temperatures may slow down the process due to hindered water transport and that there was also an upper temperature level above which the ice would not be able to exert pressures high enough to damage the stone. The authors also studied this phenomenon in granite with pre-existing cracks and again found that ice would grow by consuming water from an outer source. Hallet *et al* further point out that cyclic freezings need not be the worst case. In fact, sustained periods of constant sub-zero temperatures, along with a temperature gradient and access to moisture, may be even more likely to produce damage.

Hallet *et al* also discuss the mechanism proposed by Dunn and Hudec and say that Dunn and Hudec, due to the common lack of knowledge about the physics of frozen porous media at the time they forwarded their hypothesis, perhaps did not realise that less frozen water at a certain temperature implies more unfrozen water which in turn will increase the hydraulic conductivity of the material and will thus facilitate segregation ice growth. Finally, Hallet *et al* say that sorptive and frost effects at subzero temperatures are difficult to separate and that because they arise from identical surface–liquid interactions, it may not be worthwhile doing so.

One possible mechanism of frost-induced deterioration is based on the large coefficient of thermal volume change of ice as compared to water. Thus if ice forms within the pores, then the amount of ice forming in a certain pore at a certain temperature is adjusted so that its volume suits that particular pore. On subsequent heating, if there is a true (in contrast to super-cooling) hysteresis between freezing and melting, this ice will expand more than the cementitious matrix and expansion will occur. To the knowledge of the author, this mechanism has not been published anywhere, but was proposed and discussed by Mette Geiker at a seminar on the mechanisms of frost- and salt-frost deterioration of building materials held at our division in Lund, Sweden, in April 1996.

Summarising section 4.2.1, the three most commonly recognised mechanisms are:

- Closed container: high pressures develop when a pore volume initially contains so much water that it cannot accommodate the ice (and eventual remaining water) which forms during freezing.
- Hydraulic pressure: although the volume increase due to ice formation is not enough to completely fill the pore system, the pressure arising in the pore water due to the low permeability of the matrix surrounding the pore in which water freezes is too low.
- Osmotic ice body growth (macro/micro): due to differences in level of free energy, thermodynamically unstable water diffuses towards pores in which ice has formed.

This may occur both on a macroscopic scale, as in soil heaving, and on a microscopic scale, as in cement-bound materials or in natural stone.

Which of these mechanisms is the most important has yet to be determined.

4.2.2 Critical degrees of saturation

Since the proposed mechanisms require precise knowledge of several parameters and are also complicated to treat mathematically, simpler ways of estimating frost resistance have been developed. One such technique is based on the concept of a critical degree of saturation. Because some of the results from such studies may help in understanding the mechanisms of frost deterioration of concrete, a few works in this area will be mentioned.

From the description above concerning freezing of water in a closed container, it can be clearly seen that when the water content exceeds a certain value, deterioration is likely to occur. The degree of saturation at which this occurs is defined as the Critical Degree of Saturation, S_{cr}. In many types of building materials, however, not all water freezes at 0°C, (*e.g.* figure 2.3.3). Thus a larger degree of saturation than the above mentioned 91.7% may be allowed. To allow for this, the *effective* degree of saturation should therefore be defined:

$$S_{eff} = \frac{V_f}{V_f + a} \qquad (4.2.1)$$

in which V_f is the volume of freezable water and a is the volume of air contained in the pore system. In real materials, it is often difficult to accurately determine the amount of freezable water and therefore eq. (4.2.1) has found little use. Whiteside and Sweet [W 1954] and Vuorinen [V 1969] seem to be the only researchers who have used this definition of the degree of saturation to any appreciable extent.

A simpler definition of the degree of saturation is the straight forward:

$$S = \frac{V_w}{V_{pore}} = \frac{V_w}{V_w + a} \qquad (4.2.2)$$

Although physically less well founded than eq. (4.2.1), this definition has been shown to be very useful for studies of frost deterioration, *e.g.* Breyer [B 1955], Watson [W 1964] and Fagerlund [F 1972], [F 1977].

The concept of critical degree of saturation has proven successful in distinguishing between materials of good and poor frost resistance, at least in the laboratory. Whiteside and Sweet [W 1954] studied critical degrees of saturation and found this parameter to be determinative of the severity of damage freezing would cause in a material. The authors defined the degree of saturation according to eq. (4.2.1). The amount of freezable water V_f was calculated according to expressions derived by Powers and Brownyard [P 1948]. This procedure is very doubtful, partly because the amount of freezable water in a specific concrete is very much dependent on its microstructure, which is in turn dependent on factors such as type of cement, mixing and casting technique and also storing, and partly because the Powers and Brownyard expression was valid for freezing at -20°C, while Whiteside and Sweet froze their specimens only to -10°C. Since the

authors also emphasise the importance of small variations in amount of freezable water, and that this may easily overshadow other factors, it seems hazardous to use this very simplified technique for determining amounts of freezable water. Furthermore, since thawing was done in water, the degree of saturation may have varied considerably during the test.

Watson [W 1964] studied the frost resistance of bricks and also discussed the mechanisms responsible for deterioration and explained his results with an hypothesis somewhat similar to the concept of critical degree of saturation. Watson cooled his specimens to -2 – -5°C rapidly and then held the surroundings at constant temperature. This usually resulted in super-cooling which, when annulled, resulted in rapid ice formation. Watson discusses the possibility that when ice formation starts in brick, the surface layer is sealed with ice, and subsequent freezing will thus cause an increased degree of saturation in the specimen interior so that finally the brick is frozen like a ”closed container”, *i.e.* like in a vessel with perfectly non permeable walls which is saturated in excess of S = 0.917. However, one cannot tell from Watson’s paper, whether ice formation started at the surfaces and spread inwards. Thus one cannot say whether this ”closed container” model is correct. Watson concludes that ”for frost-resistance tests on porous materials, too slow, as well as too rapid, freezing is to be avoided.”

The proposed sealing of the specimen surfaces with ice requires that most of the water freezes in a narrow temperature interval, since otherwise many pores would still be open to moisture transport. This may be the case for brick, but for cement-bound materials, which have very spread-out pore size distributions and large freezing point depressions, such sealing seems unlikely, especially when cooling is slow. Ice-induced surface sealing to so vast an extent that subsequent freezing acts like that in a closed container, seems unrealistic.

Fagerlund [F 1972, F 1977] continued the study of critical degree of saturation and showed its validity for a large number of different materials. In contrast to Whiteside and Sweet, though, Fagerlund used the definition in eq. (4.2.2). By combining the levels of critical degree of saturation with the rate of moisture absorption (under constant climatic conditions), Fagerlund was able to estimate what he calls the ”potential service life” of a material. This term is used to emphasise that the true service life cannot be determined, since this will be heavily affected by the way the micro structure of a certain material changes in the very environment to which it is exposed, and also because the mechanisms of water uptake (after the nick-point level in a test on capillary suction) and the way these develop over time are not known. This way of comparing critical degrees of saturation with the rate of moisture uptake may be seen as a parallel to determining, on the one hand, the strength of a load-bearing structure and, on the other hand, the various loads to which it is assumed to be subjected. In [F 1977], Fagerlund presented results from an international test involving five laboratories. Two concretes, one of *w/c* ratio 0.57 with air-entrainment and the other of *w/c* ratio 0.50 without air-entrainment, were tested. Despite rather large variations in the frost cycles used by the laboratories, the results showed small variations and all laboratories rated the frost resistance of the two concretes in the same way. It therefore seems safe to say that frost resistance is not very dependent on cooling rate and also that this test method is simple enough to give reproducible results (in the interval $0>\theta>-17$°C, the cooling rates varied from 1.8 to 5.8°C/h, the total duration of freezing varied from 7.5 to 14 h, while minimum temperature varied only in the interval $-18>\theta>-22$°C). From the calculated critical degrees of saturation and the air void characteristics, Fagerlund calculated the critical air content (*i.e.* the volume of air in

a specimen when critically saturated), to be 1.5% and 4.2%, respectively, for the 0.50 and for the 0.57 concrete.

Despite its seeming simplicity and reproducibility, to the knowledge of the author, the test method described by Fagerlund [F 1977] has been adopted as a standard test method only in Switzerland. (The Swiss, however, have introduced some minor changes as compared to the original procedure described by Fagerlund, see *e.g.* Studer [Sr 1993])

4.2.3 Mechanisms involving effects of the air pore system

The air pore system has a large influence on the frost resistance of concrete and thus its properties and the time dependent changes of its properties must be considered when trying to estimate future behaviour of concrete under frost attack. Such work has been carried out and published in a series of reports by Fagerlund [*e.g* F 1977, F 1982, F 1990, F 1994]. For example, in [F 1977] it was shown that after 14 days continuous water storage, 35% of the air pore volume in a non air-entrained concrete was filled with water and that the corresponding value for an air-entrained concrete was about 10%. Fagerlund has described the mechanisms of water uptake in the air pores and has shown how the air pores are inactivated after long periods of continuous water storage [F1996].

Helmuth [H 1961] points out that water in entrained air pores serves to keep the capillaries completely saturated during cooling. This means that the air pores, or rather the water held in them, reduces the positive effect on the degree of saturation caused by a temperature drop. This might partly explain why the critical degree of saturation is lower for an air-entrained concrete than for a plain one. (Results from Fagerlund [F 1977] show that air-entrainment reduces the critical degree of saturation more than may be expected from a simple calculation of the change in porosity caused by the use of air-entrainment.)

4.2.4 Proposed mechanisms of combined salt- and frost attack

Neither Arnfelt [A 1943] nor Verbeck and Klieger [V 1957] gave any mechanistic explanation of their observations. Nevertheless, in both reports it was concluded that the mechanism is of a physical rather than purely chemical character.

Powers [P 1965] proposed that the detrimental effect of de-icing salts was due to a combined effect of osmotic and hydraulic pressures. The osmotic pressures would be due to the presence of salts and, since this would draw more moisture into pores where ice and salt existed together, the subsequently increased ice formation in these pores would cause increased hydraulic pressure when water was expelled from these pores. Powers also states that de-icing salts will spread much faster in the capillary pores than in the gel pores and that the salt concentration gradients thereby formed between gel pores and capillary pores would promote this mechanism.

Powers' explanation seems dubious because of the following: after freezing has begun in a salt solution, the chemical potential of the remaining salt solution will be equal to that of the ice. Thus, at a given temperature, the combined ice and salt solution mixture would have no more intense ability to attract water than would a pure ice body at the same temperature. As seen in chapter 2, the presence of salts (or any other dissolved matter which acts to lower the freezing point of water) will reduce the pressure difference needed for equilibrium between ice and pore water. This means that the presence of salts in the pores should reduce the severity of frost attack. Furthermore, it was subsequently shown that it is the outer salt concentration that is the main factor in salt frost scaling tests.

Snyder [Sy 1965] refers to *Hartmann [H 1957]* and concludes that neither crystallisation of de-icing salts within the pores, nor chemical reactions between the salt and the cement compounds, nor osmotic pressures super-imposed on hydraulic freezing pressures, nor heat of solution effects resulting in temperature differentials during thawing can possibly be the reason for ”salt scaling". Instead, Snyder found that scaling would appear when there was a steep salt gradient beneath the concrete surface. Snyder also used water as outer liquid but arranged his test so that the interior froze before the outer water had frozen (using an immersion heater). When the interior had frozen, the heater was turned off whereupon the outer water froze. This resulted in relatively rapid scaling. Snyder's interpretation was that it was the temperature gradient that was critical. He thus concluded that ”The development of a concentration gradient through the depth of the concrete is the primary cause of scaling. The ultimate effect of the concentration gradient probably is to produce excessive thermal and hydraulic pressures through its effect on the freezing point of the liquid phase within the concrete.” Snyder also thought that osmotic pressures caused by the salt in the pores was not the reason for deterioration.

By keeping the outer water in the liquid state after the inner parts had frozen, I believe Snyder created ideal conditions for micro ice lens growth beneath the surface. This is also an essential part of the mechanism proposed in chapter 6.

Litvan [L 1974] studied the effect of de-icers on thin (1.27 mm) discs of cement paste. The discs were stored in NaCl solutions for 120 days in order to equally distribute the salt throughout the specimens. Expansion measurements (during cooling at 20°C/h) showed that specimens that had been stored in a 5% solution expanded more than those stored in both weaker and stronger solutions. It seems that the degrees of saturation were not determined. Litvan's hypothesis on salt-free frost deterioration was used to explain this behaviour: as cooling proceeds, moisture starts migrating out of the pores towards the specimen surface (because Litvan had found that freezing could not take place in the capillary pores). When the moisture reaches the outside, it freezes. However, Litvan claims, if the migrating water contains low levels of salt, it will freeze at the mouth of the capillaries and thus cause a blockage which will in turn lead to ”…highly non-equilibrium conditions…” which, according to Litvan's earlier findings, is the reason for frost deterioration. It seems to me this does not explain why surface damage is non-existent when there is no outer solution. Furthermore, Litvan does not explain why a low amount of salt in the pore system would be able to cause more ”blocking” than what will be the case if the pore solution is pure water. In such a case there is nothing to stop the ”blocking effect” proposed by Litvan and thus it should be even easier to reach states of non-equilibrium with pure water.

Browne and Cady [B 1975] explained the optimum in scalings obtained with a moderately concentrated calcium chloride solution. They assumed the optimum was the result of two conflicting mechanisms, the first a physical one and the second a purely chemical one. The physical one comprises two effects: firstly, the stronger a calcium chloride solution, the lower its freezing point and, thus, the more calcium chloride there is in the pores the less ice will form, which in turn will act to reduce the hydraulic pressure. Secondly, the vapour pressure of the calcium chloride solution (outside the specimen surface) decreases with increasing concentration and thus acts to draw moisture out of the pores. Further, it was known that calcium chloride solutions cause disintegration of concrete and the authors hold this to be the chemical mechanism responsible for the increase in damage obtained when using strong solutions. They also claimed that the effect of strong sodium chloride solutions on concrete, in the absence of

freeze-thaw cycles, had not been well documented. Clearly, this hypothesis is in conflict with the conclusions drawn both by Arnfelt and by Verbeck and Klieger and it does not explain why there is a ”pessimum” de-icer concentration even for ethyl alcohol and other chemicals which are known not to damage concrete by any chemical mechanism.

MacInnis and Whiting [M 1979] ran dilation tests to investigate a hypothesis proposed by Litvan, according to which salt in the pores acts to retain more moisture under given climatic conditions, which in turn might lead to more severe frost deterioration. Prisms ($150 \cdot 25 \cdot 12.5$ mm^3, non specified qualities) were dried in 0% R.H. two days and then saturated with NaCl solutions (0, 1.5, 3 and 10%) by vacuum treatment. The specimens were then stored at different relative humidity (100, 88, 72, 47 and 30%) until the weight changes were less than 0.002 g/day.

After this conditioning, it was seen that the moisture content was higher the higher the NaCl concentration used for impregnation. Upon subsequent dilation testing, however, specimens stored at a relative humidity of 88% or less were not affected by freezing. (The NaCl concentrations in the pores were not corrected with regard to moisture loss due to drying. No salt concentration measurements were given.) For specimens tested in a fully saturated condition, different results were obtained depending on the number of frost cycles: after the first cycle, expansion was largest for specimens impregnated with pure water and considerably less for specimens containing salts. (The numbers of specimens impregnated with 1.5% and 10% NaCl solutions were too small for any safe trend to be discerned between specimens containing salt). After 5 cycles, however, the cumulative residual expansions were equal in specimens impregnated with water and those impregnated with the 3% solution, while those impregnated with 1.5 or 10% solutions showed less than half as much expansion. The authors concluded that a 3% concentration results in the most severe expansion. However, the mean difference was less than 10% and thus it seems one should not draw overly far-reaching conclusions from the results. Unfortunately, again, the numbers of specimens impregnated with 1.5% and 10% NaCl solutions were small, but from the reported values it seems that both of these caused less damage than did the 0% and 3% solutions. From the results by Fagerlund, *e.g* [F 1977], it can be seen that even very small variations in moisture content may cause large changes in measured deterioration due to frost attack. Thus, if the pre-storage procedures used by MacInnis and Whiting resulted in varying degrees of saturation *in addition* to varying salt concentrations, it may well be that it is primarily the moisture content effect that was seen in their results.

Since only fully saturated specimens or specimens in equilibrium with 88% RH or less were tested, it cannot be said whether the hypothesis (that salt content will lead to more severe frost-induced damage due to the increased moisture content) is correct.

Rösli and Harnik [R 1980] hypothesised that severe tensions in a concrete surface layer may be caused by thermal shock when an ice cover is removed by salting. Such a mechanism may be active in the field where de-icing salts are used, but it does not explain why salt scaling occurs when the salt solution is already present on the surface when freezing sets in (as in most laboratory testing and also in marine environments). Their calculations show that under laboratory conditions and with an ice layer of 2 mm thickness and strong salt solutions, it is possible to obtain temperature shocks which in turn may produce tensions of up to 4 MPa. Field studies showed that the temperature shocks were never large enough to cause tensions in excess of 1.4 MPa. Thus, the investigation shows that only in exceptional cases will temperature shock be the cause of disintegration. The mechanism therefore cannot be considered to be of any major

importance, even though it may, through repeated temperature shocks, cause micro crack formation which can later lead to changes in moisture content and amount of freezable water. It definitely cannot be active under circumstances where the salt solution is already present before freezing sets in.

Petersson [P 1984] proposed a mechanism based on the effect of super-cooling on hydraulic pressures. When the outer liquid is pure water, this will freeze and initiate freezing in the pores. Thus no super-cooling will occur and hydraulic pressures will be rather low. When the outer liquid is a salt solution, it does not help initiate freezing in the pores close to the surface and thus super-cooling may become considerable and on its annulment large hydraulic pressures may occur. This hypothesis thus requires that hydraulic pressure is the main cause of disintegration. When extensive super-cooling occurs, this might perhaps be possible, but it seems likely that the conditions for super-cooling in the pore liquid would be at a maximum when the surface is exposed to air, and thus surface scaling should also appear in the absence of an outer liquid. This, as far as I know, has never been reported. From determinations of critical air void spacing and related calculations on critical thicknesses, it also seems unreasonable that hydraulic pressures, or even osmotic ice lens growth in moisture isolated specimens, could possibly cause the thin flaking which is often observed.

Sellevold [Sd 1988] carried out an extensive investigation of the qualitative effects of different parameters in salt frost scaling tests. Among other things, he tested the importance of primary ice formation inside the specimens by taking them out of the cooling cabinet as soon as the minimum temperature was almost reached (after 4-6 h). This resulted in low scaling (as compared to specimens run in the usual way) and Sellevold therefore concluded that more time at the minimum temperature was needed for scaling to become severe and thus the mechanism was, somehow, an osmotic one. Obviously, this is in sharp contrast to what Snyder (above) thought and will be discussed in chapter 7.

Pühringer [Pü 1996] studied the effect of de-icers within the pore system on the frost resistance of cementitious materials. He explains that the detrimental effects of salts (and other dissolved substances) are due to changes in compressibility and temperature of maximum density of the salt concentration as compared to water. He says that, during thawing, a properly concentrated salt solution will expand more than does non-frozen water (at the same temperature). If there is still some ice blocking the pores, this will lead to high expansive pressures, especially since the compressibility of the salt solution is higher than that of water. According to Pühringer, increasing the salt concentration will lead to higher pressures during thawing, while lower concentrations will lead to higher pressures during cooling, because the volumetric expansion following upon ice formation is larger the purer the solution. When cooling and thawing are combined to form a frost cycle, Pühringer states there will be some intermediate de-icer concentration that produces the most severe stresses. Pühringer calculates this will be obtained with concentrations close to 2.5% b.w. for 9 different salts.

The hypothesis obviously requires that salts are present within the pore system. It does not provide an explanation as to why scaling does not occur in the absence of an outer solution, nor why a prolonged frost cycle produces more scaling, nor why it seems to be primarily the concentration of the outer solution that is important (as shown by Sellevold [Sd 1988] and also in section 5.1 of this report.)

While the physical effects may be dominant, chemical effects may also play a significant role in salt frost scaling. For instance, Stark and Ludwig [Sk 1997] propose

that in concretes containing granulated blast furnace slag (GBFS), carbonation may cause formation of unstable forms of $CaCO_3$ (vaterite and aragonite) which are dissolved in the presence of an NaCl solution. As a result, badly crystalline calcite is formed which, according to the authors, scales off quickly during salt frost scaling tests. The authors propose that this may explain why concrete containing GBFS is severely damaged by salt frost attack (after some carbonation has occurred) despite having air void systems of a quality that would normally be regarded as fully satisfactory.

4.2.5 Conclusions

It seems that no mechanism, either alone or in combination with other mechanisms, has yet been put forward which can explain all the observations mentioned in chapter 4.1.

4.2.6 Final remark

It has been determined on several occasions that the permissible spacing factor is some 0.25 mm. Fagerlund [F 1986] used this to calculate the critical thickness of a thin sheet of cement-paste. According to his results, a completely water-saturated specimen of cement paste will be frost resistant if its thickness is less than approximately a millimetre. Direct measurements support this finding [L 1991], [F 1993]. The flakes which are obtained in salt frost scaling tests are often considerably thinner than this. Flakes of a thickness of 0.2 mm, and even less, are common. Obviously, regardless of whether it is hydraulic pressures or osmotic ice lens growth that is the primary cause of frost deterioration in moisture-sealed specimens, neither of them can fully explain the phenomenon of salt frost scaling, unless some other factor is also considered. In chapter 6.1, a mechanism is proposed which draws primarily on the mechanism of osmotic ice lens growth, but which adds the improved moisture conditions for micro ice lens growth that result from the presence of an outer, liquid phase. Such a mechanism may explain the occurrence of such thin flakes.

5

INITIAL LABORATORY STUDIES

The following preliminary laboratory studies were undertaken:

- A study of the existence of a ”pessimum” salt concentration on the effect of minimum temperature and the effect of cooling rate
- A study of the salt frost scaling resistance of high strength concrete (”pessimum” salt concentration and effect of temperature)
- A study of chloride ion transport over short time periods

The first study was motivated by the fact that there have been very few tests in which the effects of de-icer concentration have been reported. Neither had the effects of minimum temperature and cooling rate been much investigated at the time these tests were run.

The second test was undertaken as a part of the Swedish National Program on High Performance Concrete, which was run during the years 1991–1997. The purpose was to study whether high performance concrete could be made immune to salt frost attack without the use of an air entraining agent. Furthermore, one questioned whether the ”3% pessimum” also existed for these high quality materials.

The study of the effect of salt concentration on capillary suction was run mainly as part of another project. Some of the results though were also interesting for this project, in that it showed that there is nothing in the pure capillary suction properties of cement-bound materials which might explain the existence of a ”3% pessimum”.

Finally, as an indication of the depth to which the mole fraction of water in the pore solution is affected by the presence of an outer salt solution during the hours preceding the start of freezing in a salt frost scaling test, a study was run on chloride ion transport into the concrete surface.

5.1 INFLUENCE OF TESTING CONDITIONS ON SALT FROST RESISTANCE OF CONCRETE

5.1.1 Introduction

This chapter describes results from studies of the salt frost scaling (SFS) resistance of three different concretes, two of which were high performance concretes. The main objective of the study was to detect a salt concentration which would produce maximum scaling in a traditional salt frost scaling test, similar to what had been found for ordinary concretes by Arnfelt [A 1943] and Verbeck and Klieger [V 1957]. Such knowledge may be essential in designing a test method for high performance concrete and the laboratory results may also be valuable when trying to understand the mechanism of salt frost deterioration.

The experiments presented in this section were originally carried out as part of the National Program for High Performance Concrete which was run in Sweden (and which included participants from Norway) during the years 1991-1997. The project was financed by the Swedish state through the Swedish Council for Building Research (BFR) and the Swedish National Board for Technical and Industrial Development (NUTEK) and through the private companies, Cementa, Euroc Beton, NCC, SKANSKA, Strängbetong and Elkem Materials of Norway.

This chapter is a compilation of three earlier reports from the National Program for High Performance Concrete. A few minor changes have been introduced.

5.1.2 Objective

The questions asked in this preliminary study were:

1. How is scaling affected by salts in the pores and salts in the test solution?
2. How does the shape of the frost cycle affect the test result?
3. Is it possible to establish a precise value for the most detrimental salt concentration, the ”pessimum” concentration?
4. Can high strength concrete be made salt frost resistant without air entrainment?

Three test series were run. In the first, the main purpose was to study the effects of frost cycle design and different combinations of salt concentrations. This was done using one single concrete quality, five different frost cycles and three different salt concentrations in the outer test solution as well as in the pore solution (the ”inner” solution) - a total of 45 variable combinations.

In the second series an attempt was made to precisely evaluate the ”pessimum” concentration, *i.e.* the concentration which would result in the most severe damage in a high quality concrete of water-cement ratio 0.35 without air entrainment. Ten different salt concentrations were used in the outer solution (no salt in the pores). Since the first series had shown ”pessimum” salt concentration to be independent of frost cycle design, this time only one frost cycle was used.

In the third series a concrete of even higher quality was tested with respect to different minimum temperatures, different salt concentrations in the outer solution, and with and without a short period of drying before testing.

For each combination of variables, three specimens were used.

5.1.3 Test method

The test arrangement is shown in figure 1. The test method resembles the Swedish standard SS13 72 44, known as ”The Scandinavian Slab Test”. The thickness of the specimens was reduced to 25 mm instead of the prescribed 50 mm in order to make measurements of resonance frequencies more distinct.

The concretes were cast in PVC-tubes of 350 mm in height and 127 mm in diameter. Specimens were then cut from these tubes with the PVC-tube still on. The specimens were moisture isolated with PVC-rings and then heat isolated with 20 mm cellular plastic as shown in figure 1. The surface was then covered with 40 ml of test solution (corresponding to a depth of 3.2 mm) and a plastic foil lid was put on. The salt solutions were mixed from tap water and sodium chloride.

After 7, 14, 28, 42 and 56 cycles, scaled-off material was brushed off the specimen surface, dried (105°C) and weighed. According to the Swedish Standard Test Method, the maximum allowable accumulated scaling after 56 cycles is 1,0 kg/m². Furthermore, scaling must not show a tendency to increase. This is measured by comparing the accumulated scaling after 56 cycles with that obtained after 28 cycles. The former must not be greater than the latter by more than a factor of 2.

Only those parts of the test procedure which were common to the three tests have been set out here. Details of each test are given below.

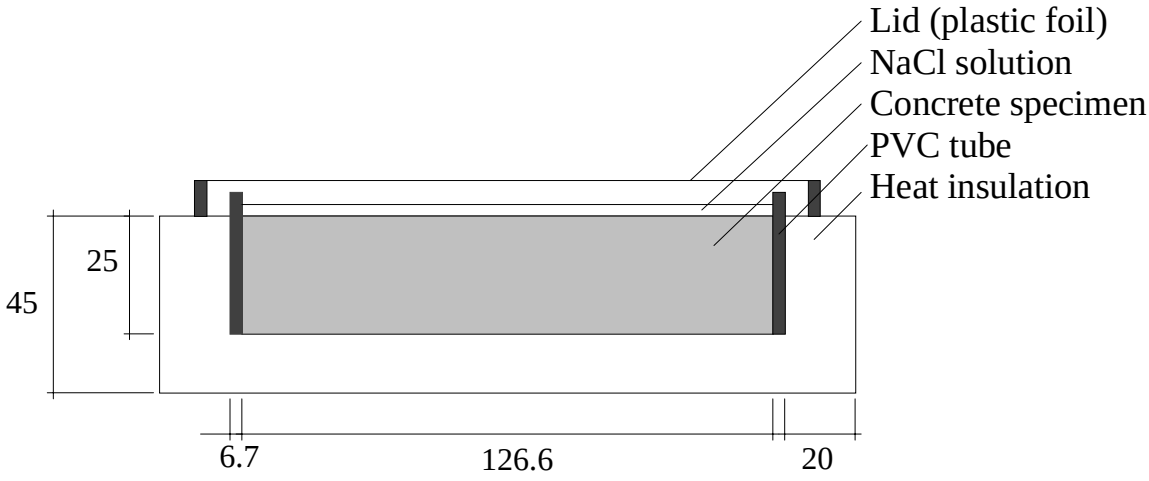

Figure 5.1.1. Test arrangement (dimensions in mm)

5.1.4 Series 1: Effects of salt concentrations, salt distributions and frost cycle design

The first questions were:

- Is it salts in the outer solution or salts in the pores close to the surface of the material that lead to the dramatic increase in scaling that is usually observed when testing a concrete specimen for salt frost resistance?
- Or is it only the difference between inner and outer salt concentrations that matters, *i.e.* is it the gradient across the uppermost millimetre of the material?
- How important is the shape of the frost cycle?
- Is it true that rapid cooling will result in more severe damages than slow cooling, as might be predicted from the Powers' Hydraulic Pressure Model?

The outcome of this series would decide which topics to concentrate on in the subsequent series.

Concrete

The concrete recipes of all three series are given in table 1. In the first series, a concrete of water-cement ratio 0.40 was used. It had only a small amount of air entrainment and its maximum aggregate size was 8 mm. The concrete was designed in this way in order to produce sufficiently even and severe scaling. The concrete was cast and membrane cured in the mould for six days. The specimen slices were then cut out, with the PVC-tube still mounted, and the specimens were distributed among their different salt solution baths.

Salt concentrations

By using different concentrations of salts in the outer solution and by pre-storing specimens for long periods (>6 months) in salt solutions of different concentrations, different combinations of inner and outer salt concentrations were obtained. The chosen concentrations were 0, 3 and 6% by weight. Accordingly, nine different combinations of

Table 5.1.1: Concrete mixes. The cement is the Swedish Anläggningscement, a low alkali, sulphate resistant Portland cement. Plasticiser additive: Melamin resin. Air entraining agent: Vinsol resin. Compressive strength was measured on 10 cm cubes.

Component		Series 1	Series 2	Series 3
Water cement ratio		0.40	0.354	0.299
Water binder ratio		0.40	0.337	0.271
Gravel	kg	---	977 (8-12)	1030 (12-16)
Aggregate (0-8)	kg	1315,5	800	746
Cement*	kg	622,9	466	480
Silica	kg	---	23,3 (dry)	48 (slurry 50/50)
Water	kg	249,2	164,8	143,3
Plasticiser, % by cement weight		---	0.84% (dry subst.)	1,3%
Air entraining agent	kg	0.013 (dry)	---	---
Air content, fresh		5,3%	0.2%	1,1%
Compressive strength		65, 28 days	114, 28 days	136, 90 days

**Swedish Anläggningscement, General Appendix 2.*

inner and outer salt concentrations were obtained. The specimens were pre-stored in their salt solutions for between 6 and 11 months (this pre-storage was begun at an age of 7 days). The salt concentration of the pore liquid of the specimens was not determined, but it seems safe to say that to a depth of 4-5 times the average thickness of the flakes scaled off during testing, *i.e.* between 1 and 2 mm, the salt concentrations were markedly different between specimens stored in different salt solutions.

Frost cycles

The different frost cycles used are shown in figure 2. These temperature curves were measured in pure water covering the specimens. When salt is added, quite another shape is obtained depending on the salt concentration, because salt lessens the amount of frozen water at each individual temperature level. For example in the case of cycle E, in which a rapid cooling is obtained once the pure water is completely frozen, this leads to a slower and more prolonged cooling phase. This will be commented on later in the report. The characteristics of the frost cycles are summarised in table 2.

Results

Average accumulated scaling for the three specimens tested in each frost cycle and with each salt concentration combination is set out in table 3. Generally, scaling is low and it is seen in Appendix 5.1.1 that the differences between individual specimens is so

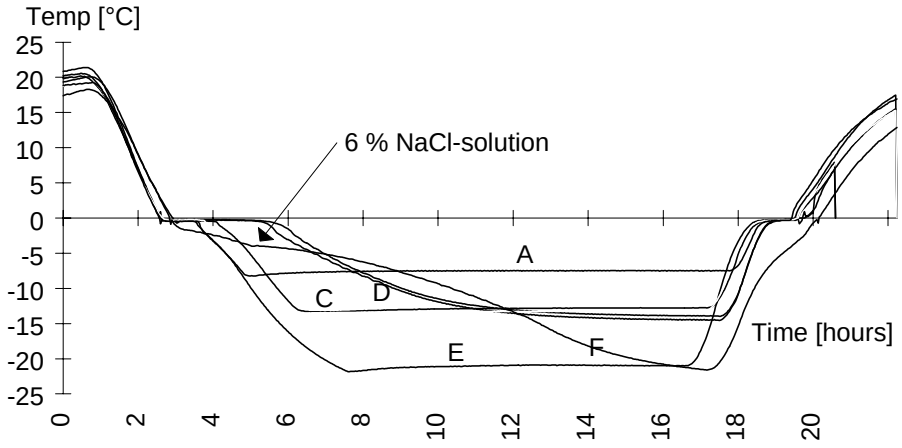

Figure 5.1.2: Frost cycles used in series 1. Cycle F measured in 6% NaCl solution.

Table 5.1.2: Characteristics of frost cycles in Series 1.

Frost cycle	Max. cooling [°C/h]	Minimum temperature [°C]
A	-5.5	-7
C	-5.5	-14
D	-2	-14
E	-5.5	-22
F	-2	-22

Table 5.1.3: Accumulated scalings [kg/m²] for different frost cycles (56 cycles), mean values for three specimens. *indicates a case where one specimen was missing, which means the mean value is calculated from only two specimens.

Outer salt concentration [%]	Desired inner salt concentration [%]	A -5.5°C/h -7°C	C -5.5°C/h -14°C	D -2°C/h -14°C	E -5.5°C/h -22°C	F -2°C/h -22°C
0	0	0.13	0.04	0.10	0.26	0.14
0	3	0.13	0.13	0.16	0.36	0.18
0	6	0.15*	0.40	0.30	0.45	0.41
3	0	0.20	0.38	0.45	1.79	0.58
3	3	0.17	0.64	0.57	1.66	0.48
3	6	0.17	0.84	0.73	1.53	0.57
6	0	0.22	0.29	0.49	0.33*	0.42
6	3	0.23	0.23	0.26	0.34	0.27
6	6	0.22	0.29	0.38	0.45	0.42

Approximate duration of pre-storage in salt solutions (≈age of specimens), months: A 7½, C 6, D 11½, E 7½, F 7½.

large that the significance of the differences between the different series must be questioned. An indication of the precision in this kind of test, although obtained with the CDF test method, was given by Setzer [S 1993], who reported that in the CDF test method, the coefficient of variation is some 15-30% at total scaling of 100-400 g/m² (28 cycles). The scatter increases with decreasing scaling. For example, the high average scaling obtained in cycle D with outer concentration 6% and inner concentration 0% is due to one ”flyer”, *i.e.* one of the three specimens shows about 3.5 times more scaling than the other two. Omitting this specimen lessens the mean value to 0.27 kg/m².

Dependence of scaling on salt concentrations

It can be seen from table 3 that for each cycle, except A, the most severe damage is observed to occur when the salt concentration of the outer solution is about 3%, regardless of the salt concentration present in the pores. With respect to cycle A, it can be seen that this frost cycle causes worse scaling as the outer salt concentration increases, and that an outer concentration of about 3% is not the worst case. Differences are small but very clear, even when considering each individual specimen.

When the outer concentration is 0%, damage tends to increase as the ”inner” concentrations increase. This is further commented in chapter 6.

Dependence of scaling on frost cycle design

For every salt combination, cycle E (-5.5°C/h, -22°C) causes the most severe scaling, with one exception: when the outer concentration is 6% and at the same time the inner one is 0%, cycles D and F give higher mean values. Although, as stated above, the value obtained for cycle D is suspect. Omitting the ‘flyer’ reduces the mean value from 0.49 to 0.27, which leaves cycle F the only cycle ”worse” than cycle E.

As for the rest of the cycles, it can be seen that A (rapid cooling to about -7°) gives very moderate scaling, while the others seem to be equally destructive.

By comparing cycles E (rapid cooling, low minimum temperature) and F (slow cooling, low minimum temperature), it can be seen that cycle E results in worse damage in the cases where the outer salt concentration is 3%, while the two cycles seem equally detrimental when the outer concentration is increased to about 6%. This may be caused by what was earlier described as the slowing effect on temperature drop in the specimen

surface due to the gradual freezing of a salt solution, which might result in the specimen surfaces in case E as well as in case F being cooled rather slowly. (Exact temperature cycles of individual specimens were not registered.)

5.1.5 Series 2: Study on the ”pessimum” salt concentration for a concrete of water-cement ratio 0.35

The results observed in series 1 made it desirable to clarify in greater detail what would be the ”pessimum” concentration for a high quality concrete. It also seemed interesting to see whether a high quality concrete could be made salt frost resistant without adding an air entraining agent.

Specimens were cast using a concrete of water cement-ratio 0.35 without air entraining agent, but this time with silica fume added (5% of the cement weight, giving a water binder ratio of 0.337). The complete composition is given in table 2. The test arrangement was identical to that of series 1 (figure 5.1.1).

Salt concentrations

Ten different salt concentrations were used: 0, 1.0, 1.5, 2.0, 2,5....5.0%. As in the other series, solutions were prepared from tap water and sodium chloride.

Frost cycle

Since cycle E had proved to be the most detrimental, and since the high concrete quality made it reasonable to assume that scaling would be very small, and since too little scaling might make it difficult to identify the ”pessimum” concentration, this cycle was chosen for series 2. Furthermore, in deciding whether or not a high strength concrete could be made salt frost resistant without air entrainment, using a harsh frost cycle would be ”on the safe side”.

Pre-treatment

In this series, the effect of a short period of drying and remoisturising before testing was also studied. Such a procedure has proved to increase the amount of freezable water in concrete (Sellevold and Bager, [B2 1986]), which in turn might lead to increased damage. It is also possible, depending on how severe the drying and how long the time for resuction, that the specimens, at the beginning of the test, are saturated to a lesser extent, making them, at least initially, more resistant. Which of these two effects will dominate for a given drying procedure, depends on the concrete quality.

In the series in question, specimens were cut out of their moulds one day after casting, and then stored in water for six weeks. Then half of the specimens were taken up to dry in dry air for one week (30±2%R.H./21°C) and then all the specimens were again stored in water for another week before beginning the test.

Results from Series 2

Figures 5.1.3 and 5.1.4 show the results for non-dried and dried specimens, respectively. It can be observed that dried specimens in general show a somewhat increased deterioration as compared with never dried ones.

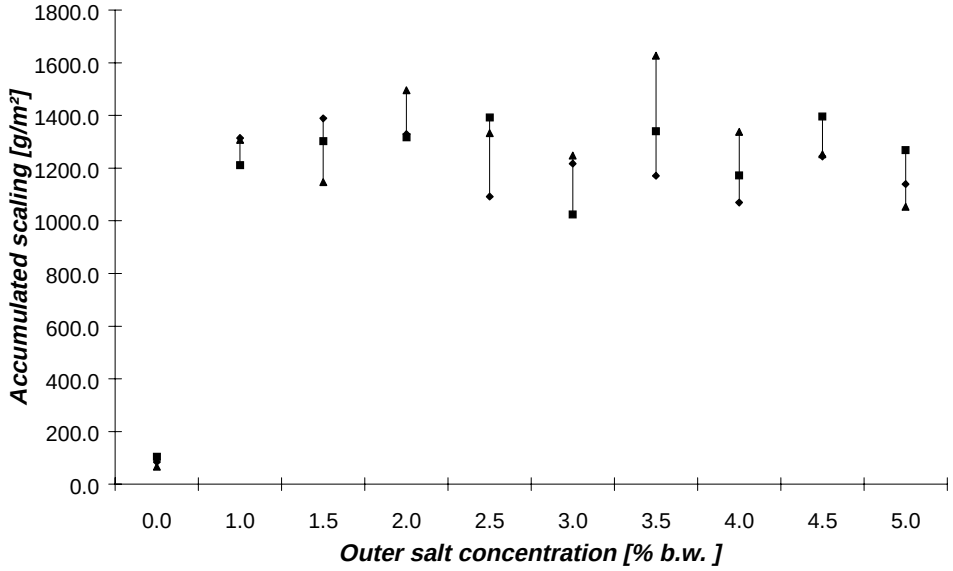

Figure 5.1.3: Accumulated surface scaling after 56 cycles in relation to salt concentration of the outer solution. Concrete w/c 0.35. Never dried specimens. One dot = one specimen.

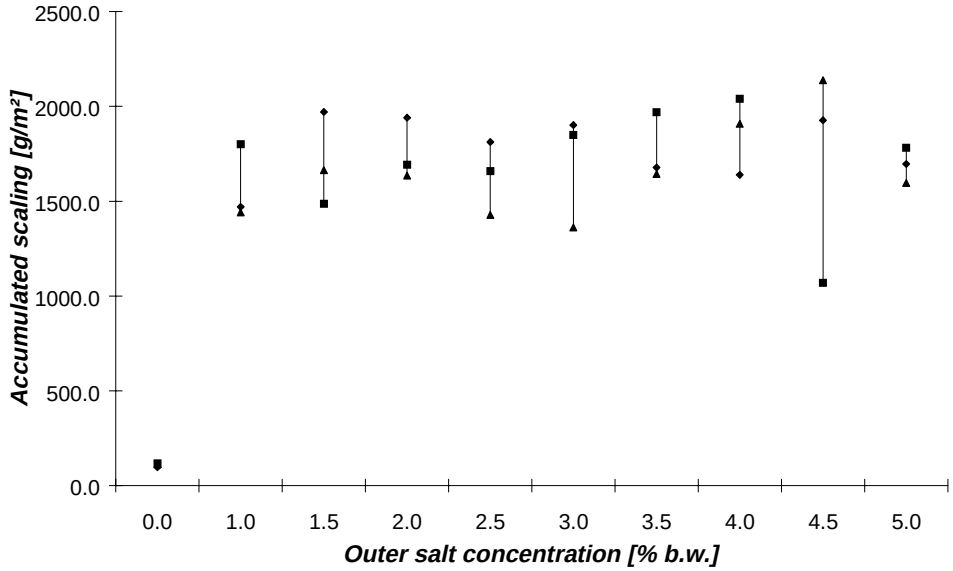

Figure 5.1.4: Accumulated surface scaling after 56 cycles in relation to salt concentration of the outer solution. Concrete w/c 0.35. Dried and remoistened specimens. One dot = one specimen.

Obviously, scaling is dramatically increased when salt is present in the test solution in comparison with pure water and it is an astonishing fact that no pessimum salt concentration can be distinguished for this concrete quality. This is contradictory to Arnfelt [A 1943] and Verbeck and Klieger [V 1957] but has been reported by Sellevold [Sd 1988]. This result is interesting in that it shows that the mechanism causing maximum scaling for a moderately concentrated solution on a conventional concrete is not active in this case. Of course, it might be that the ”pessimum” concentration is above the range tested,

i.e. more than 5%, but that seems unlikely, since the obtained scaling shows neither an increasing nor a decreasing tendency with salt concentration. The reason for this behaviour will be discussed in chapter 6.

A possible explanation as to why the salt concentration is insignificant might be that the very low temperature applied overshadows the effect of a varying salt concentration. To check this out, two different minimum temperatures were used in series 3.

5.1.6 Series 3: Effect on scaling of salt concentration and minimum temperature for concrete of water-cement ratio 0.30.

In the last series, concrete of water-cement ratio 0.30 was tested with respect to salt concentration of the outer solution and minimum temperatures. This concrete was made with silica fume (10% by weight of the cement, water binder ratio 0.27) but again without air entrainment. No specimens were allowed to dry before testing.

Pre-treatment

Specimens were cut out of the cast cylinders the day after casting and were then stored in water for eight weeks until testing began.

Temperatures and salt concentrations

In order to clarify whether or not the choice of minimum temperature might have an overshadowing effect on the choice of salt concentration described above, two different minimum temperatures were used in this series: -15° and -22°C. Since it had been decided to use two different minimum temperatures after the specimens had been prepared, only three levels of salt concentration could be used: 0, 3 and 4.5%.

Number of frost cycles

As scaling was very low in this series, testing was continued for another 28 cycles, *i.e.* to a total of 84 cycles. The scaling rate was almost constant, which means values for comparison at 56 cycles can be obtained by multiplying the ones shown by 2/3.

Results

The accumulated scaling for series 3 in relation to minimum temperature and salt concentration of the outer solution is shown in figure 5.1.5. The margin of experimental error is about 20 g/m² (*i.e.* error due to material inhomogeneity not included). Thus, one must avoid far-reaching conclusions from the differences between specimens tested with salt solutions. Still, it can be safely stated that the presence of salt increases scaling, but that the exact salt concentration seems to be less important. Taking into account the margin of error, it cannot be concluded that a very low minimum temperature overshadows the level of salt concentration, but a tendency in this direction can be discerned: at a minimum temperature of -15, 3% causes worse damage than 4.5%, while the two concentrations seem equally destructive at the lower temperature. Again, this may be too far-reaching a conclusion, and further research would be interesting.

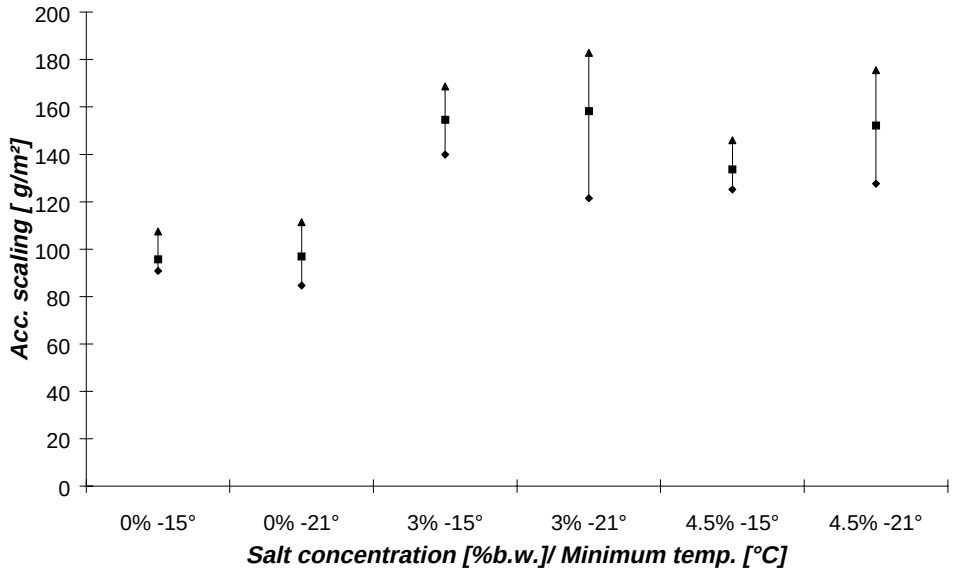

Figure 5.1.5: Accumulated scaling after 84 cycles in relation to salt concentration and minimum temperature for series 3. One dot = one specimen.

5.1.7 Conclusions

Effects of different combinations of salt concentrations in the pore solution and the surface-covering solution, frost cycle design, and water-cement ratio were studied in three series of salt frost resistance tests.

For concrete of water-cement ratio 0.40 with a moderate air content, the most severe damage was observed when the salt concentration of the surface-covering solution, the ”outer” solution, was about 3% and no salt was present in the pores. Damage got worse the lower the minimum temperature used in the frost cycle.

Concrete of *w/c* = 0.35 and with *s/c* = 5% without air entrainment showed bad SFS resistance, independent of salt concentration. No ”pessimum” concentration could be detected. Damage was even and equally severe regardless of salt concentration within the range tested: 0-5% b.w.

Concrete of *w/c* = 0.30 and *s/c* = 10% silica fume without air entrainment showed very good SFS resistance. Taken together with results reported in the literature, this indicates that concrete of *w/c* ratio 0.30 or lower is resistant to salt frost attack. At present, however, it cannot be said whether this resistance will be affected by possible microstructure changes occurring over time in field applications.

The results indicate that the choice of minimum temperature may have a decisive effect on test results.

Appendix 5.1.1: Accumulated scalings after 56 frost cycles for individual specimens in Series 1

Accumulated scaling after 56 cycles, Series 1: Concrete w/c 0.40, Dmax 8 mm.
Weights in grams per specimen
Specimen surface area = 0.127m²

Acc. scale: Accumulated scaling after 56 cycles
Dev, %: Deviation of individual specimen from group mean value

Frost cycle:				**A**			**C**			**D**			**E**			**F**		
	Conc.	Conc.		Acc. scale	Mean	Dev.	Acc. scale	Mean	Dev.	Acc. scale	Mean	Dev.	Acc. scale	Mean	Dev.	Acc. scale	Mean	Dev.
w/c	out	in		dry	value	%	dry	value	%	dry	value	%	dry	value	%	dry	value	%
40	0	0	A	1.6		1.5	0.41		-15.2	1.41		11.3	5.83		77.0	1.66		-4.8
40	0	0	B	1.64	1.58	4.0	0.57	0.48	17.9	1.18	1.27	-6.8	2.06	3.29	-37.4	1.85	1.74	6.1
40	0	0	C	1.49		-5.5	0.47		-2.8	1.21		-4.5	1.99		-39.6	1.72		-1.3
40	0	3	A	1.54		-6.7	2.9		74.7	1.78		-13.5	3.25		-28.8	1.72		-23.0
40	0	3	B	1.74	1.65	5.5	0.42	1.66	-74.7	2.38	2.06	15.7	7.57	4.57	65.8	3.13	2.23	40.1
40	0	3	C	1.67		1.2	1.66		0.0	2.01		-2.3	2.88		-36.9	1.85		-17.2
40	0	6	A	1.81		43.3	6.11		21.3	2.74		-27.4	4.54		-19.4	6.57		28.6
40	0	6	B	1.98	1.26	56.7	4.46	5.04	-11.4	3.78	3.78	0.1	6.13	5.63	8.8	3.54	5.11	-30.7
40	0	6	C	missing		-	4.54		-9.9	4.81		27.4	6.23		10.6	5.22		2.2
40	3	0	A	2.81		13.3	7.85		63.8	5.42		-5.3	30.87		36.7	3.61		-50.5
40	3	0	B	2.23	2.48	-10.1	3.29	4.79	-31.4	6.23	5.72	8.9	4.49	22.59	-80.1	14.99	7.29	105.6
40	3	0	C	2.4		-3.2	3.24		-32.4	5.52		-3.6	32.41		43.5	3.27		-55.1
40	3	3	A	2.14		0.9	11.83		46.7	8.86		23.0	23.39		12.2	10.61		77.3
40	3	3	B	2.05	2.12	-3.3	8.87	8.07	10.0	6.09	7.20	-15.5	19.78	20.85	-5.1	3.15	5.98	-47.4
40	3	3	C	2.17		2.4	3.5		-56.6	6.66		-7.5	19.39		-7.0	4.19		-30.0
40	3	6	A	2.01		-8.2	14.07		33.8	8.63		-6.2	20.96		9.1	7.91		9.5
40	3	6	B	2.45	2.19	11.9	9.43	10.51	-10.3	9.5	9.20	3.2	17.52	19.21	-8.8	5.89	7.23	-18.5
40	3	6	C	2.11		-3.7	8.04		-23.5	9.48		3.0	19.15		-0.3	7.88		9.0
40	6	0	A	2.47		-9.1	2.76		-23.8	3.15		-48.8	missing			7.62		44.7
40	6	0	B	2.66	2.72	-2.1	5.14	3.62	42.0	11.66	6.15	89.7	4.83	4.24	13.9	4.44	5.27	-15.7
40	6	0	C	3.02		11.2	2.96		-18.2	3.63		-40.9	3.65		-13.9	3.74		-29.0
40	6	3	A	2.78		-3.1	4.14		41.1	2.61		-18.6	4.02		-7.4	3.34		-0.8
40	6	3	B	2.88	2.87	0.3	2.19	2.93	-25.3	3.02	3.21	-5.8	4.24	4.34	-2.3	2.79	3.37	-17.1
40	6	3	C	2.95		2.8	2.47		-15.8	3.99		24.4	4.76		9.7	3.97		17.9
40	6	6	A	2.91		4.2	3.7		1.7	3.56		-26.6	4.86		-15.3	4.31		-18.8
40	6	6	B	2.61	2.79	-6.6	4.49	3.64	23.5	5.07	4.85	4.5	7.67	5.74	33.7	6.7	5.31	26.3
40	6	6	C	2.86		2.4	2.72		-25.2	5.92		22.1	4.68		-18.4	4.91		-7.5

5.2 STUDY OF CHLORIDE ION TRANSPORT INTO THE SURFACE LAYER OF HCP OVER SHORT TIME PERIODS

5.2.1 Introduction

In an SFS resistance test, like the Swedish SS 13 72 44, the salt solution is applied to the specimen surface shortly before cooling from room temperature begins. From the time of application until freezing starts (and possibly even after that), there is an ion exchange between the pore solution and the outer salt solution. If the net change in amount of dissolved ions in the pore solution increases, the freezing point of the pore solution will be depressed. This may cause the initial freezing in the pore solution to take place at some depth beneath the surface, despite the shape of the temperature gradient. If ice lens growth through segregation is the dominating means of ice formation and if one single ice lens is able to dominate subsequent ice lens formation, as indicated by the existence of a critical thickness and the Powers' spacing factor, such disturbance of the ice formation pattern may be of great importance in the subsequent surface scaling process.

To study this early intrusion of chloride ions into Portland cement-bound materials, a series of diffusion tests in neat hardened cement paste were carried out. The main purposes were:

1. to study how far into the specimen chloride ions are transported during the time from application until freezing begins, in a test such as the SS 13 72 44
2. to investigate whether there is anything in this transport process that may explain the "3%-pessimum" reported in the literature
3. to study whether the chloride ions are mainly transported and spread in the capillary pores or whether the entire pore system is involved (*i.e.* both gel- and capillary pores)
4. to study the extent to which this early chloride ion intrusion may be described as a pure diffusion process

If it turned out that the process is a pure diffusion-type process, transport coefficients were to be determined.

The experiments were run by Mr. Gyula Pinter. I wish to thank him for carrying out this very demanding work (requiring patience, skill and care) with excellence and enthusiasm.

5.2.2 Experiments

The investigations were carried out by soaking water-saturated circular discs of pure cement paste (*w/c* 0.4, 0.5 and 0.65) in NaCl solutions (0.5, 3 and 8% b.w.) for various time periods (0.5, 1 and 3h) and then, by grinding off layer by layer and leaching out the chloride ions (some 20h in distilled water), analysing the variation in chloride ion concentration with depth (details are given below). The following main series were run

Series 1 – Pure diffusion (at +18°C)
Series 2 – Capillary suction of salt solutions
Series 3 – Effect of leaching time (over night / 4 min.)
Series 4 – Effect of temperature level (+5°C)

The results from Series 2 are not reported because of the overly large scatter obtained.

Finally, the contents of chloride ions and certain other ions were determined by X-ray mapping on specimens run parallel to some of the specimens in Series 1.

5.2.3 Material

Cement pastes of *w/c* ratios 0.35, 0.50 and 0.65 were used. The cement was a low alkali Portland cement produced by Cementa AB, Sweden (chemical composition in General Appendix 2). The cement pastes were mixed in batches of 1.5 l using a hand-held electric mixer (household type) for 3 minutes. The pastes were cast in cylindrical plastic tubes (ϕ58·200mm) which were then rotated for one day at a speed of 3-4 revs/min in order to avoid sedimentation (This rotation technique had earlier been tested with similar materials and moulds and had been found to produce even density throughout the specimen volume [L 1991].

The cylinders were de-moulded two days after casting and were then cut with a diamond saw into discs of a thickness of 4-5 mm. These discs were stored in a small amount of tap water (until testing began). The storage time varied from 5 to 7 months for specimens in series 1 and from 11 to 12 months for specimens in series 2, 3 and 4.

A few days before testing, each specimen was ground on an abrasive cloth (silicon carbide, produced by 3M, USA) in order to make the circular surfaces plane-parallel (grinding tool described below). This was done in water and was stopped when the thickness, as measured with a sliding caliper, varied by less than 0.1 mm across the surface.

To make the transport of chloride ions one-dimensional, the edges of the specimens were sealed with a plastic coating a few days before testing. This was done by removing the specimens from the water bath, slightly drying them and then sealing the edges by rolling the specimens on their edges in a small pool of plastic sealant intended for the moisture protection of electrical circuits. The sealant hardens within a minute. The specimens were immediately returned to the storage water in order to recover the moisture loss caused by the slight drying.

5.2.4 Equipment

Balance

A balance with a resolution of 0.001g was used. In order to avoid systematic errors in the weighings due to a non-calibrated balance, the balance was checked daily by weighing a reference weight of mass 200.000 g. Throughout the entire test period, the registered value was 200.006±0.003. This small systematic error has been neglected.

Grinding equipment

A grinding tool was designed which could be adjusted (steplessly) to grind off layers of a thickness of approximately 0.1 mm (the scale had a resolution of 0.1 mm). The

grinding tool is shown in figure 5.2.1. Measuring errors caused by the grinding tool are discussed below.

The abrasive cloths were cut circular to fit in the petri dish. The abrasive cloth was tested to ensure that no chloride ions could be leached out of it.

Chloride ion analysis equipment

The leach water was analysed using automatic potentiometric titration equipment produced by Corning, England, figure 5.2.1. The equipment measures chloride ion concentrations in the interval 10–999 mg Cl^-/l. According to the producer, the repeatability is ±1.5% at an absolute level of 200 mg Cl^-/l.

Calibration

The potentiometric analysis equipment is calibrated by analysing a 500 µl sample of a standard calibration liquid supplied by the equipment producer. This liquid contains 200 mg Cl^-/l. A potentiometer is adjusted until the correct reading is obtained.

However, calibrating by adjusting the potentiometer is time-consuming. In the present tests, it was not possible to spend that kind of time. Instead, the calibration liquid was analysed five times and a correction coefficient was calculated as:

$$k = \frac{C_{corr}}{m_{corr}} \cdot \frac{m_{mean}}{C_{mean}} = \frac{200}{500} \cdot \frac{m_{mean}}{C_{mean}} \qquad (5.2.1)$$

in which C_{corr} and m_{corr} are the correct values of the analysis result and the sample mass (mg) and C_{mean} and m_{mean} are the mean values of analysis results and sample masses for the five subsequent analyses. The values 200 and 500 are the correct reading (200 mg/l) obtained with a correct mass of the calibration liquid (500 mg).

This correction factor was determined before and after each and every specimen was analysed (*i.e.* 25 layers/50 analyses). The adjusted value of chloride content in any one single specimen layer was then obtained from:

$$C_{cal} = 500 k_{mean} \frac{C_{meas}}{m_{smp}} \qquad (5.2.2)$$

in which C_{cal} is the calculated chloride ion concentration of the sample, C_{meas} is the obtained reading, m_{smp} is the mass of the analysis sample (leach water) and k_{mean} is the average correction coefficient obtained from the analyses of the calibration liquid made before and after the 25 layers were analysed. Measuring errors caused by the analysis equipment are discussed below.

Fig 5.2.1: Grinding tool (far left), petri dish with abrasive cloth and specimen, pipette and potentiometric titration apparatus.

5.2.5 Experimental procedures

The specimens were wiped off with a moist cloth and weighed.
The disc thickness was measured with a digital sliding caliper (resolution 0.01 mm).
The specimens were placed in some 30 ml of salt solution in a plastic beaker (ϕ60 mm, with a lid on) for the intended process duration.
Specimens were taken up, wiped off with a moist cloth and weighed.
A first layer (thickness appr. 0.1 mm) was ground off on an abrasive cloth placed in a plastic petri dish. (The petri dish and the abrasive cloth had previously been weighed).
The petri dish, with its abrasive cloth, and the ground-off dust from the specimen, were weighed. (Meanwhile, the grinding tool, with the mounted specimen, was put on a table surface so as to avoid any drying of the specimen).
The next layer (appr. 0.1 mm) was ground off into another petri dish and weighed as before.

This was repeated until a sufficient depth was reached (in almost all cases it was decided to grind off 25 layers, *i.e.* a total of 2.5 mm). The total time for this grinding procedure varied from 0.5 to 1 h (depending on material quality). After grinding, the thickness of the remaining disc was measured.

After the grinding procedure was finished, de-ionised water was added (appr. 30 ml) to all petri dishes. The dishes were left over night (some 20 h with a lid on) to leach out the chloride ions from the grinding dust. (In series 3, the dishes were left for only 4 minutes in order to study the effect of leaching time.)

The following day, the petri dishes were weighed in order to determine the water content.

A sample for analysis was taken with a pipette (500-900 µl). The sample was weighed and analysed with the potentiometric analysis equipment. A further sample was analysed identically. The analysis equipment was checked with a calibration liquid once before the samples were analysed and once afterwards.

For each combination of variables, two specimens were run, and for each layer ground off, two chloride ion concentration analyses were done.

5.2.6 Evaluation of measured data

Degree of hydration

The degree of hydration of each specimen was determined by drying (105°C) and igniting (1050°C) the thin discs (typically 1.5 – 2 mm) which remained after grinding.

The weight of the crucibles was taken before heating to 105°C and denoted m_c. The specimens (in their crucibles) were allowed to cool over silica gel in an exsiccator and were then weighed. This mass was denoted $m_{c+s,dry}$. The weight of the dry specimen was calculated as:

$$m_{dry} = m_{c+s,dry} - m_c \qquad (5.2.3)$$

After igniting to 1050°C over night, the specimens were again allowed to cool over silica gel in an exsiccator. The weight of the crucible and specimen was denoted $m_{c+s,1050°}$. The specimen weight after ignition was determined by:

$$m_f = m_{c+s,1050} - m_c \qquad (5.2.4)$$

Since the specimens were pure cement pastes, this is the weight of the unhydrated cement, m_{cem}.

The mass of chemically-bound water was determined as:

$$m_n = m_{dry} - m_f \qquad (5.2.5)$$

Assuming $m_{n,max} = 0.25C$ [P 1948], the degree of hydration was determined from:

$$\alpha = \frac{m_n}{0.25C} \qquad (5.2.6)$$

Complete data are reported in Appendix 5.2.1. The errors are discussed below. No correction was made to compensate for possible hydration taking place in the cement before mixing.

Porosity and density

To calculate chloride ion concentration in the pore solution, data on density and porosity are needed. In the calculations, values for these parameters have been determined from data on the degree of hydration. The porosities and densities, as determined by the Archimedes principle, were used only for comparison. Such data were determined for only a few specimens using the following procedure:

The specimens (discs remaining after grinding) were dried at 105°C.
Specimens were allowed to cool over silica gel in an exsiccator.
Specimens were weighed in air (m_{dry}).
Specimens were put under vacuum for at least 6 hours.
Specimens were impregnated with de-ionised water over night.
Specimens were weighed under water ($m_{sw,w}$).
Specimens were wiped off with a moist cloth and weighed in air ($m_{sw,a}$).

Specimen volumes were calculated from:

$$V = m_{sw,a} - m_{sw,w} \qquad (5.2.7)$$

(assuming the water density to be 1000 kg/m^3.) The specimen densities were calculated:

$$\rho_{dry} = \frac{m_{dry}}{V} \qquad (5.2.8)$$

No corrections for incomplete vacuum or water density deviations were made. Complete data are given in Appendix 5.2.2. Errors in the determination of density and porosity are discussed below.

Determination of chloride ion concentration in pore solution

The potentiometric analysis apparatus was calibrated as described above.

The following weighings were done:
m_p = weight of empty petri dish
$m_{p,g}$ = weight of petri dish with abrasive cloth
$m_{p,g,s}$ = *ditto* plus weight of grinding dust
$m_{p,g,s,sol}$ = *ditto* plus de-ionised water
m_a = mass of the analysis sample (the leach water)

The following parameters were calculated from the degree of hydration:
ρ_d = specimen dry weight
ρ_s = specimen water-saturated density
P = specimen porosity (as determined from data on degree of hydration)

The following calculations were made:

Mass of the ground-off layer: $m_s = m_{p,g,s} - m_{p,g}$ *(5.2.9)*

Dry weight of the ground-off layer: $m_{dry} = m_a \cdot \frac{\rho_d}{\rho_s}$ *(5.2.10)*

Mass of the added de-ionised water: $m_{sol} = m_{p,g,s,sol} - m_{p,g,s}$ *(5.2.11)*

The concentration of chloride ions in the leaching water, C_{sol}, was determined by potentiometric titration. Total amount of chloride ions in the layer was calculated:

$$m_{Cl} = C_{sol} \cdot m_{sol} \qquad (5.2.12)$$

(assuming the leach water density to be 1000 kg/m^3)

The mass of chloride ions, $m_{Cl,s}$, per gram of dry ground-off dust was calculated:

$$m_{Cl,s} = \frac{m_{Cl}}{m_{dry}} \qquad (5.2.13)$$

The thickness of the ground-off layer was determined from:

$$d = \frac{m_{dry}}{A \cdot \rho_d} \qquad (5.2.14)$$

with A = cross section of the circular specimens, 26.42 cm².
The volume V_s of the ground-off layer was calculated:

$$V_s = \frac{m_{dry}}{\rho_d} \qquad (5.2.15)$$

Total pore volume in the layer was calculated:

$$V_{P,tot} = V_s \cdot P_{tot} \qquad (5.2.16)$$

in which P_{tot} had been calculated from the mean degree of hydration for each material quality (by use of equations set up by Powers and Brownyard [P 1948]).

Finally, the concentration of chloride ions in the pore solution was calculated as:

$$C_{Cl,Ptot} = \frac{m_{Cl,s}}{V_{P,tot}} \qquad (5.2.18)$$

(under the assumption that the specimen remained water-saturated during both the process duration and the grinding procedure).

5.2.7 Error estimation

The errors in the finally calculated chloride ion concentration profiles are due to

- errors in chloride ion concentration, and to
- errors in the determination of layer thicknesses.

While both of these are due to errors in estimated porosity and incomplete water saturation, the former is also due to titration errors and the latter is also due to errors caused by the grinding procedure. The following constitutes an attempt to estimate the extent of the errors induced by these error sources.

Errors in values on density and porosity used in the evaluations

Values on degree of hydration, density and porosity as measured by ignition and by the Archimedes principle are given in Appendix 5.2.2. There, it can be seen that the minimum and maximum values of density and porosity deviate from the respective mean values by up to 3.8% (as determined from degree of hydration) and 4.8% (as determined by the Archimedes principle). The maximum coefficient of variation (ratio of standard deviation to mean value) is 2.2% (values in italics omitted.).

On comparing the porosities obtained by the two techniques used here, it can be seen that those measured by the Archimedes principle are, on average, some 2 percentage points higher than those calculated from the measured degrees of hydration. This discrepancy may well be attributable to unintended air voids resulting from insufficient compaction. If so, the measured values are in good conformity. Furthermore, since such air voids, if actually filled with air, would not contribute to the diffusion of ions, the porosities used for the evaluation of chloride concentrations are those calculated from the degree of hydration. For the sake of convenience, the average value of degree of hydration is used for all materials having one and the same *w/c* ratio. These values, together with the thus calculated porosities and densities, are given in table 5.2.1.

Errors due to incomplete water saturation

If the pore system of the specimen is not completely water-saturated at start of the test, the calculated transport coefficients will be erroneous since some suction of the outer liquid into the pores may possibly occur. This source of error was avoided as far as possible by keeping the specimens in water from casting until testing, except for those few minutes when the specimen edges were sealed with plastic as described above. There is nothing in the calculated concentration profiles from Series 1 to indicate that there was any convective transport of chloride ions into the specimens.

Table 5.2.1: Degrees of hydration (α) used in all evaluations of measured data. Porosities and densities as calculated from degree of hydration. Measured by ignition.

w/c	Number of specimens	α, mean	Porosity [%]	Dry density [g/cm^3]	Wet density [g/cm^3]
0.35	10	0.6851	0.3304	1.7601	2.0905
0.50	14	0.7907	0.4289	1.4687	1.8976
0.65	12	0.8186	0.5122	1.2476	1.7596

If the specimens do not remain completely saturated during grinding, the calculation of layer thickness will yield erroneous values because it involves the use of the wet density of the material. Unintentional drying therefore had to be avoided as far as possible. This was done by keeping the specimen enclosed in the grinding tool while weighing the petri dish (the grinding tool was put on a table surface so that the specimen was completely shut in). Since the grinding took about half an hour, there still must have been some drying. However, a simple calculation of the possible rate of drying shows the effect to be negligibly small: for a cement paste specimen of *w/c* ratio 0.50 and α = 0.80, the calculated dry and wet densities are 1.472 and 1.898 g/cm^3, respectively. The ratio of these two, which is used in the calculation of layer thickness is ρ_{dry}/ρ_{wet}=0.775. The maximum possible drying would be obtained if the specimen was allowed to dry in the prevailing climate (+18°C/60%R.H.) during the approximately 30 minutes that were required for the entire grinding process. An approximative calculation (using moisture transport coefficients from Hedenblad [H 1993] reveals that the degree of saturation might be lowered from 1.0 to 0.98. This would reduce the ratio of the wet (although less than saturated) weight of the material to that of the dry material to 0.772, *i.e.* a change of some 0.5%. Since the specimens were always protected, as far as possible, against loss of moisture during grinding, it is concluded that unintentional moisture loss did not affect the measured values in any significant way.

Errors due to imprecise chloride ion concentration analysis

The potentiometric analysis equipment was calibrated as described above. The analysis samples of leaching water were always weighed in order to reduce pipetting errors. (When necessary, this also provides a means for taking into account the varying density of differently concentrated solutions.)

The precision of the read values decreases with decreasing concentration. In order to test this, the calibration liquid was diluted by the addition of distilled water and analysed. The results are shown in figure 5.2.2. From these results, equation (5.2.18) was derived to be used for adjusting all analyses taken from the tested specimens.

$$C_{adj} = 1.0111 C_{cal} - 2.7144 \qquad (5.2.18)$$

Here, C_{adj} is the adjusted concentration and C_{cal} is the concentration calculated from eq. (5.2.2).

It can also be seen in figure 5.2.2 that the scatter is rather large at low concentrations. After correcting the obtained results with equation (5.2.18), the standard deviation of this scatter is 8% of the adjusted calculated value. However, the scatter increases with decreasing concentration and thus the scatter for values lower than 50 mg/l is estimated to be 9%. In the final results, layers in which the analysis result (*i.e.* the value read on the analysis apparatus) was less than some 13 mg/l have not been used for the final evaluation of chloride ion transport coefficient. (In most cases, the readings did not exceed 100 mg/l). The depth at which such low concentrations were obtained are marked in the figures in the Results section with “Depth of unreliable analysis”.

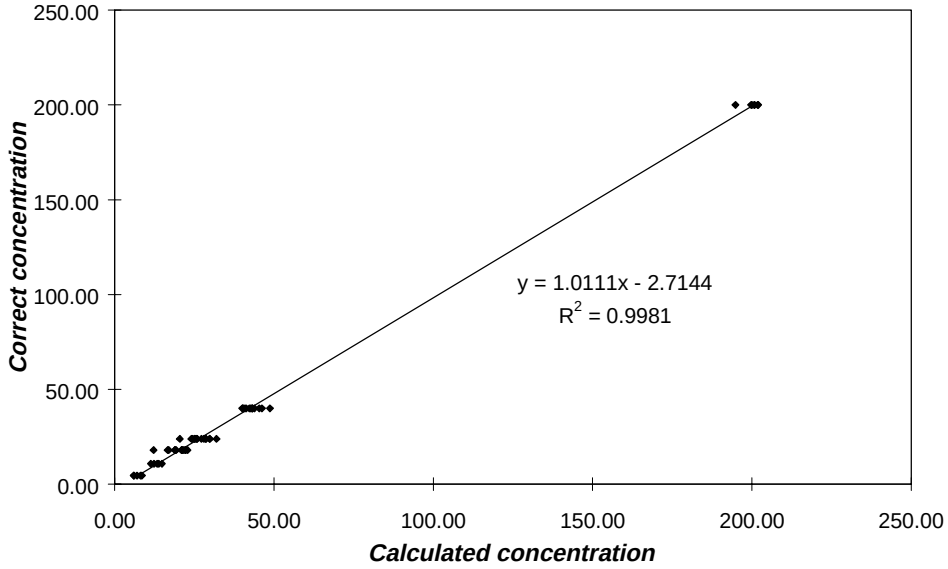

Figure 5.2.2: Correct chloride ion concentration vs. calculated same. Data obtained both from calibration liquid, diluted calibration liquid and weak NaCl solutions. Concentrations in mg Cl^-/l.

Errors due to the grinding procedure

Because of the interaction of the grinding tool and the grinding cloth, a certain amount of steel dust from the grinding tool found its way into the grinding dust. The additional weight of this steel makes the calculated layer thicknesses too high. This was dealt with by summing the individual layer thicknesses and comparing it to the thickness of the specimen as measured before and after grinding. From this, a correction factor K was calculated:

$$K = \frac{D_i - D_f}{\sum_{n=1}^{N} d_n} \qquad (5.2.19)$$

in which D is the specimen thickness before (i) and after (f) grinding, d_n is the thickness of layer number n calculated from its weight and N is the total number of layers (usually 25, in a few cases 15). The mass (and thus the thickness and the pore volume) of each and every layer was adjusted by multiplying the measured mass by K. Usually, K ranged from 0.8 to 1. A few examples are given in table 5.2.2.

Further remarks on possible errors

Apart from the errors mentioned above, the following possible error sources also need to be considered:

- contamination of grinding dust from one layer by dust from another
- non plane-parallell layers
- continued diffusion inside specimens during grinding

Table 5.2.2: Comparison of specimen thicknesses with sum of measured ground-off layer thicknesses as calculated from the weights. Diff = Thickness before - thickness after.

File	*w/c*	Thickness [mm] before	after	Diff.	Sum of layers [mm]	Number of layers	K (eq.(5.2.19))
960409A	0.35	4.00	2.20	1.8	2.179	25	0.826
960410A	0.35	4.23	2.42	1.81	2.002	25	0.904
960423A	0.35	4.07	2.12	1.95	1.992	25	0.979
960403A	0.65	3.38	0.99	2.39	2.583	25	0.925
960403B	0.65	3.59	1.04	2.55	2.845	25	0.896
960415A	0.65	3.31	0.84	2.47	2.418	25	1.022

Contamination of grinding dust from one layer by dust from another was reduced as far as possible by carefully brushing the grinding tool with a soft paint brush after each layer had been ground off.

If the specimen surfaces are not plane-parallel, the first layer cut off will not be of even thickness. However, since each specimen was ground (a few days before testing) until its thickness varied by less than 0.1 mm and since the half thickness was usually more than twice the penetration depth, errors caused by this non-parallelity may be disregarded.

It is possible that chloride ions which have been transported into the pore system during exposure to an outer chloride ion solution will continue spreading in the pore system during the grinding process. Especially in specimens exposed for only 30 minutes, this may cause a flatter slope of the chloride ion concentration profile than was actually obtained during exposure. However, the possibility of convective transport towards the specimen surface due to drying may cause even larger effects. Because of the shape of the finally obtained concentration profiles, any effects due to these phenomena could not be detected.

5.2.8 Estimation of total absolute errors

Absolute errors in estimated mean depth of the layers

The estimated layer thicknesses were adjusted by use of eq. (5.2.19). The error in the measurement taken with the sliding caliper is estimated to be less than 0.05 mm. If the errors in the two measurements taken before and after grinding are in opposite directions, the maximum total error may thus be some 0.1 mm. Since the total thickness change obtained after grinding off 25 layers is approximately 2.5 mm, this means the maximum error in estimated depths and layer thicknesses should be 4%.

Absolute errors in estimated chloride ion concentrations

The chloride ion concentration in each layer is calculated from the layer volume (which is corrected to within 4% according to eq. (5.2.19), the porosity (the error of which may estimated at 2% on average), and the titration result (the error of which may be estimated at 9%) The total error thus may amount to some 15%.

5.2.9 Results

Series 1 and 3 – Pure diffusion and effect of leaching time

The calculated chloride ion concentration profiles are shown in figures 5.2.3–5.2.18. Unfortunately, some data were lost and thus in some figures data for only one specimen are given. The chloride ion concentrations have been calculated both under the assumption that the ions are present only in the capillary pore volume and under the assumption that they are present in the whole pore volume, *i.e.* both in capillary pores and in gel pores. The volumes of each of these groups of pores have been calculated from the degree of hydration (in accordance with equations from Powers and Brownyard [P 1948]). The indicated depth of unreliable analysis is the approximate depth at which the absolute analysis result, as obtained from the potentiometric analysis apparatus, showed less than 13 mg Cl^-/l.

Figure 5.2.18 shows results from the experiments on the effect of leakage time. For this purpose, four specimens of *w/c* ratio 0.50 were tested in an 8% NaCl solution for one hour. For two of these specimens, the leaching time was reduced from 24 hours to 4 minutes. Because the specimen thicknesses were not registered, it was not possible to adjust these results for steel grinding dust. Nevertheless, because a qualitative comparison is wholly satisfactory, this was not a serious drawback. Also, the results shown in figure 5.2.10 (in this case not compensated for steel grinding dust) have been included in figure 5.2.18. Although there is a great deal of scatter in the curves, the results indicate that the measured concentrations are independent of the leaching time used, 4 minutes or 24 hours.

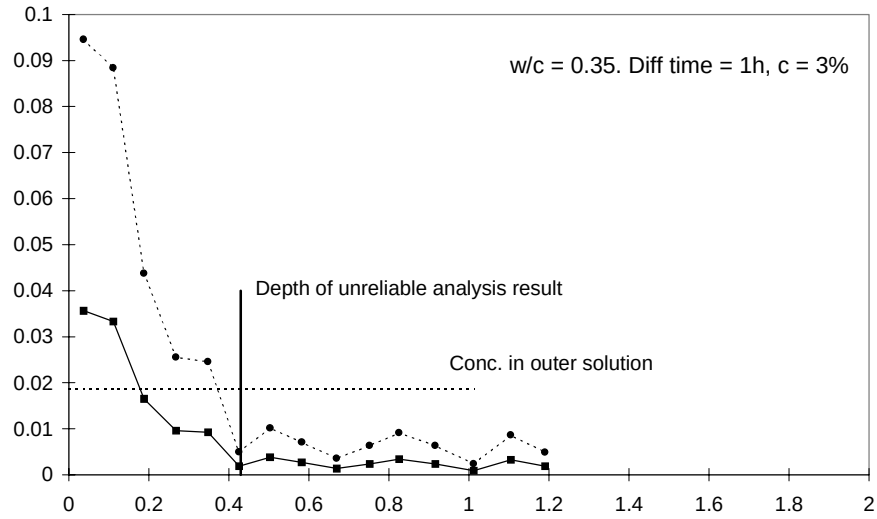

Figure 5.2.3: Measured Cl^- concentration [mg/mm^3] in pore solution vs. depth beneath surface [mm]. Solid line: Cl^- ions assumed equally distributed in all pores. Dashed line: Cl^- ions assumed present only in capillary pores. (one line = one specimen)

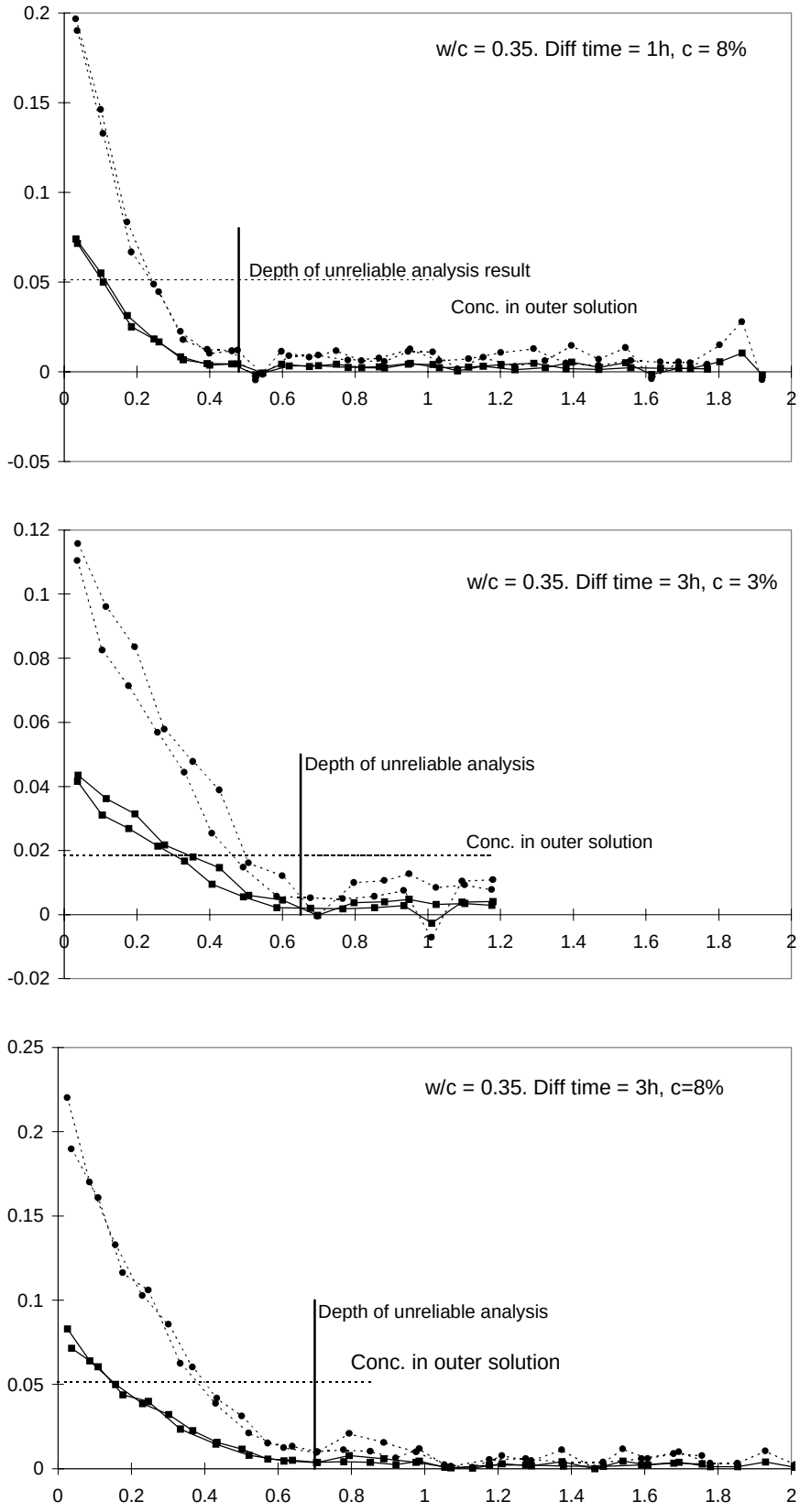

Figure 5.2.4-5.2.6: Measured Cl^- concentration [mg/mm^3] in pore solution vs. depth beneath surface [mm]. Solid line: Cl^- ions assumed equally distributed in all pores. Dashed line: Cl^- ions assumed present only in capillary pores. (one line = one specimen)

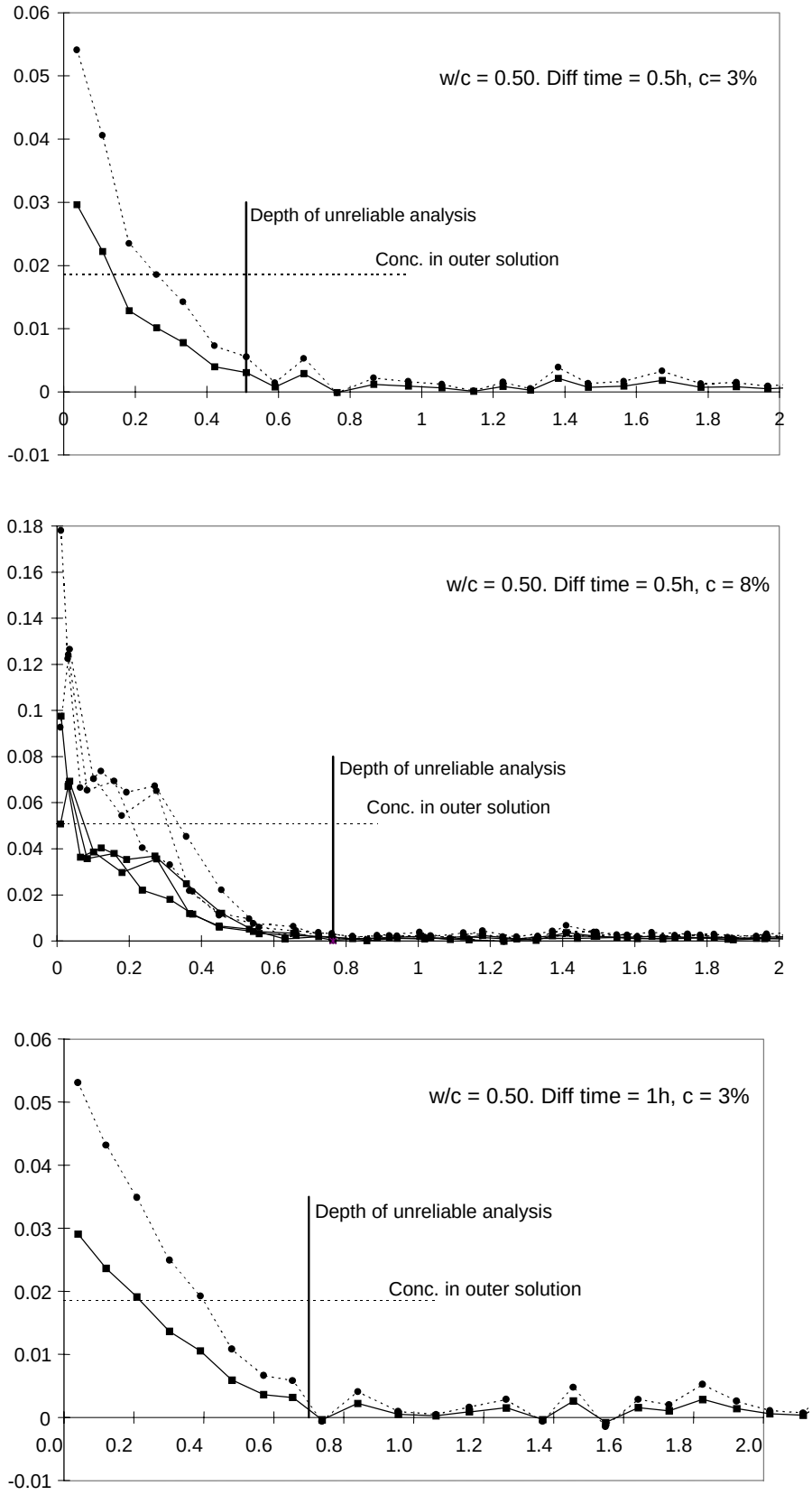

Figure 5.2.7-5.2.9: Measured Cl^- concentration [mg/mm^3] in pore solution vs. depth beneath surface [mm]. Solid line: Cl^- ions assumed equally distributed in all pores. Dashed line: Cl^- ions assumed present only in capillary pores. (one line = one specimen)

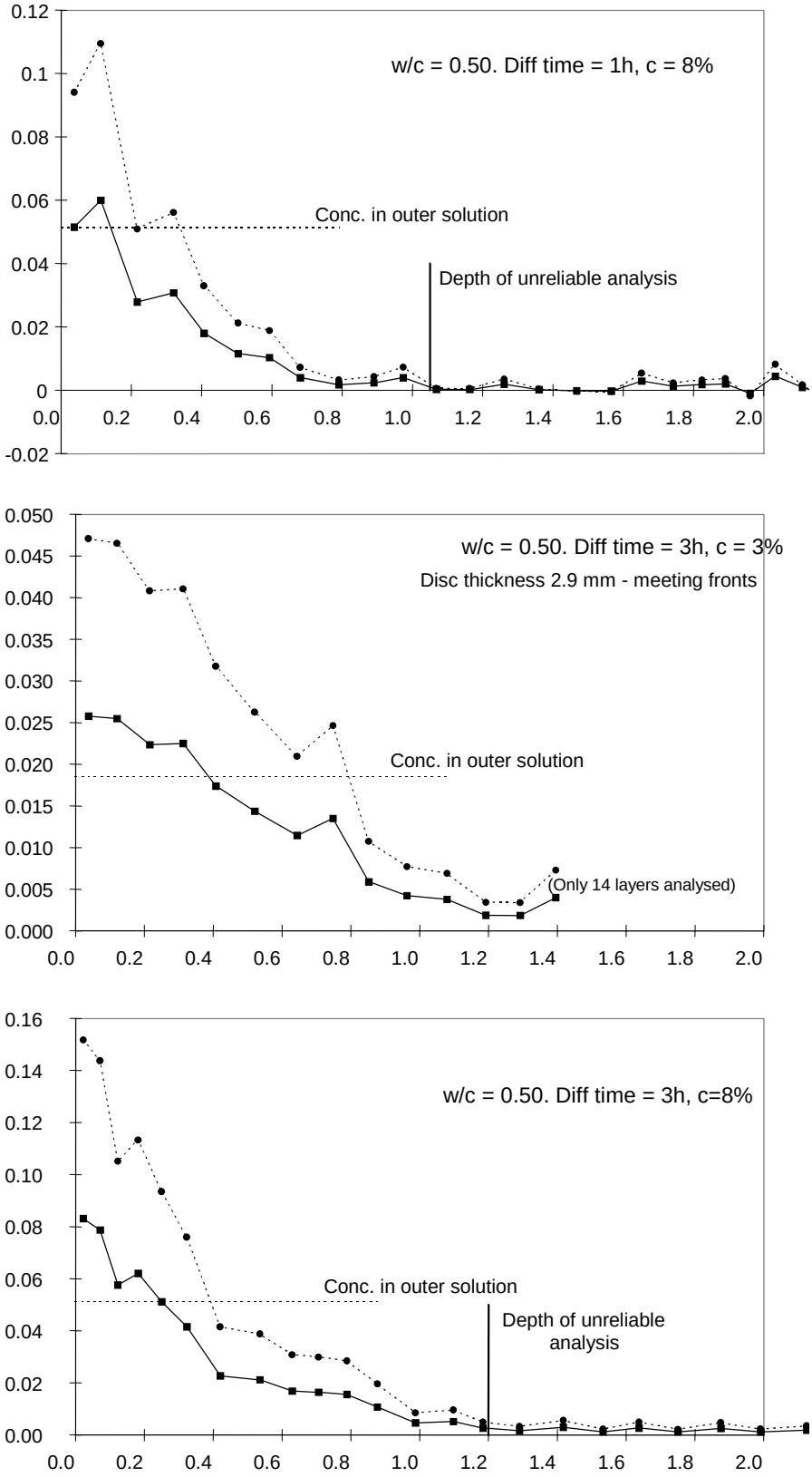

Figure 5.2.10-5.2.12: Measured Cl^- concentration [mg/mm^3] in pore solution vs. depth beneath surface [mm]. Solid line: Cl^- ions assumed equally distributed in all pores. Dashed line: Cl^- ions assumed present only in capillary pores. (one line = one specimen)

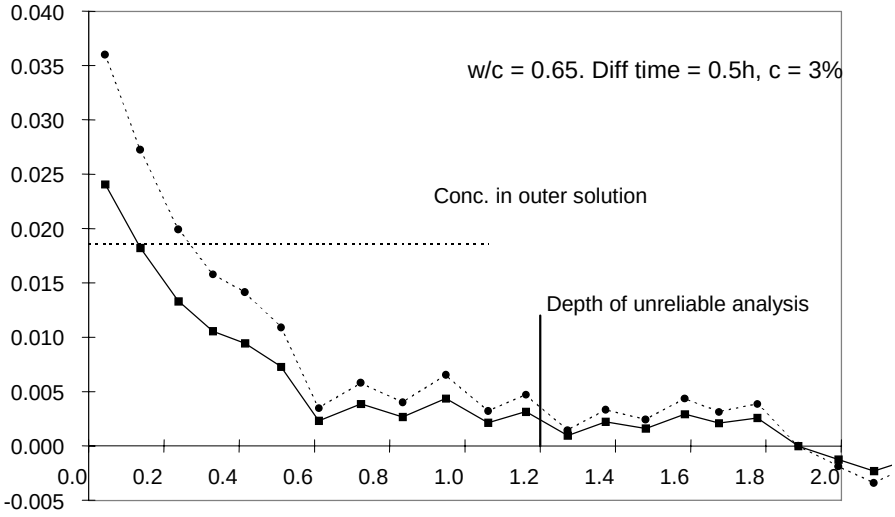

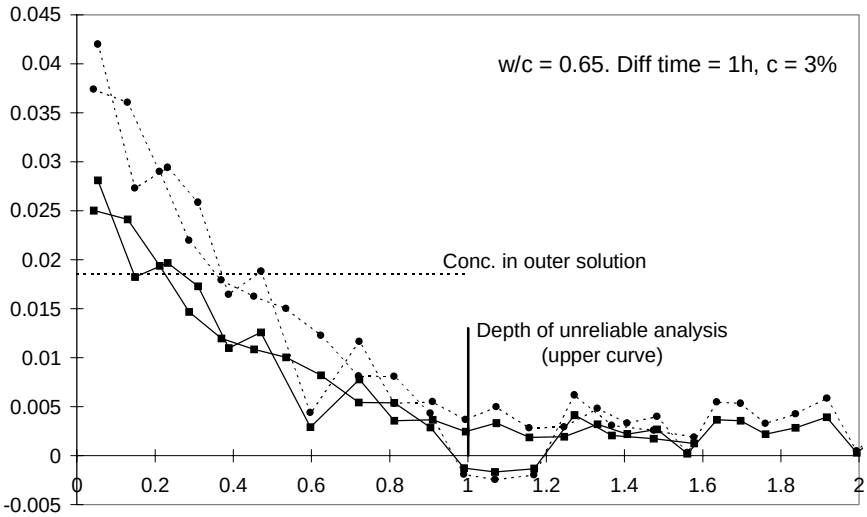

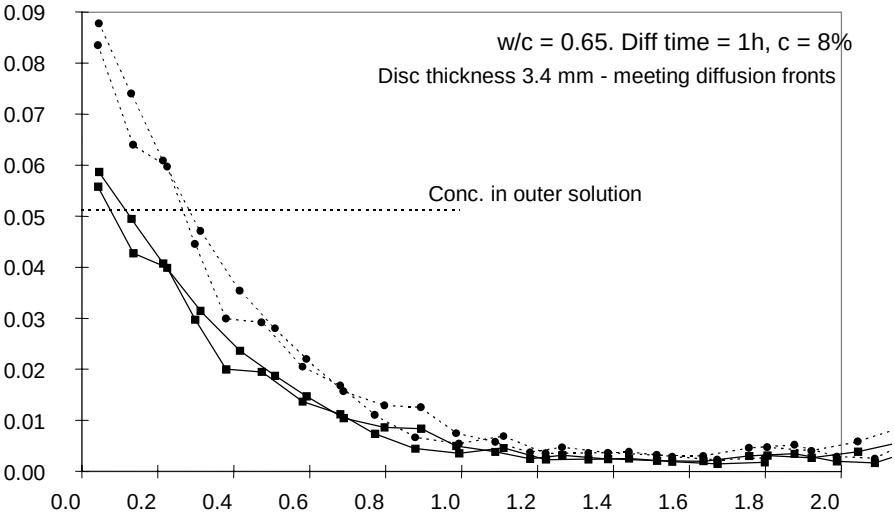

Figure 5.2.13-5.2.15: Measured Cl^- concentration [mg/mm^3] in pore solution vs. depth beneath surface [mm]. Solid line: Cl^- ions assumed equally distributed in all pores. Dashed line: Cl^- ions assumed present only in capillary pores. (one line = one specimen)

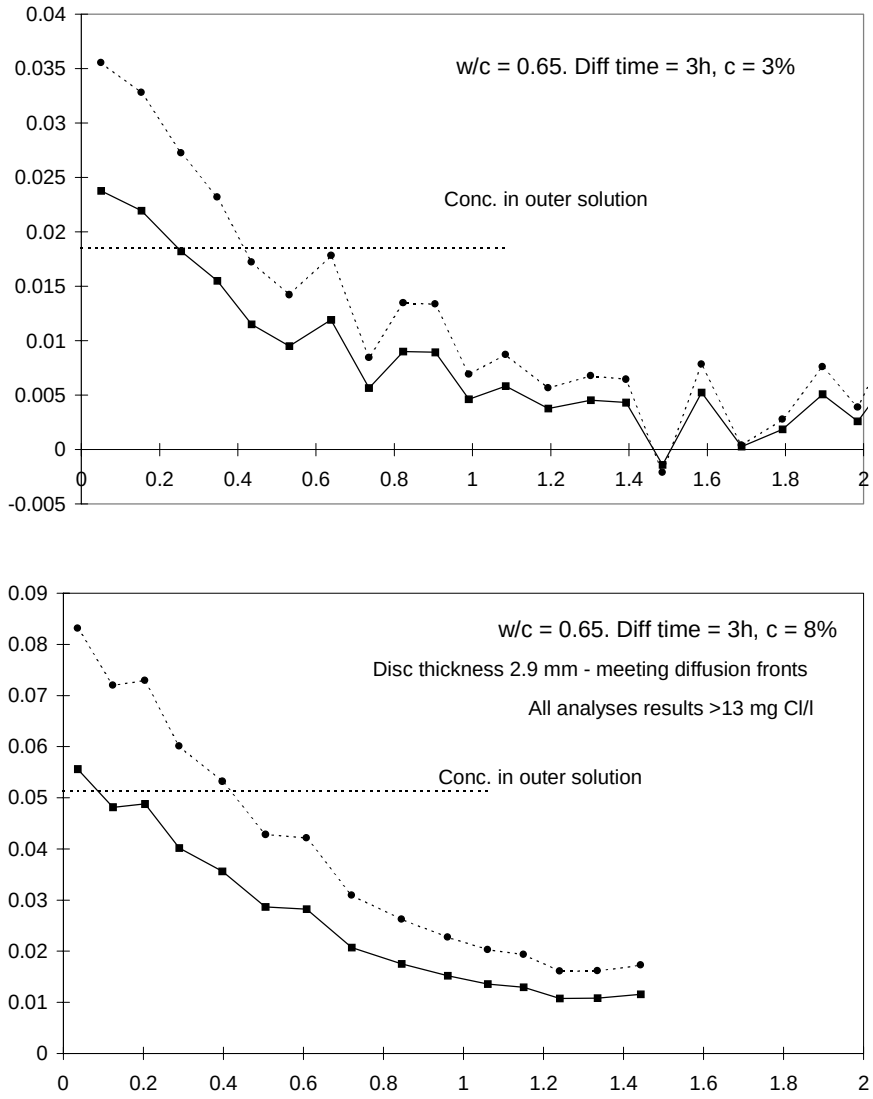

Figure 5.2.16-5.2.17: Measured Cl^- concentration [mg/mm^3] in pore solution vs. depth beneath surface [mm]. Solid line: Cl^- ions assumed equally distributed in all pores. Dashed line: Cl^- ions assumed present only in capillary pores. (one line = one specimen)

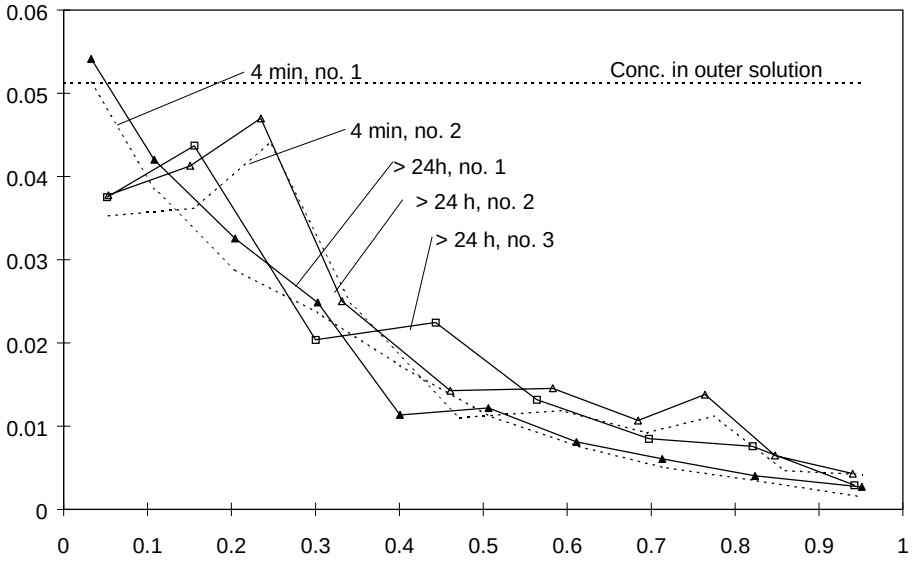

Figure 5.2.18: Effect of leaching time. Cl^- concentration [mg/mm^3] in pore solution vs. depth beneath surface [mm]. Cl^- ions assumed equally distributed in all pores. Not compensated for moisture loss or grinding dust from grinding tool.

5.2.10 Discussion

General

Generally, from the shape of the profiles, it seems that the intrusion of chloride ions is a diffusion-controlled process. However, in most cases, the concentration measured in the outermost layer is higher than that of the test solution. The concentrations, even when assuming the chloride ions are spread throughout the entire pore volume, exceed even the upper concentration limit as estimated from the possible maximum errors described above (*i.e.* they are in excess of the outer concentration by more than 15%). Unless the chemical composition of the pore solution and the changes taking place in it during testing plays a significant role, the concentration of dissolved ("free") chloride ions reasonably cannot be higher in the pore solution than it is in the outer solution. This indicates that the intrusion of chloride ions is not a pure diffusion process. Instead, some of the chloride ions seem to be "bound" to the pore walls. This matter of "binding" has been extensively studied in recent years, but the mechanisms still are unknown. In fact, it is not even known whether or not all the pore solution acts as a solvent. (The state of the art is described by Nilsson *et al*, who present a list of almost 2000 published references, [N 1996].) Typically, binding has been studied in experiments of much longer duration than has been the case here. Often, an acid is used in order to detect all chloride ions present in the material, they being either physically or chemically bound. In this study, no chemically bound ions are detected, since only de-ionised water was used for leakage. From the results shown in figure 5.2.18, no dependence of measured concentrations on leakage time can be determined. Since the longer leakage time is much longer than the entire time of diffusion, thus providing good conditions for unbinding any physically-bound chloride ions, we may assume that unbinding of physically bound chloride ions is complete in those tests where the longer leakage time was used. Since the profiles

obtained with a leakage time of only 4 minutes yield the same results, we may further assume that unbinding is a fast process (still referring to physically-bound ions only). This makes it likely that the physical binding involved in these experiments is also a fast process and thus that the relation between the amount of physically bound and dissolved ions in the outermost layer may be assumed to have reached a state of equilibrium, thereby revealing the binding capacity of the material. This is further strengthened by the fact that the excess concentration (defined and calculated below) is material-dependent, but independent of experiment duration. The results, however, are too uncertain (and even incomplete) to permit any meaningful determination of the relation between free (*i.e.* truly dissolved) and loosely-bound chloride ions.

However, the aim of this study was merely to study how far beneath the concrete surface *free* chloride ions may reach during the hours between the application of the salt solution and the beginning of freezing in an SFS resistance test, since it is only ions dissolved in the pore solution which will affect its freezing point. Of course, as mentioned above, the freezing point of the pore solution is not determined simply by the presence of chloride ions. But the chloride ion concentration may be taken as an indication of the depth to which the chemical composition of the pore solution is affected by the outer salt solution.

Determination of transport coefficients

There must be dissolved (free) chloride ions present at the largest depth of penetration observed. Assuming the mode of transport to be pure diffusion, the profile showing the concentration of "free" chloride ions may thus be sketched as a typical diffusion profile between the level of concentration of the outer solution at the surface to a point of zero concentration at the depth of maximum penetration. Any chloride ions in excess of this must be more or less bound. From such a profile, "effective" diffusion coefficients may be calculated. The word "effective" is used because, if "binding" is sufficiently fast in relation to the diffusion process itself, the net diffusion of chloride ions is reduced as a result of the binding of ions to the pore wall. It seem reasonable that the concentration at a given depth at a certain time would be higher if binding was not a factor. As long as the mechanisms of binding are not known, such "effective" diffusion coefficients determined from these results are valid only for conditions very similar to those of this test.

A concentration profile for pure diffusion in one dimension is described by:

$$C(x,t) = C(0,0) \cdot erfc\left(\frac{x}{\sqrt{4Dt}}\right) \qquad (5.2.20)$$

in which $C(x,t)$ = concentration
x = distance from the surface
t = time
D = diffusion coefficient

Since the measured concentrations in the pores exceed those of the outer solutions, the outer concentration cannot be used for $C(0,0)$ when fitting equation (5.2.20) to the obtained concentration profiles. Instead, a computer program has been used to find a combination of an outer "fictive" concentration and a transport coefficient which produces the best fit according to the method of least squares. The difference between

this fictive outer concentration and the true concentration is here called the excess concentration, *i.e.*:

$$C_{ex} = C_{fic} - C_{true,out} \qquad (5.2.21)$$

The terms involved are explained in figure 5.2.19. The results are given in table 5.2.3. Only layers which produced reliable potentiometric analysis results were used.

For the specimen denoted 960415B (figure 5.2.13), a *w/c* ratio 0.65 specimen tested for 30 minutes, only the first 7 layers have been used for the estimation of a transport coefficient, despite the fact that reliable analysis results were obtained even for the 14th layer. This is because the concentration profile is disturbed at depths beyond the 7th layer such that the final results cannot reasonably be trusted. This disturbance might be due to a crack, although no such observation was made.

For the specimen denoted 960326A (figure 5.2.12), a *w/c* ratio 0.50 quality specimen tested for 3 hours, the calculated transport coefficient is unusually low as compared to the other 0.50 samples. The excess Cl^- ion concentration is also unusually high. No explanation of these deviations has been found.

It can be seen in table 5.2.3 that the results of specimens tested at +5°C do not allow any definite conclusions to be drawn. However, as expected, the calculated transport coefficients are lower at the lower temperature.

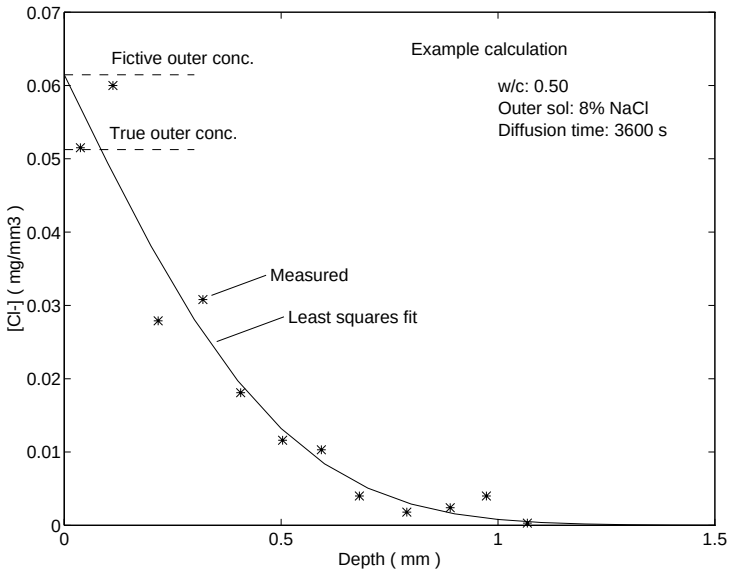

Figure 5.2.19: Terms used in the calculation of transport coefficients.

Table 5.2.3: Calculated fictive outer concentrations and transport coefficients.

Specimens tested at +18°C - Adjusted for steel grinding dust

File	W/C	Duration [s]	Disc thickness	Outer salt conc. [% NaCl, b.w.] and (mg / mm^3)	C_{fic} Fic. out conc. [mg / mm^3]	10^{12}*D [m^2 / s]	Depth at which C(x) = 0.01 * C_{fic} at given time [mm]	Depth at which C(x) = 0.001 * C_{fic} at given time [mm]	Excess Cl^- conc. (C_{fic} - C_{out})	Sum of squared errors	Layers used for fitting
960501A	0.35	1800	3.91	3 (0.01856)	0.04654	7.9	0.43	0.56	0.028	2.43E-05	1 - 6
960501B	0.35	3600	4.29	3 (0.01856)	0.04380	7.9	0.61	0.79	0.025	4.87E-05	1 - 6
960410A	0.35	3600	4.23	8 (0.05126)	0.08424	5.2	0.50	0.63	0.033	3.37E-05	1 - 8
960423A	0.35	3600	4.07	8 (0.05126)	0.08658	5.4	0.51	0.65	0.035	2.50E-05	1 - 7
960507B	0.35	10800	4.13	3 (0.01856)	0.04839	6.5	0.97	1.24	0.030	2.87E-05	1 - 9
960513B	0.35	10800	4.02	3 (0.01856)	0.04407	5.5	0.88	1.13	0.026	1.96E-05	1 - 8
960409A	0.35	10800	4	8 (0.05126)	0.08371	5.0	0.84	1.08	0.032	4.56E-05	1 - 10
960423B	0.35	10800	4.28	8 (0.05126)	0.07865	5.2	0.86	1.11	0.027	1.15E-04	1 - 13
960416A	0.5	1810	4.45	3 (0.01856)	0.03261	18.5	0.67	0.85	0.014	1.29E-05	1 - 7
960320A	0.5	**1920**	4.95	8 (0.05126)	0.05944	21.2	0.74	0.94	0.008	3.66E-04	1 - 8
960326B	0.5	**1930**	4.45	8 (0.05126)	0.06723	22.1	0.75	0.96	0.016	3.86E-04	1 - 9
960320B**	0.5	**2790**	4.45	8 (0.05126)	0.07379	16.7	0.79	1.01	0.023	0.001564	1 - 10
960422B	0.5	3600	4.04	3 (0.01856)	0.03206	20.0	0.98	1.25	0.014	2.26E-06	1 - 8
960328B	0.5	3600	*4.14*	8 (0.05126)	0.06146	22.6	1.04	1.33	0.010	2.86E-04	1 - 12
*960506A**	*0.5*	*10800*	*4.92*	*3 (0.01856)*	*0.02898*	*26.8*	*1.96*	*2.50*	*0.010*	*3.77E-05*	*1 - 14*
960326A	*0.5*	*10905*	*4.16*	*8 (0.05126)*	*0.08237*	*11.3*	*1.28*	*1.64*	*0.031*	*3.22E-04*	1 - 14
960327A	0.5	11760	4.42	8 (0.05126)							
960415B	0.65	**1790**	3.44	3 (0.01856)	0.02550	49.0	1.08	1.38	0.007	2.54E-05	1 - 7
960403A	0.65	3600	3.38	8 (0.05126)	0.05745	33.5	1.27	1.62	0.006	7.75E-05	1 - 16
960403B	0.65	3600	3.59	8 (0.05126)	0.06086	36.9	1.33	1.70	0.010	3.21E-05	1 - 13
960429A	0.65	3615	3.37	3 (0.01856)			Meeting fronts				
960429B	*0.65*	*3630*	3.01	*3 (0.01856)*	*0.02754*	*40.6*	*1.40*	*1.79*	0.009	*2.55E-05*	*1 - 10*
960415A	0.65	10800	3.31	3 (0.01856)			Meeting fronts				

Specimens tested at +5°C

961009A5	0.5	10800	5.94	8% (0.05126)	0.05638	11.1	1.26	1.61	0.005	4.45E-05	1 - 14
961009B5	0.5	10800	5.92	8% (0.05126)	0.04022	20.8	1.73	2.21	-0.011	1.48E-05	1 - 11
961009A6	0.65	10800	4.38	8% (0.05126)	0.06291	15.8	1.51	1.93	0.012	2.77E-05	1-10,12-13
961009B6	0.65	10800	3.89	8% (0.05126)	0.05869	20.2	1.70	2.17	0.007	3.11E-05	1 - 15

** Initial specimen thickness uncertain* *** Non-diffusion type concentration profile*

Relation between true outer salt concentration and fictive outer concentration

As described above, because unbinding seems to be as large after 4 minutes as after 24 hours, it may also be assumed that binding is fast. Thus, the difference between the fictive outer concentration and the true outer concentration may be taken as a measure of the binding capacity. (Of course, this is true only for the kind of binding detected with these methods. Chloride ions which cannot be unbound unless an acid is used are not included in this "capacity".) This hypothesis requires that the excess concentrations are equal to or greater than zero. From table 5.2.3, it can be seen that a negative excess concentration was obtained in only one case; a specimen tested at +5°.

From table 5.2.3, it can also be seen that the excess chloride ion concentration (in the outermost layer) is relatively constant for each material quality and is also independent of diffusion time and concentration of chloride ions in the outer solution, fig. 5.2.20. This implies that this binding reaches its final value after a period of time shorter than the shortest time used in these tests, *i.e.* half an hour. However, if this binding is so fast that maximum (loose physical) binding is completed long before the experiment is terminated, then the concentration profile should not be a typical diffusion profile. More data than were obtained in this study are required for a more complete description of the diffusion and binding processes.

Correlation with pore system structure

The transport coefficients were not determined here under conditions of steady state. Therefore, there are most likely binding phenomena going on, and we should not expect to find any simple relation between the material pore structure parameters and the transport coefficients. Still, it may be interesting to see the extent to which such relations exist, despite the lack of steady state.

In figure 5.2.21 an attempt has been made to correlate the transport coefficients to porosity. This was done by assuming, on the one hand, that all the pore volume is active in chloride transport and, on the other hand, that only capillary pores are active in the transport. Straight line curve fits have been added. The results are unsatisfactory because both equations predict non-zero transport coefficients at zero porosity.

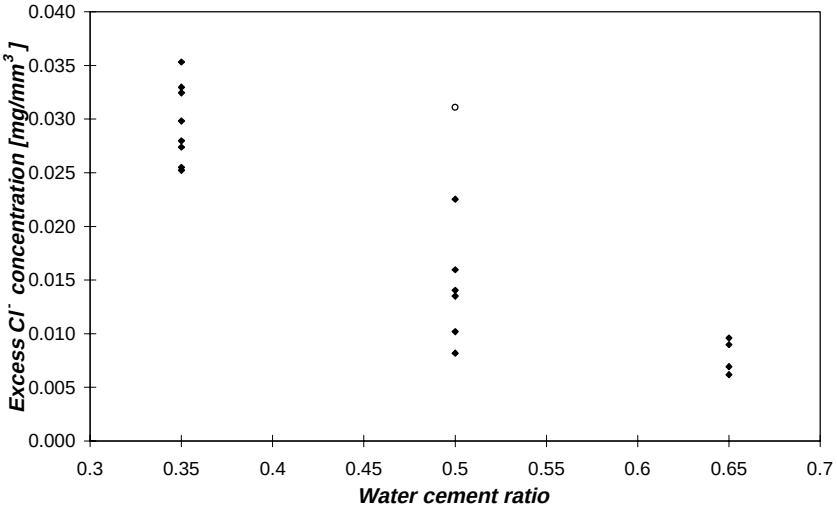

Figure 5.2.20: Excess concentration as defined by eq. (5.2.21) and fig 5.2.19. Unfilled circle: Specimen 960326A (extreme excess concentration and diffusion coefficient, tab. 5.2.3).

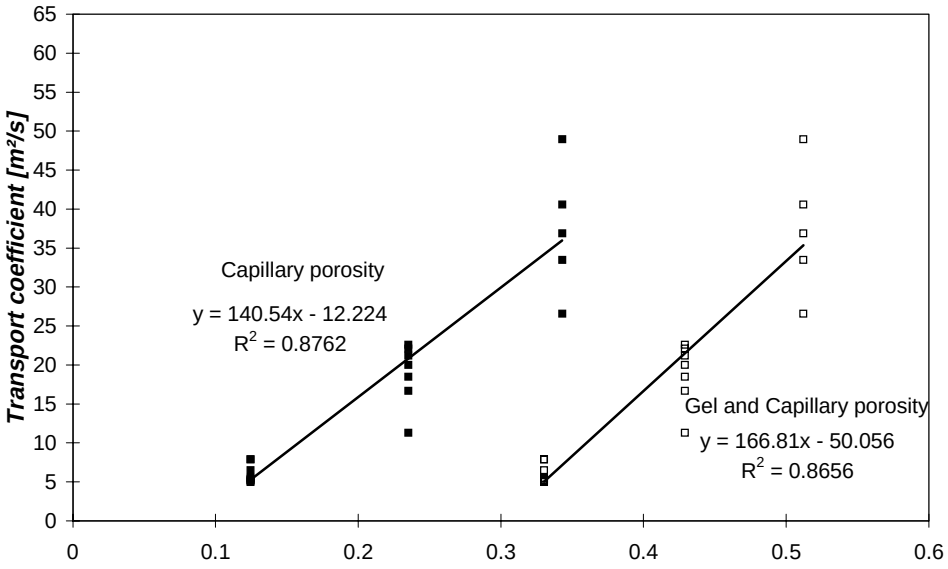

Figure 5.2.21: Calculated transport coefficients vs. capillary porosity and total porosity (gel and capillary porosity), respectively.

The left curve of figure 5.2.21 however suggests that a power function be used. This in turn suggests that the transport coefficients may be related to the pore structure somewhat as predicted for water transport by the Kozeny-Carman equation, according to which the permeability *K* to water for a substance is expressed [S 1960]:

$$K = \frac{P^3}{k \cdot S_w^2 (1-P)^2} \qquad (5.2.22)$$

in which *P* is the porosity, *k* is the Kozeny constant (taking into account a turtuosity factor), and S_w is the area of walls wetted by the streaming water per unit volume of the *solid* phase, *i.e.:*

$$S_w = \frac{a}{1-P} \qquad (5.2.23)$$

in which *a* is the internal pore wall area per unit volume of the porous material. Combining equations (5.2.22) and (5.2.23) we get:

$$K = \frac{P^3}{k \cdot a^2} \qquad (5.2.24)$$

If the chloride ion transport is related to pore structure in the same way as water transport is, there should be a proportionality such that:

$$D \propto \frac{P^3}{a^2} = KC \qquad (5.2.25)$$

in which D is the transport coefficient calculated in table 5.2.3. For the sake of convenience, the right hand side of eq. (5.2.25) will here be denoted by the geometry factor KC of the Kozeny-Carman equation.

The internal area a expressed in m^2/m^3 material may be calculated [P 1948]:

$$a = 3570000 \cdot k \cdot 0.25\alpha \cdot C_v \qquad (5.2.26)$$

in which α is the degree of hydration and C_v is the content of unhydrated cement per unit volume of hardened paste [kg/m^3]. The factor k is the ratio of the monolayer capacity to the amount of chemically-bound water (estimated from the present cement composition to be 0.255 using an equation from Powers and Brownyard) and 0.25 is an approximation of the amount of chemically-bound water per unit weight of cement at complete hydration.

The degrees of hydration, cement contents and calculated specific surfaces and geometry factors KC for the materials used in this study are given in table 5.2.4. A plot of D *versus* KC is given in figure 5.2.22. A straight line fit reveals a good correlation in the sense that zero porosity yields a transport coefficient almost equal to zero. When the lowest transport coefficients obtained for the 0.50 and 0.65 qualities are omitted (because these are probably erroneous), the equation fit changes only slightly, figure 5.2.23. As an approximation, the following equation applies:

$$D = 11.5 \cdot 10^6 KC \qquad (5.2.27)$$

As pointed out above, the transport coefficients were determined under transient conditions and thus binding of chloride ions and leaching of naturally occurring ions make it unreasonable to expect a simple relation between the parameter KC and the transport coefficient. Nevertheless, the results indicate that such a relation may exist. It should be possible to establish a more exact relation from steady state experiments. Since the parameter KC is dependent on cement content and degree of hydration, this will yield an expression for the transport coefficient which takes into account both composition and age (or, rather, degree of hydration) of a Portland cement-bound material. As porosity decreases and specific surface increases as hydration proceeds, the parameter KC will decrease, thus predicting a reduction in the transport coefficient over time. For instance, for a concrete of water/cement ratio 0.50 having reached a degree of hydration of 0.85, which may be the case after a few years of hardening, the transport coefficient as calculated from equation (5.2.27) would be some 30% of the value obtained at an early testing when the degree of hydration is only 0.6 (using equations for the porosity and specific surface by Powers and Brownyard [P 1948]). For higher quality concretes, the reduction would be even larger. Tang [T 1996] published results from measurements of the development of the diffusion coefficient, figure 5.2.24. It is seen in this figure that, during the first two years, the diffusion coefficient is reduced by a factor 2–5 (depending on *w/c* ratio), which indicates that eq. (5.2.27) may be relevant.

It seems reasonable to expect the turtuosity factor in the original Kozeny-Carman equation to be dependent on the relation of gel pores to capillary pores. From the equation fit in figures 5.2.22 and 5.2.23, however, this seems to be of minor importance.

Again, it must be emphasised that the equation (5.2.27) was obtained from chloride ion transport coefficients determined under non-steady state conditions. Therefore, it cannot be expected that this simple relation will hold in all situations. It does however form an interesting basis for future work.

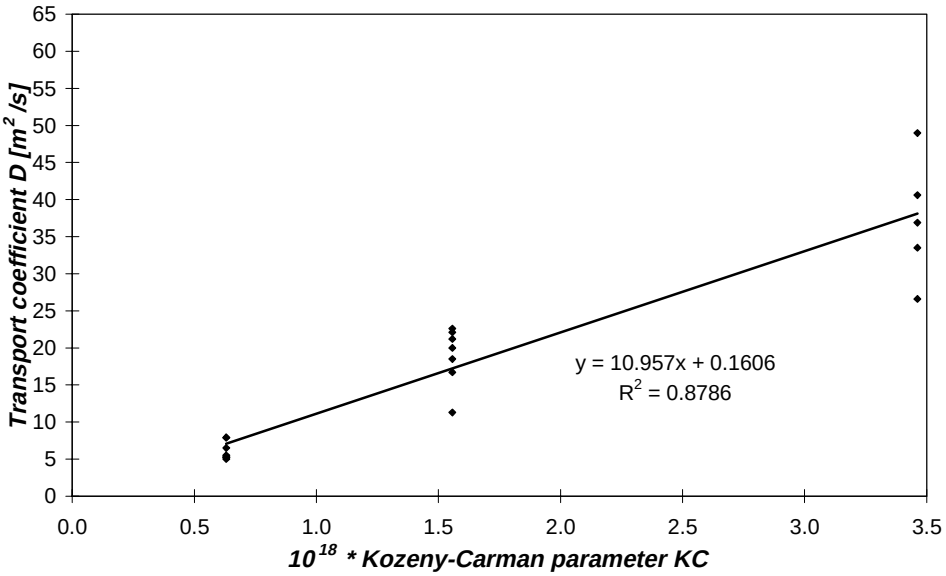

Figure 5.2.22: Relation between calculated transport coefficients and pore structure parameter KC in the Kozeny-Carman equation.

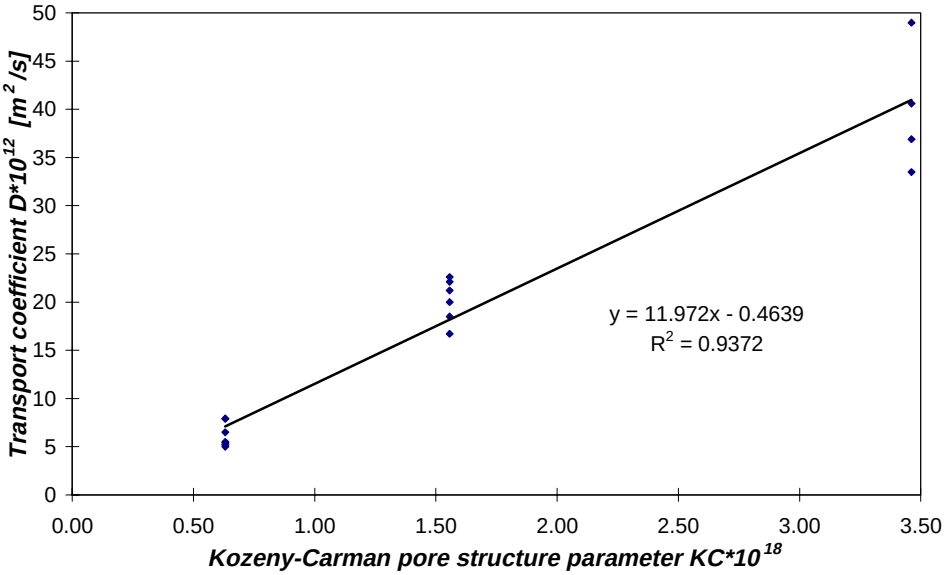

Figure 5.2.23: Relation between calculated transport coefficients and pore structure parameter KC in the Kozeny-Carman equation. Extreme values omitted (described in text)

Table 5.2.4: Parameters used for calculating the pore structure parameter KC in equation (5.2.24).

w/c	α	C_v	*P*	*a* [m²/m³]	*KC*
0.35	0.685	1502.7	0.330	$2.39 \cdot 10^{8}$	$6.30 \cdot 10^{-19}$
0.50	0.791	1226.3	0.429	$2.25 \cdot 10^{8}$	$1.56 \cdot 10^{-18}$
0.65	0.819	1035.8	0.512	$1.97 \cdot 10^{8}$	$3.46 \cdot 10^{-18}$

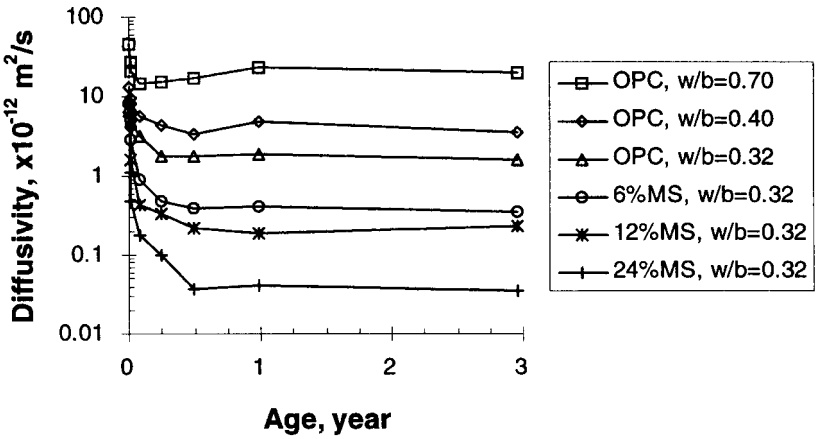

Figure 5.2.24: Examples of age dependence of coefficient of chloride ion diffusion. OPC: Ordinary Portland Cement, MS: Micro Silica.[T 1996]

5.2.11 X-ray mapping

As a comparative check, an X-ray mapping was performed by Senior Lecturer Staffan Hansen at the Division of Organic Chemistry, Lund Institute of Technology.

Two discs of each material quality were exposed to a salt solution, as in the experiments reported above. The salt solution was a 3% NaCl solution and the duration was 3 hours.

After 3 hours, the discs were taken up and broken so that plates of a thickness less than the specimen thickness were obtained. Those surfaces through which chloride ions had come into the specimens were protected against evaporation in order to make evaporation perpendicular to the direction of diffusion, figure 5.2.25. In this way, it was thought the location of the chloride ions along the path they had come into the specimens would not be affected by evaporation. If evaporation were to cause movement of the chloride ions toward the surface of evaporation, the absolute concentrations would be increased, thus facilitating detection of the chloride ions. Due to calibration difficulties, no quantitative analysis was done.

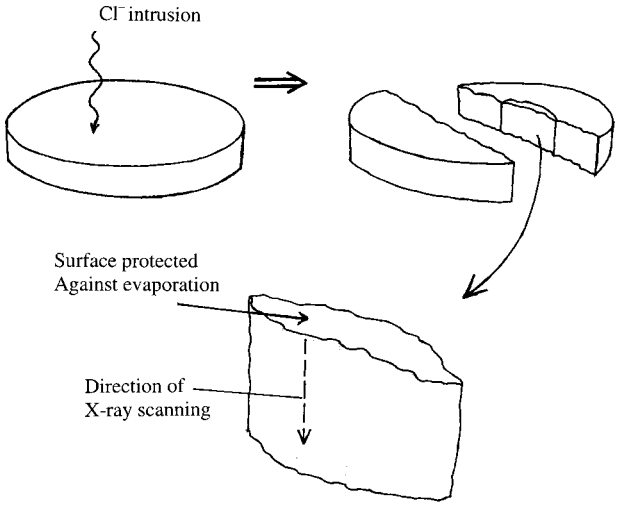

Figure 5.2.24: After the time period of diffusion, the specimens were broken into pieces suitable for X-ray mapping. The directions were chosen so as to minimise any effect of evaporation on the maximum depth of penetration.

The results are given in figure 5.2.25. Unfortunately, the chloride ion concentrations were so low that the general noise in the signals effectively shades the exact depths of penetration. Still, the values which are possible to estimate from the X-ray analyses agree rather well with the calculated 3 hour depths in table 5.2.3.

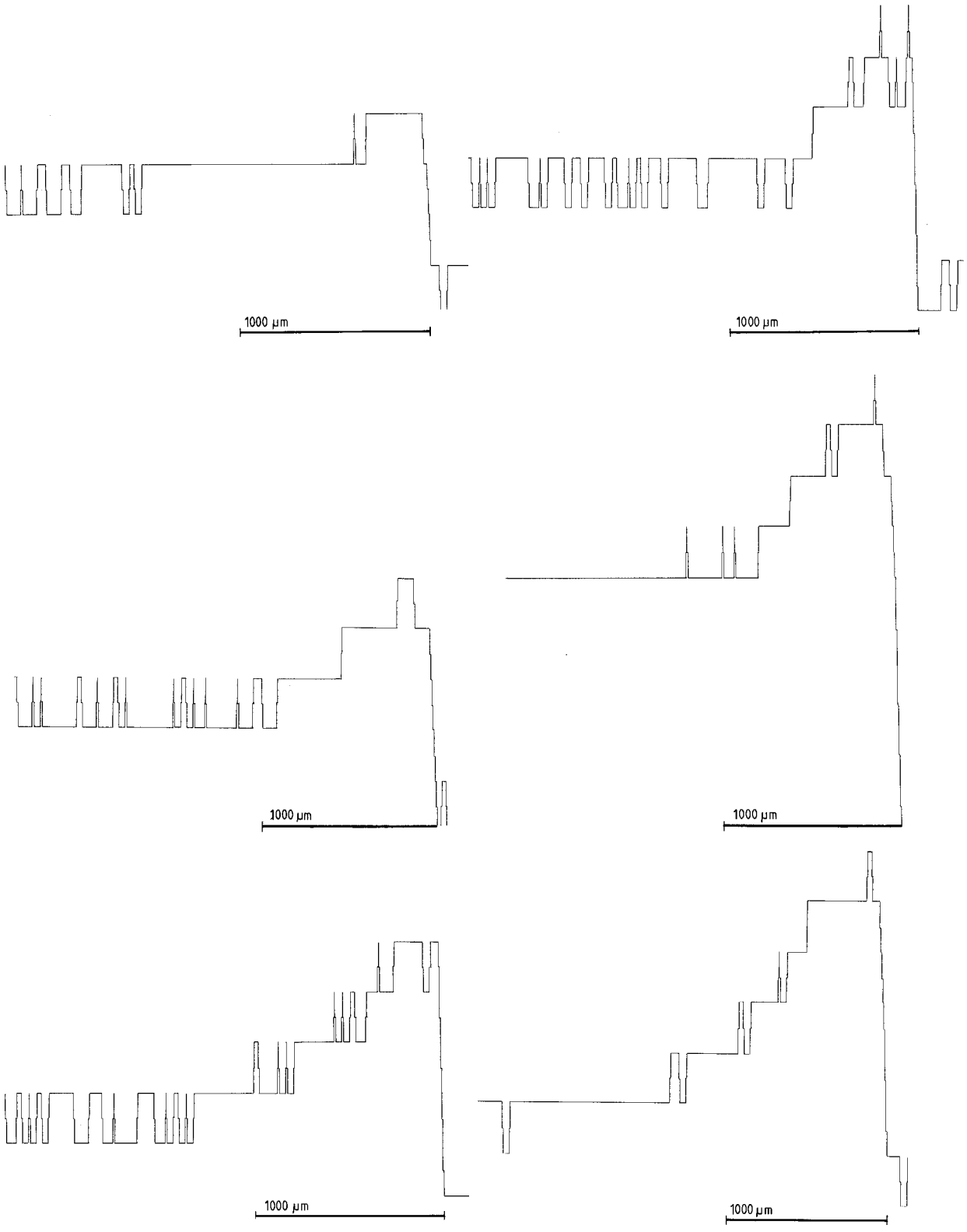

Figure 5.2.25: Chloride ion concentration profiles as detected by X-ray mapping. One sample per profile, two samples per w/c ratio. Upper two profiles: w/c 0.35, middle two: w/c 0.50, lower two: w/c 0.65. Absolute concentrations unknown.

5.2.12 Conclusions

Circular discs of neat Portland cement pastes were subjected to NaCl solutions of different concentrations and for different periods of time. Thin layers were ground off the discs and the ground dust was analysed with respect to Cl^- ions. All concentrations were determined as mass per unit volume of pore solution. The main findings were:

1. The obtained distribution of chloride ions seems to be controlled mainly by a diffusion process.
2. Some loosely ”bound” chloride ions were detected.
3. The amount of ”bound” chloride ions increased with decreasing water/cement ratio.
4. The maximum depth of penetration after 3 hours (at +18°C) was approximately 0.55, 1.0 and 1.3 mm for the neat Portland cement pastes of water/cement ratios 0.35, 0.50 and 0.65, respectively.
5. The transport coefficients for this early stage diffusion depend on the water/cement ratio as expected from previous knowledge. The average values obtained were $6 \cdot 10^{-12}$, $20 \cdot 10^{-12}$ and $40 \cdot 10^{-12}$ m²/s for the water/cement ratios 0.35, 0.50 and 0.65, respectively.
6. The transport coefficients were satisfactorily related to the micro structure of the materials by use of the Kozeny-Carman equation.
7. The maximum depth of penetration as determined by this grinding and leakage method agree fairly well with those observed through X-ray mapping.
8. The total change in pore solution composition was not determined.
9. No conclusions can be drawn as to whether the transport coefficient is affected by the outer salt concentration or the exposure time.
10. There is nothing in the results indicating any anomalous behaviour at a 3% NaCl concentration in the outer concentration.

The possible absolute error in the determination of depth of penetration was estimated to be less than 4% of the calculated value. The possible absolute error in the determination of chloride ion concentration was estimated to be less than 15% of the calculated value.
Due to the too low amount of determinations of transport coefficients at +5°C, it is not possible to make any more precise temperature-dependent calculation of the depth to which chloride ions penetrate the pore system during the hours from beginning of cooling to beginning of freezing.

Data

The complete set of measured data is available from this division.

Appendix 5.2.1: Degree of hydration.

(Calculations described in text.)

Degree of hydration

measurements and calculation of porosities and densities

Assumed weighing errors (±): 0.003 g

Degree of hydration $\alpha = W_n/C/0.25$

Porosity $P = (w/c-0.19\alpha)/(1/\rho_c+w/c)$

Density $D = (1+0.25\alpha)/(1/\rho_c+w/c)$

Cement density $\rho_c = 3.17$ kg/dm^3

(Min and Max values obtained by combining the assumed maximum errors to optimum values)

Specimen	**w/c**	Crucible	Specimen	Crucible + specimen (dried 105°)	Crucible + specimen (ignited 1050°)	Ignited specimen (=C)	Hydr. water (= W_n)	Degree of hydration α	α, min	α, max	**Calc. Porosity %**	min	max	**Calc. density g/cm^3**	min	max
960410	**0.35**	69.955	11.227	81.182	79.531	9.576	1.651	0.690	0.687	0.693	**0.329**	0.328	0.330	**1.762**	1.761	1.763
960410	**0.35**	69.955	11.227	81.182	79.531	9.576	1.651	0.690	0.687	0.693	**0.329**	0.328	0.330	**1.762**	1.761	1.763
960513	**0.35**	75.03	12.908	87.938	86.042	11.012	1.896	0.689	0.686	0.691	**0.329**	0.329	0.330	**1.761**	1.760	1.762
960513	**0.35**	75.03	12.908	87.938	86.042	11.012	1.896	0.689	0.686	0.691	**0.329**	0.329	0.330	**1.761**	1.760	1.762
0.35 4,00	**0.35**	74.873	12.987	87.861	85.946	11.073	1.915	0.692	0.689	0.694	**0.328**	0.328	0.329	**1.763**	1.762	1.764
960423A	**0.35**	76.705	9.197	85.905	84.554	7.849	1.351	0.688	0.685	0.692	**0.329**	0.328	0.330	**1.761**	1.760	1.763
960423B	**0.35**	105.430	9.277	114.707	113.347	7.917	1.360	0.687	0.684	0.691	**0.330**	0.329	0.331	**1.761**	1.760	1.762
960501A	**0.35**	74.816	12.828	87.645	85.821	11.005	1.824	0.663	0.660	0.666	**0.337**	0.336	0.337	**1.752**	1.751	1.753
960501B	**0.35**	75.026	14.363	89.389	87.289	12.263	2.100	0.685	0.683	0.687	**0.330**	0.330	0.331	**1.760**	1.759	1.761
960507B	**0.35**	74.800	13.136	87.935	86.030	11.230	1.905	0.679	0.676	0.681	**0.332**	0.332	0.333	**1.758**	1.757	1.759
960513A*	**0.35**	76.757	5.209	81.966	81.097	4.340	0.869	*0.801*	*0.794*	*0.808*	***0.297***	*0.299*	*0.295*	***1.804***	*1.801*	*1.806*
							Mean:	**0.6851**			**0.3304**			**1.7601**		
							Std-dev	**0.009**			**0.002**			**0.003**		

*not included in mean value calculation

Specimen	w/c	Crucible	Specimen	Crucible + specimen (dried 105°)	Crucible + specimen (ignited 1050°)	Ignited specimen (=C)	Hydr. water (= W_n)	Degree of hydration α	α, min	α, max	**Calc. Porosity %**	min	max	**Calc. density g/cm³**	min	max
960320	**0.5**	76.697	8.844	85.542	84.079	7.382	1.463	0.793	0.789	0.797	**0.428**	0.428	0.429	**1.469**	1.468	1.471
960320	**0.5**	76.697	8.844	85.542	84.079	7.382	1.463	0.793	0.789	0.797	**0.428**	0.428	0.429	**1.469**	1.468	1.471
960326	**0.5**	74.927	8.101	83.028	81.67	6.743	1.358	0.806	0.801	0.810	**0.425**	0.424	0.426	**1.473**	1.472	1.475
960326	**0.5**	74.927	8.101	83.028	81.67	6.743	1.358	0.806	0.801	0.810	**0.425**	0.424	0.426	**1.473**	1.472	1.475
960417	**0.5**	105.602	8.591	114.192	112.805	7.203	1.387	0.770	0.766	0.774	**0.434**	0.433	0.435	**1.462**	1.461	1.464
960417	**0.5**	79.511	6.954	86.466	85.295	5.784	1.171	0.810	0.805	0.815	**0.424**	0.423	0.426	**1.475**	1.473	1.476
960320A	**0.5**	105.441	10.330	115.767	114.072	8.631	1.695	0.786	0.782	0.789	**0.430**	0.429	0.431	**1.467**	1.466	1.468
960326A	**0.5**	79.528	6.529	86.057	85.010	5.482	1.047	0.764	0.759	0.769	**0.435**	0.434	0.436	**1.461**	1.459	1.462
960327A	**0.5**	74.973	6.431	81.409	80.316	5.343	1.093	0.818	0.813	0.824	**0.422**	0.421	0.424	**1.477**	1.476	1.479
960328B	**0.5**	69.956	7.345	77.302	76.071	6.115	1.231	0.805	0.801	0.810	**0.426**	0.424	0.427	**1.473**	1.472	1.475
960416A	**0.5**	105.624	8.941	114.563	113.155	7.531	1.408	0.748	0.744	0.752	**0.439**	0.438	0.440	**1.456**	1.454	1.457
960422B	**0.5**	79.522	6.590	86.121	85.016	5.494	1.105	0.805	0.799	0.810	**0.426**	0.424	0.427	**1.473**	1.471	1.475
960506A	**0.5**	74.928	12.964	87.893	85.829	10.901	2.064	0.757	0.755	0.760	**0.437**	0.436	0.437	**1.458**	1.458	1.459
960508B	**0.5**	69.953	10.365	80.320	78.573	8.620	1.747	0.811	0.807	0.814	**0.424**	0.423	0.425	**1.475**	1.474	1.476
							Mean:	**0.7907**			**0.4289**			**1.4687**		
							Std-dev	**0.022**			**0.005**			**0.007**		

Specimen	w/c	Crucible	Specimen	Crucible + specimen (dried 105°)	Crucible + specimen (ignited 1050°)	Ignited specimen (=C)	Hydr. water (= W_n)	Degree of hydration α	α, min	α, max	**Calc. Porosity %**	min	max	**Calc. density g/cm³**	min	max
960415	**0.65**	105.425	2.569	107.995	107.549	2.124	0.446	0.840	0.826	0.854	**0.508**	0.505	0.511	**1.253**	1.250	1.257
960415	**0.65**	105.425	2.569	107.995	107.549	2.124	0.446	0.840	0.826	0.854	**0.508**	0.505	0.511	**1.253**	1.250	1.257
960429	**0.65**	74.794	3.992	78.785	78.103	3.309	0.682	0.824	0.816	0.833	**0.511**	0.509	0.513	**1.249**	1.247	1.252
960429	**0.65**	74.794	3.992	78.785	78.103	3.309	0.682	0.824	0.816	0.833	**0.511**	0.509	0.513	**1.249**	1.247	1.252
960401A	**0.65**	74.814	2.690	77.508	77.053	2.239	0.455	0.813	0.800	0.826	**0.513**	0.511	0.516	**1.246**	1.243	1.250
960401B	**0.65**	105.692	1.801	107.494	107.174	1.482	0.320	0.864	0.844	0.883	**0.503**	0.499	0.507	**1.259**	1.254	1.265
960403A	**0.65**	76.701	3.191	79.893	79.346	2.645	0.547	0.827	0.816	0.838	**0.510**	0.508	0.513	**1.250**	1.247	1.253
960403B	**0.65**	105.618	3.183	108.801	108.265	2.647	0.536	0.810	0.799	0.821	**0.514**	0.512	0.516	**1.246**	1.243	1.248
960415B	**0.65**	75.025	2.696	77.724	77.263	2.238	0.461	0.824	0.811	0.837	**0.511**	0.509	0.514	**1.249**	1.246	1.252
960429B	**0.65**	76.710	2.561	79.273	78.875	2.165	0.398	0.735	0.722	0.748	**0.529**	0.526	0.531	**1.226**	1.223	1.230
960507C	**0.65**	105.610	4.545	110.158	109.381	3.771	0.777	0.824	0.817	0.832	**0.511**	0.510	0.513	**1.249**	1.247	1.251
960508A	**0.65**	74.928	4.572	79.502	78.742	3.814	0.760	0.797	0.790	0.805	**0.516**	0.515	0.518	**1.242**	1.240	1.244
*960424A**	***0.65***	*75.026*	*2.573*	*77.600*	*77.206*	*2.180*	*0.394*	*0.723*	*0.710*	*0.736*	***0.531***	*0.528*	*0.534*	***1.223***	*1.220*	*1.226*
960424B*	**0.65**	75.070	1.737	76.806	76.483	1.413	0.323	*0.914*	*0.894*	*0.935*	***0.493***	*0.489*	*0.497*	***1.273***	*1.267*	*1.278*
							Mean:	**0.8186**			**0.5122**			**1.2477**		
							Std-dev	**0.031**			**0.006**			**0.008**		

*not included in mean value calculation

Appendix 5.2.2: Data on density and porosity.

(Calculations described in text.)

Determination of porosities and densities
(Arkimedes type measurement)

Assumed errors:
Weighing in air, ±: 0.003 g
Weighing in water, ±: 0.010 g

(Min and Max values obtained by combining the assumed maximum errors to optimum values)

C= Coefficient of variation = standard dev / mean value

Volume = Ws,a - Ws,w
Density = Wdry / Volume
Pore volume =Vp= Ws,a - Wdry
Porosity = Vp / V

$W_{s,a}$ = Weight in air, saturated
$W_{s,w}$ = Weight saturated in water
W_{dry} = Weight in air, dry

W/C = 0.35

Nr	Spec.	w/c	W_{dry}	$W_{s,w}$	$W_{s,a}$	Volume	min	max	**Density**	min	max	Pore vol.	min	max	**Porosity**	min	max
33	*960513A*	*0.35*	*5.213*	*3.265*	*7.763*	*4.498*	*4.485*	*4.511*	*1.159*	*1.155*	*1.163*	*2.550*	*2.544*	*2.556*	*0.5669*	*0.565*	*0.569*
18	*960423A*	*0.35*	*9.419*	*5.785*	*10.988*	*5.203*	*5.190*	*5.216*	*1.810*	*1.805*	*1.815*	*1.569*	*1.563*	*1.575*	*0.3016*	*0.300*	*0.303*
11	960410B	0.35	11.206	7.062	13.424	6.362	6.349	6.375	**1.761**	1.757	1.765	2.218	2.212	2.224	**0.3486**	0.347	0.350
19	960423B	0.35	9.255	5.849	11.066	5.217	5.204	5.230	**1.774**	1.769	1.779	1.811	1.805	1.817	**0.3471**	0.346	0.349
24	960501A	0.35	12.812	8.078	15.351	7.273	7.260	7.286	**1.762**	1.758	1.765	2.539	2.533	2.545	**0.3491**	0.348	0.350
25	960501B	0.35	14.316	9.029	17.108	8.079	8.066	8.092	**1.772**	1.769	1.775	2.792	2.786	2.798	**0.3456**	0.345	0.347
27	960507B	0.35	13.167	8.256	15.756	7.500	7.487	7.513	**1.756**	1.752	1.759	2.589	2.583	2.595	**0.3452**	0.344	0.346
34	960513B	0.35	12.931	8.099	15.474	7.375	7.362	7.388	**1.753**	1.750	1.757	2.543	2.537	2.549	**0.3448**	0.344	0.346
								Mean:	**1.763**						**0.347**		
								Std-dev	**0.008**						**0.002**		
								min:	1.753						0.345		
								max	1.774						0.349		

W/C = 0.50

Nr	Spec.	w/c	W_{dry}	$W_{s,w}$	$W_{s,a}$	Volume	min	max	**Density**	min	max	Pore vol.	min	max	**Porosity**	min	max
1	960320A	0.5	10.315	6.480	13.459	6.979	6.966	6.992	**1.478**	1.475	1.481	3.144	3.138	3.150	**0.4505**	0.449	0.452
2	960320B	0.5	8.834	5.548	11.478	5.930	5.917	5.943	**1.490**	1.486	1.493	2.644	2.638	2.650	**0.4459**	0.444	0.447
3	960326A	0.5	6.565	4.108	8.530	4.422	4.409	4.435	**1.485**	1.480	1.490	1.965	1.959	1.971	**0.4444**	0.442	0.446
4	960326B	0.5	8.084	5.073	10.530	5.457	5.444	5.470	**1.481**	1.477	1.485	2.446	2.440	2.452	**0.4482**	0.447	0.450
5	960327A	0.5	6.358	4.018	8.282	4.264	4.251	4.277	**1.491**	1.486	1.496	1.924	1.918	1.930	**0.4512**	0.449	0.453
6	960328B	0.5	7.355	4.581	9.515	4.934	4.921	4.947	**1.491**	1.486	1.495	2.160	2.154	2.166	**0.4378**	0.436	0.440
14	960416A	0.5	8.883	5.611	11.561	5.950	5.937	5.963	**1.493**	1.489	1.497	2.678	2.672	2.684	**0.4501**	0.449	0.452
15	960417A	0.5	6.987	4.345	9.133	4.788	4.775	4.801	**1.459**	1.455	1.464	2.146	2.140	2.152	**0.4482**	0.446	0.450
16	960417B	0.5	8.557	5.380	11.215	5.835	5.822	5.848	**1.466**	1.463	1.470	2.658	2.652	2.664	**0.4555**	0.454	0.457
17	960422B	0.5	6.641	4.150	8.560	4.410	4.397	4.423	**1.506**	1.501	1.511	1.919	1.913	1.925	**0.4351**	0.433	0.437
26	960506A	0.5	12.992	8.068	16.982	8.914	8.901	8.927	**1.457**	1.455	1.460	3.990	3.984	3.996	**0.4476**	0.447	0.449
31	960508B	0.5	10.395	6.470	13.529	7.059	7.046	7.072	**1.473**	1.469	1.476	3.134	3.128	3.140	**0.4440**	0.443	0.445
								Mean:	**1.481**						**0.447**		
								Std-dev	**0.015**						**0.006**		
								min:	1.457						0.435		
								max	1.506						0.456		

W/C = 0.65

Nr	Spec.	w/c	W_{dry}	$W_{s,w}$	$W_{s,a}$	Volume	min	max	**Density**	min	max	Pore vol.	min	max	**Porosity**	min	max
7	*960401A*	*0.65*	*2.762*	*1.714*	*2.642*	*0.928*	*0.915*	*0.941*	*2.976*	*2.932*	*3.022*	*-0.120*	*-0.126*	*-0.114*	*-0.1293*	*-0.135*	*-0.124*
8	*960401B*	*0.65*	*1.830*	*1.129*	*0.519*	*-0.610*	*-0.623*	*-0.597*	*-3.000*	*-3.060*	*-2.942*	*-1.311*	*-1.317*	*-1.305*	*2.1492*	*2.184*	*2.115*
10	960403B	0.65	3.182	2.016	4.664	2.648	2.635	2.661	**1.202**	1.195	1.209	1.482	1.476	1.488	**0.5597**	0.556	0.563
12	960415A	0.65	2.561	1.611	3.750	2.139	2.126	2.152	**1.197**	1.189	1.206	1.189	1.183	1.195	**0.5559**	0.551	0.561
13	960415B	0.65	2.711	1.694	3.963	2.269	2.256	2.282	**1.195**	1.187	1.203	1.252	1.246	1.258	**0.5518**	0.547	0.556
20	960424A	0.65	2.577	1.632	3.560	1.928	1.915	1.941		1.326	1.347	0.983	0.977	0.989		0.505	0.515
21	960424B	0.65	1.731	1.086	2.523	1.437	1.424	1.450	**1.205**	1.192	1.218	0.792	0.786	0.798	**0.5511**	0.544	0.558
22	960429A	0.65	3.950	2.506	5.799	3.293	3.280	3.306	**1.200**	1.194	1.205	1.849	1.843	1.855	**0.5615**	0.558	0.565
23	960429B	0.65	2.579	1.659	3.777	2.118	2.105	2.131	**1.218**	1.209	1.227	1.198	1.192	1.204	**0.5656**	0.561	0.570
29	960507C	0.65	4.615	2.851	6.582	3.731	3.718	3.744	**1.237**	1.232	1.242	1.967	1.961	1.973	**0.5272**	0.525	0.530
30	960508A	0.65	4.621	2.918	6.778	3.860	3.847	3.873	**1.197**	1.192	1.202	2.157	2.151	2.163	**0.5588**	0.556	0.561
9	960403A	0.65	3.188	2.008	4.590	2.582	2.569	2.595	**1.235**	1.227	1.242	1.402	1.396	1.408	**0.5430**	0.539	0.547
								Mean:	**1.209**						**0.553**		
								Std-dev	**0.016**						**0.012**		
								min:	1.195						0.527		
								max	*1.237*						0.566		

6

HYPOTHESIS REGARDING THE MECHANISM OF SALT FROST SCALING

In this chapter, a mechanism for salt frost scaling on Portland cement-bound materials is proposed. It is hypothesised that ice bodies inside the material are able to grow and to exert disruptive pressures because the outer liquid phase can be sucked into the pores, thereby acting to maintain the free energy of the pore solution in the immediate vicinity of the ice body. The basic mechanism is principally the same as that responsible for macro ice lens formation in soils. Explanations of phenomena observed in salt frost scaling tests are proposed. Different ways of further testing the relevance of the hypothesis are also proposed.

Section 6.2 presents results from two tests which were run in order to reject the hypothesis in the event their results deviated from what had been predicted by the proposed mechanism. Experimental results show that water is taken up during freezing and that a salt solution has a drying effect on specimens stored in water - two facts which support the hypothesis.

An initial discussion of the hypothesis was presented at the RILEM TC-117 meeting in Helsinki, Finland, August 1996. Since then, the hypothesis has been further developed and more laboratory tests have been run.

6.1 HYPOTHESIS

6.1.1 Introduction

In order to predict the service life of a concrete structure in a certain environment, it is necessary to know the true mechanism(s) causing destruction. In this chapter, a hypothesis for such a mechanism is presented which may be used to explain many of the experimental results reported from laboratory studies.

The proposed mechanism basically relies on the phenomenon of osmotic ice body growth which is due to differences in level of free energy between an ice body and the moisture in its surroundings. Such ice body growth has previously been proposed to be the reason for soil heaving [T 1930] and to be the cause of frost destruction in the interior of concrete [P 1953]. The present description differs from previously proposed mechanisms regarding the salt frost resistance of concrete in that it emphasises the possibility which exists for concrete exposed to a salt solution to take up liquid during freezing. As compared to the mechanisms of soil heaving, which may be seen as an open system, it also considers the effects of salts. The present hypothesis therefore should not be regarded as something entirely new; rather, it is a new application of well-known basic mechanisms.

If further laboratory studies make it seem reasonable that this is the major mechanism, it should be possible to apply the mechanism, with due consideration of all the various environmental conditions and the way in which these affect the material, to estimations of the service life of concrete structures.

The hypothesis is first briefly described in its entirety before a more detailed description and the physical principles are dealt with.

Brief description

The main principle of the mechanism proposed here is that osmotic ice body growth in a concrete specimen is significantly facilitated, as compared to the situation in the interior of a moisture isolated specimen, when the pore liquid is connected to a reservoir of liquid in which the liquid pressure remains atmospheric. It is the central role of the salt in the outer solution to provide such a reservoir of liquid at temperatures below the freezing point of the pore solution.

Osmotic ice body growth occurs in the pore system of hardened cement paste when the free energy of the pore liquid is higher than that of the existing ice. The free energy of either phase is changed if their respective temperatures or pressures are changed. In addition, the free energy of the pore liquid is changed if its mole fraction of water is changed. At the interface between the two phases, the temperature difference between the ice and the liquid will be practically insignificant and the mole fraction of the liquid may be changed only slowly by the addition of solutes from an outer source. The remaining possibility of achieving equilibrium thus lies in the possibility of establishing a pressure difference between the two phases. If the pore liquid is connected to a large source of liquid in which the atmospheric pressure is maintained, and provided replacement of pore liquid by liquid from that outer source is not hindered by too high a resistance to the flow of liquid into the pore system, the pressure of the liquid close to the ice body cannot be reduced to establish equilibrium. The only remaining possibility is that of increasing the ice pressure. Such pressure will arise when the growing ice body meets the walls of the pore in which it is growing. However, the pressure needed for equilibrium may easily

reach such magnitudes that normal, porous building materials are deteriorated (chapter 2.4 and below).

The effect of the outer liquid on the possibilities of ice body growth in the interior of the specimen is actually twofold: firstly, it allows ice body growth to proceed much further than would be possible if only the natural pore solution were available. Secondly, since there will be thermodynamically unstable water in small pores for a much longer time than in a specimen frozen without access to an outer liquid, the probability of *in situ* ice formation, through annulment of super cooling, increases. Such *in situ* ice formation in saturated small pores may cause disruptive pressures.

Before outlining the details of the processes which are to be expected from the proposed hypothesis, the principles of micro ice body growth are described.

6.1.2 Osmotic ice body growth in porous systems

At the triple point of water, ice and water are in equilibrium, *i.e.* their levels of free energy are equal. When the system is further cooled, the free energy of the water increases more than that of the ice, because the entropy of liquid water is higher than that of ice; $dG/dT = -S$ (chapter 2.4). Consequently, transition of molecules from the liquid to the ice will reduce the free energy of the system. Thus, continued ice formation is a spontaneous process, which will not stop until some of the thermodynamic parameters of either or both of the phases have been changed sufficiently to make the free energy of the two phases equal.

For a system of liquid in a narrow, conical cylindrical pore of radius r_l and an ice body in a somewhat wider cylinder of radius r_s (figure 6.1.1), equilibrium is established when an exchange of water molecules between the ice and the liquid causes no change in free energy of the system, *i.e*:

$$\frac{dG_{sys}}{dn} = 0 \qquad (6.1.1)$$

in which n is the number of molecules in either the ice or the water. Since the total number of molecules must remain constant in a closed system, $dn_s = -dn_l$. Setting $dn = dn_s = -dn_l$, we get (from eq. (2.4.5)):

$$dG_{sys} = dn(\mu_s - \mu_l) \qquad (6.1.2)$$

Thus, if the chemical potential of the ice is lower than that of the liquid, ice formation will be a spontaneous process. By setting $\Delta\mu = \mu_s - \mu_l$ and using equation (2.4.36), we get:

$$\begin{aligned}\Delta\mu = &-S_{m,s}(T_s - T_{ref}) + V_{m,s}(P_s - P_{ref}) + \frac{2\Delta\sigma_{s-m}}{r_s}V_{m,s} \\ &+ S_{m,l}(T_l - T_{ref}) - V_{m,l}(P_l - P_{ref}) - \frac{2\Delta\sigma_{l-m}}{r_l}V_{m,l} - RT\ln(X_{H_2O})\end{aligned} \qquad (6.1.3)$$

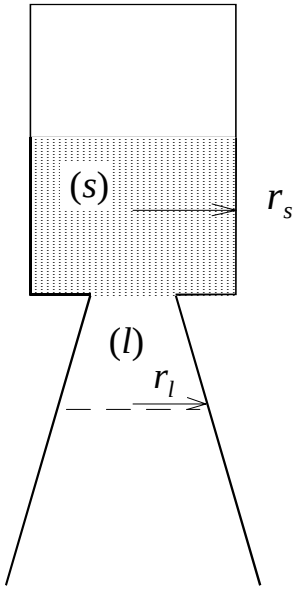

Figure 6.1.1: Model for eq. (6.1.3): Two cylindrical pores of circular cross section. Ice body of radius r_s growing in the larger one. The smaller one, which is somewhat conical and open to the surroundings at its lower end, is filled to such an extent that the meniscus is located where the radius of the conical pore is r_l

The interpretation of eq. (6.1.3) is that transfer of moisture from the liquid to the ice body is spontaneous when the difference in chemical potential, $\Delta\mu$, is negative.

An example will illustrate how drainage of the pore system or an increase in the pressure on the ice affects the equilibrium. Suppose an ice body of radius 1 µm exists in a pore connected to a water filled, conical channel (fig. 6.1.1) at T = 263.15 K (-10°C). In order to establish equilibrium between the ice and the liquid water without any increase in ice pressure, it can be calculated from eq (6.1.3) that the conical pore must be drained to the extent that the water-air meniscus will be located where the radius of the conical pore is r_l = 12 nm. However, if the drained water is continuously replaced with liquid water from an outer source, the required radius will never be reached. Instead, equilibrium will be established when the pressure on the ice body reaches 11.9 MPa. (Additional examples were given in chapter 2.4.)

Suppose equilibrium has been established between the ice and the water in the model in figure 6.1.1. When temperature drops, the equilibrium will be disturbed and phase transition will take place. From eq. (6.1.3), the following ways of re-establishing equilibrium may be identified:

- Raising the temperature of the ice to a level sufficiently above that of the liquid, and/or
- Reducing the mole fraction of water in the liquid phase, *e.g.* by adding some salt to it, and/or
- Increasing the pressure of the *ice* phase, and/or
- Reducing the pressure of the liquid phase, and/or
- Partially draining the pore system, by which process the meniscus separating liquid from air will move through the pore system towards more narrow pores, thereby increasing the total interface energies of the system and also increasing the rate at which

the interface energy increases in relation to the amount of water drained out of the pores.

Often, changes in free energy of the system that are in fact due to interface area changes are described (by use of the radius of curvature of the meniscus separating the liquid phase from the vapour) as being due to changes in pressure. However, since the shape of the meniscus is a consequence of the interface energies (of three interfaces), it is more straightforward to describe the changes in free energy of the system in terms of changes in interface areas (and possibly changes in interface energy per unit area). The pressure in the liquid should therefore be avoided as an explanation, unless the pressure of the liquid is in fact affected in some way, for instance by mechanical pressure applied to the entire system.

In practice, however, the temperature of an ice body in the interior of a porous specimen cannot enduringly adopt a different temperature than its surroundings. This way of re-establishing equilibrium therefore must be considered impossible.

The possibility of re-establishing equilibrium by any of the other means varies depending on whether or not the system is capable of exchanging matter with its surroundings, *i.e.* whether the system is a closed or an open one. A specimen subjected to a salt-frost scaling test may be considered to be an open system and this is where the present hypothesis applies. Before outlining the principles of the hypothesis, some comments on osmotic ice body growth in closed systems may be appropriate.

Ice body growth in a moisture isolated specimen

In a closed system, neither the number of water molecules nor the amount of dissolved ions can change (provided no chemical reactions with the solid matrix occur). Thus, partially draining the pore system and/or increasing the pressure of the ice are the only means of re-establishing equilibrium (this change will also cause a change in the mole fraction of water in the pore solution, but the amount of dissolved substances will remain constant). The reason for the ”and/or” is the fact that while the ice pressure will not increase unless partial draining occurs (because the ice grows by consuming water from the solution, thus reducing the volume of the solution), partial drainage may occur without simultaneous ice pressure increase if the ice is growing in a non-saturated pore.

Thus, if the permeability to water flow is high enough, moisture will be transported from the pore solution to the ice body until the required drainage is attained. If the degree of saturation is too high, equilibrium will not be established by the time the ice body starts exerting pressure on the pore walls. Since the ice body pressure required for equilibrium easily attains several MPa, many building materials are readily destroyed soon after the pore containing an ice body is completely filled. On the other hand, if there is ample room for the ice bodies to grow, equilibrium may be attained before the material is damaged by partial drying of the pore system. This was proposed by Powers and Helmuth [P 1953] as the explanation of the function of entrained air pores. Furthermore, since the pore system is no longer saturated, it may now be described as being in a state of suction.

If the permeability to moisture flow is too low in relation to the heat flow rate, moisture may not be transported from the surrounding pores to the growing ice bodies fast enough. Instead, new ice bodies may form in the surrounding pores. Of course, such *in situ* ice formation blocks the pores and reduces permeability even more. It most probably also causes high hydraulic pressures and may possibly be considered to be like the freezing of water in a closed container. Such *in situ* ice formation is highly dependent on

the possibilities of nucleation *in situ*, *i.e.* it is highly dependent on the possibilities of heaving any local super-cooling. This possibility increases as temperature decreases, but if a high cooling rate is used, the time available for heaving of super-cooling is also decreased. According to Helmuth [H2 1960], the mechanism of ice formation in hardened cement paste is osmotic ice body growth even at rates of cooling of 30°C/h.

6.1.3 Micro ice body growth in non moisture isolated systems – Proposed mechanism of ”salt frost scaling”

The second case of interest is that of ice body growth in a non-sealed specimen, especially in its surface region, figure 6.1.2. Here, the ”outer environment” may be air, pure water or a solution containing some kind of de-icing agent.

- If the outer environment is air, ice bodies close to the surface will have less moisture accessible to them than to crystals in the interior. (Here, ”close to” means about half a millimetre from the surface, a value based on the critical thickness of cement paste with regard to frost attack, see below.) Therefore, the partial drainage required for equilibrium is more readily established here than in the interior of the specimen and, consequently, the surface is likely to suffer less damage than the interior. Just like in a closed system, because the pores are partially drained, the system may be considered to be in a state of suction. (This first case may, to some extent, be seen as a special case of ice body growth under conditions of moisture isolation. It also explains why surface scaling rarely occurs on specimens isolated from moisture exchange.)

- If the surface is covered with pure water, and provided the specimen is unidimensionally cooled via that surface, an outer ice layer will form before any ice forms in the capillary pores. Menisci between outer ice and the pore solution form at B and C (fig. 6.1.2). Now, as cooling proceeds, moisture will move from the pore solution to the outer ice, a process by which the uppermost part of the specimen is protected from frost deterioration, in the same way ice bodies in entrained air pores protect the surrounding paste from frost deterioration, as proposed by Powers and Helmuth [P 1953].

- The final case, in which the surface is covered with a de-icing agent solution, is where the proposed mechanism applies: for temperatures between the freezing point and the eutectic temperature of a salt solution, the outer solution will be a mix of ice and liquid solution. Thus there will be no meniscus between the outer solution and the pore solution, only a diffuse zone where the salt (if that is the de-icing agent) concentration varies. When ice bodies inside the specimen start consuming the pore solution close to them, the outer solution is sucked into the specimen and the drainage required for equilibrium is never reached. Instead, ice bodies are able to grow and to exert pressure on the pore walls to the depth to which moisture may flow sufficiently easily. This will continue as long as the de-icing agent in the outer solution is not transported into the growing ice body to such an extent that its concentration in the pore liquid immediately surrounding the ice body is high enough to restore equilibrium.

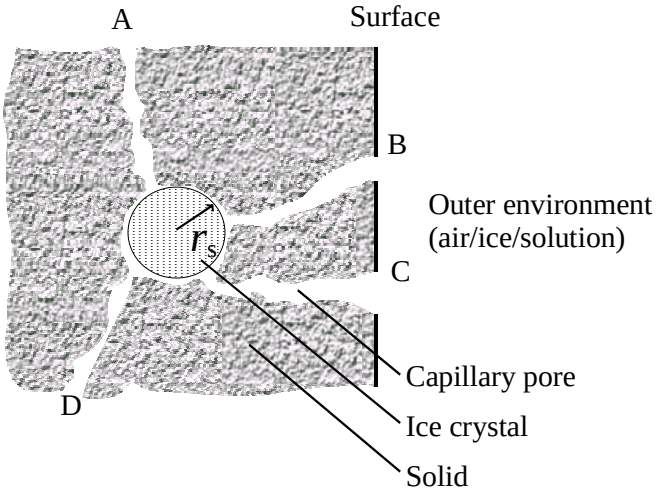

Figure 6.1.2: Ice body growing close to the surface of a micro-porous material.

Counter-force

At every temperature above its eutecticum, the chemical potential of the outer solution will be as low as that of bulk ice (and even lower if temperature is above the freezing temperature of the solution). The outer solution therefore ought to have the same draining effect on the pore solution as outer ice has. Thus, moisture absorption during freezing might be thought to be impossible. As will be seen in section 7.1, such (partial) drainage does in fact occur at room temperature. At freezing temperatures, however, the net effect is moisture uptake. Thus the suction caused by the growing ice bodies dominates the draining caused by the outer solution. In fact, it can be seen that the inner ice bodies dominate even when the chemical potential of the outer solution is lower than that of bulk ice at the same temperature!

The following is thought to be a reasonable explanation. Moisture flows along with and proportionally to its gradient in chemical potential (*e.g.* [A 1990]). The gradient in chemical potential between the pore water and the growing ice body occurs across the meniscus separating the two phases, *i.e.* over a distance of approximately one molecule diameter. Thus the gradient is steep and provides a large force for moisture flow. Furthermore, this gradient is mechanically fixed to the position of the ice body. The gradient in chemical potential due to the presence of dissolved substances will not be as steep, as this drop occurs over a larger distance (the diffuse zone of varying concentration of solutes) and, more importantly, this zone is mobile; when suction occurs at the ice/pore liquid interface, the entire pore solution may move through the pores.

6.1.4 The ice body growth process – a coupled heat and mass transfer process

Suppose a tensionless ice body exists at a certain depth below the specimen surface as shown in figure 6.1.2. Suppose also that the permeability of the material allows moisture from outside to flow into the pore system rapidly enough to keep the non ice-filled part of the pore system at a constant level of saturation, *i.e.* the chemical potential of the pore

solution remains at a constant level (of course this means disregarding the effects of the incoming solutes).

The driving force for the phase transition, and thus for the moisture flow rate, is then the temperature-induced difference in chemical potential $\Delta\mu$ between the ice body and the pore solution, eq. (6.1.3). When phase transition occurs, heat is released and the temperature is raised. Thus the driving force decreases.

The temperature rise causes a heat flow from the site of freezing proportional to the rate of phase transition. If the heat released is lead away rapidly enough, the temperature will remain constant, despite the heat released by ice formation, and the driving force for moisture flow will remain unchanged. The system thus may be described as being in a state of dynamic equilibrium.

If a heat flow rate larger than that required for dynamic equilibrium is applied, the specimen temperature will drop. This increases the driving force for ice body growth and thus even greater moisture absorption will occur (provided moisture is available and the pore system is not clogged by ice forming in the smaller pores).

The described ice body growth does not take place at one single depth. Instead, it is likely to occur at several depths and under varying conditions (due to the variation with depth of the temperature, moisture content, and mole fraction of water in the pore solution). This means the dynamic equilibrium described above is adjusted so that there is a balance between moisture accessibility, heat flow rate and the rate of ice body growth at each and every depth.

Since there is no analytical solution which may be used to illustrate the complete phenomenon (including varying temperature, changing mole fraction of water, varying permeability etc.), a numerical solution is needed. Thus far, however, no such complete numerical solution has been carried out successfully. Therefore, the following discussion of the importance of different parameters must necessarily be a qualitative one.

6.1.5 Effect of micro pore structure on the rate of moisture absorption

The micro pore structure affects the described processes indirectly because it affects the coefficient of heat transfer, the amount of ice formed at a given temperature, and the material's intrinsic permeability to flow of water. From the above description, it should be clear that the described osmotic ice body growth is facilitated if the value of any of these parameters is increased.

The coefficient of heat transfer is dependent on the coefficients of heat transfer of each of the constituents (the solid matrix, the water and the ice). For a normal Portland cement-based material, the largest coefficient of heat transfer is that of the solid phase. Thus, the less pore space, the larger the total coefficient of heat transfer will be and the more the osmotic ice body growth will be facilitated. However, for normal Portland cement-based materials, the relative amounts of the constituents varies within a very small interval and, thus, the total changes in coefficient of heat transfer are small compared to the effects of, for example, permeability.

It was shown in figure 2.1.2 that permeability increases rapidly with increasing capillary pore space. Thus, an increased micro pore porosity will facilitate osmotic ice body growth. Since capillary porosity increases with increasing *w/c* ratio, moisture absorption during freezing should therefore increase with increasing *w/c* ratio. This was shown to be true by Jacobsen [J 1995] and it is also shown in the laboratory tests reported in the next chapter. Thus, so far, the proposed mechanism accords with reality.

Moisture absorption increases as the number of ice bodies increases, since there are then more ice bodies consuming pore liquid. The number of existing ice bodies is mainly dependent on micro-pore size distribution and, again, we can see that increasing the water/cement ratio indirectly increases moisture absorption. Whether the dominating effect of the micro-pore size distribution is that on the permeability or that on the number of ice bodies is impossible to say at present.

If the pores are single-sized, then the first freezing will take place in all pores at the same temperature (except for effects of super-cooling). In such a case, permeability will be reduced to such an extent that the subsequent in-flow of water, and thus also the ice body growth, may stop. The only remaining possibility for moisture transport will be via the liquid-like layer which may exist between the ice bodies and the pore walls (chapter 2.3). This should be true both for coarse and fine porous materials, the difference being in the temperature level at which ice formation begins. For materials with well-spread pore size distributions, the remaining permeability may be high enough to allow moisture to be transported into the growing ice bodies. While cement-based materials have this type of well-spread pore size distribution, other materials, *e.g.* some sandstones, may have narrow pore size distributions and may therefore behave differently from cement-based materials in salt frost freezing experiments.

6.1.6 Effect of environmental conditions on the rate of moisture absorption

The following discussion is intended to shed some light on the ways in which final scaling may be affected by the variation of some or all those parameters which, according to the proposed hypothesis, affect the scaling process. If it turns out that a change in any single parameter also affects other parameters, then experiments in which the effect of one parameter is studied by changing only that single parameter may produce seemingly strange results, which are actually the results of some other variation caused by the ”thought-to-be” single parameter variation.

Effect of temperature

The main effect of a low temperature is that it increases the driving force for ice body growth (eq. (6.1.3)) and thus the ice pressure needed for equilibrium, provided the chemical potential of the pore water is not changed in any other way. Furthermore, at lower temperatures, more of the initially present pore solution will be freezable. This will increase the number of ice bodies that may grow by the described mechanism and thereby add to the pressures inside the material.

At low temperatures, the resistance to moisture flow increases because of the temperature dependence of the viscosity of water. This effect, however, is small in comparison to the increased driving force: while a temperature change from 0°C to -20°C increases the viscosity by a factor of about 2 (fig. 2.2.4), it increases the driving force from 0 to some 25MPa (fig. 2.4.5).

In chapter 4, it was seen that a reduced minimum temperature of the frost cycle has been reported several times to result in more scaling. Thus, the predicted effect of a lower temperature is confirmed.

Effect of cooling rate (cooling heat flow rate)

The cooling rate influences moisture absorption in at least two ways. Firstly, rapid cooling means there will be less time for moisture absorption during cooling and thus that scaling is likely to decrease with increasing cooling rate (if the rest of the frost cycle is unchanged). Secondly, an intense heat flow rate means the balance between heat flow rate and moisture flow rate will be displaced towards the specimen surface, thus reducing the zone in which ice body growth may cause disruption. However, scaling may be repeated several times during the cooling phase, so the final result cannot be qualitatively predicted. Furthermore, if cooling rate is reduced, the time for moisture absorption is prolonged at temperatures at which only a little ice forms in the pores, thereby reducing permeability. As was seen in chapter 4, it has not been possible as yet to determine experimentally any significant effect of the cooling rate.

Effect of de-icer distribution

To illustrate the basis for the following discussion, we shall first re-visit figure 6.1.2 and assume that the previously described dynamic equilibrium has been established. Then, for an infinitesimal time interval and for a given situation (in terms of temperature and mole fraction of water in the pore solution close to the ice body), the following discussion applies.

Figure 6.1.3 illustrates three principal cases in which the surface of a specimen of a material of well-spread pore size distribution (like that of HCP) is exposed to a salt solution and to a heat flow rate perpendicular to the surface. At each and every depth, $D\mu$ is the difference in chemical potential between the ice bodies and the surrounding pore solution, eq. (6.1.3). The temperature is below the freezing point of the pore solution and the temperature gradient is small. The cases are as follows:

- In the first case, figure 6.1.3A, the de-icer concentration is zero in the pore solution and thus the driving potential for ice body growth is not disturbed by any dissolved substances. The maximum driving potential, as described by equation (1), is reached. This ice body growth consumes moisture from the pore solution and so moisture is sucked into the specimen from the outer liquid phase. At every depth, ice body growth takes place at a rate determined by the balance between heat withdrawn and the flow of moisture reaching each depth. Since the resistance to moisture transport increases with the depth of each ice body, the ice bodies closer to the surface will grow faster than the more deeply lying ones. Thus, in this case, ice body growth takes place immediately, from the surface inwards, its intensity diminishing with depth.

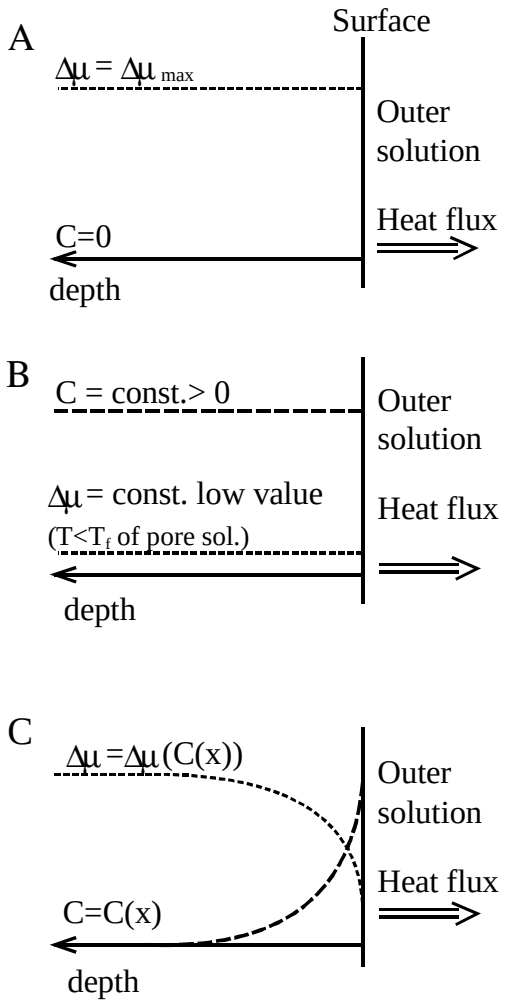

Figure 6.1.3: Illustration of the variation in driving chemical potential difference with depth and salt concentration. Temperature is below the freezing temperature of the solution and its gradient is too small to significantly affect the equilibria. No mechanical pressures in ice or solution. Δμ is the difference in chemical potential between large ice bodies and the surrounding pore solution (eq. 6.1.3).

- In figure 6.1.3B, the de-icer is present everywhere at a given, constant concentration. The first effect of this concentration is that no ice forms until the temperature has reached a lower level than that needed in the first case. Furthermore, at each and every temperature below the freezing temperature, the driving chemical potential difference is reduced, as compared to the first case.

At any given temperature, these two effects lead to reduced rate of moisture uptake as compared to the first case and thus probably also to less damage. (This was actually shown in a laboratory study by Sellevold and Farstad [Sd 1991]: the more salt present in the specimens, the less the scaling.) Since less ice forms, the remaining permeability will be higher and thus moisture transport will be facilitated. The pattern of ice body growth is still the same, *i.e.* immediately from the surface inwards, diminishing with depth.

- In the last case, Figure 6.1.3C, the de-icer is present at a concentration diminishing with depth. Now, the first ice body is likely to form at some distance from the surface, the exact location being dependent on the cooling rate: the higher the cooling rate, the

steeper the temperature gradient and, consequently, the location of the initial ice formation varies. With a very steep temperature gradient, the pore solution of the outermost part of the specimen may freeze first, despite its higher de-icer concentration. In natural environments, however, cooling is usually so slow that the interior-most part probably freezes first. Under such circumstances, the permeability of the unfrozen zone close to the surface will remain undisturbed and moisture therefore may be easily transported into the ice bodies further in. This means the pattern of ice body growth will be different from those in the former cases: here, the rate of ice body growth may be higher at a depth beneath the surface than it is closer to the surface. This in turn may cause heavy scaling.

6.1.7 Proposed explanations of observed phenomena

In the literature, some interesting phenomena have been reported which are yet to be explained. The following shows how the proposed mechanism may be used to explain some of these phenomena.

Reasons for a ”3% pessimum”

Most-discussed among the reported phenomena is the apparent existence of a ”pessimum” de-icer concentration: Arnfeldt [A 1943] and Verbeck and Klieger [V 1957] reported that a de-icer concentration of about 3% b.w. in the outer solution would cause the most severe damage. According to the present hypothesis, the following factors may be distinguished as those which act to cause such a ”pessimum”:

- From the hypothesis, it is clear that a certain de-icer concentration is needed in the outer solution, since otherwise there will be no liquid phase available during freezing. The higher the de-icer concentration in the outer solution, the larger the amount of moisture available at each temperature during freezing. This ”positive” effect of the outer salt concentration is opposed by the following:

In tests such as those run by Arnfelt or Verbeck and Klieger, and in modern standard test methods, the outer solution is left on the specimen surface during the period of temperatures above 0°C. During this time, the de-icer may enter the pores of the specimen, and possibly decrease the mole fraction of water in the pore solution (depending on the concentration of the outer solution and the total ion exchanges). During the next freezing, this will make the pore solution in the outermost part of the specimen freeze at a lower temperature than the natural pore solution would. This will reduce the driving force for ice body growth and for moisture flow and will also reduce the maximum possible ice body pressure, thus reducing the risk of damage. The first formed ice bodies will be displaced to a greater depth and their growth will be limited by the increased resistance to moisture flow that the longer flow distance represents. Furthermore, the increased deicing agent content of the pore solution will reduce the number of (potentially) growing ice bodies, thereby reducing moisture uptake.

However, if a different type of frost cycle is used, the choice of de-icer concentration may be overshadowed by the choice of duration of the thawed state, since this has a major influence on the distribution of de-icer in the pore solution, which in turn has a major influence on the location of first ice formation. Thus, it is the combination of time for penetration of de-icers, absolute concentration of de-icer in the outer solution, and the diffusion coefficient of the de-icer present in the material that will be important. With these in mind, a test was designed and run, the results of which are presented in the next chapter. From the results, which do not contradict the present reasoning, it may be con-

cluded that the importance of using a 3% b.w. NaCl solution in standard test methods must not be exaggerated, especially since damage also occurs when testing with considerably higher concentrations [Sd 1991], [A 1943], [V 1957].

- Lastly and probably of lesser importance, the outer de-icer solution may have a drying effect on the specimen: the higher the outer de-icer concentration, the more effective the drying during the thawed state and, for a given ice body growth-induced moisture absorption, the longer the time needed during subsequent freezing before ice bodies start exerting disruptive pressures. (From the concentration of naturally occurring dissolved reaction products in a cement-based material, the relative humidity of the pore solution at capillary saturation may be calculated to be in the interval 96-99% [H 1994], depending somewhat on cement type and water/cement ratio. For a NaCl solution, RH 98% is reached at a concentration of approximately 3% and thus, ideally, a more concentrated outer NaCl solution will have a drying effect on the specimen, while a lower concentration will allow moisture to move into the specimen even during the thawed state.)

Effect of entrained air

Entrained air may prevent, or at least delay, damage, provided the air content is high enough. Upon cooling, air contracts and sucks pore solution into the pore. When this water freezes, the mechanism is activated; moisture flows into the specimen and accumulates in the air pores. On melting, the air expands and presses out as much water as was sucked in due to its contraction during cooling. Thus in a frost cycle in which the duration of the thawed state is long enough, the air pore system will be completely restored and will have regained its full protective function for the next freezing. If, however, the compressed air can find some way out, the moisture uptake will be permanent and thus the protective effect of the air voids will be reduced in the next frost cycle.

If the frost cycle is changed so that temperature oscillates between the freezing point of the pore solution and some lower temperature, say -3° and -10°C, the ice in the air pores never melts and more and more ice will gather in the air pores. After several cycles, the air pores will be completely filled and the material surface will deteriorate.

It follows naturally that the required air content is higher in a specimen subjected to combined salt and frost attack than in one subjected to pure frost attack. While the air pores in the latter will need only to protect the material against freezing of its original water content, the air pores in a specimen subjected to salt frost attack also must provide ample space for accumulation of the ice which forms from incoming moisture. Whether the required true spacing between air voids needs to be shorter than in ordinary, pure water frost attack, cannot be said.

Effect of carbonation

According to some reports, carbonation has a limiting effect on surface scaling, *e.g.* [Sk 1997], [P 1995]. The effect of carbonation is probably due mainly to its effect on the permeability of the surface zone. Different effects on the surface layer are obtained depending on cement type and admixers. For ordinary Portland cement-based materials, carbonation causes a denser pore structure [K 1986], while cements containing ground, granulated blast furnace slag (GBFS) become coarser [M 1995]. According to what was reported by Powers *et al* [P 1954] on the dependence of permeability on pore size distribution and total porosity, it thus seems that carbonation will cause a reduction of the permeability of pure Portland cement materials, while that of materials containing GBFS

will be increased. The role of permeability was discussed above: Portland cement material will probably benefit from carbonation while GBFS material will become more sensitive to salt frost attack.

Stark and Ludwig [Sk 1997] also found that concretes containing high amounts of granulated blast furnace slag would suffer severe scaling even though the air void system was of remarkably good quality. This cannot be explained by the osmotic ice body growth mechanism described here. However, as was mentioned above, the presence of an outer liquid solution will make thermodynamically unstable water remain in the micro pores for a longer time than in ordinary experiments on moisture sealed specimens because the micro ice body growth in such specimens will use up the thermodynamically unstable water rather quickly. Thus, the risk of *in situ* nucleation is increased and disruptive pressures may be exerted. This destruction probably cannot be avoided by the presence of air voids. However, this explanation is speculative and needs further examination.

According to Stark and Ludwig, their results were due to the formation of forms of calcite which are unstable in the presence of NaCl. Of course, it would have been interesting to run those tests again, using some other de-icing agent.

Finally, the phenomena reported in the literature (reviewed in chapter 4) should be given some attention. The conclusions in chapter 4.1 were:

1. ”Surface scaling almost never appears in the absence of an outer solution which to some extent remains liquid at temperatures lower than the normal freezing point of the pore solution of HCP. It may even be noted that in the two reports in which scaling is reported when the outer solution was pure water, either the outer water was rich in naturally occurring ions [Sk 1994] or the specimen surface had been exposed to a salt solution prior to testing so that the pore system did contain some salt [S 1965].
2. Portland cement-bound materials with proper air void systems are able to withstand combined salt and frost attack, at least in laboratory tests.
3. The chemical composition of the de-icing agent seems to be of no importance.
4. Without actual freezing temperatures, no scaling occurs.
5. Use of a lower minimum temperature will produce more scaling, at least for minimum temperatures in the interval $0°C > \theta > -20°C$.
6. Coarse porous materials are more sensitive to salt frost attack than dense materials.
7. Purely chemical mechanisms are of little importance in comparison to physical mechanisms.□

The explanation of the first point should be rather obvious from the above reasoning. The role of the high amounts of naturally-occurring ions in the outer water will be the same as that of salt in a salt solution; these ions will serve to depress the freezing point of the outer solution. Considering the low quality of the materials used in their study (a w/c ratio 0.60 concrete without air entrainment), the scaling reported by Stark and Ludwig in [Sk 1994] must be regarded as very small: after 28 frost cycles, the accumulated scaling obtained with a water quality containing the highest amounts of solutes was only 0.49 kg/m² for the concrete made with pure Portland cement. In a traditional salt frost scaling test, using a 3% NaCl solution, such a low quality concrete would be expected to be very much more damaged (see, for example, the tests reported in the next chapter).

In Snyder’s results [S 1965], scaling was obtained when the specimen was covered with pure water after first having been exposed to a salt solution. It seems reasonable that this previous exposure to a salt solution must have resulted in some salt being left in the

pores close to the specimen surfaces. During the subsequent freezing tests, this salt may have served to provide a liquid phase during at least a part of the frost cycle.

The second point concerns the effect of entrained air voids and was discussed above.

The third point also follows logically from the described mechanism, since the important role of the de-icing agent is to provide a liquid phase. However, in the results by Arnfelt and Verbeck and Klieger, it can be seen that optimum scaling is actually dependent on the de-icing agent used to bring about a freezing point depression of approximately 2°C. This may be because the rate of diffusion of different de-icers into the pore system varies, and/or because the eutecticum, below which there will be no liquid phase remaining on the specimen surface, varies by type of de-icer.

The fourth and fifth points need no further comment.

Point six is mainly explained by the effect of micro pore structure on intrinsic permeability and on the amount of ice formed at a given temperature.

The final point stands on its own.

Finally, there are other phenomena which are not straightforwardly explained by the described mechanism. For example, the sudden increase in scaling on high performance concretes containing silica fume (fig 4.1.6) cannot be explained, unless the described mechanism causes successive accumulation of moisture in the pores of such materials. Further research is needed.

In chapter 5.1, Series 1, it was found that when the outer concentration was 0%, scaling would increase as the "inner" concentration increased. This might be because salts from the pore solution are transported out to the outer "solution" (pure water) during the thawed state, thereby making a small amount of liquid available during subsequent freezing. Naturally, the amount of liquid will be greater the higher the salt concentration in the pores.

6.1.8 Conclusions

The proposed mechanism is robust in the sense that it requires no unusual circumstances for it to function. Rather, it will be active as long as permeability is high enough and the heat released on freezing is conducted away at a sufficient rate. Furthermore, the mechanism is sensitive to small changes in material properties and test procedure, a fact which is likely to make final scaling sensitive to such variations. For example, Sellevold [Sd 1988] pointed out that final scaling seemed to be highly dependent on structural differences between specimens cut out from different sites within a single, large block of concrete. On a qualitative basis, laboratory results found in the literature and results from our own investigations are in accord with predictions made from the hypothesis.

6.2 PROPOSED TESTS OF THE HYPOTHESIS

From the description in section 6.1, the effect of various changes in a test procedure may be predicted. If a test is designed in accordance with the predictions, but the results are contradictory to what was foreseen, the hypothesis either needs to be revised or completely rejected. Such tests, however, are difficult to design, since a change in one parameter is liable to change some other important parameters.

The following tests however were designed and carried out:

1. According to the hypothesis, the rate of moisture uptake should increase with decreasing temperature (unless the pore system is clogged with ice) and it should be reduced by the presence of any de-icing agent in the pore system. Results from such a test are described in section 7.1.
2. It is hypothesised that scaling will be independent of the concentration of de-icer in the outer solution if the de-icer can be hindered from penetrating into the pore system. Such a test has been carried out and is reported in section 7.2.
3. It is hypothesised that scaling will be significantly reduced if the pore system is rich in salts or other de-icing agent. Results from such a test are described in section 7.2.

7

TESTS OF THE HYPOTHESIS

In this chapter, the results from two series of tests of the hypothesis are reported. The tests were designed with the intention that their results would reveal whether the hypothesis is incorrect and should be rejected.

In chapter 7.1, results from tests on weight changes occurring during freezing are presented. The major intention was to confirm that moisture is taken up during freezing and that the presence of salts in the pore system reduces this uptake.

The second test, reported in chapter 7.2, is a modified standard salt frost scaling test. The modification of the ordinary test method is that the salt solution was removed from the specimen surface at temperatures >0°C. According to the hypothesis, this should eliminate or at least very significantly reduce any ”3% optimum”, such as reported by Arnfelt [A 1943], Verbeck and Klieger [V 1957], and in chapter 5.1, and as indicated in Sellevold’s results [Sd 1988].

7.1 FIRST TEST OF THE HYPOTHESIS: STUDY OF WEIGHT CHANGES DURING FREEZING IN SALT SOLUTIONS AT CONSTANT TEMPERATURE

Abstract

According to the hypothesis proposed in chapter 6, as a result of ice body growth in the pore system of a specimen, moisture uptake from the outer brine should occur during salt frost testing. This should cause weight gain. To test this and the qualitatively predicted dependence of such weight changes on temperature and salt distributions, discs of Portland cement mortar were frozen by submerging them in pre-cooled salt solutions and then the weight changes occurring at constant sub-zero temperatures were observed. Mortar specimens of *w/c* ratios 0.40, 0.55 and 0.65 were tested. Also mortars of *w/c* ratios 0.40 and 0.65 with additional air-entrainment were tested. Specimens were pre-stored in lime water or strong salt solutions (6.6, 14.4, 19.7% b.w.) for 12 weeks. In addition, a set of specimens were pre-stored in weak salt solutions (1, 3, 5% NaCl b.w.) for 19 days. Tests were run at -4°C, -10°C, -16°C, and at room temperature. Other reasons for weight changes during this kind of test were examined. From the hypothesis, it was predicted that larger weight increases would be observed the lower the temperature and the lower the concentration of salt in the pore system. The predicted results were fulfilled. In addition, two unexpected results were obtained. The results are not interpreted as evidence against the proposed mechanism.

7.1.1 Introduction

In chapter 6, an hypothesis for a major mechanism causing salt frost scaling on porous, brittle materials was put forward. It is partly based on an earlier description of how micro ice bodies in relatively large pores are able to consume moisture from nearby pores as long as the vapour pressure of the remaining moisture is high enough [P 1953]. In a moisture isolated specimen, ice formation and the resulting consumption of moisture will, by partial drying, lower the vapour pressure of the moisture in the surrounding pores. The key idea of the hypothesis put forward in chapter 6 is that in a specimen in contact with a source of liquid, partial drainage due to micro ice body growth is prevented through replacement of lost moisture by liquid from that outer source.

As a consequence, specimens in contact with an outer salt solution at a temperature between the freezing point and the eutectic temperature of that outer salt solution, will take up moisture from the brine remaining after freezing has been initiated. This will be observed as an increase in weight.

The primary purpose of this study was to check that such moisture uptake occurs and also to investigate its dependence on temperature, salt distribution, and salt concentrations for cement mortars of various qualities.

The hypothesis predicts that the pattern of ice formation in a zone with a depth of a few millimetres close to the surface will be changed if there are salts present in the pore solution. If the presence of an outer salt solution results in a reduction of the mole fraction of water in the pore solution as compared to the mole fraction of water that is obtained in the pore solution when the specimen is tested with pure water on the surface, then the driving force for moisture uptake during freezing will be reduced. The measured water uptake therefore should be less in specimens pre-stored so that the mole fraction of

water in the pore solution is significantly reduced, *e.g.* after storage in a strong salt solution.

7.1.2 Method

The intention was to study weight changes occurring at constant sub-zero temperature. Therefore, circular discs (ϕ100·5 mm) were immersed in salt solutions which had previously been cooled to the desired test temperature (-4, -10 or -16°C) and the temperature was then maintained as constant as possible. The specimen weights were registered approximately once an hour by lifting the specimens out of the salt solution (one at a time), wiping them off with a moist cloth and weighing them. Each specimen was put back immediately after weighing. The time required for this procedure was approximately 20-30 s for each disc.

The salt solution was kept in an open plastic box which in turn was lowered into a glycol bath cooled by a cryostat (Lauda, RK 20, Germany). A heat insulating lid was put on during the experiments. The salt solution volume was some 4 l. The specimens were mounted in a frame to keep them standing vertically, thus making them easily accessible for weighing. At the most, 12 specimens were tested at the same time. Because it is difficult to seal a wet concrete surface and because the results obtained were to be used only for internal, qualitative comparisons, the specimen circumferential edges were not sealed to moisture exchange. The equipment used for the tests is shown in figure 7.1.1.

The temperature of the salt solution was slightly affected by the removal and reimmersion of the specimens. This is commented on further below.

Figure 7.1.1: Cryostat, salt solution container and frame holding the specimens.

7.1.3 Experiments

The main purpose was to study weight changes in specimens kept at constant temperatures in a salt solution so concentrated that its vapour pressure is equal to that of bulk ice at the same temperature. For these tests, the temperatures -4°, -10° and -16°C were chosen. The salt solutions were prepared with NaCl and, in order to obtain the desired vapour pressure at the chosen temperatures, the concentrations were 6.6, 14.4 and 19.7 % b.w. The reason for choosing salt concentrations which yield the same vapour pressure as bulk ice at the prevailing temperature is twofold: first and most importantly, during testing of concrete for salt frost resistance, such as the Swedish SS 13 72 44, the outer salt solution is successively concentrated as more and more ice forms in it as temperature drops. Provided an equilibrium path is followed, the concentration of the remaining brine will be such as to produce the same vapour pressure as that of the ice which has thus far formed. Furthermore, because of the way the tests were carried out, a completely liquid outer solution was needed in order to make the specimens accessible for weighing.

The following experiments were carried out:

1. Moisture content changes due to osmosis. Room temperature
2. Weight changes at constant temperatures <0°C in ”temperature matched” salt solutions, no inner salts, both never-dried and dried and re-moistened specimens.
3. Weight changes at constant temperatures <0°C in ”too strongly” concentrated salt solutions, no inner salts
4. Weight changes at constant temperatures <0°C, specimens pre-stored and tested in ”temperature matched” salt solutions.
5. Weight changes at constant temperatures <0°C, specimens containing less than ”temperature matched” salt concentrations, outer solution concentration ”temperature matched”
6. Weight changes at constant temperatures -10°C, specimens pre-stored in weak salt solutions, tested in ”temperature matched” solution
7. Effect of reduced specimen thickness on rate of weight changes at -10°C, ”matched ” outer solution.

The term ”matched ” is used to denote that the concentration of NaCl was chosen so that the salt solution would be in equilibrium with bulk ice at the chosen test temperature. The term ”too strong” means a salt concentration more concentrated than that corresponding to ”matched”.

Intended as a reference test, the first test was run in order to estimate effects caused purely by differences in salt concentration between the inner and the outer solution. Specimens both with and without salt in the pores were tested in both pure water and different salt solutions at +21°C. Those specimens which were to contain salt in the pore system during testing were stored in the relevant salt solution from one week after casting until testing began 12 weeks later. Also, the weight changes caused by submersing specimens (containing their natural pore solutions) in various weak salt solutions (1, 3, 5% NaCl) were studied.

Next, the effect of salts in the pore solution on the rate of moisture uptake during freezing was studied.

These tests were complemented by experiments in which the concentration of salt in both the outer salt solution and the pore solution was different from that required for thermodynamic equilibrium with bulk ice at the prevailing temperature.

Specimens containing only the natural pore solution were tested both in a never-dried state and after drying and re-moistening. Drying was done by storing the specimens for two days in a plastic box in which a relative humidity of approximately 65% was main-

tained by use of a saturated salt solution. The relative humidity was disturbed when placing the specimens in the box and equilibrium was probably not re-established prior to the specimens being removed. This drying procedure was, however, enough to cause drastic differences in weight changes during the experiments as compared to the never-dried specimens. Re-moistening was done by letting the specimens soak up tap water for two days.

A few tests were run in which the inner salt concentrations were obtained by storing the samples in weak NaCl solutions (1, 3 and 5% b.w.). These were tested in 14.4% NaCl solutions at -10°C.

The effect of the specimen size was studied by repeating the experiments carried out at -10°C/14.4% with samples of half the thickness of the ordinary specimens, *i.e.* approximately 2 mm instead of 5 mm.

The chloride concentration obtained in the pore solution after pre-storage in various salt solutions was determined on a few specimens.

7.1.4 Materials

Five Portland cement mortar qualities were used; water/cement ratios 0.40, 0.55 and 0.65 with additional air-entrainment and water/cement ratios 0.40 and 0.65 without additional air-entrainment. The materials without additional air-entrainment were so severely deteriorated that the results could not be used. The material compositions are given in table 7.1.1.

The mortars were cast in steel cylinder moulds of 100 mm diameter and 200 mm height. The cylinders were demoulded on the day after casting, stored for a week in lime-saturated water, and afterwards cut into discs of a thickness of approximately 5.1±0.5 mm.

The discs were then stored in lime water or salt solutions (6.6, 14.4 and 19.7 % b.w. NaCl, with lime) until testing began 12 weeks after casting. The major part of the tests were run over a period of 16 days (12 work days). A few complementary tests were run 2-4 weeks later.

Table 7.1.1: Material compositions

Mix:	0.40	0.40 AE	0.55 AE	0.65	0.65 AE
Water/cement ratio	0.40	0.40	0.55	0.65	0.65
Water [kg/m^3]	290	290	290	290	290
Cement [kg/m^3]	725	725	527	446	446
Sand (0-3mm) [kg/m^3]	1272	1272	1438	1506	1506
u, %	8.8	7.8	7.0	6.4	5.7
Fresh Air content [%]	appr. 3 %	13	11.5	(not reg.)	13.5
AEA dosage	----	36	26	----	22
Plasticiser	1.7	1.7	1.2	1.03	1.03

u: Moisture content in sand, % by weight.
AEA: Tall oil, weight of effective substance, g/m^3 ("Cementa L14", produced by Cementa AB, Sweden)
Plasticiser: Melamin Resin, weight of effective substance, kg/m^3 ("Cementa V33" , produced by Cementa AB, Sweden)
Cement type:"Anläggningscement", produced by Cementa AB, Sweden. Described in General Appendix 2.

Specimens tested with weak salt concentrations (1, 3 and 5%) in their pore solutions were stored in lime water for 10 weeks after casting and then in the respective salt solutions prepared from de-ionised water for 9 days, after which testing began.

The chloride ion content of the specimens was determined by the use of field equipment (Rapid Chloride Test, RCT, from Germann Instruments, Denmark) in which an acid is used to dissolve all chloride ions.

Porosity and density

The average porosity and density was determined on a few parallel specimens for each quality. The measurement was carried out using the Archimedes principle (described elsewhere). The complete results are set out in Appendix 7.1.1. The average values are given in table 7.1.2.

7.1.5 Results predicted from the hypothesis

From the hypothesis, some predictions of the results may be made. If these are contradicted by the actual results, then the hypothesis will need either revision or complete rejection.

1. First and most importantly: specimens without salt in their pore system should gain weight because of the uptake of the outer liquid which results from micro ice lens growth. This may be very much reduced if too little ice forms in the specimens or if the permeability of the material is too low. Too low permeability may be due to a very dense cement paste (which is usually due to a low water/cement ratio) or it may be due to clogging of the pore system with ice.
2. There should be competition between the outer bulk ice and inner ice crystals for the moisture available within the pore system. This competition may cause specimen weight reduction if the salt concentration of the outer solution is high enough. Weight losses should be observable particularly at room temperature, since there is then no ice in the pore system to consume moisture. Also, at mild frost temperatures, an outer salt solution may cause weight loss in the specimen, since there is only a little ice present at high temperatures and the driving force for continued ice lens growth is limited by the temperature.
3. Specimens containing ”temperature matched” salt solutions should show no weight increases due to cryosuction, since no ice should form in such specimens. Furthermore, there should be less moisture uptake the more salt there is in the pore system.

Table 7.1.2: Average porosity and density as determined on parallel specimens.

Material (*w/c*)	Dry density [kg/m^3]	Wet density [kg/m^3]	Porosity [%]	Degree of saturation after pre-storage [%]
0.40	2090	2303	21.7	99
0.40 AE	1865	2098	30.5	76
0.55 AE	1851	2084	30.9	75
0.65	2032	2265	24	97
0.65 AE	1796	2030	33.1	71

7.1.6 Reasons for weight changes other than micro ice lens growth-induced moisture uptake

There are several reasons why the weight of a specimen with a certain moisture content and at a certain temperature should change (more or less abruptly) when the specimen is suddenly immersed in a salt solution of different temperature. Those reasons are discussed here and an estimation is made of the magnitude of these weight changes. This is necessary in order to distinguish ice lens-induced weight gain from weight gain caused by other phenomena.

Apart from the growth of micro ice bodies, which this entire chapter is about, the following phenomena may cause weight changes:

- Thermally-induced contraction of entrapped air leading to water uptake
- Changes in salt content
- Changes in water content due to osmosis
- Temperature-induced changes in the density of the pore solution, leading to changes in total moisture content
- Thermally-induced volume change in the specimen, leading to changes in pore volume and thus changes in pore solution content
- Redistribution of liquid between gel and capillary pores as described by Helmuth [H 1961], leading to suction and thereby to changes in total content of pore solution (same effect as causing increased adsorption at lower temperatures)

Thermally-induced contraction of entrapped air leading to water uptake

When temperature is lowered, the entrapped air shrinks. As a consequence, moisture is sucked into the pore system. The weight change is calculated:

$$\Delta m = \Delta V_a \cdot \rho_{w,f} = V_{a,i} \cdot \left(1 - \frac{T_f}{T_i}\right) \cdot \rho_{w,f} \qquad (7.1.1)$$

At +20°C, the air content of air-entrained specimens of water/cement ratios 0.40 and 0.65 was approximately 2.89 cm^3 and 3.90 cm^3, respectively, and for the corresponding qualities without additional air-entrainment it was 0.12 and 0.30 cm^3, respectively. Using the values for the density of water given in chapter 2.2, the calculated weight changes accompanying a temperature change from +20° to -16°C are +0.48 g for the air-entrained *w/c* ratio 0.65 quality and only +0.015 g for the non air-entrained *w/c* ratio 0.40 quality. It will be seen in the results section that these values agree fairly well with those measured during the first hour of freezing.

Time required for moisture uptake caused by contraction of confined air

The pressure change causing the suction described above may be satisfactorily calculated from the ideal gas law as:

$$P_f = P_i \frac{T_f}{T_i} \qquad (7.1.2)$$

with indici *i* and *f* denoting initial and final values, respectively. The volume of water required to replace air in order to re-establish atmospheric pressure in the entrapped air is also calculated from the ideal gas law.

The time required for water to flow into the specimen and replace/compensate for the reduced air volume was calculated numerically. Using a value for the permeability coefficient of $500 \cdot 10^{-15}$ s (reasonable according to [B 1982]), a disc thickness of 5 mm, and an air content of 9% b.v., such a calculation reveals that the required time is less than 20 minutes. (In this calculation it was assumed that no moisture inflow occurs across the edges of the disc.)

It was assumed in this calculation that the temperature is momentarily reduced to its final value. From the measurements of temperatures during testing (fig. 7.1.4), it can be seen that cooling is almost completed after approximately 1 hour. Since this is slower than the 20 minutes calculated above, it may be assumed that the refilling is finished by the time the cooling to the set temperature is finished.

Changes in salt content and changes in water content due to osmosis

During the freezing tests, some ion exchanges may occur which may affect the weight of the specimen in a significant way. To test this, pure diffusion tests were run on identical specimens at room temperature. Specimens of the air-entrained material qualities were exposed at room temperature for 5 hours to NaCl solutions of concentrations 1, 3 and 5% b.w., respectively. Unfortunately, the subsequent evaluation of the chloride ion

Table 7.1.3: Total weight change and amount of chloride ions detected after 5 hours of soaking in different NaCl solutions at +21°C. The development of the weights vs. time during testing are shown in figures 7.1.2 a-c.

Material	Solution Conc [% b.w.]	Appr. Thickness [mm]	Initial weight [g]	Final weight [g]	Net weight change [g]
0.40 AE	1	5.7	94.3	94.29	-0.01
0.40 AE	1	4.7	77.33	77.28	-0.05
0.40 AE	3	4.8	79.62	79.54	-0.08
0.40 AE	3	4.7	78.11	78.04	-0.07
0.40 AE	5	5.2	86.18	86.02	-0.16
0.40 AE	5	4.7	78.19	78.07	-0.12
0.55 AE	1	5.7	92.68	92.61	-0.07
0.55 AE	1	5.2	84.62	84.55	-0.07
0.55 AE	3	5.4	87.82	87.75	-0.07
0.55 AE	3	5.6	92.44	92.37	-0.07
0.55 AE	5	5.1	83.09	82.95	-0.14
0.55 AE	5	5.4	88.09	88.00	-0.09
0.65 AE	1	5.5	87.15	86.95	-0.20
0.65 AE	1	5.3	83.91	83.70	-0.21
0.65 AE	3	5.8	91.71	91.58	-0.13
0.65 AE	3	5.2	83.54	83.36	-0.18
0.65 AE	5	5.2	82.16	82.05	-0.11
0.65 AE	5	5.1	81.12	81.00	-0.12

contents failed. The amount of chloride ions taken up during these tests may however be estimated from the results in chapter 5.2: under the assumption that conditions for

diffusion of chloride ions into the specimens used in these room temperature experiments were comparable to those of the tests reported in chapter 5.2, the total mass of chloride ions having penetrated into the pore system of a mortar specimen of *w/c* ratio 0.65 after 5 hours exposure to a 5% NaCl solution at room temperature may be estimated, by numerically integrating eq. (5.2.20), to be 0.08 g (using $D = 30 \cdot 10^{-12}$ m²/s and ignoring effects due to the non-sealed edges of these specimens).

The tests and this calculation thus indicate that weight increases registered during the freezing tests are not due to diffusion of ions from the outer solution into the pore solution.

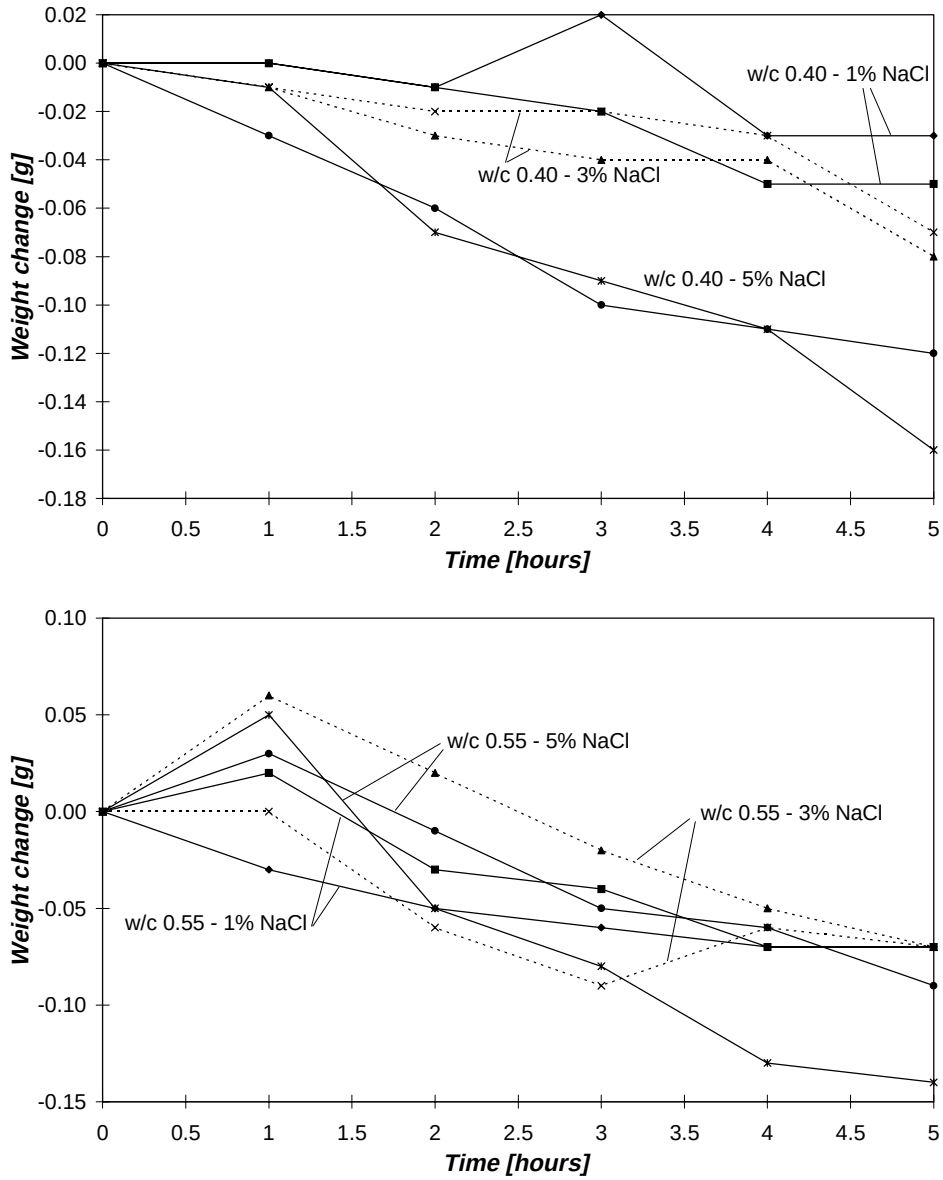

Figure 7.1.2 a-b: Weight changes of circular (ϕ100·5 mm) mortar specimens submerged in NaCl solutions of indicated concentrations. Specimens pre-stored in lime water. Note scales

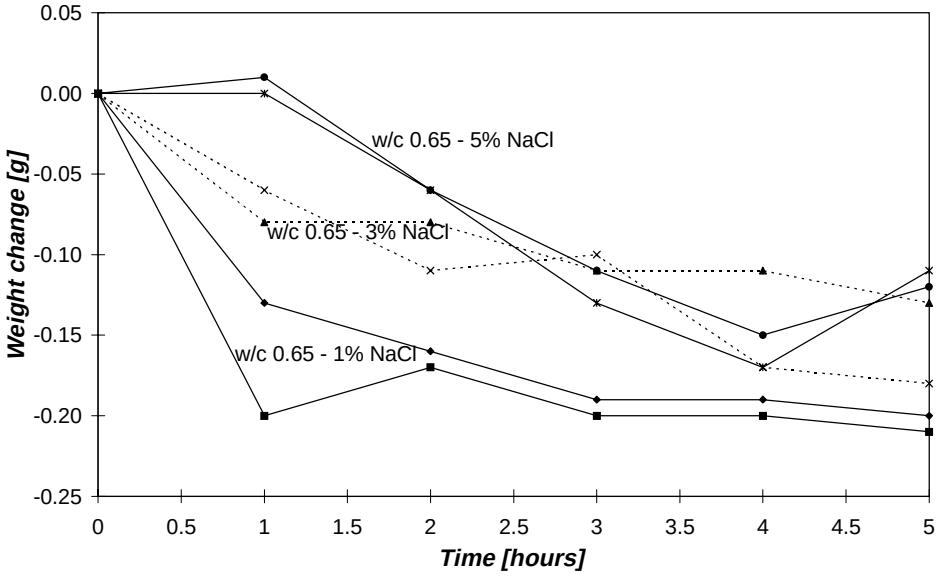

Figure 7.1.2 c: Weight changes of circular (ϕ100·5 mm) mortar specimens submerged in NaCl solutions of indicated concentrations. Specimens pre-stored in lime water. Note scales!

Furthermore, specimens pre-stored in 19.7% NaCl solution (as described above) were tested in pure water (tap water) and specimens stored in lime water were tested in 19.7% NaCl solutions at +21°C. The results of these tests are shown in figure 7.1.3.

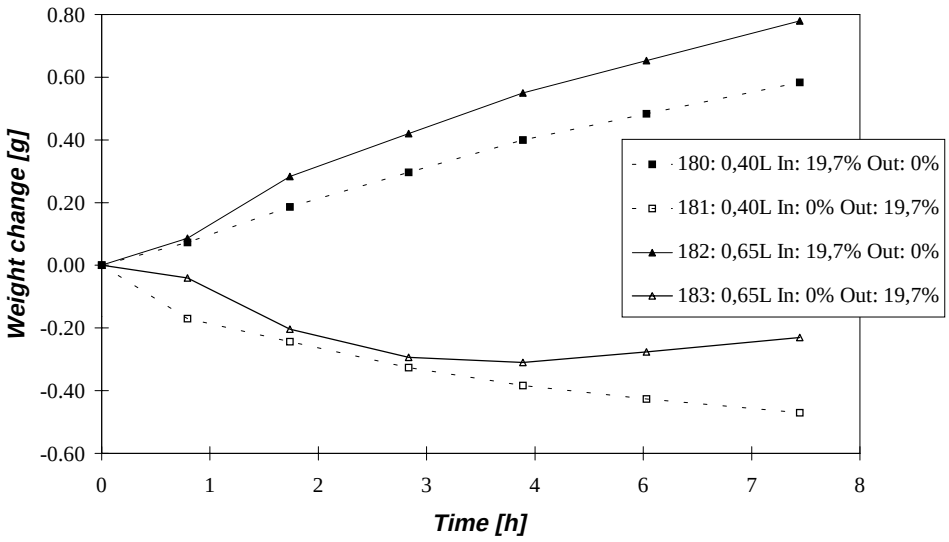

Figure 7.1.3: Weight changes for specimens tested +21°C. Different pre-storage and test solutions. "In" denotes intended concentration in pore solution, "Out" denotes outer (test) solution. Each line represents mean values from three specimens.

The results shown in figures 7.1.2 and 7.1.3 all indicate that specimens pre-stored in water (lime-saturated or tap water) lose weight when immersed in a salt solution. As will

be shown in the results section below, when specimens pre-stored in water are frozen in a salt solution, the opposite result is obtained: such specimens gain weight!

Temperature-induced changes of the density of the pore solution leading to changes in total moisture content

The density of water varies with temperature and reaches its maximum value of 999.97 kg/m^3 at +4°C. As a consequence of this, water held in a specimen at +20° "shrinks" when the specimen temperature is lowered to +4°. If the specimen is in contact with a water source, more water will be sucked into the specimen. On continued cooling, the pore solution will expand and press water out of the pore system, causing a loss of weight. Assuming the pore solution density reacts to temperature changes in the same way as pure water, the weight changes may be calculated as:

$$\Delta m = V \cdot P \cdot S\left\{\rho(T_f) - \rho(T_i)\right\} \qquad (7.1.4)$$

The temperature dependence for water was described in chapter 2.2. For the materials of highest porosity used in this study (appr. 24%), the weight change accompanying a temperature decrease from +20 to -4°C is:

$$\Delta m = 40 \cdot 10^{-6} \cdot 0.24 \cdot 1 \cdot (999.414 - 998.204) = 0.012\,g$$

In the same way, on cooling from +20 to -16°C, the specimen weight changes by -0.024 g. It will be seen that these changes, although the maximum possible for the specimens used here, are small in comparison to the weight changes occurring during freezing.

Thermally-induced volume change of the specimen leading to changes in pore volume and thus changes in content of pore solution

The specimens contract on cooling. Thus the absolute pore volume decreases and some of the pore solution is pressed out. The weight change due to this effect alone is:

$$\Delta m = \rho \cdot \Delta V_p \qquad (7.1.5)$$

with ρ denoting the pore solution density and ΔV_p the change in pore volume, which is:

$$\Delta V_p = V_i \cdot P \cdot \left(\left(1 + \alpha_T \cdot \left(T_f - T_i\right)\right)^3 - 1\right) \qquad (7.1.6)$$

An approximate value of the coefficient of thermal contraction α_T for concrete and similar materials is $11 \cdot 10^{-6}$ K^{-1} [H 1961]. The volume of the specimens used in this study was approximately 40 cm^3 and the maximum temperature change was -37°C (from +21°C to -16°C). The porosity of the *w/c* ratio 0.65 quality without additional air-entrainment was some 24%. Setting the pore solution density to 1000 kg/m^3, one finds that the amount of liquid pressed out of the pore system is 0.011 g. Also, for specimens containing air, pore solution will be pressed out, but the process will run more slowly, since the pressure changes can be accommodated through compression of the entrapped air.

Redistribution of liquid between gel and capillary pores

This phenomenon was described by Helmuth in [H 1961]. Because of the different entropies of water held in narrow (gel) pores and water held in larger (capillary) pores, a temperature change will cause a difference in level of free energy between these different groups of water, causing a flow of water from the large pores into the narrow ones. As a result, the large pores will be partly emptied. If a sample of cement paste is in contact with water when the temperature change takes place, more water will be sucked into its pores. Helmuth produced an equation for estimating the amount of water taken up in this way when cooling a sample from +25° to ±0°C. The equation comprises effects that are the result of thermal contraction of the sample, temperature dependence of the pore solution density, and differing entropies. For neat cement pastes having reached a degree of hydration of 0.86, Helmuth derived the following expression:

$$\Delta w = 0.0194 w_g + 0.0024 w_c \qquad (7.1.7)$$

in which w_g is the amont of water held in the gel pores and w_c is the water present in the capillary pores.

Helmuth related both gel water and capillary water to the amount of chemically-bound water. The gel water was calculated:

$$w_g = 0.74 w_n \qquad (7.1.8)$$

in which w_n is the amount of chemically-bound water, which is calculated:

$$w_n = 0.25 \alpha \cdot C \qquad (7.1.9)$$

in which α is the degree of hydration and C is the cement weight (calculated from the mix proportions). For the present samples (the volume of which was approximately 40 cm^3) of water/cement ratios 0.40 and 0.65, C is approximately 29 and 17.8 g, respectively. Estimating the degrees of hydration to be 0.5 and 0.65 for *w/c* ratios 0.40 and 0.65, respectively, w_g is estimated to be 2.68 g for *w/c* ratio 0.40 and 2.14 g for *w/c* ratio 0.65.

The water held in the capillary pores is calculated from the capillary porosity (eq. (2.1.5)), which yields:

$$w_c = V \cdot \rho_w \cdot V_p \cdot \frac{w/c - 0.39\alpha}{0.32 + w/c} \qquad (7.1.9)$$

in which V_p is the volume fraction of cement paste in the specimen and *w/c* is the water/cement ratio. For the present materials of water/cement ratio 0.40 and 0.65, the former is 0.52 and 0.43, respectively. Together with the above assumed values for degree of hydration, this yields w_c = 5.9 g for *w/c* ratio 0.40 and w_c = 7.0 g for *w/c* ratio 0.65.

Helmuth's expression (eq. (7.1.7)) for the weight change accompanying a temperature change from +25° to ±0°C now yields:

$$\Delta w = 0.0194 w_g + 0.0024 w_c = 0.0194 \cdot 2.68 + 0.0024 \cdot 5.9 \approx 0.066 g$$

for *w/c* ratio 0.40 and for *w/c* ratio 0.65 it yields:

$$\Delta w = 0.0194 w_g + 0.0024 w_c = 0.0194 \cdot 2.14 + 0.0024 \cdot 7.0 \approx 0.058 g$$

These values may be compared to those calculated above from equations (7.1.4)–(7.1.6). For a temperature decrease from +25° to ±0°C those equations yield weight changes of 0.017 g for a specimen of *w/c* ratio 0.40 and 0.019 g for one of *w/c* ratio 0.65. Helmuth's equation thus yields higher values, indicating that the entropy effects are comparatively large. Both types of calculations however show that temperature change-induced weight changes are considerably smaller than the weight changes registered in the measurements.

Helmuth's paper [H 1961] was commented on by Hansen [H 1963, p 944], who pointed out that weight changes estimated in the way proposed by Helmuth are very uncertain. The reason is that when moisture moves from coarse to narrow pores, its interaction with the pore wall is changed and thus the water structure and water volume are changed. According to Hansen, little is known about these phenomena. Since the volume change is what determines the weight changes, the precise weight changes cannot therefore be predicted.

Summary

The total sum of the weight changes described by equations (7.1.2)–(7.1.6) may be obtained from a single expression:

$$\Delta m = m_{w,f} - m_{w,i} = \rho_{w,f} \cdot V_i \cdot P \cdot \left\{ \left(1 + \alpha\left(T_f - T_i\right)\right)^3 - \left(1 - S_i\right) \cdot \frac{T_f}{T_i} \right\} - V_i \cdot P \cdot S_i \cdot \rho_{w,i} \qquad (7.1.10)$$

From the above calculations, it is clear that the single largest cause of weight change results from the temperature-dependent contraction of entrapped air. This effect is clearly seen in the results presented below.

7.1.7 Results from tests of experimental conditions

This section sets out, firstly, the results of tests on salt concentrations obtained in specimens pre-stored in salt solutions, followed by a description of the measurement of temperature events and, finally, a discussion of repeatability between specimens (in the same series).

Salt content in specimens pre-stored in salt solutions

Field test equipment from Germann Instruments, Denmark, was used to check possible salt concentration gradients. Layers of approximately 0.5 mm thickness were milled off from the specimen surfaces. The dust was weighed and dissolved in an acid (part of the field equipment). The chloride ion content was then measured with a chloride ion-sensitive electrode. A calibration chart is used to express chloride content in % by weight of mortar weight. Measurements were taken on samples of *w/c* ratios 0.40 and 0.65. The results are set out in Appendix 7.1.3.

Since only chloride ions were detected, the total effect on the mole fraction of water in the pore solution could not be determined. The change in mole fraction of water in the

pore solution might not be as large as that indicated by the concentration of chloride ions, especially in specimens pre-stored in weak salt solutions.

Specimens pre-stored in salt solutions for 12 weeks

For specimens pre-stored in 19.7% solutions, the Cl^- concentrations in the specimens were above the limit of detection for the instrument. Allowing for a 10% error in measured values, the measured chloride ion content is almost constant across the specimen thickness in specimens stored in 6.6% solutions. For the specimens pre-stored in 6.6% NaCl solutions, the concentration of chloride ions were recalculated (using values from table 7.1.3) into a fictive NaCl concentration (fictive because the concentration of Na^+ ions is not known). It can be seen in Appendix 7.1.3 that this fictive concentration of NaCl is lower than that in the storage solution, despite the lack of a gradient. The reason for this is unknown. It might simply be due to poor precision in the measurements.

Specimens pre-stored in salt solutions for 19 days

These specimens were pre-stored in 1%, 3%, and 5% NaCl solutions. For the 0.40 quality, no gradient could be detected for a specimen stored in the 1% solution. While a vague concentration gradient (weaker concentration in the centre) was detected for a specimen stored in the 3% solution, the results for the specimen stored in the 5% NaCl solution showed slightly higher concentration in the centre of the specimen than at its edges. Taken together, these results indicate no or very small differences in chloride ion concentration in specimens of this quality. For the specimens pre-stored in 1% NaCl solutions, the absolute concentrations of chloride ions in the pore solution (expressed in relation to pore solution volume) correspond to approximately 2.5 times those in the outer solution. For specimens pre-stored in 3% solutions the ratio is approximately 1.3 and for specimens pre-stored in 5% solutions the ratio is approximately 1. The reason why the concentration of chloride ions in the pores is higher than that corresponding to the outer solutions is probably that some amount of the chloride ions are bound, somehow, to the pore walls.

For the 0.65 quality, no gradient was found in the specimen stored in the 1% solution. The amount of detected chloride ions, however, corresponds to a concentration twice as high as that in the outer solution. In specimens stored in 3% or 5% solutions, the results indicate that the concentration at the centre of each specimen was some 70-75% of that at the edges. Again, the amount of chloride ions detected in the specimens corresponds to a concentration in the pore solution larger than that in the outer solutions.

Obviously, there are many uncertainties in the measured chloride ion concentrations. It was never the purpose of the present experiments to study chloride ion diffusion. The intention was merely to check that the storage of the specimens in salt solutions had been sufficiently long to affect the entire pore volume. This seems to have been achieved.

Temperatures

For practical reasons, it was not possible to measure the temperature of each and every specimen. Therefore, temperatures were supervised using a thermocouple inside a disc of acrylic plastic of a size and shape equal to the specimens. This was used as an indicator during the experiments simply to check that nothing unexpected occurred. The temperature of the specimens was afterwards measured in a separate test with a thermocouple inside a mortar specimen, figure 7.1.4. Another example of the bath temperature is given in figure 7.1.23. It can be seen that the intended temperature was never completely reached. Thus, the intended equilibrium between the outer salt solution and bulk ice was never reached and thus the vapour pressure of the outer solution was slightly less than

that of bulk ice. This provides a force for water to move out of the specimens. Further, it can be seen that the test temperature was reached within the first hour of submersion. As described above, this will cause large weight changes during this first hour. Finally, it can be seen that the temperature rose several degrees during the 20-30 seconds that the specimen was out of the salt solution during weighing. It regained its previous temperature almost completely within some 30 s of being returned to the solution (indicated in figure 7.1.4).

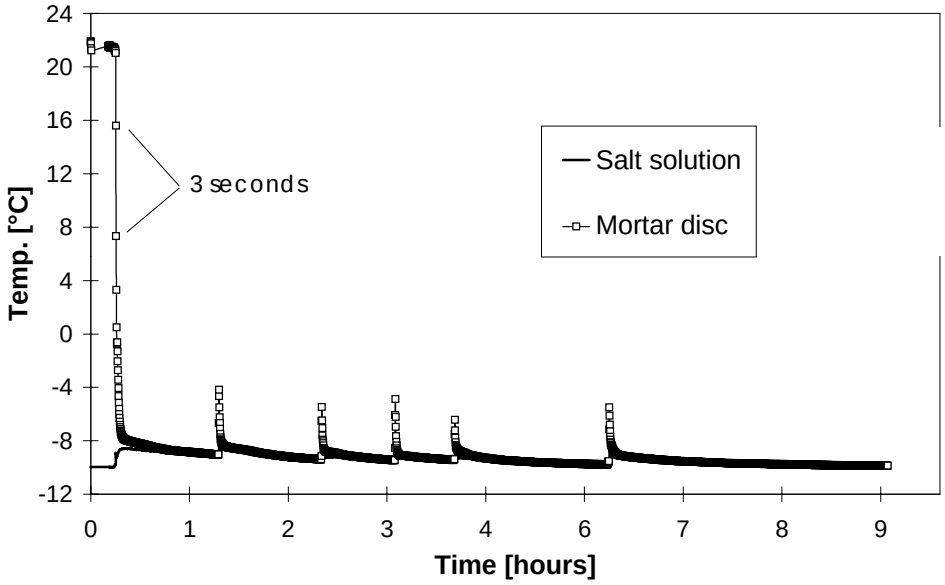

Figure 7.1.4: Temperatures registered in specimen and in salt solution. Intended temperature -10°C. Time between measurements 3 seconds.

Repeatability of results obtained on specimens within a single series

In the main description of the obtained results, only curves showing mean values from three specimens are shown. In figure 7.1.5-7.1.9, a few examples are given of the spreading between the three specimens used in each series.

The first three figures were chosen arbitrarily. The last two (fig:s 7.1.8 and 7.1.9) were chosen in order to show how the scatter affects the possibility of distinguishing the effect on the final results of varying one parameter. For this case, it can be seen that the scatter is clearly less than the entire effect of changing the outer salt concentration from 14.4% to 19.7%.

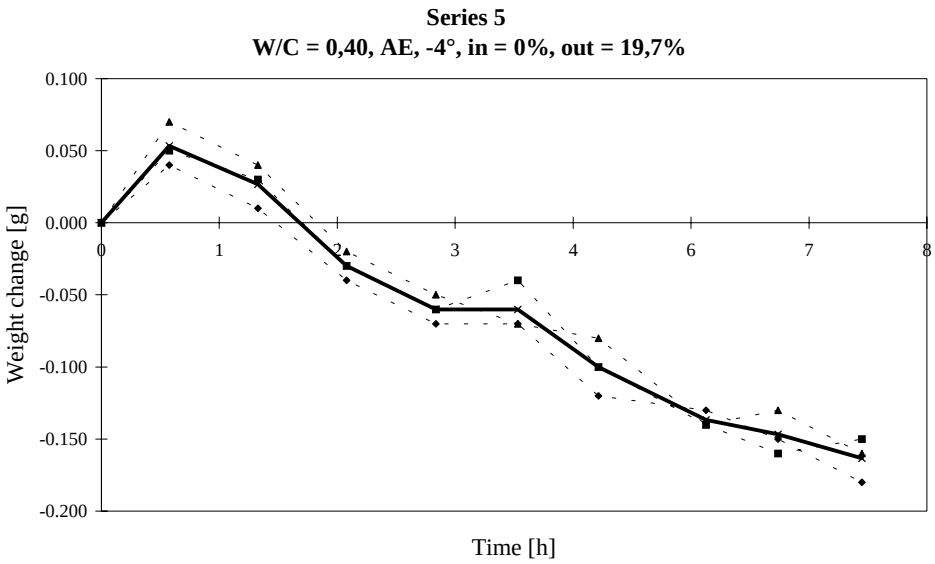

Figure 7.1.5: Example of scatter between specimens. Dashed lines: Single specimens. Solid line: Mean value for the three specimens.

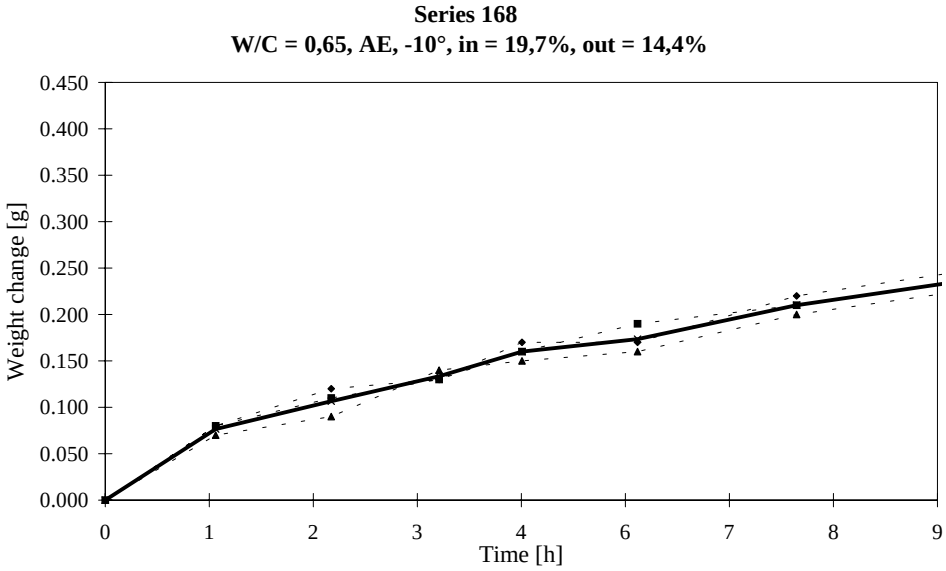

Figure 7.1.6: Example of scatter between specimens. Dashed lines: Single specimens. Solid line: Mean value for the three specimens.

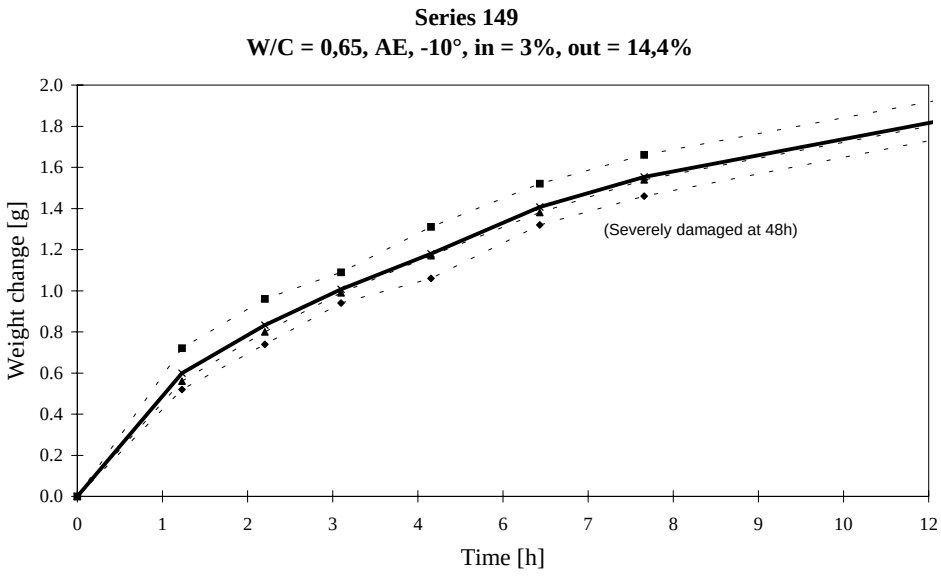

Figure 7.1.7: Example of scatter between specimens. Dashed lines: Single specimens. Solid line: Mean value for the three specimens.

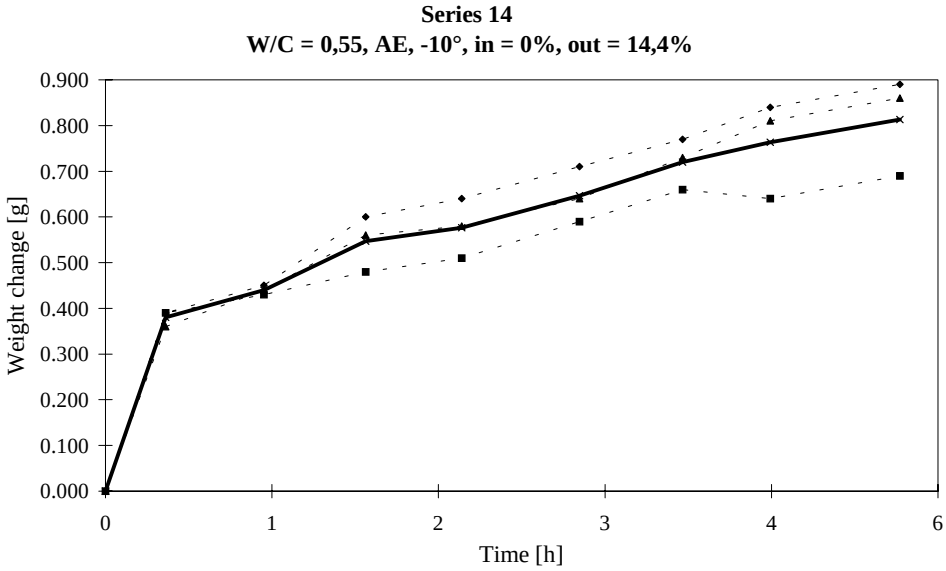

Figure 7.1.8: Example of scatter between specimens. Dashed lines: Single specimens. Solid line: Mean value for the three specimens.

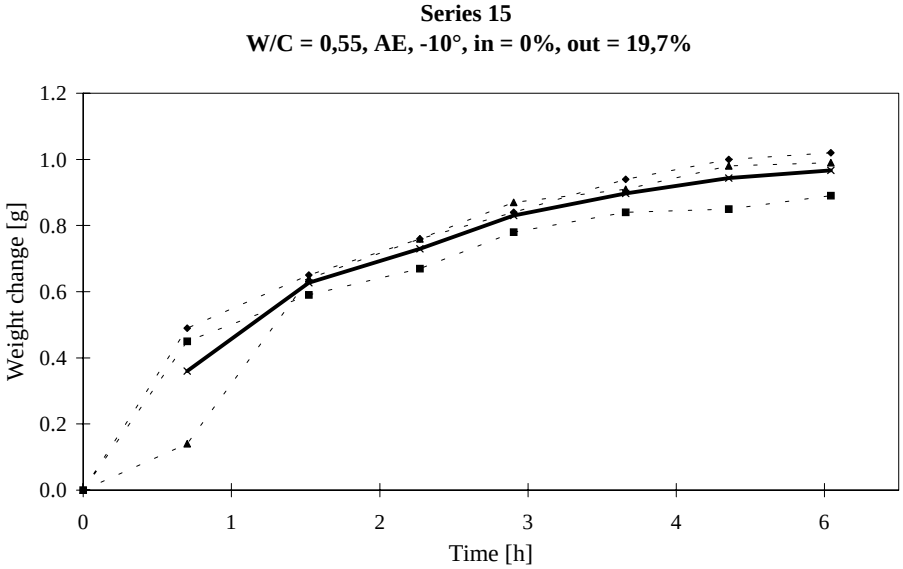

Figure 7.1.9: Example of scatter between specimens. Dashed lines: Single specimens. Solid line: Mean value for the three specimens.

7.1.8 Main Results

Only graphs showing weight changes are presented here. The complete set of measured data is available from our division.

1: Moisture content changes due to osmosis. Room temperature.

The aim of the first series was to check what weight changes would occur as a result of salt concentration changes only. The results are shown in figure 7.1.3. These are the most extreme salt concentration changes occurring in the tests. It can be seen that after 7.5 hours of storage in a 19.7% NaCl solution, *w/c* ratio 0.40 specimens have lost 0.5 g in weight. When a similar specimen is put into a tap water bath after being pre-stored in a 19.7% NaCl for 12 weeks after casting, it *gains* the same amount of weight. Considering the different mole fractions of water in the inner and outer solutions, these results are to be expected.

The two *w/c* ratio 0.65 specimens behave somewhat differently: while the ones pre-stored in salt solution and tested in water gain weight throughout the entire test, those pre-stored in lime water and tested in salt solution initially lose weight and then, after some 4 hours, start gaining weight again. This curve shape is not caused by one single, misbehaving specimen. All three specimens in that series behave in the same way. A possible explanation for this might be that, initially, water moves out of the specimen pores at a rate high enough to cause a net loss in weight, despite the simultaneously occurring transport of chloride ions (and possibly Na^+ ions). After some 4 hours, however, the driving potential for water transport has been lowered and water transport slows down. Transport of chloride ions into the pore solution continues and, after a time, when the mole fraction of dissolved ions begins to even out, some of the initially lost water is taken up again. It must be stressed that this is merely a hypothetical explanation.

2: Weight changes at constant temperatures <0°C in ”temperature matched” salt solutions, no inner salts, both never-dried and dried and-re-moistened specimens.

The weight changes registered for never-dried specimens tested at various temperatures in ”matched” NaCl solutions are shown in figures 7.1.10-7.1.12. The corresponding results for specimens once dried and re-moistened are shown in figures 7.1.13–7.1.15.

Scaling occurred on some samples. Since 12 samples were tested in the same beaker, it was not possible to determine exactly how much material was scaled off from each specimen. For each and every one, however, it was noted in the laboratory protocol when scaling was first observed. After testing, the approximate distribution of the total amount of scaled off material from the specimens tested was noted. The scaled off material was collected, dried at 105°C and weighed. To compensate for scaling (as shown in figures 7.1.11 and 7.1.12), this dry material was spread out on all weighings for those specimens on which scaling occurred, assuming scaling took place at a constant rate throughout the entire test after scaling was first observed. Obviously, this is just an approximate compensation. Since the dry weight of the scaled off material was used, it tends to underestimate the true weight gain in these samples.The term ”temperature matched” was explained above.

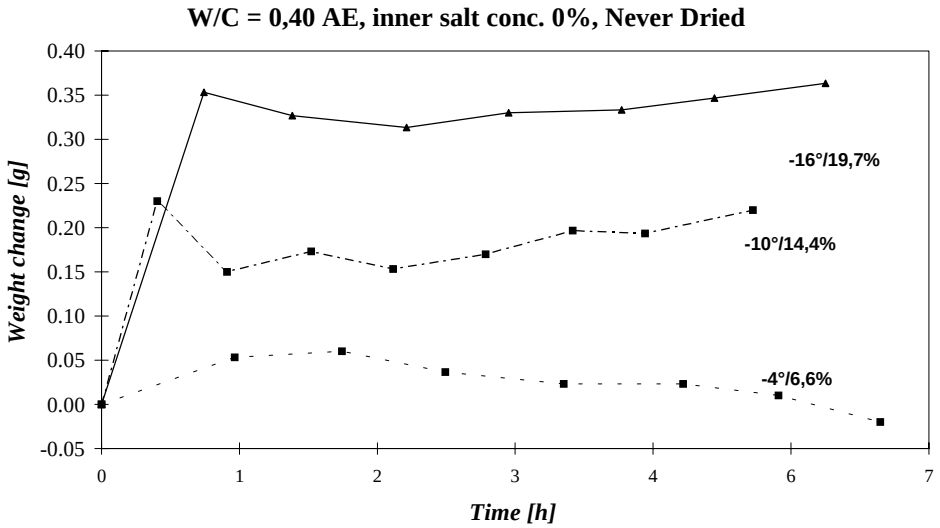

Figure 7.1.10: Weight changes for never-dried specimens tested in ‘temperature matched’ salt solutions (explained in the text).

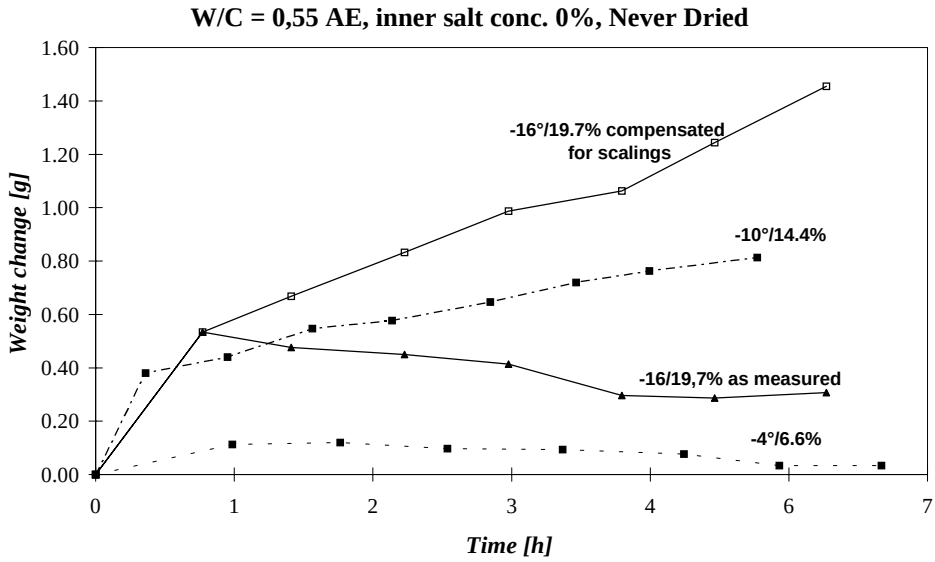

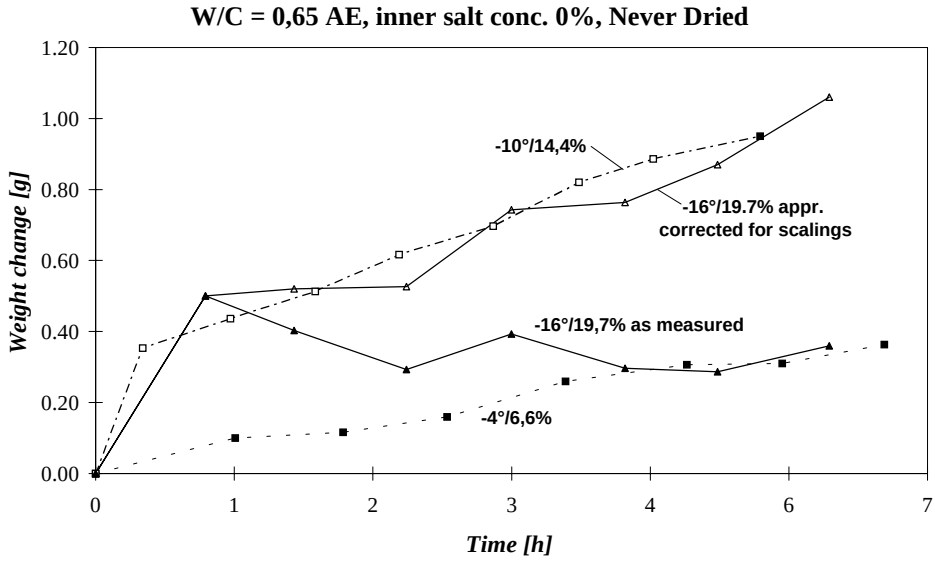

Figure 7.1.11–7.1.12: Weight changes for never-dried specimens tested in 'temperature matched' salt solutions (explained in the text).

It is seen that large weight increases occur during the first hour of submersion. This is due to the above described effect of air contraction due to the temperature change. The exact amount of weight increase is dependent on the degree of saturation of each individual specimen.

It can be seen in the figures that for all materials, at temperatures -10°C and -16°C, large weight increases occur (after the increase during the first hour), despite the fact that specimens tested in equally strong salt solutions at room temperature lose weight. For the 0.40 specimens however, weight changes are very small (after the first hour).

It can be further seen that the moisture uptake after the first hour is larger the higher the *w/c* ratio. This is probably due both to the higher permeability linked to an increasing *w/c* ratio and the larger amount of ice forming in higher *w/c* ratio materials. The latter means there is a larger surface of ice against water inside the high *w/c* ratio materials at which moisture consumption can occur.

At -4°C however, only the *w/c* ratio 0.65 specimens gain weight. This may be because at this temperature very little ice, if any, forms in the specimens of lower *w/c* ratios. If super-cooling occurs and prevents ice formation, then of course no moisture uptake due to ice lens growth will occur. Instead the salt effects dominate and, as can be seen in the figures, at this mild temperature the higher quality materials lose weight.

Taken together, these results do not contradict the hypothesis put forward in chapter 6.

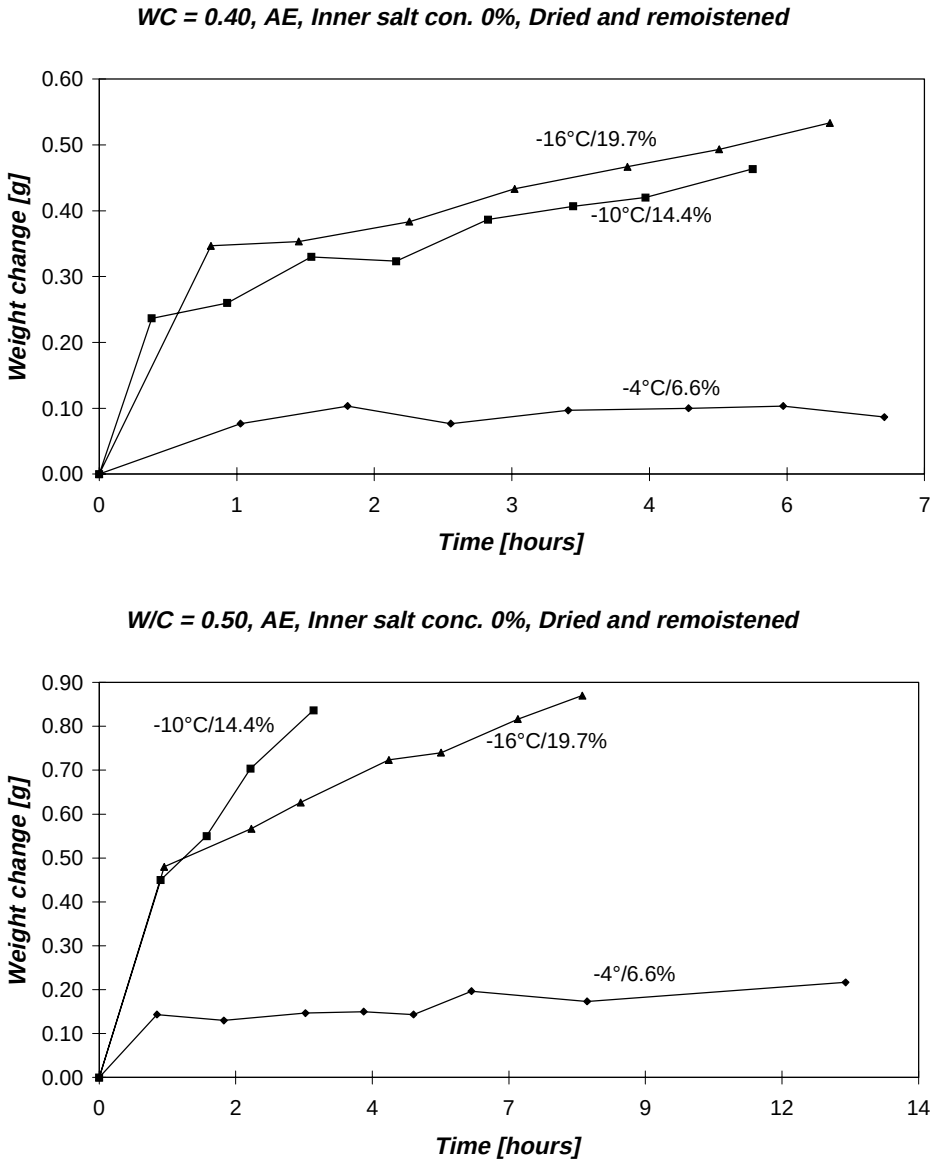

Figure 7.1.13–7.1.14: Weight changes for dried and re-moistened specimens frozen in 'temperature matched' salt solutions. Each curve represents mean values from three specimens.

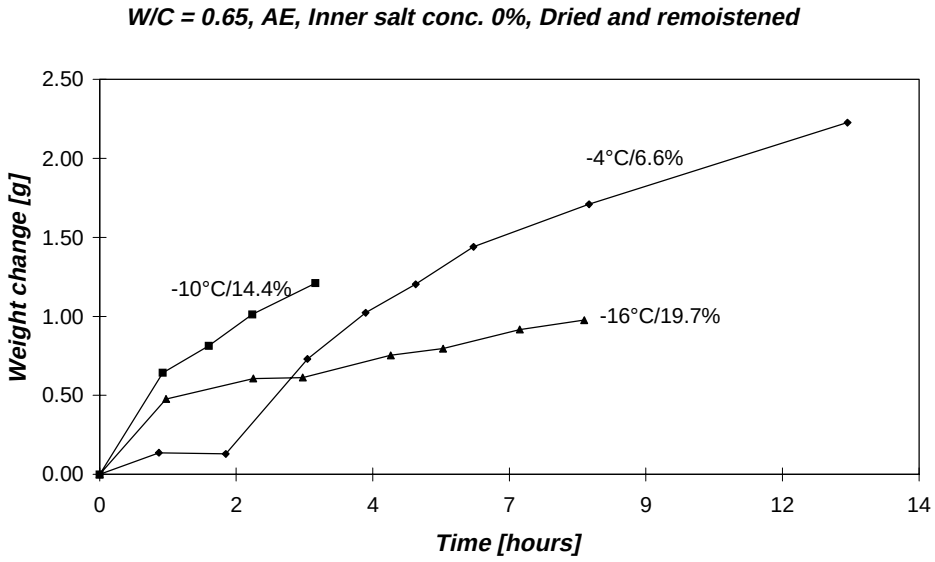

Figure 7.1.15: Weight changes for dried and re-moistened specimens frozen in 'temperature matched' salt solutions. Each curve represents mean values from three specimens.

The drying and re-moistening procedure obviously causes some changes (figures 7.1.13–7.1.15.). For the 0.40 specimens, significant weight changes after the first hour occur at temperatures -10°C and -16°C. This is probably due to the combined effect of the increase in ice formation [B2 1986] and the increase in permeability [P 1954] that is due to the pre-drying of the samples. The *rate* of weight change however is the same at both these temperature levels. At -4°C, the weight almost does not change at all after the first hour. This is in contrast to the non-dried specimens, which lost weight under the same conditions. The differences between the dried and non-dried specimens are small, but all three specimens in each series behave consistently, as is shown in figure 7.1.16: The changes during the first hour, when cooling effects are dominant, are qualitatively the same. All specimens increase in weight due to air contraction, although the mean increase for the non-dried specimens is a little less than that for dried and re-moistened specimens. This may be because the degree of saturation was somewhat higher in the never-dried specimens. From equation (7.1.10) it can be seen that the initial degree of saturation has a dominant influence on initial weight changes.

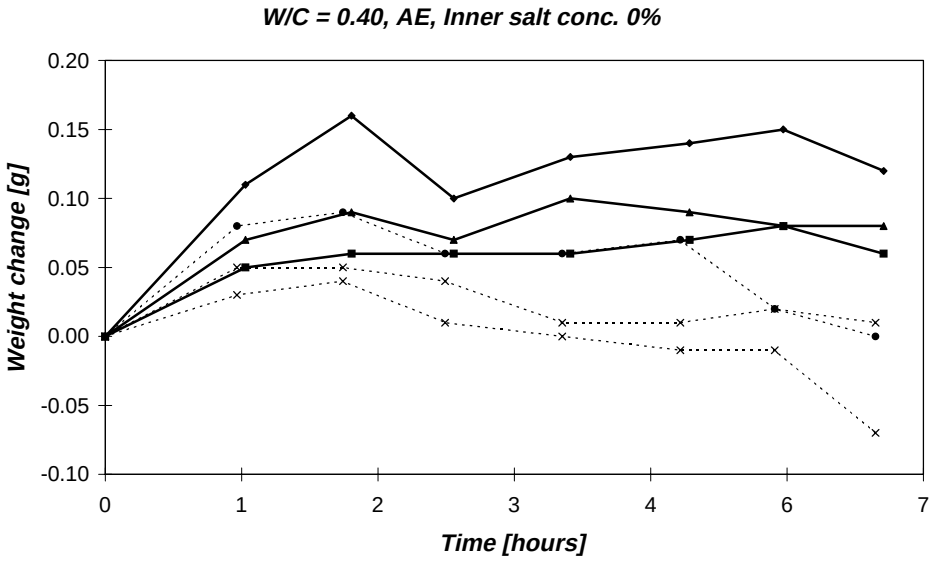

Figure 7.1.16: w/c ratio 0.40 specimens tested at -4°C/6.6% NaCl. Each line represents one single specimen. Solid lines: Dried and re-moistened specimens. Dashed lines: Never-dried specimens.

As for the *w/c* ratio 0.50 quality, it might seem an unexpected result that the rate of weight gain after the first hour is higher for specimens tested at -10°C/14.4% than for those tested at -16°C/19.7%. This however may be because ice formation has clogged so much of the pore volume that permeability sets a lower limit to the rate of weight gain at this temperature than at -10°C, notwithstanding the larger driving force for ice lens growth linked to the lower temperature (eq. (6.1.3)). This is further enhanced by the lowering of the pore solution viscosity which follows on a temperature decrease. Both of these phenomena were foreseen in the description of the hypothesis.

3: Weight changes at constant temperatures <0°C in ”too strongly” concentrated salt solutions, no inner salts

The term “too strongly” is used to denote the fact that the vapour pressure of the salt solution is lower than that of bulk ice at the prevailing temperature (described above).

The results for *w/c* 0.40 mortars are shown in figure 7.1.17 (all three specimens for each variable combination are shown in order to illustrate the order of magnitude of the scatter in relation to the total levels).

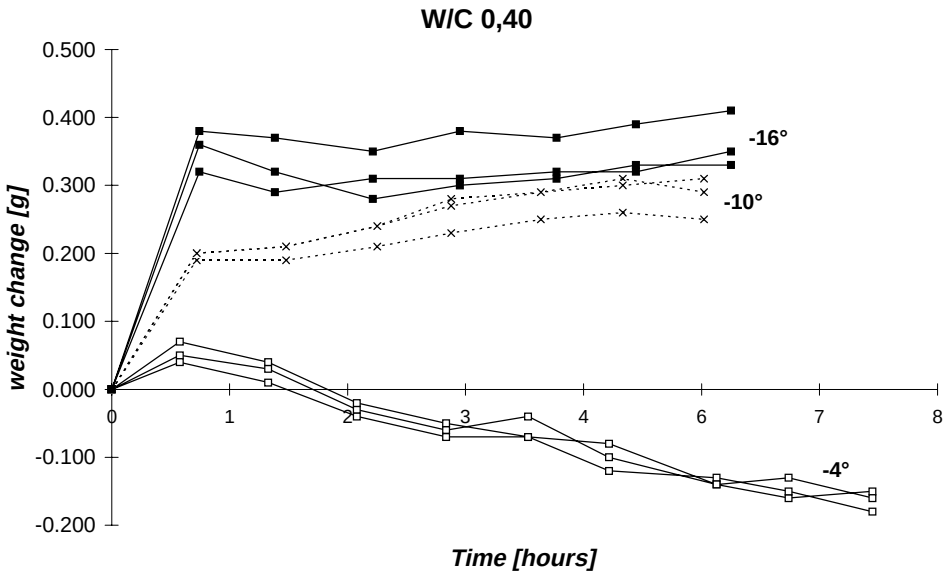

Figure 7.1.17: Effect of 'too strong' outer salt solution. W/C ratio 0.40, never-dried specimens. Outer salt concentration 19.7%. Inner salt concentration 0. One line: one specimen. Uppermost curve: Matched salt concentration (from figure 7.1.9).

At -4°C the outer salt solution seems to have the same kind of drying effect on these specimens as was seen at room temperature, figure 7.1.3. This is to be compared with the results shown in figure 7.1.16, in which it was shown that the weight decreases only slightly in similar specimens tested at -4°C with a 'matched' (6.6%) outer solution.

The results obtained at -10°C are to be compared with those in figure 7.1.9, which, apart from the registered weight loss between the first and the second hour, show a rate of weight gain approximately equal to that shown in figure 7.1.17. A straight line fit to the last seven registrations in figure 7.1.9 and the mean values for the seven registrations shown in figure 7.1.17 (referring in both cases to the -10°C results), shows that the rate of weight change in figure 7.1.9 is 0.131 g/h while that in figure 7.1.17 is 0.179 g/h, *i.e.* some 35 - 40% higher. Although the exact rates are uncertain because of the uncertainties in the weighings, the results indicate that weight gain is faster when the outer salt solution is "too concentrated". This is an unexpected result. Since the density of the 'too concentrated' solution is only a few percent higher than that of the 'temperature matched' solution, the difference in rate of weight gain cannot be due solely to the liquid density. It is clear however, that the weight gain for specimens tested at -10°C in the 'too strong' solution (fig. 7.1.17) is quick initially, but also that it slows down with time so that, after 5 hours, there is a tendency for the weights to decrease. This is in contrast to the specimens tested in 'matched' solutions (fig. 7.1.9, -10°C) which keep increasing at an almost constant rate throughout the entire test. The slow down in rate of weight gain may be due to the fact that after a few hours, so much of the outer, "too concentrated" solution has been sucked into the pore system that ice growth cannot proceed.

It can also be seen in figure 7.1.17 that the rate of weight gain is higher at -10°C than at -16°C when the outer concentration is 19.7%, despite the greater driving force created at the lower temperature. This may be because *in situ* ice formation has blocked the pore system, rendering the specimens impermeable to continued moisture transport at -16°C.

When using once dried and re-moistened specimens of *w/c* ratio 0.40, the results are as shown in figure 7.1.18.

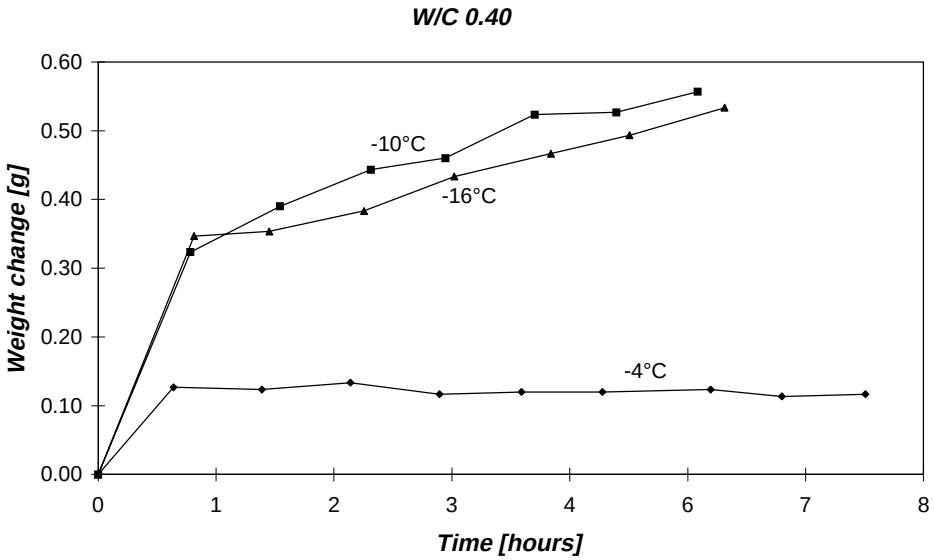

Figure 7.1.18: Effect of 'too concentrated' outer salt solution. w/c ratio 0.40, dried and re-moistened specimens. Outer salt concentration 19.7%. Inner salt concentration 0. One line: mean value from 3 specimens. Middle curve: Matched salt concentration (from figure 7.1.23).

For specimens tested at -4°C, the drying and re-moistening procedure has resulted in no weight changes occurring after the first hour of submersion. A drying and re-moistening procedure coarsens the pore structure and thereby leads to increased amounts of ice at a given temperature [B2 1986]. Together with the results obtained at -4°C for non dried specimens, this indicates that the increased amount of ice inside the specimen is enough to prevent the weight loss (probably from partial drying) seen in figure 7.1.17.

Just as for the non-dried specimens, a "too strongly" concentrated salt solution cannot prevent weight gain at -10°C. The rate of weight gain for the dried and re-moistened specimens tested at -10°C with the "too concentrated" solution in figure 7.1.17 is 0.3 g/h, while the rate for the dried and re-moistened specimens tested in a 'temperature matched' solution (fig. 7.1.13) is 0.23 g/h. As above, the rate of weight gain is actually higher when testing in a 'too concentrated' solution.

The same type of comparison for the 0.50 (series 14 *vs.* 15 and 38 *vs.* 39) and 0.65 mortars (series 22 *vs.* 23 and 46 *vs.* 47) yields the same result: At -10°C, the rate of weight gain is higher when the outer salt solution concentration is "too concentrated". The approximate rates are gathered in table 7.1.4. These rates have been evaluated by fitting a straight line (a least squares fit) to those weights measured after the first hour of submersion.

In table 7.1.4, the identification numbers of the baths in which these test were run have also been included. It can be seen that the increased rates of weight gain obtained with the "too strong" outer solution cannot entirely be explained as being due to some systematic error originating from, for example, erroneous salt concentrations or temperatures.

Table 7.1.4: Approximate rates of weight gain [g/h] occurring after the first hour for specimens tested in 'temperature matched' (-10°C/14.4% NaCl) and 'too strong' concentrations (-10°C/19.7% NaCl). (Series indicated in parenthesis, followed by bath identification number).

	Never dried		**Dried and remoistened**	
Mortar	-10°C / 14.4%	-10°C / 19.7%	-10°C / 14.4%	-10°C / 19.7%
0.40 AE	0.13 (6) 6a	0.18 (7) 7b	0.23 (30) 6a	0.30 (31) 7c
0.50 AE	0.38 (14) 6a	0.51 (15) 7b	0.29 (38) 6b	0.55 (39) 7c
0.65 AE	0.30 (22) 6a	0.53 (23) 7c	0.21 (46) 6b	0.56 (47) 7c

The effects of using 'too concentrated' solutions (the 19.7% NaCl solution) at -4°C on the 0.55 and 0.65 mortars are shown in figures 7.1.19 and 7.1.20. The weight losses registered for never-dried specimens of *w/c* ratio 0.50 are possibly due to the fact that no or too little ice forms in these specimens at this temperature. (It may even be that ice actually can form but that it is prevented by super-cooling, which easily exceeds 4°C, *e.g.* [P 1953], [B1 1986])

In figure 7.1.20 it can be seen that the specimens tested at -4°C/6.6% suddenly start gaining weight after about 2 hours of submersion. All three specimens among those dried and re-moistened behave in the same way. One of the never-dried specimens also behaves this way (all three are shown). This may be due to the fact that super-cooling is annulled at this time. If so, it strengthens the reasoning above. The reason that super-cooling is annulled in several specimens at one and the same time may be that some ice had formed in the outer solution which then seeded ice formation in the pore solutions. Ice formation in the outer solution easily occurred when the equilibrium temperature was reached. This result thus strengthens the idea that super-cooling acts to hide the "true" results, *i.e.* those results which may be foreseen when an equilibrium path is followed. All results obtained at -4°C therefore must be handled carefully when comparing them to what was foreseen in chapter 6.

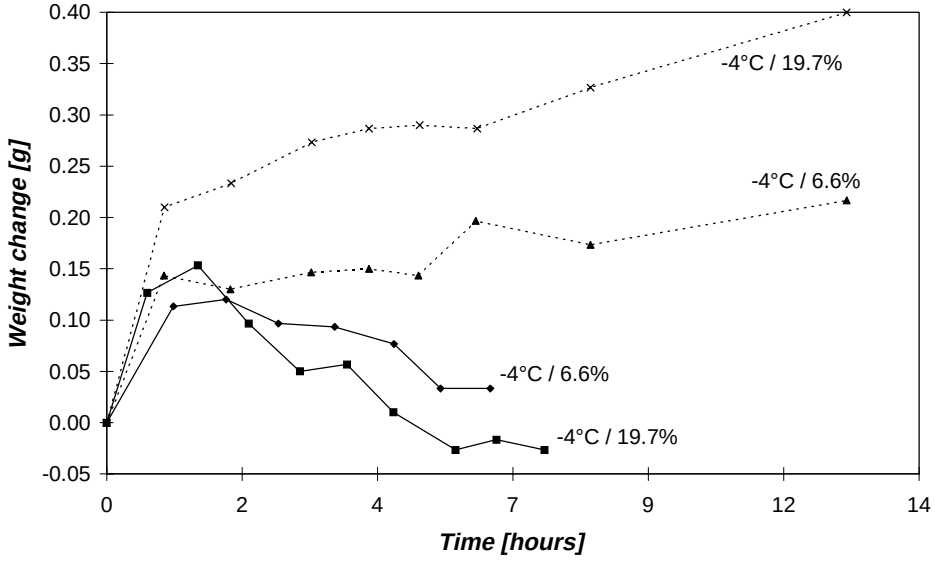

Figure 7.1.19: Weight changes for w/c ratio 0.50 mortars. Mean values for three specimens. Dashed lines: Dried and re-moistened specimens, solid lines: Never-dried specimens.

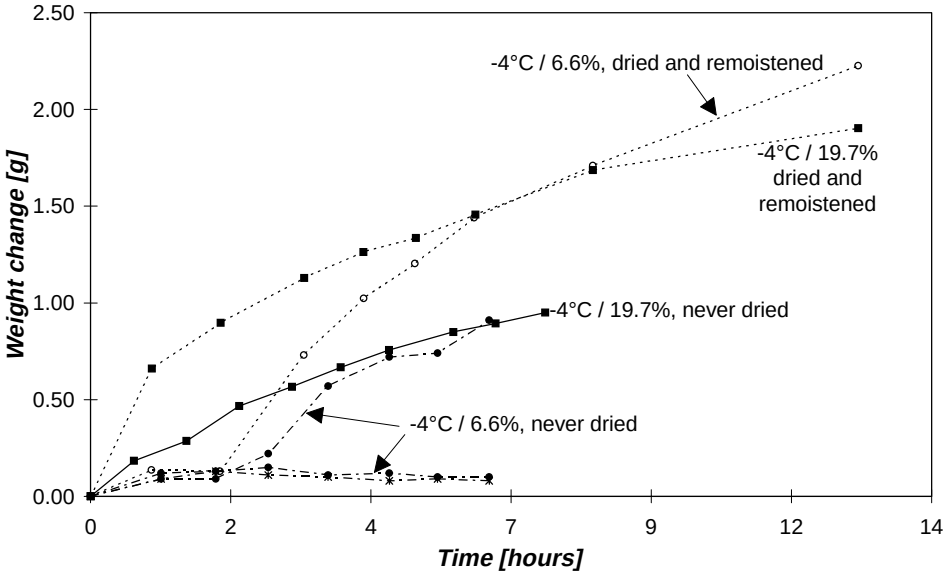

Figure 7.1.20: Weight changes for w/c ratio 0.65 mortars. Mean values for three specimens except for -4°C/6.6% never-dried for which all three are shown.

4: Weight changes at constant temperatures <0°C, specimens pre-stored and tested in "temperature matched" salt solutions.

According to the hypothesis, the presence of salts in the pore system should reduce both the amount of ice formed at each and every temperature and the driving force for micro ice lens growth. In the series presented here, the inner concentration was intended to be high enough to precisely prevent ice formation in the pore system. The relevant series are nos. 65 (-4°C) and 72 (-16°C) for *w/c* 0.40 and 89 (-4°C) and 96 (-16°C) for *w/c* 0.65. (This was not tested on *w/c* ratio 0.50 specimens).

The results for *w/c* ratio 0.40 at -4°C are shown in figure 7.1.21. All registered weight changes are very small and the differences cannot safely be said to be significant, especially since the above mentioned super-cooling effects may also play a role. Nevertheless, the results are as expected: the specimen pre-stored in a 6.6% solution, *i.e.* the same concentration as the test bath, undergoes almost no weight change after the initial cooling-induced weight change. Meanwhile, the specimens pre-stored in lime water seem to be somewhat drained, just as was found for specimens containing natural pore solution and tested in a strong solution at room temperature. These two results are reasonable, provided ice formation is negligible. This was indicated to be true for this material at this temperature in the results described above.

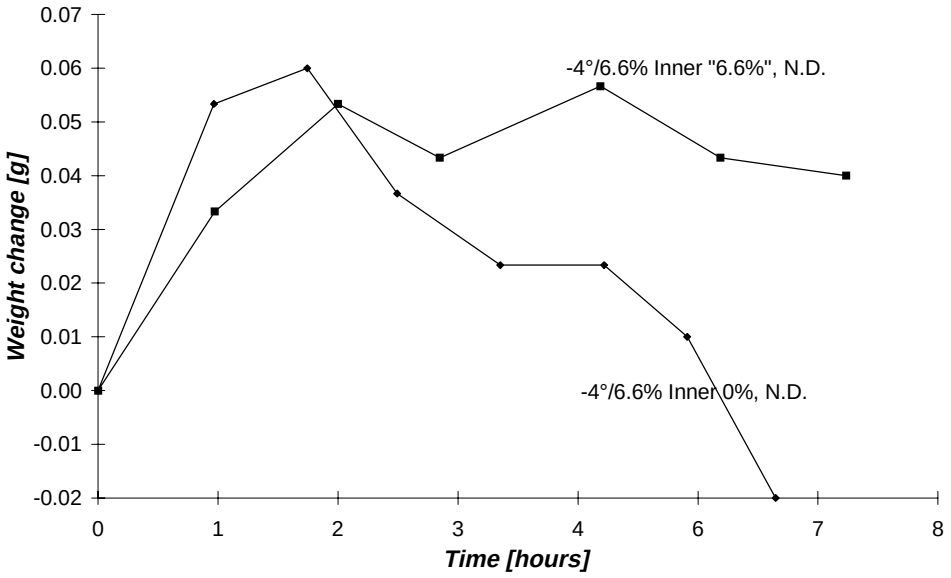

Figure 7.1.21: Effect of (intended) inner salt concentration 6.6% on w/c ratio 0.40 specimen weights at -4°C. Each line represents three specimens. N.D: Never-dried.

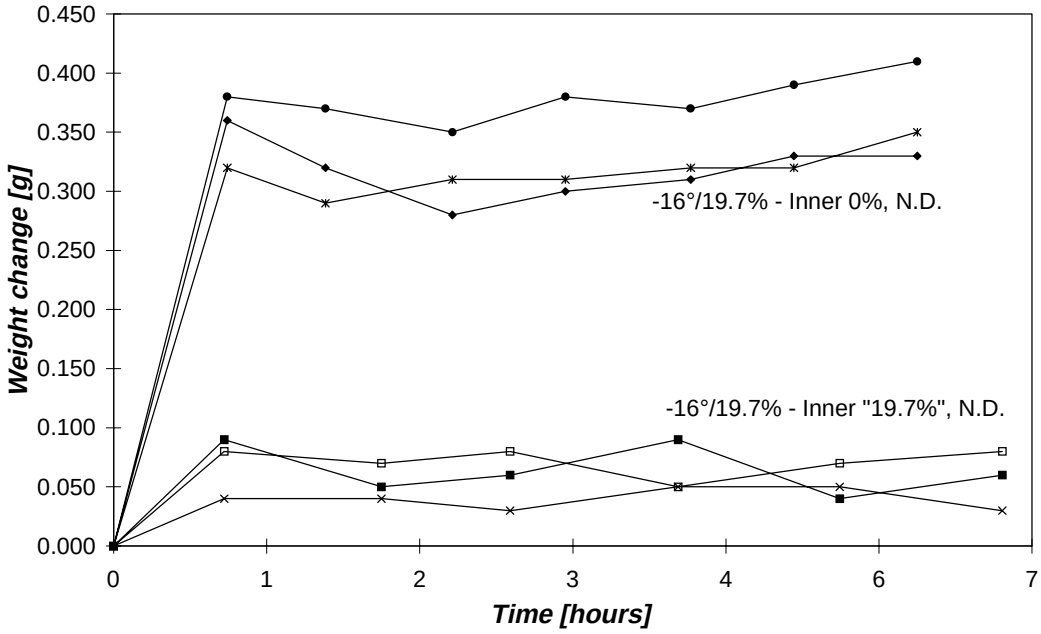

Figure 7.1.22: Effect of (intended) inner salt concentration 19.7% on w/c ratio 0.40 specimen weights at -16°C. Each line represents one specimens. N.D: Never-dried.

The results for *w/c* ratio 0.40 at -16°C are shown in figure 7.1.22. As is seen in this figure, the never-dried specimens pre-stored in 19.7% NaCl solutions undergo only small weight changes due to air contraction. All three specimens behave the same. The bath temperature, shown in figure 7.1.23, is normal. The weight development after the first hour is, however, as expected: no weight changes occur, probably because no ice forms inside the specimens and because the inner and the outer salt concentrations are equal.

This kind of reduced weight gain, despite the lowering of temperature, was also seen for the corresponding specimens of *w/c* ratio 0.65, figure 7.1.25.

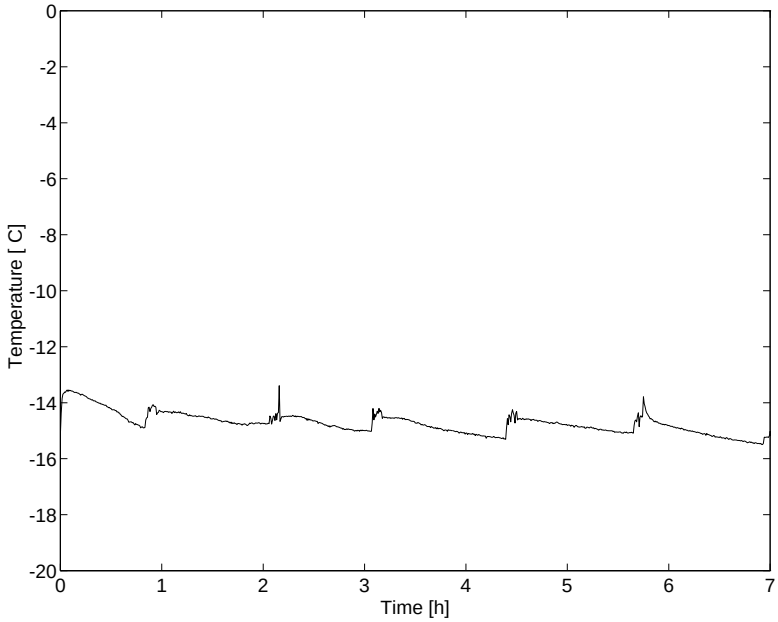

Figure 7.1.23: Bath temperature vs time. Used for specimens of w/c ratio 0.40 pre-stored in 19.7% NaCl solution, shown in figure 7.1.22.

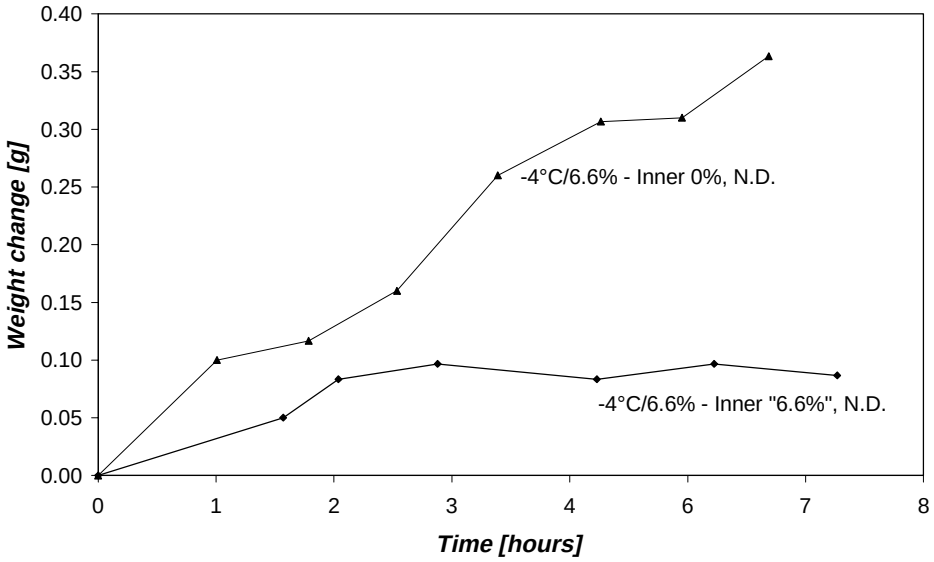

Figure 7.1.24: Effect of (intended) inner salt concentration 6.6% on w/c ratio 0.65 specimen weights at -4°C. Each line represents three specimens. N.D: Never-dried.

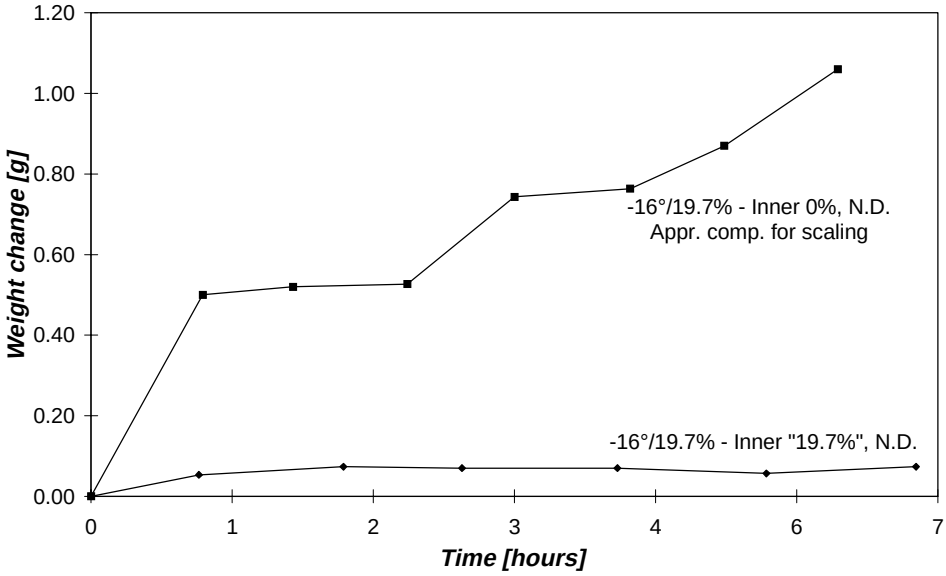

Figure 7.1.25: Effect of (intended) inner salt concentration 19.7% on w/c ratio 0.65 specimen weights at -16°C. Each line represents three specimens. N.D: Never-dried.

The corresponding results for the *w/c* ratio 0.65 mortar are shown in figures 7.1.24 and 7.1.25. It can clearly be seen in figure 7.1.24 that an inner salt concentration reduces the weight increases.

Heavy scaling occurred on 0.65 specimens pre-stored in lime water and tested at -16°C. The mean value curve shown in figure 7.1.25 has been approximately compensated for scaling as described above. The difference between the upper curve and that for the specimens pre-stored in 19.7% NaCl clearly shows that the presence of a 'matched' inner salt concentration effectively stops weight changes at constant temperature.

The small weight increase during the first hour for specimens pre-stored in the strong salt solution is similar to what was observed on specimens of w/c ratio 0.40, figure 7.1.22. The reason for these small weight changes is unknown. (Other specimens tested in the very same baths show normal (large) weight increases during the first hour, thus there was nothing amiss with the test bath.) If the pre-storage had caused increased degrees of saturation, the decreased air content would provided an explanation. From the registered weights, it is not possible to evaluate whether or not this was the case. These series should therefore be run again.

5: Weight changes at constant temperatures <0°C, specimens containing less than "temperature matched" salt concentrations, outer solution concentration "temperature matched"

Specimens of water/cement ratios 0.40 and 0.65 pre-stored in 6.6, 14.4 and 19.7% were tested in a 19.7% solution at -16°C. The results are shown in figures 7.1.26 and 7.1.27.

For *w/c* ratio 0.40, the weight gain, after the initial cooling has stopped, is very slow for the specimens stored in lime water (uppermost curve, from figure 7.1.10). For the specimens containing some salt, the weights remain rather constant or possibly decrease. Again, as for many other series, it can be seen that the initial weight change (during initial cooling) is much smaller for specimens containing salt than for those containing the natural pore solution. This indicates a higher degree of saturation in the specimens stored in salt solutions.

For the specimens of water/cement ratio 0.65, there is a clear trend that the higher the inner salt concentration, the slower the rate of weight gain. This is in accord with what may be predicted from the proposed mechanism. (Here, as well, the weight gain during the first hour is less, the higher the concentration of the pre-storage solution.)

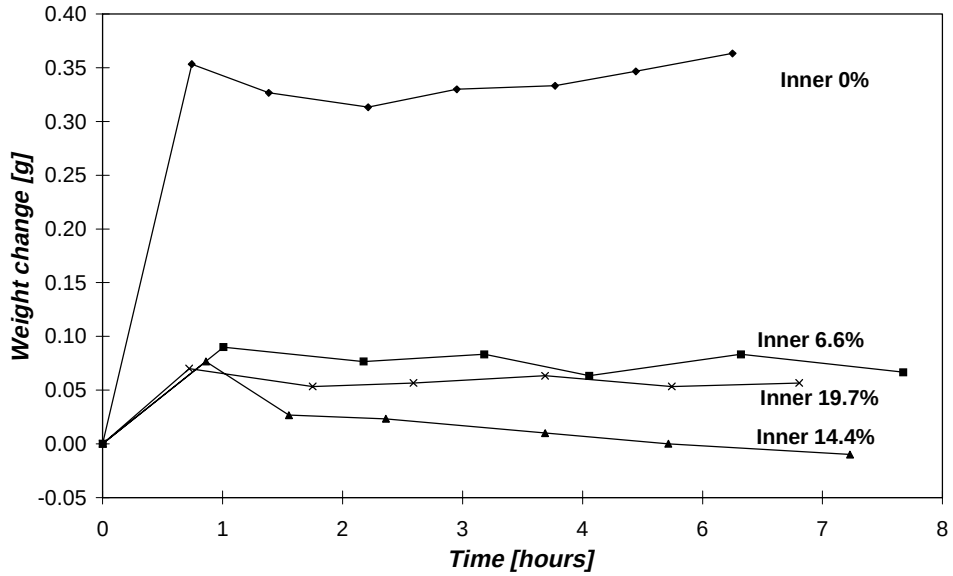

Figure 7.1.26: Weight changes in w/c ratio 0.40 specimens tested at -16°C in a 19.7% outer solution after being pre-stored in different salt solutions (as indicated). One line: Mean value for three specimens.

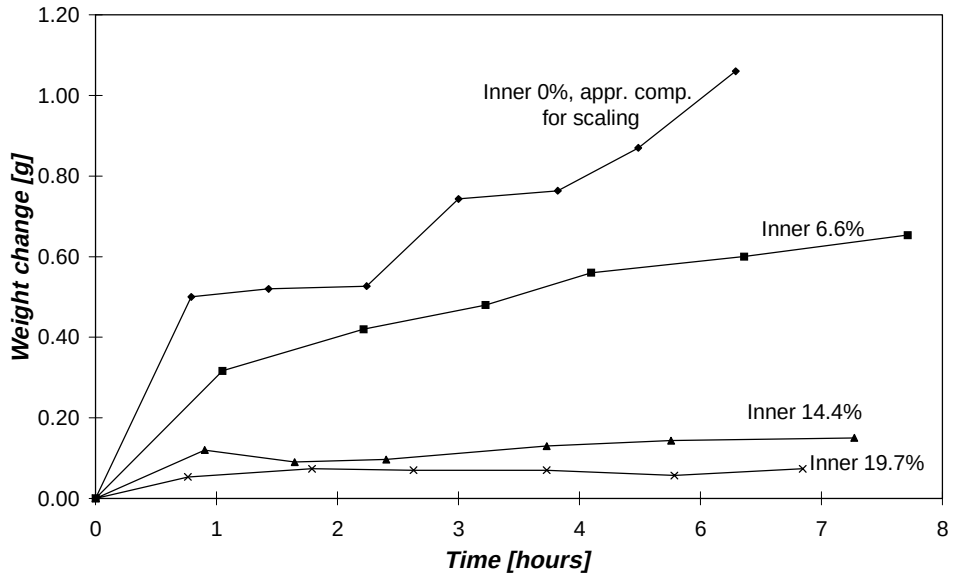

Figure 7.1.27: Weight changes in w/c ratio 0.65 specimens tested at -16°C in a 19.7% outer solution after being pre-stored in different salt solutions (as indicated). One line: Mean value for three specimens.

6: Weight changes at constant temperatures -10°C, specimens pre-stored in weak salt solutions, tested in ”temperature matched” solution

In all the above tests, the concentration of salt in the pore solution was intended to be 6.6% or more. Such high salt concentrations are not to be expected in the pore solution of a specimen tested in a standard salt frost scaling test, at least not during the initial temperature cycles. Therefore, experiments on weight changes obtained in specimens containing low amounts of salts were also run.

These tests were run only on air-entrained qualities of *w/c* ratios 0.40 and 0.65.The specimens were stored in lime water for 14 weeks and then moved to weak NaCl solutions and stored for another 19 days before testing. The solution concentrations were 1%, 3% and 5% NaCl.

The results for the *w/c* ratio 0.40 specimens during the first 8 hours are shown in figure 7.1.28. As was seen above, the weight gain during the first hour is smaller, the higher the salt concentration in the pores. After the initial cooling almost no weight increases seem to occur.

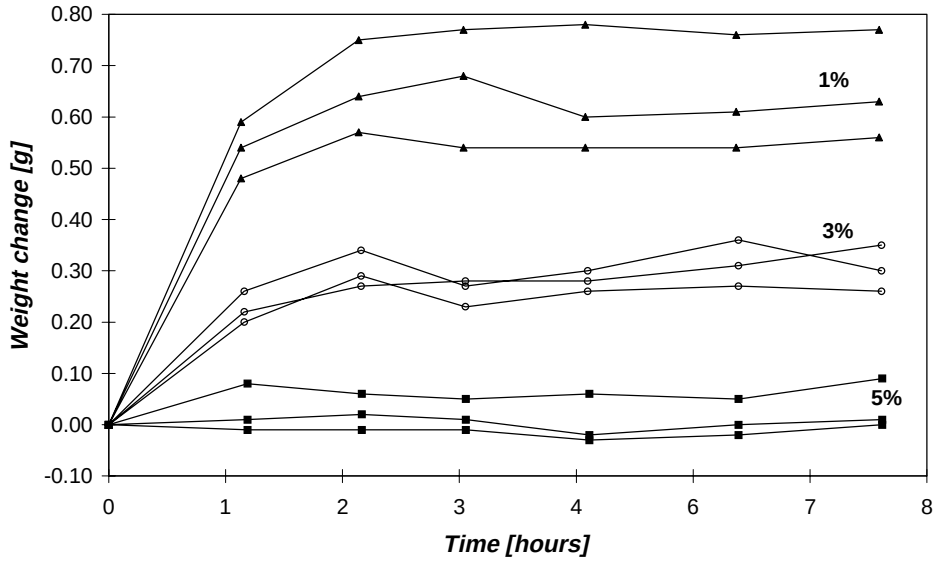

Figure 7.1.28: Weight changes occurring during the first 8 hours for specimens of w/c ratio 0.40 after 19 days pre-storage in weak NaCl solutions (concentrations indicated). Temperature -10°C, outer solution: 14.4% NaCl.

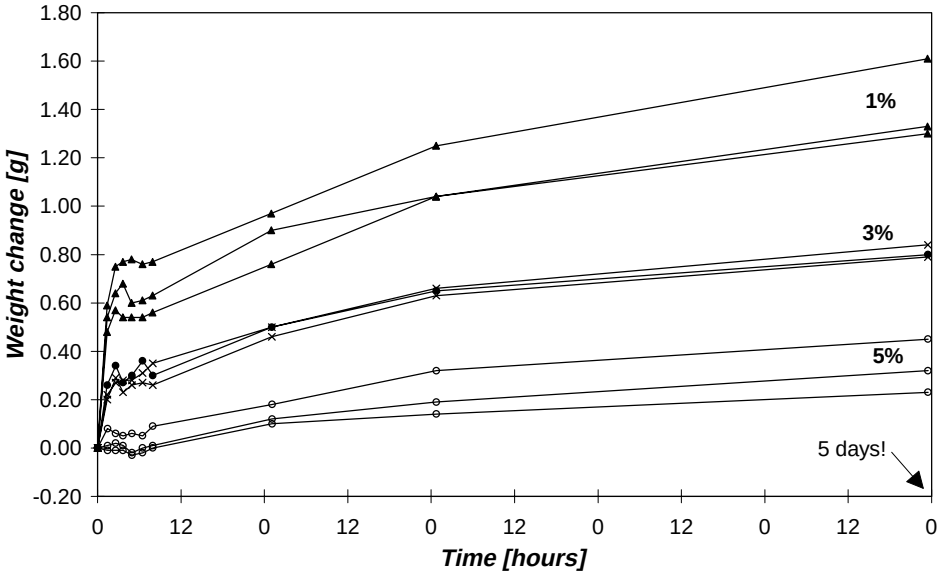

Figure 7.1.29: Weight changes occurring over 5 days for specimens of w/c ratio 0.40 after 19 days pre-storage in weak NaCl solutions (concentrations indicated). Outer solution 14.4% NaCl. Temperature -10°C.

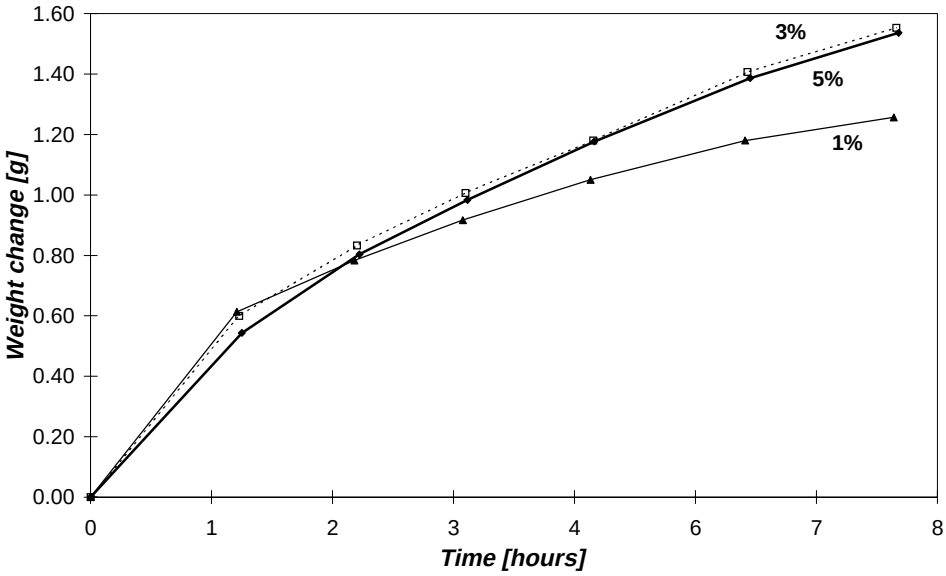

Figure 7.1.30: Weight changes for specimens of w/c ratio 0.65 after 19 days pre-storage in weak NaCl solutions (concentrations indicated). Each line represents the mean value for three specimens. Temperature -10°C, outer salt solution 14.4% NaCl.

The results for *w/c* ratio 0.65 specimens are shown in figure 7.1.30. A plot of each and every specimen for the series shown in figure 7.1.30 reveals that the scatter is large enough to make the apparent differences shown in figure 7.1.30 insignificant. Furthermore, some scaling occurs on all of these specimens after approximately 2 hours and thus the weights are not exact. Since this scaling was rather small, no compensations have been made to the curves in figure 7.1.30.

Figure 7.1.31: Crack in the center of w/c ratio 0.65 specimen stored in 3% NaCl solution for 19 days prior to test at -10°C, bath salt concentration 14.4%. (Two views)

For one of the samples of *w/c* ratio 0.65, pre-stored in 3% NaCl, a remarkable result was obtained after breaking the specimen in two pieces: a large, surface-parallel crack was observed in the centre of the specimen, figure 7.1.31. A similar but less easily distinguishable crack was found in one companion specimen and also in one specimen pre-stored in the 1% NaCl solution. I believe this crack was formed by ice lenses growing in the centre of the specimen. The reason that ice lens growth would be most favourable there is simply that this is where the salt concentration should have been the lowest. This strengthens the hypothesis of chapter 6.

7: Effect of reduced specimen thickness on rate of weight changes at -10°C, ”matched ” outer solution.

A few experiments were run with specimens with a thickness of approximately 2 mm. These tests were run at -10°C/14.4% NaCl. The results for *w/c* ratio 0.40 specimens are shown in figure 7.1.32. The thin discs of *w/c* ratio 0.65 were completely destroyed within one hour of testing.

It can be seen in figure 7.1.32 that the rate of weight increase is higher in the thinner specimens than in the 5 mm specimens reported above. These thin specimens were destroyed within a few hours after start of freezing. ”Destroyed” does not mean that scaling occurred. Instead these specimens fell apart, with cracks going straight through the disc, from one side to the other, somewhat concentrically, figure 7.1.33.

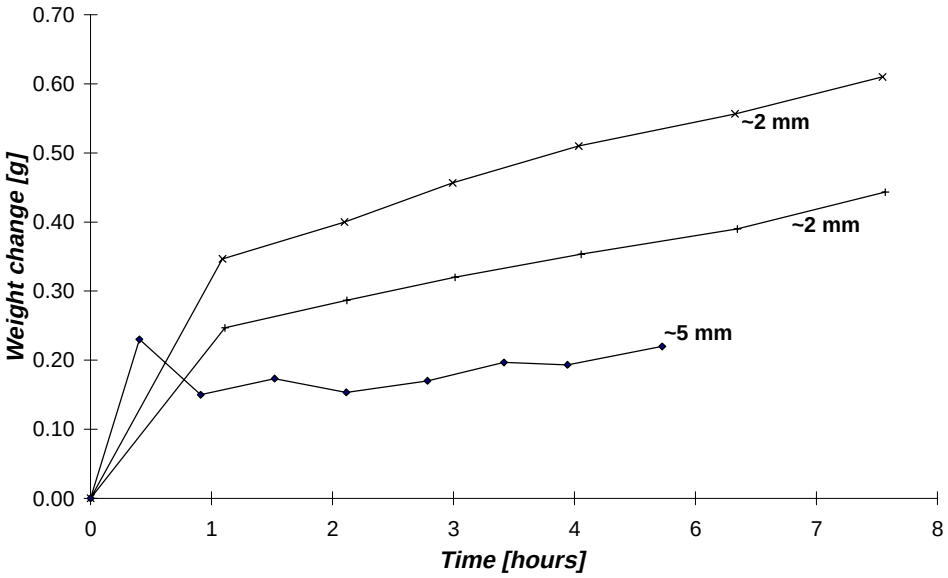

Figure 7.1.32: Effect of specimen thickness. w/c ratio 0.40. Temp -10°C, outer salt conc 14.4%. Thinner discs did not "scale", but were cracked straight through, perpendicular to the surfaces

Figure 7.1.33: Cracks in thin specimen (appr. 2 mm). w/c ratio 0.40. Temperature -10°C, outer concentration 14.4% NaCl, inner concentration 0%.

7.1.9 Discussion and Conclusions

The results predicted in section 7.1.5 were fulfilled. These results however were complemented by two non-predicted results.

The first non-predicted result was the increase in rate of weight gain when a "too concentrated" outer solution is used as compared to that obtained when freezing a specimen

in a ”matched” salt concentration (table 7.1.4). Although not predictable from the hypothesis, these results do not contradict the hypothesis that the pore solution is consumed by growing ice bodies and replaced by the outer solution. These tests should be run again in order to exclude the possibility that the results were due to some unusual circumstance.

The second non-predicted result was that, while the weight increase for specimens pre-stored in lime water during the first hour, which is when the major part of the temperature change takes place, were qualitatively predictable from the measured air contents, specimens pre-stored in salt solutions showed smaller weight increase during this first hour, the stronger the salt solution in which they had been pre-stored. This was seen in figures 7.1.22 and 7.1.25-7.1.28. This observation is also not direct proof against the hypothesis, but it does require an explanation. It might be explained as being due to a higher degree of saturation in these samples. However, determinations of density and porosity made after the entire test series had been finished showed that the degree of saturation in specimens pre-stored in salt solutions had been less than that in specimens pre-stored in lime water. The results from this determination are given in Appendix 7.1.3. These determinations were made after the specimens had been left in the drying oven at 105°C for about a month. Thus it might be that the porosities had been affected, so that the calculated degree of saturation at the start of freezing was erroneous. It can in fact be seen in Appendix 7.1.3 that the porosity of all these samples was less than that determined on specimens pre-stored in lime water before the test series was carried out. If the degree of saturation after pre-storage is determined from the values of porosities as determined before the tests were carried out on specimens pre-stored in lime water (Appendix 7.1.1), then the calculated degrees of saturation after pre-storage in salt solution becomes even lower, making the observed reduced weight increases even more difficult to explain.

The final conclusion drawn from the results of these tests is that the hypothesis cannot be rejected. In fact, the cracks observed in the centre of some specimens actually strengthen the hypothesis.

Appendix 7.1.1

POROSITY AND DENSITY AS DETERMINED ON DUPLICATE SAMPLES

Values determined by the Archimedes principle, (calculations described in Appendix 3.1)
Values not corrected for exact density of water or incomplete vacuum.
Specimens were weighed and dried to determine water content after pre-storage. Then, specimens were let to suck water for 2 days and then dried again. The period of capillary suction results in less moisture content than the (natural) water content after pre-storage.

Data on Porosity, Density, Degree of saturation and air content after pre-storage in lime water

Remaining pressure after evacuation in vacuum chamber: 3 mBar

Assumed water density: 1.0 kg/l

Spec.	After pre-storage	Dry (105°C)	2 days cap. suct.	Dry (105°C)	Watersaturated in Water	Watersaturated in air	Volume	Pore vol.	**Density**	**Porosity**	**S-natur**	**Air content as pre-stored**	Air content after cap. suct.	Wet dens after pre-storage
40L1	74.91	66.68	73.82	66.71	41.82	77.47	35.65	10.79	1870.41	30.3	76.3	7.2	10.2	2101.3
40L2	75.95	67.31	74.78	67.4	42.26	78.7	36.44	11.39	1847.15	31.3	75.9	7.5	10.8	2084.2
40L3	84.06	74.79	82.88	74.88	46.89	86.96	40.07	12.17	1866.48	30.4	76.2	7.2	10.2	2097.8
40L4	76.93	68.43	75.8	68.5	42.93	79.43	36.50	11	1874.79	30.1	77.3	6.8	9.9	2107.7
40L5	73	64.95	71.98	65	40.75	75.56	34.81	10.61	1865.84	30.5	75.9	7.4	10.3	2097.1
								Mean :	**1864.93**	**30.5**	**76.3**	**7.2**	**10.3**	**2097.6**
								Std. Dev. :	**10.57**	**0.4**	**0.6**	**0.3**	**0.3**	**8.6**
								Coeff. of variation (%) :	**0.57**	**1.4**	**0.8**	**3.5**	**2.9**	**0.4**
65L1	81.33	71.8	80.7	71.92	45.06	85.45	40.39	13.65	1777.67	33.8	69.8	10.2	11.8	2013.6
65L2	81.37	72.29	80.59	72.41	45.37	85.26	39.89	12.97	1812.23	32.5	70.0	9.8	11.7	2039.9
65L3	82.73	73.1	82.08	73.23	45.88	86.84	40.96	13.74	1784.67	33.5	70.1	10.0	11.6	2019.8
65L4	85.03	75.18	84.32	75.33	47.19	88.91	41.72	13.73	1802.01	32.9	71.7	9.3	11.0	2038.1
65L5	85.74	75.95	85.12	76.04	47.63	89.7	42.07	13.75	1805.32	32.7	71.2	9.4	10.9	2038.0
								Mean :	**1796.38**	**33.1**	**70.6**	**9.7**	**11.4**	**2029.9**
								Std. Dev. :	**14.58**	**0.6**	**0.8**	**0.4**	**0.4**	**12.3**
								Coeff. of variation (%) :	**0.81**	**1.7**	**1.2**	**4.0**	**3.7**	**0.6**
401	99.55	90.32	98.68	90.42	56.5	99.84	43.34	9.52	2083.99	22.0	97.0	0.7	2.7	2297.0
402	99.82	90.49	98.83	90.56	56.56	99.95	43.39	9.46	2085.50	21.8	98.6	0.3	2.6	2300.5
403	105.94	96.18	105.13	96.25	60.09	105.9	45.81	9.72	2099.54	21.2	100.4	-0.1	1.7	2312.6
								Mean :	**2089.68**	**21.7**	**98.7**	**0.3**	**2.3**	**2303.4**
55L1	84.76	75.45	83.92	75.59	47.33	88.03	40.70	12.58	1853.81	30.9	74.0	8.0	10.1	2082.6
55L2	87.73	77.73	86.65	77.86	48.7	90.68	41.98	12.95	1851.60	30.8	77.2	7.0	9.6	2089.8
55L3	84.16	74.86	83.27	74.93	46.93	87.42	40.49	12.56	1848.85	31.0	74.0	8.1	10.2	2078.5
								Mean :	**1851.42**	**30.9**	**75.1**	**7.7**	**10.0**	**2083.6**
651	101.38	90.84	100.4	90.93	56.87	101.65	44.78	10.81	2028.58	24.1	97.5	0.6	2.8	2264.0
652	99.22	89.23	98.31	89.33	55.85	99.59	43.74	10.36	2040.01	23.7	96.4	0.8	2.9	2268.4
653	82.62	74.05	81.89	74.12	46.4	82.92	36.52	8.87	2027.66	24.3	96.6	0.8	2.8	2262.3
								Mean :	**2032.08**	**24.0**	**96.8**	**0.8**	**2.8**	**2264.9**

Appendix 7.1.2

CHLORIDE ION CONTENT IN SPECIMENS PRE-STORED IN NACL SOLUTIONS

Chloride ion contents determined by milling layers off the samples and leaching chlorides out with acid. Chloride ion content determined with chloride ion sensitive electrode. (Complete field equipment from Germann Instruments, Denmark)

Appendix 7.1.2

Chloride ion content in specimens pre-storedin NaCl solutions

Specimen	Storage time days	Read value mV	Eval. % Cl b.w.	Remark	Calculated NaCl conc.(fic.) [%]
0,40:6,6%:1 mm	84	-13.9	0.43		6.4
0,40:6,6%:2 mm	84	-10.1	0.38		5.7
0,40:6,6%:3 mm	84	-8.8	0.36		5.4
0,40:19,7%:1:mmProv 1	84	-34.5	> 0,5		
0,40:19,7 %:2 mmProv 1	84	-28.7	> 0,5		
0,40:19,7 %:3 mmProv 1	84	-29.1	> 0,5		
0,40:19,7%:1 mmProv 2	84	-40.3	> 0,5		
0,40:19,7 %:2 mmProv 2	84	-36.2	> 0,5		
0,40:19,7 %:3 mmProv 2	84	-29.8	> 0,5		
0,40:1%:0,5 mm	19	12.8	0.16		2.5
0,40:1 %:1 mm	19	13.4	0.16		2.5
0,40:1 %:2 mm	19	36.1	0.065	0,584 g	2.6
0,40:3 %:0,5 mm	19	-2.7	0.29		4.4
0,40:3 %:1 mm	19	-0.8	0.26		4.0
0,40:3 %:2 mm	19	4.1	0.22	1,407 g	3.6
0,40:3 %:3 mm	19	3	0.23		3.5
0,40:5 %:0,5 mm	19	-7.9	0.34		5.1
0,40:5 %:1 mm	19	-6.9	0.33		5.0
0,40:5 %:2 mm	19	2.5	0.235	0,930 g	5.7

Specimen		mV	% Cl-	Remark	Calculated NaCl conc.(fic.)
0,65:6,6%:1 mm	84	-12.8	0.41		5.4
0,65:6,6%:2 mm	84	-11.4	0.39		5.2
0,65:6,6%:3 mm	84	-10.6	0.38		5.0
0,65:19,7%:1:mm	84	-37.1	> 0,5		
0,65:19,7 %:2 mm	84	-35.2	> 0,5		
0,65:19,7 %:3 mm	84	-32.8	> 0,5		
0,65:1%:0,5 mm	19	25.7	0.1		1.4
0,65:1 %:1 mm	19	20	0.125		1.7
0,65:1 %:2 mm	19	17.2	0.135		1.8
0,65:1 %:3 mm	19	19	0.128		1.8
0,65:3 %:0,5 mm	19	-3.1	0.29		3.9
0,65:3 %:1 mm	19	1.4	0.245		3.3
0,65:3 %:2 mm	19	4.7	0.22		3.0
0,65:3 %:3 mm	19	5.7	0.21		2.8
0,65:5 %:0,5 mm	19	-9.5	0.36		4.8
0,65:5 %:1 mm	19	-5.1	0.31		4.1
0,65:5 %:2 mm	19	-4.3	0.305		4.1
0,65:5 %:3 mm	19	-1.1	0.27		3.6

Appendix 7.1.3

APPROXIMATE DETERMINATION OF DEGREE OF SATURATION AT START OF FREEZING TESTS FOR SAMPLES PRE-STORED IN NACL SOLUTIONS.

Samples had been dried at 105°C for one month prior to determination. Calculations as described in Appendix 3.1 (though not compensated for incomplete vacuum)

Appendix 7.1.3: Degrees of saturation at start of test as function of pre-storage solution

Assumed water density: 0.9983 kg/l
Density of pore solution after pre-storage assumed = density of pre-storage solution
(calculations described elsewhere)
(specimens dried 1 month at 105° prior to porosity determination (after freeze test)

		(1)	(2)	(3)	(4)	(5)	(6)	(7)	(8)	(9)	(10)
Spec.	W/C ratio	Pre-storage solution (%NaCl)	Density of pre-storage sol. (g/cm^3)	Weight at start of freezing (g)	Dry (105°C) (g)	water saturated in water (g)	air (g)	Volume [cm^3]	Porosity [%]	Volume of pore solution after pre-storage (cm^3)	Degree of saturation after pre-storage (%)
67B	0.4	6.60	1.05	91.53	82.68	51.16	95.16	44.07493	28.4	8.5	67.7
67C	0.4	6.60	1.05	100.53	90.95	56.35	104.77	48.50245	28.5	9.2	66.2
69A	0.4	19.70	1.15	93.08	84.18	51.88	96.4	44.59581	27.4	7.8	63.5
69B	0.4	19.70	1.15	93.55	84.59	52.14	96.94	44.87629	27.6	7.8	63.2
69C	0.4	19.70	1.15	94.85	85.86	52.96	98.47	45.5875	27.7	7.8	62.1
90A	0.65	19.70	1.15	75.85	68.28	42.11	78.29	36.24161	27.7	6.6	65.9
90B	0.65	19.70	1.15	82.16	73.58	45.17	84.81	39.7075	28.3	7.5	66.6
90C	0.65	19.70	1.15	80.05	72.06	44.42	83.1	38.74587	28.5	7.0	63.1
91B	0.65	6.60	1.05	90.42	81.32	50.08	94.38	44.37544	29.5	8.7	66.5
91C	0.65	6.60	1.05	90.35	81.17	50.15	94.4	44.32535	29.9	8.8	66.2
93A	0.65	19.70	1.15	84.66	76.42	46.84	87.58	40.80938	27.4	7.2	64.4
93B	0.65	19.70	1.15	80.25	71.92	43.92	82.72	38.86607	27.8	7.3	67.2
93C	0.65	19.70	1.15	77.82	69.88	42.8	80.32	37.58389	27.8	6.9	66.3

7.2 SECOND TEST OF THE HYPOTHESIS: EFFECT OF VARYING TIME OF SALT PENETRATION INTO THE PORE SOLUTION IN SALT FROST SCALING TESTS

7.2.1 Abstract

Two series of salt frost scaling tests were run in order to test whether the results predicted by the hypothesis would occur. In the first series, the intention was to avoid the presence of salts in the pore solution. This should, according to the hypothesis, make scaling independent of the outer concentration used. Furthermore, it should make scaling more severe than in an ordinary test in which the de-icing agent is permitted to affect the pore solution. The second test series sought to have the outer salt solution considerably influence the pore solution. The hypothesis predicted this should reduce scaling. While the predictions for test 1 were fulfilled, the results from series 2 were somewhat obscured because the tests had to be discontinued after only a few frost cycles. Extrapolation, however, indicates that the predicted results would have been achieved.

7.2.2 Introduction

According to the proposed hypothesis, scaling should be independent of the salt concentration in the outer solution if the composition of the pore solution remains undisturbed, *i.e.* if no ion exchange occurs between the inner and the outer solution. (Possibly, scaling may increase with increasing salt concentration, since this will make more liquid available in the outer solution throughout the entire frost cycle.) Thus, if an SFS resistance test could be run in such a way that the penetration of ions from the outer solution to the pore solution was prevented, the 3% optimum in scaling reported by Arnfelt [A 1943] and Verbeck and Klieger [V 1957] should not appear. This is the basis for the qualitative tests of the hypothesis presented in this chapter.

Using a modified version of the Swedish SS 13 72 44 test method, two series of tests were run on mortar specimens. In the first series, the outer salt solution was applied to the specimen surfaces only during that part of the frost cycle when the temperature was below 0°C. During the period of temperatures >0°C, tap water was applied to the specimen surfaces. Of course this does not completely stop penetration of salts into the pore solution. But it will, nevertheless, very much reduce the salt content, both because diffusion is slower the lower the temperature and because the pure (tap) water applied to the surfaces during the part of the frost cycle when the temperature was above 0°C should serve as a leaching liquid for any salts present in the pore system.

This study was divided into one pre-series, which was carried out on samples of mortar of *w/c* ratio 0.50, and a main series, carried out on mortars of *w/c* ratios 0.45 and 0.65, respectively. In addition to the scaling tests, a small study of the concentration of chloride ions in the outer solution (before and after testing) was also undertaken. This was to check that the intended salt concentrations had been achieved and that salt had not penetrated into the specimens.

In the second test, the opposite conditions were striven for. Thus, the salt solutions were applied to the specimen surfaces for a week between every frost cycle. In this way, the mole fraction of water in the pore solution (close to the surface) was assumed be significantly reduced. This, according to the hypothesis, should reduce scaling.

7.2.3 Series 1 - Minimised intrusion of salt into the pore solution

Experimental

Three materials (Portland cement mortar, *w/c* ratios 0.45, 0.50 and 0.65) were tested with 4 different salt concentrations (0, 1, 3 and 7.5% b.w.), which were applied to the specimen surface at 0°C. The salt solutions were removed from the specimen surfaces when the temperature reached 0° during thawing. When removing the salt solutions, scaled off material was also collected and thus the scaling was evaluated day by day.

First, a pre-series of tests were performed on the *w/c* ratio 0.50 mortar and then the *w/c* ratio 0.45 and 0.65 mortars were used for the main series.

Expected results

According to the hypothesis, scaling should be reduced when the outer salt has penetrated into the pore solution. This is because the pressure difference required for thermodynamic equilibrium is reduced and thus both the driving force for moisture flow and the possible ice lens pressure are reduced.

Materials

The mortar mixes are set out in table 7.2.1. The mortars were cast in PVC tubes of 127 mm diameter and 300 mm height. On the day after casting, discs of a thickness of 25 mm were cut from the cylinders. Immediately after cutting, the discs were stored in lime water.

Pre-storage

Both discs that had never been dried and discs that had been dried once and re-moistened were used. All discs were stored in water for a minimum of 6 weeks. The discs tested last were water-stored for 11 weeks (see part 2). Those discs in the main series which were to be dried and re-moistened were stored for two days in 60%R.H./18°C and were then water-stored for another three days until being tested. The corresponding specimens in the pre-series (*w/c* 0.50) were dried for three days.

Table 7.2.1: Mortar mixes

w/c:	0.45	0.50	0.65	
Water	262	280	266	kg/m^3
Cement*	582	560	409	kg/m^3
Sand, 0-3 mm	1295	1275	1424	kg/m^3
Sand moisture content, % b.w.	5.8	4.8	5.6	%
Fresh air content	6.6	6.2	6.7	%

**Cement type "Anläggningscement", General Appendix 2*
Mix water was reduced for moisture content in sand

Test set-up

The test set-up is shown in figure 7.2.1. The specimen discs had been cut from the PVC mould so that a ring of PVC was left around the specimen edges. This ring was displaced approximately 15 mm up the edges of the specimen. In the pre-series, a hardening silicon sealant was applied along the edge where the PVC ring meets the upper surface of the specimen. This, however, turned out to be unsuitable because when scaling starts the sealant loosens and the solution leaks out. In the main series and in Series 2, the specimens were sealed at the lower end of the displaced PVC-ring, fig 7.2.1. This time, a polyester resin (Plastic Padding ”hemical Metal”) was used, fig. 7.2.1. This served well in the main series of Series 1, but failed in Series 2, see below.

The discs were then heat isolated by mounting them in extruded polystyrene forms. The intention was to keep heat flux as one-dimensional as possible. A lid, made of plastic film wrap, was put on to prevent evaporation from the solution applied to the specimen surface.

Salt concentration combinations and application of salt solution

The intention was to clarify whether there is an optimum in scaling when the outer solution consists of a 3% NaCl solution, even when the salt is added in such a way that the time available for diffusion of ions into the pore solution is very limited. This was done by pouring 26 ml of de-ionised water on the specimen surfaces at the beginning of cooling (*i.e.* at +20°C) and then, when the temperature reached ±0°C, adding another 13 ml of salt solution (pre-cooled to ±0°C) with a concentration three times higher than that intended (an injection syringe was used for this purpose). In this way the salt was properly dissolved without causing any heat effects due to dissolution.

The total volume of salt solution, 39 ml, corresponds to a solution depth of 3 mm, which is prescribed in the Swedish SS137244.

When the temperature reached ±0°C during thawing, the scaled off material was collected and the salt solutions were replaced with 26 ml of de-ionised water. Next time the temperature reached ±0°C, some 8 hours later, new concentrated solution was added.

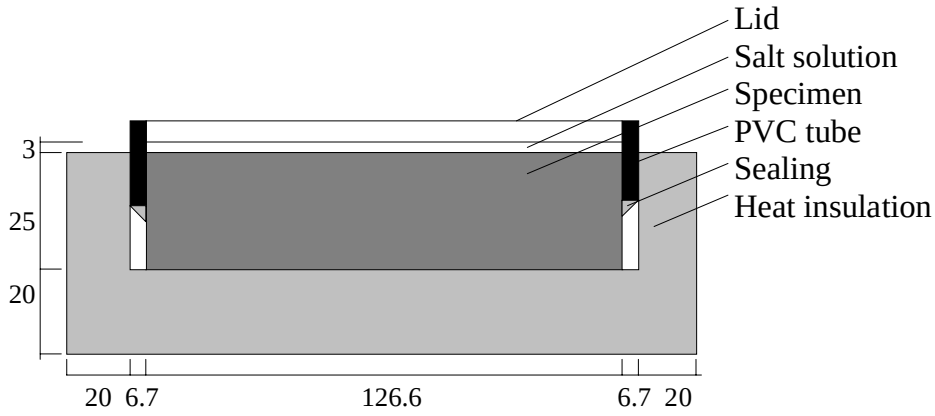

Figure 7.2.1: Test set-up.

Nomenclature

The specimens were denoted by *w/c* ratio, pre-storage procedure (ND: Never-dried, D: Dried and re-moistened), salt concentration and a letter to mark the individual specimen. Two specimens of each variable combination were used, thus the final letter is either A or B. For example, the notation 45D3A signifies a water cement ratio 0.45 specimen, dried and re-moistened before testing, tested with a 3% NaCl solution. This is specimen A of two identical specimens. (The specimens tested with a 7.5% solution were denoted 75.)

Temperature cycle

The temperature cycle is shown in figure 7.2.2. The temperatures were measured in the solutions. It would be desirable that the temperature cycles be the same for all specimens. However, salt content and the addition of salt solution affect the obtained temperatures, as shown in figure 7.2.2: While cooling proceeds at a slow rate in a salt solution, it stops at 0°C in tap water until all of it has transformed into ice. Thereafter, the temperature decrease is faster in this ice than in salt solution until approximately -13°C is reached.

7.2.4 Results and discussion, Series 1

General

The development of scaling and the final accumulated scaling are shown in figures 7.2.3 – 7.2.11. Due to leakage of the salt solutions, the test had to be discontinued after some 9-10 frost cycles. Otherwise, the following disturbances were noted:

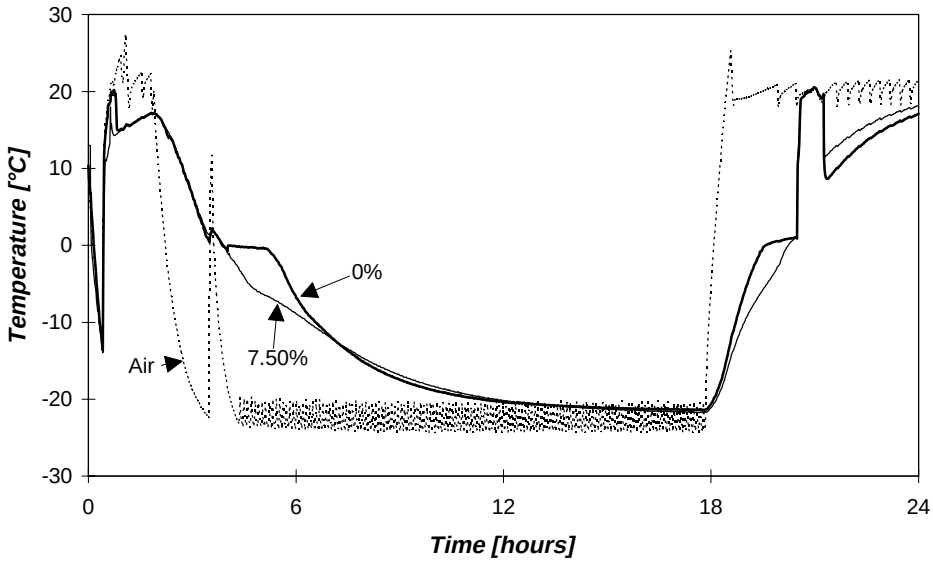

Figure 7.2.2: Temperature cycles. Peaks close to 0°C appear when the cabinet door was opened.

Main series 1: *w/c* ratio 0.45

1. Due to a malfunctioning thermostat, frost cycle number 2 went approximately 2 hours too long. The effect on the results is estimated to be negligible.
2. Specimen ND1B had a double dosage of concentrated salt solution during the first cycle. The true concentration was thus 1.5% instead of the intended 1%. No effect of this can be seen in the results.

Main series 2: *w/c* ratio 0.65

In the last cycle, the salt solution covering specimen 65D3A leached out. The concentration therefore may not have been the intended 3%.

Pre-series: *w/c* ratio 0.50

Due to erroneous mix proportions, the intended salt concentrations were not achieved. Instead, the specimens were tested with outer salt concentrations 1.1, 2.3 and 5.6 % NaCl.

Effect of salt concentration on the scaling process

Figures 7.2.3–7.2.8 show the accumulated scaling *vs.* number of run cycles. It should be noted that those specimens of the 0.50 quality which were dried once and re-moistened, were dried for three days, whereas those of the other qualities were dried for only two days. This is probably the reason why the dried and re-moistened 0.50 mortars started scaling rather late and at a low rate.

It can be seen that the specimens start scaling after different numbers of run cycles. When scaling starts, it initially occurs at somewhat different rates, but during the later cycles, the rate is approximately the same for all specimens of the same *w/c* ratio, irrespective of outer salt concentration. The differences in final accumulated scaling shown in figures 7.2.3-7.2.5 are largely due to the different start times of scaling. Specimens that have been dried once and re-moistened, however, are destroyed at a somewhat lower rate. The reason for this may be the possibly different moisture content profile obtained in these specimens, which would in turn be due to the drying and re-moistening procedure. It can also be seen that the scatter is larger for specimens dried once and re-moistened than for those that have never been dried.

Although there is a general trend, independent of outer salt concentration, for the rate of scaling to become the same after several cycles have been run, there is a trend that scaling accelerates the slowest on specimens tested with an outer salt concentration of 1%. This is logical, from the hypothesis, since this low amount of salt in the outer solution results in very little liquid being available during the freezing period.

Only very slight scaling occurs during the first cycle. Considering the proposed hypothesis, this is a remarkable result, since it cannot be directly predicted. Indirectly, though, it may be explained as being due to one of the following reasons, or a combination of them:

1. It may be because the specimens initially contain so little water that no destructive pressures due to ice body growth are reached for the duration of the first cycle. As the number of cycles increases, moisture accumulates in the specimens and deterioration begins.
2. It may be that during the first freezing of never-dried specimens, a rather small amount of water is freezable, causing only minor ice lens growth. This first freezing however leads to structural changes (as in drying) that lead to larger amounts of water

being freezable in subsequent cycles. (For the dried once and re-moistened specimens, this structural change has probably already been established. Instead, these specimens are not as saturated as the never-dried specimens and thus do not scale during the initial cycles.)

Finally, it may be an indication that the mechanism causing scaling is not the one described in chapter 6.

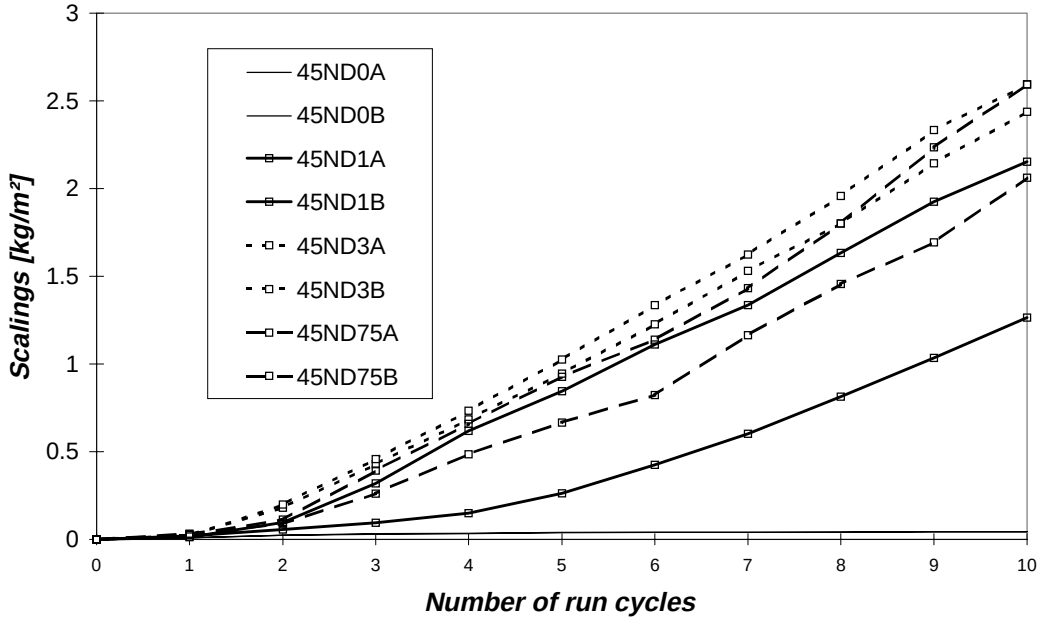

Figure 7.2.3: Accumulated scaling vs. number of cycles for never-dried specimens of w/c ratio 0.45 mortars.

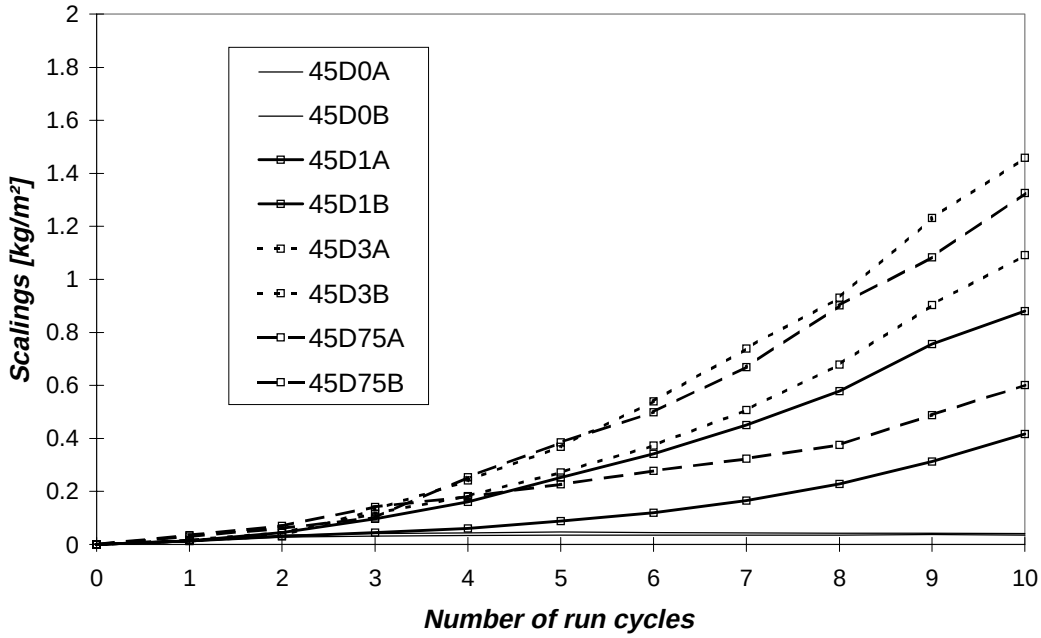

Figure 7.2.4: Accumulated scaling vs. number of cycles for dried and re-moistened specimens of w/c ratio 0.45 mortar.

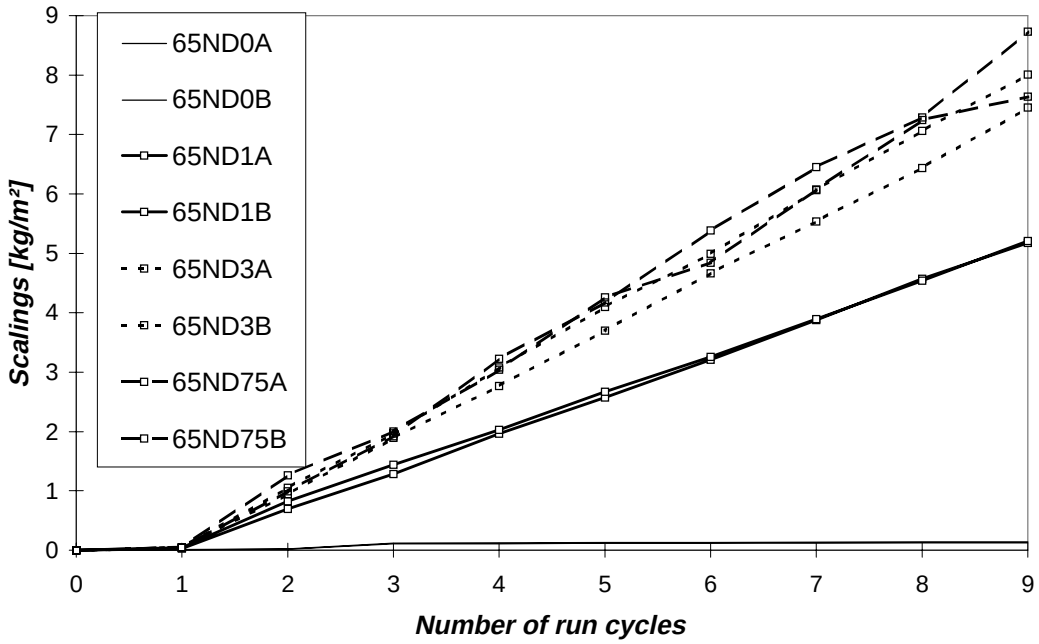

Figure 7.2.5: Accumulated scaling vs. number of cycles for never-dried specimens of w/c ratio 0.65 mortar.

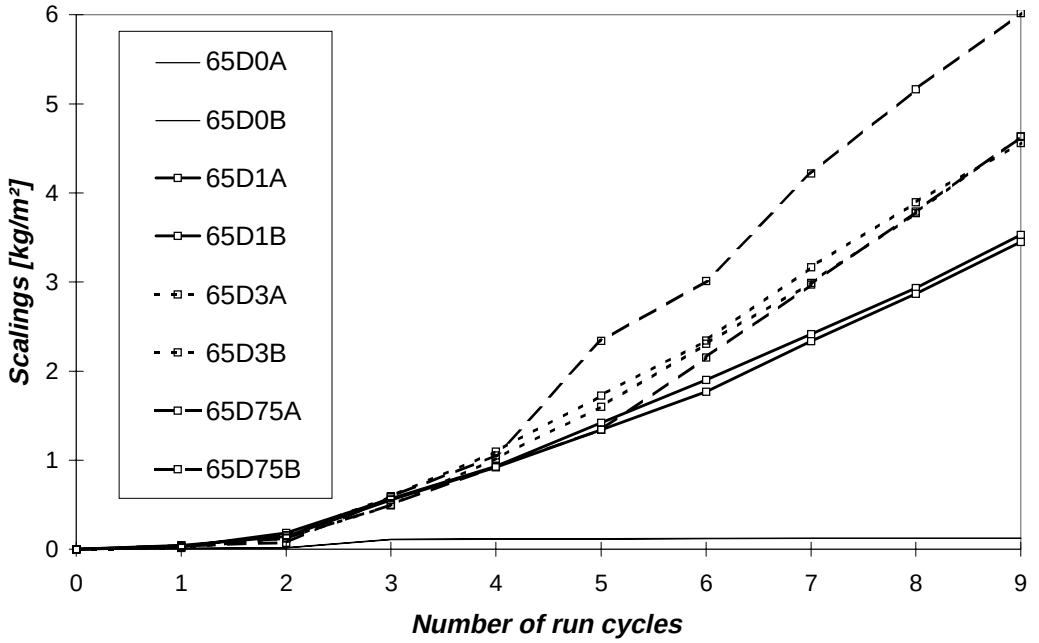

Figure 7.2.6: Accumulated scaling vs. number of cycles for dried and re-moistened specimens of w/c ratio 0.65 mortar.

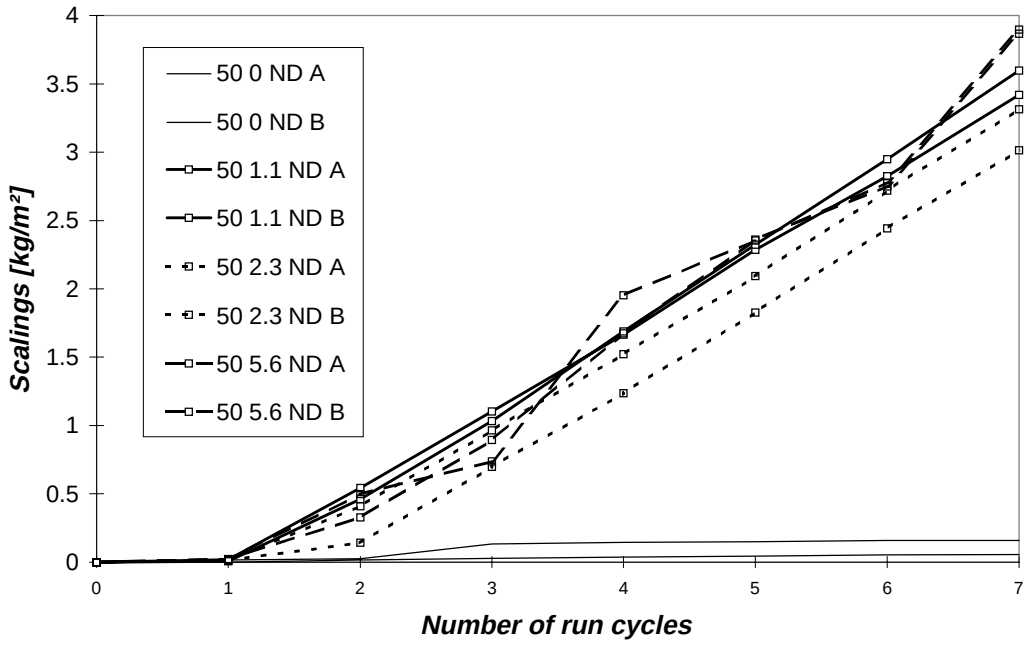

Figure 7.2.7: Accumulated scaling vs. number of cycles for never-dried specimens of w/c ratio 0.50 mortar. Note different salt concentrations.

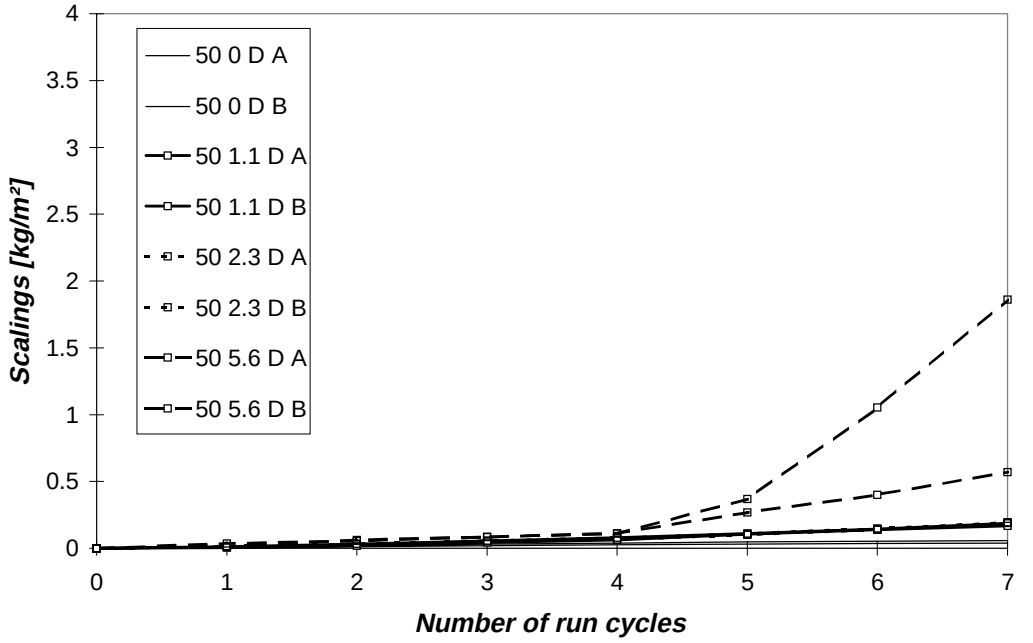

Figure 7.2.8: Accumulated scaling vs. number of cycles for dried and re-moistened specimens of w/c ratio 0.50 mortar. Note different salt concentrations.

Final accumulated scaling – effect of outer salt concentration

The final accumulated scaling for each individual specimen is shown in figures 7.2.9-7.2.11. The first observation is that specimens tested in pure water are almost completely undamaged. The amounts of scaling noted in the figures are so small that the specimens seem completely unharmed on visual inspection. This is important since it shows that none of the materials tested here were of such low quality that the high amount of scaling obtained for specimens tested with salt solution could be explained as simply being due to inferior material quality. Furthermore, it can be seen that scaling decreases with *w/c* ratio.

The accumulated scaling from specimens that had not been dried prior to testing seems to be almost independent of salt concentration. There are differences, but these are neither as clear nor as consistent as those reported by Arnfelt [A 1943], or Verbeck and Klieger [V 1957], or those reported in chapter 4.1. (As pointed out above, the differences in final scaling are largely due to the different times required for initiation of scaling.) It thus seems that scaling is dependent on whether or not there was salt in the outer solution during freezing, rather than on the concentration of the outer solution.

For those specimens which had been dried and re-moistened, scaling is clearly reduced. It can be seen in figures 7.2.3 - 7.2.8 that the dried once specimens start scaling somewhat later and then proceed at an initially slower rate compared to the never-dried specimens. This is especially so for the 0.50 mortar. On specimens of *w/c* ratio 0.45, the rate of scaling however increases with the number of frost cycles. It seems that the specimens are being filled with moisture in each cycle so that scaling becomes more severe in the subsequent cycle. It also seems that the scaling rate of the dried once and re-moistened specimens becomes the same as that for never-dried specimens after several cycles. This might be because water successively accumulates in the air pores.

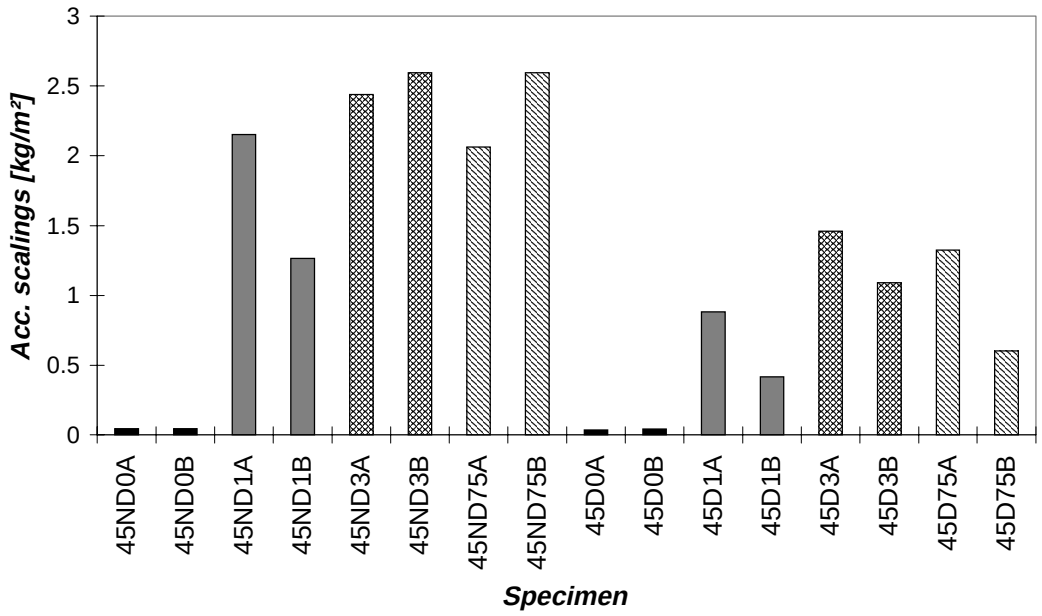

Figure 7.2.9: Final accumulated scaling for w/c ratio 0.45 mortars (10 cycles). See Experimental section for nomenclature.

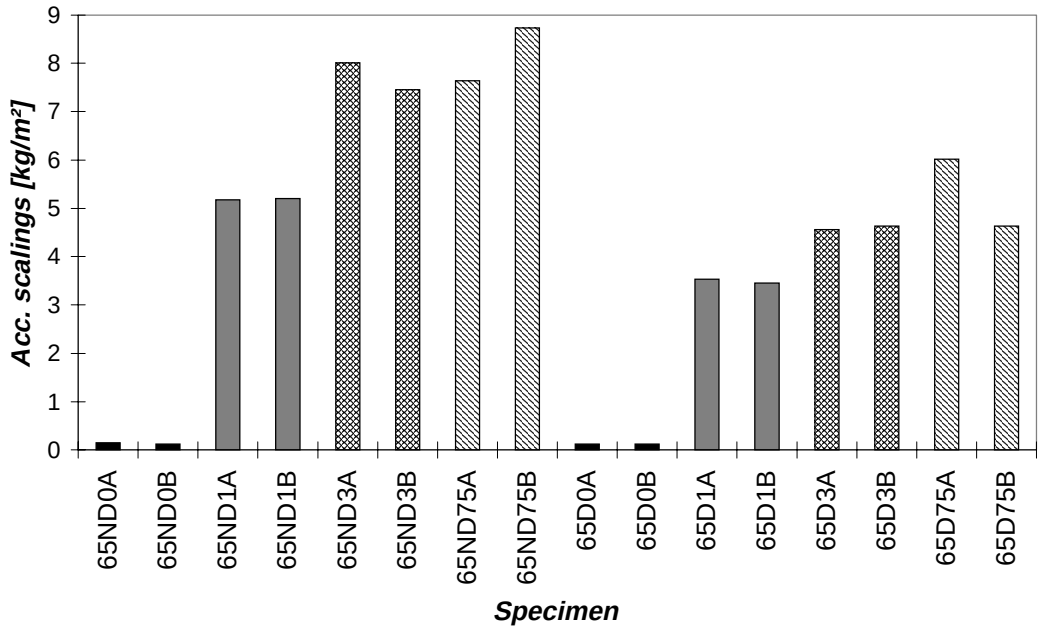

Figure 7.2.10: Final accumulated scaling for w/c ratio 0.65 mortars (9 cycles). See Experimental section for nomenclature.

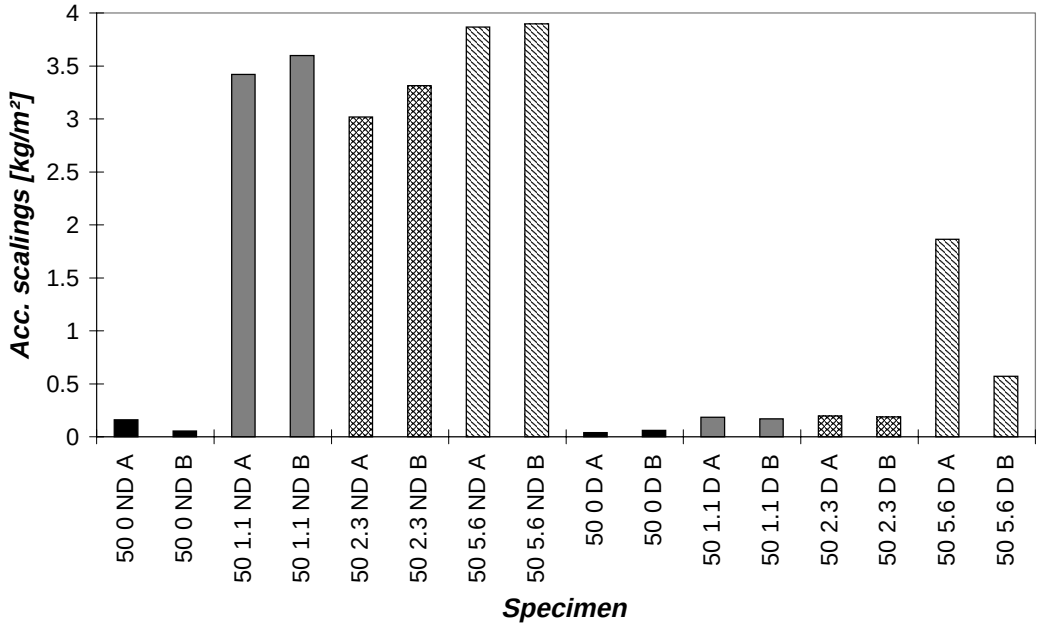

Figure 7.2.11: Final accumulated scaling for pre-series test of w/c ratio 0.50 mortars (7 cycles). Note different salt concentrations, see text. See Experimental section for nomenclature.

It can be seen in the figures that scaling was almost proportional to the number of cycles run. Such proportionality was also found by Pettersson [P 1994] who pre-stored specimens in plastic bags, thus avoiding drying of the specimens. The absence of drying reduces the variances of microstructure in the outermost part of the specimens and thus the material properties do not change as scaling proceeds.

It was foreseen from the hypothesis that scaling would be worse the lower the salt content in the pore solution. On comparing these results with those reported in chapter 4.1, which referred to a *w/c* ratio 0.45 concrete (maximum aggregate size 8mm), it can be seen that the scaling obtained for the 0.45 mortar used here is clearly larger, approximately 2 kg/m² after 10 cycles as compared to 1.5-1.8 kg/m² after 56 cycles for the 0.45 concrete in chapter 4.1 (for the comparable frost cycle E and outer salt concentration 3%). In fact, when comparing fresh air content to paste content, it seems that the mortar used here should have been better protected against salt frost attack. This prediction therefore seems to be fulfilled by the present results.

For the 0.65 *w/c* ratio mortar, scaling was somewhat unusual: after each cycle, an almost coherent layer of scaled-off material could be lifted off. (Using a spatula, it would have been possible to lift this layer off in one single piece.) ”Coherent” does not mean the layer came off as a solid thin disc. It appeared cracked and destroyed but was still coherent and thus it deviated significantly from normal scaling, which appears as finely divided gravel.

The thickness of this coherent layer was approximately 0.5 mm. The occurrence of such a layer indicates that ice lens growth (if this is what causes surface scaling) is concentrated in a rather well-defined zone beneath the surface. Of course, the exact depth must be expected to be dependent on material properties and testing conditions. This kind of coherent layer has not been previously observed in this laboratory and the author is unaware of it having been observed elsewhere either. Usually, scaled-off material is collected only once every 7 days (or even less often) and it may be that the initially coherent layer is broken down during subsequent frost cycles.

Examination of obtained salt concentrations

Because concentrated salt solutions were added to water on top of the specimen surfaces, it was necessary to check the salt concentrations actually obtained. After the first frost cycle, the surface solutions from the 0.45 mortars were collected and analysed with the potentiometric analysis equipment described in chapter 4.3 (where the analysis procedure is also described). The results are set out in table 7.2.2. The last two columns give the measured and expected concentrations in the outer solution. (The detected amount of Chloride ions have been calculated into a corresponding NaCl concentration in order to facilitate comparisons.)

Table 7.2.2: Analysis of salt concentration in salt solutions covering the mortar specimens of w/c ratio 0.45 after first frost cycle.

Specimen	Sample size [g]	Sample + dilution water [g]	Analysis result [mg Cl^-/l]	Calc. corresp. Concentration [g NaCl/l sol.]*	Expected result [g NaCl /l sol.]
ND1A	1.994	101.374	94 95 92	7,8	10
ND1B	2.989	55.518	447 445	13.4	10
ND3A	2.017	48.701	678 698	27.4	30
ND3B	2.005	89.284	375 375	27.5	30
ND7.5A	Not analysed				
ND7.5B	2.093	163.039	628 637(506mg)	80.8	75
D1A	2.991	58.354	264 268	8.6	10
D1A	2.485	184.43	76 66 83	9.2	10
D1B	2.196	57.197	190 189	8.1	10
D3A	2.024	98.428	342 344	27.5	30
D3B	Not analysed				
D7.5A	2.068	193.165	508 501	77.7	75
D7.5B	2.078	193.149	508 510	78.0	75

*not corrected for the dependence of density on NaCl concentration

From table 7.2., it can be seen that the dosage procedure followed here produced acceptable salt concentrations. However, while the concentrations were lower than expected in the solutions with expected concentrations of 1 and 3% (except for one case), it was higher than expected for the solution expected to have a concentration of 7.5% NaCl/l solution. The latter result is explained if it is assumed that some of the de-ionised water had leached out before the concentrated salt solution was added. The former (too low) results however need some other explanation. Assuming the volume of the outer solution did not change after salt was added to it, the results indicate that approximately 0.02 - 0.05 g of chloride ions had been lost from the outer solution to the specimens. (It was not possible to analyse the chloride content of the scaled off flakes, since these were washed off the specimen surfaces with tap water and their chloride content was thereby severely affected.) Although it seems natural that some chloride ions were taken up in the pore system, a closer investigation of the possible errors due to erroneous mixing and dosing was undertaken in order to reveal whether this was the true reason for the measured values.

First, the concentrated solutions which had been used to produce the surface covering solutions were analysed. The results are set out in table 7.2.3.

Table 7.2.3: NaCl concentrations measured in the concentrated solutions.

Solution	Analysis sample [g]	Sample + water [g]	Analysis result [mg Cl^-/l dilute sol.] (2st)	Calc. conc. [g NaCl/l sol.]
”3%”	2.025	85.565	431 , 436	30.2
”9%”	1.579	142.013	607 , 608	90.0
”22.5%”	0.886	165.331	730 , 729	224.3

It can be seen that none of the concentrated solutions was erroneous enough to explain the unexpected concentrations measured in the surface covering solutions. Therefore, the precision and repeatability of the dosages was checked by weighing samples taken with the injection syringe. The results are set out in table 7.2.4.

Table 7.2.4: Result from test of the reliability of the dosage syringe

Intended volume	Weights [g] Sample: No 1	No 2	No 3	No 4	No 5	No 6
20 ml	19.89	19.87	19.98	20.09	20.00	
13 ml	13.05	12.99	13.06	12.92	12.84	13.13
6 ml	6.16	6.14	6.13	6.10	6.12	

It can be seen that the maximum errors were approximately 0.15 g. Maximum dosage was 20 ml. In order to add 26 ml of de-ionised water, two dosages had to be supplied and thus the maximum error could occur twice. It could also occur once when adding the concentrated solution. The maximum possible error may be estimated by adding the errors in the worst possible case.

The correct concentration (in g NaCl / g solution) is obtained from:

$$C_{dil} = \frac{m_{conc} \cdot C_{conc}}{m_{H_2o} + m_{conc}} \qquad (7.2.1)$$

The ratio E of obtained concentration to intended concentration due to erroneous masses of added solutions is obtained from:

$$E = \frac{(m_{conc} - e) \cdot C_{conc}}{(m_{H_2o} + 2e) + (m_{conc} - e)} \Big/ \frac{m_{conc} \cdot C_{conc}}{m_{H_2o} + m_{conc}} \qquad (7.2.2)$$

in which e is the maximum error of a single dosage and in which the signs inside brackets have been chosen so as to produce maximum errors. Assuming e = 0.15g, we get:

$$E = \frac{(13 - 0.15)}{(26 + 2 \cdot 0.15) + (13 - 0.15)} \Big/ \frac{13}{26 + 13} = 0.985 \qquad (7.2.3)$$

The maximum final error is thus some 1.5%. From the concentrations of the concentrated solutions given in table 7.2.3, we might therefore expect the dilute solutions to have concentrations within the following intervals:

Dilute solution 1%: $9.85 < C < 10.16$ g/l
Dilute solution 3%: $29.55 < C < 30.5$ g/l
Dilute solution 7.5%: $73.65 < C < 75.89$ g/l

This error analysis shows that the concentrations measured in the solutions covering the specimens after the first temperature cycle cannot be explained solely by dosage errors. The conclusion is that something occurred during the temperature cycle that changed the concentrations. A first reason for this is that diffusion is not completely stopped despite the low temperatures. Another possible reason is that chloride ions are transported by convection into the pore solution if moisture is taken up from the outer solution. During thawing, it may be that not all of these chloride ions are transported out again. This would be partly due to the fact that not all the moisture taken up is expelled from the specimen during thawing (which would act to keep the outer concentration constant), and partly because some chloride ions are physically or chemically bound to the pore walls.

7.2.5 Results and discussion, Series 2

The experiments reported above deviate from normal standard tests in that a salt content in the pore solution was avoided as far as possible. Under these circumstances, the scaling turned out to be independent of outer salt concentration. This is in line with what was predicted from the hypothesis. However, this experimental result might just as well be due to some other factor. Therefore, a traditional test, in which the salt solution is left on the specimen surface during the period of temperature >0°C, should have been run in order to test that these materials in fact are most severely damaged when exposed to a 3% solution in such a test. Because the tests reported in chapter 5.1 had shown that the ”pessimum” 3% existed for material produced in the same way, in the same laboratory, with the same cement, and with a similar air content, it was judged safe enough to assume that a ”pessimum” would have been found for the present materials too. Therefore, it was determined to use the remaining specimens for a test designed in yet another way.

According to the hypothesis, scaling will be reduced if the pore solution contains a deicing agent. This is because both the number of growing ice bodies and the driving force for their growth are reduced when the solution surrounding the ice bodies contains some solute. Therefore, this time, the specimens were let stand with the salt solution on their exposed surface for one week before being frozen through one cycle. Then, the scaled off material was collected, new salt solution was poured on and the specimens were let stand for another week and then frozen again. In this way, it was ensured that salts did penetrate into the pore solution. No dried and re-moistened specimens were used.

Results

The mortar quality of *w/c* ratio 0.50 was this time not run as a pre-series test and is therefore fully comparable with the other results.

Due to leakage of the outer salt solution, the experiments had to be stopped after some 4-5 frost cycles.

The accumulated scaling is shown in figures 7.2.12- 7.2.14. The specimen L6575A (L denotes Long salt solution exposure) was tested for only two cycles as leakage made further testing meaningless. The same goes for specimen L503A, which was tested in only 3 cycles.

Discussion

Since the tests had to be stopped after only a few cycles, a direct comparison with the results reported above cannot be done. However, in figures 7.2.3 - 7.2.8 it can be seen that scaling is proportional to the number of frost cycles (for never-dried specimens). Assuming the present results are also proportional to the number of frost cycles, we may extrapolate them by the ratio of cycles run in the Series 1 tests to the number of cycles run in these tests. Thus, for *w/c* ratio 0.45, we obtain a factor of 10/4 = 2.5. On multiplying the results in figure 7.2.12 by 2.5 and comparing to figure 7.2.9, it is clear that the present tests did cause much less severe scaling.

For *w/c* ratio 0.50 the extrapolation factor is 7/4 and for *w/c* ratio 0.65 it is 9/4. Although the 0.50 quality was run with somewhat different salt concentrations in the first test, it is clear that the scaling obtained in this second test is clearly smaller. This is also true for the 0.65. (In fact there is a tendency towards maximum scaling for an outer salt concentration of 3% for the 0.65 mortar. However, due to the few specimens and the very few frost cycles run, this trend should not be dwelt upon.)

Of course, this extrapolation may be misleading, if, as was shown for some specimens in the first series, scaling is slow initially and then accelerates. However, even if the results in figures 7.2.12-7.2.14 are doubled and then extrapolated, the scaling obtained in Series 1 is still clearly larger.

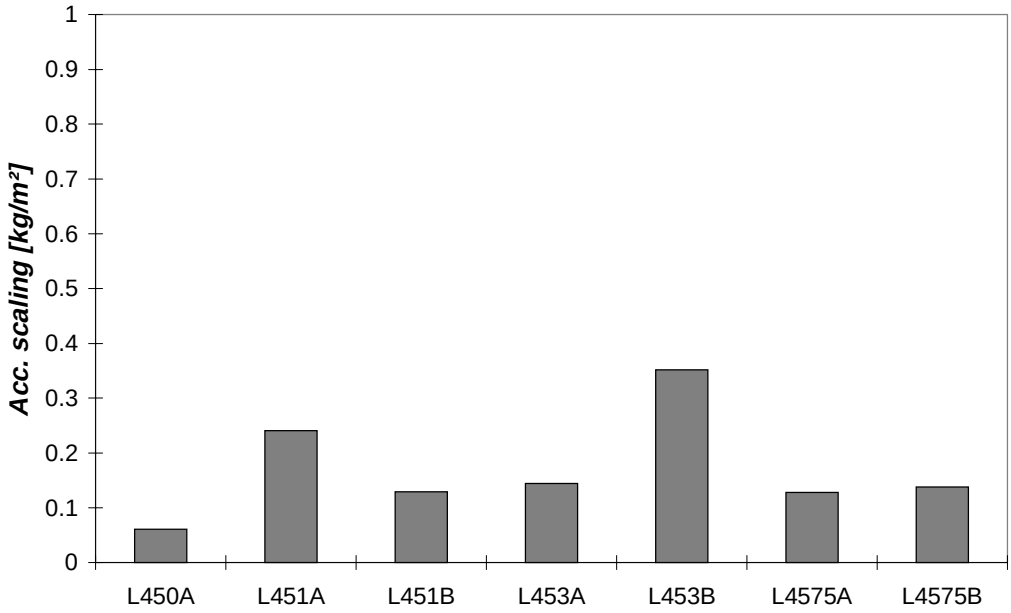

Figure 7.2.12: Mortar of w/c ratio 0.45. Accumulated scaling after 4 cycles. One week exposure to salt solution prior to freezing. Some specimens had to be stopped due to leakage.

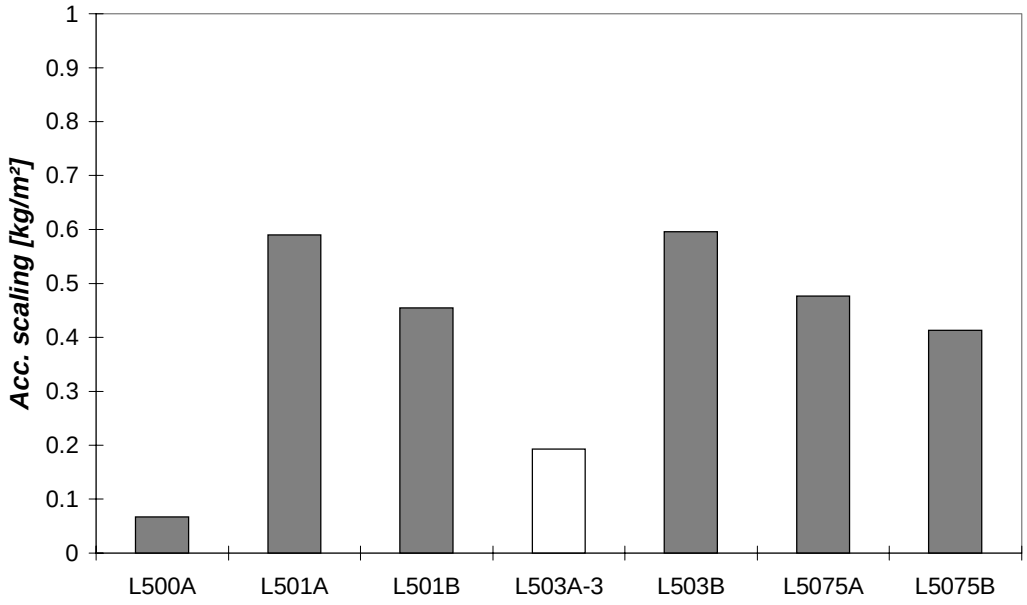

Figure 7.2.13: Mortar of w/c ratio 0.50. Accumulated scaling after 4 cycles. One week exposure to salt solution prior to freezing. Specimen L503A had to be discontinued after 3 frost cycles.

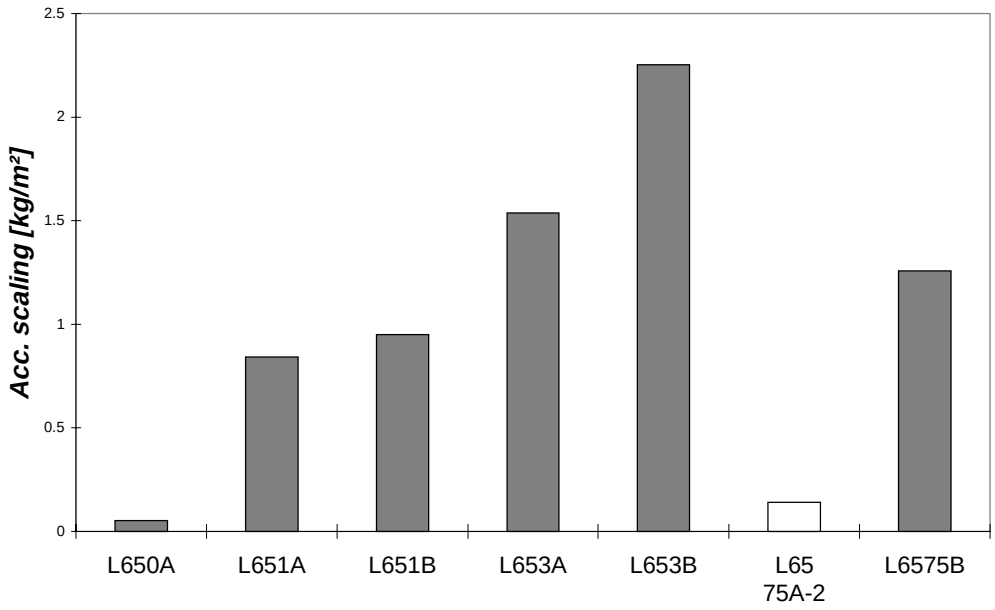

Figure 7.2.14: Mortar of w/c ratio 0.65. Accumulated scaling after 4 cycles. One week exposure to salt solution prior to freezing. Due to leakage, specimen L6575A had to be discontinued after 2 cycles.

7.2.6 Conclusions

It was expected that in a normal salt frost scaling test the materials used in the first part of these experiments would be most severely damaged by an intermediately concentrated solution. This was expected since the material composition (*w/c* ratio and air content) was normal and was such that freezing in tap water did not cause any surface scaling. The results, which showed that scaling was independent of outer salt concentration when the tests were run in such a way that penetration of salt into the pore solution was reduced as far as possible, are as predicted by the hypothesis.

The results from the second part of the experiments, in which the time for salt penetration was greatly prolonged as compared to ordinary tests, were also in line with what had been predicted by the hypothesis. These results, however, were obtained after only 4 freezings.

In Series 1, no scaling was observed on never-dried specimens during the first freezing. This was not predicted by the hypothesis and may be seen as evidence that some accumulative effect, for instance accumulation of salt in the uppermost part of the specimen, is required for scaling to start. However, since scaling was seen to start, without exception, during the second cycle for all never-dried specimens, it may well be that scaling is dependent on a first freezing to change the micro structure so that its permeability and the amount of freezable water increase.

If this explanation is accepted, then the conclusion is that none of the results herein contradict the hypothesis.

The fact that severe scaling did occur despite the very much reduced amount of chloride ions in the pore solution also shows that previously proposed hypotheses which require the presence of salt within the pores are not valid.

8 CONCLUSIONS, SUGGESTIONS FOR FUTURE RESEARCH AND DISCUSSION OF TEST METHODS

8.1 Conclusions

A mechanism for salt frost scaling on porous, brittle materials has been proposed. An undeniable consequence of the proposed mechanism is moisture uptake during freezing. From the mechanism, qualitative predictions were made concerning the effect of various parameters on this moisture uptake. The effect on final scaling is difficult to predict, since scaling may occur several times during a single frost cycle, each scaling affecting the conditions for any subsequent scaling. Still, results from scaling experiments reported in the literature seem to accord with what might be predicted from the proposed mechanism. Furthermore, results from laboratory tests carried out as part of this research do not contradict the hypothesis. In light of these findings, it seems reasonable to conclude that the described mechanism is the major mechanism causing salt frost scaling.

8.2 Suggestions for future research

Since many of the parameters involved in the described process affect each other and since the scaling process cannot be followed during actual freezing, direct evaluation of the described hypothesis through salt frost scaling experiments is difficult to do in such a way that the results undoubtedly reflect the effect of the studied parameter. Therefore, a numerical model should be designed, so that the processes can be followed and the importance of each parameter can be separately studied.

As regards laboratory work, the first thing to do would be to repeat, under better control, the experiments described in this report. Another conceivable experiment would be to fill the specimen pores with a liquid which contracts on solidification and then apply the same liquid, with an added freezing point depressing substance, to the specimen surface. The initial content of liquid in the pore system should be low enough as not to cause deterioration by itself. If scaling still occurs, it should be due to uptake of the outer solution. Of course, the test may be improved by measuring weight changes. (One requirement for the liquid, however, is that it wets the pore walls.)

Another experiment would be similar to traditional soil heaving experiments. By cooling the specimen from one side, applying the salt solution (or pure water) to the other side and then measuring temperature fields and the positions of (eventual) cracks, much information may be obtained regarding the transport of moisture within the specimen at sub-freezing temperatures.

There are other, seemingly interesting experiments which upon closer inspection, however, cannot be used. For example, it might be thought appropriate to study salt frost scaling on materials of single-sized pores. Assuming permeability would be zero in this kind of material once the pore water had frozen, the described mechanism would not be functional and no moisture uptake would occur. However, even in the ideal case where all water freezes at a single temperature, the liquid-like layer described in chapter 2.3 will make water transport possible and thus moisture will be taken up.

8.3 Test methods

The most important characteristic property of a test method is that it classifies different materials in the same way that exposure in the field would do. The test method must absolutely not allow concretes of inferior quality to be used, but at the same time must not be too restrictive.

A first way of improving test methods is to clarify the true climatic conditions which may be expected in different types of use. For example, results published by Petersson [P 1995] reveal that concrete structures in marine environments, exposed only to salts naturally occurring in sea water, are much less severely deteriorated than concrete exposed along highways, where de-icing salts and lower temperatures are common.

Obviously, the micro structure of concrete plays a central role in salt frost scaling; it affects permeability, amount of ice formed at a given temperature and the rate of penetration of de-icing agents. The second way of improving a test method therefore is to allow for the changes in micro structure which can be expected to develop during the lifetime of the concrete structure. For example, special attention must be paid to those types of concrete which are known to develop a coarser porous micro structure over time.

These two types of improvements are difficult to carry out, especially the one concerning micro structure changes. However, from the described hypothesis, it is also possible to propose some changes to the present standardised test methods. For example, the Swedish SS 13 72 44 has sometimes been criticised for being too restrictive. It may be, however, that this test method is actually too mild.

Compared to what frequently occurs in nature, the temperature cycle used in SS 13 72 44 applies a low minimum temperature for a short time. This might, according to the described mechanism, represent too mild an exposure: a low minimum temperature means a large portion of the pore system will be clogged with ice. This will reduce permeability and thus to some extent hinder micro ice body growth. Furthermore, in cold regions, the temperature of a concrete structure may remain at sub-freezing levels for much longer periods of time than the 16 hours prescribed in SS 13 72 44. This means that, in reality, there will be much more time for micro ice bodies to grow and to exert pressure.

Furthermore, as in most standard test methods, salt solution is applied to the specimen surface throughout the entire test. While this seems to be relevant for concrete exposed in a marine environment, it is doubtful whether this is a realistic simulation of conditions along a highway. Since the continuous presence of the de-icer solution may lower the freezing point of the pore solution, micro ice body growth may be reduced. In reality, however, salt is applied mainly during periods of sub-freezing temperatures and its concentration may vary from zero up to saturated solution. According to the described hypothesis, the period of above-freezing temperatures acts mainly to reduce moisture uptake and micro ice body growth.

From these considerations, it seems reasonable to test concrete intended for highways with a frost cycle which does not allow the pore solution to melt completely and which reaches a minimum temperature which is chosen on the basis of available recorded climatic data for the actual construction site. The concrete might be frozen with tap water on its surface and the salt added when freezing has begun in the pore solution. For example, the frost cycle may oscillate between -3°C and -13°C, using 12 hours for freezing and 12 hours for melting. In this way, the possibility that the de-icer will act to inhibit the severity of the salt frost attack is significantly reduced. Therefore, the number of frost cycles should be chosen from recorded climatic data. Finally, it is important that cooling acts over the surface to which the de-icer solution is applied, as otherwise the favoured depth of ice body growth will be displaced, possibly to too great a depth.

GENERAL APPENDIX 1:
STANDARD TEST METHODS

The following is a short review of the standard test methods SS 13 72 44, CDF and ASTM C672. Only the major principles are described. The reader is referred to the original references for complete descriptions.

SS 13 72 44, 3rd edition, Procedure A

Source: Standardiseringskomissionen i Sverige, Stockholm

Two procedures are described in this standard. In procedure A the specimen is exposed to a 3% NaCl solution during freezing. In procedure B, this solution is replaced by pure water. These procedures are divided into different sub-procedures. Only procedure A1, which is intended for pre-testing of concrete (*i.e.* before the concrete is used in a construction) is described here.

Concrete cubes, 150*150*150 mm^3 shall be cast according to SS 13 72 45. In short, the cubes are cast and then stored at 20±2°C for 24±2 hours. A plastic foil is applied to prevent evaporation of water from the cast concrete. On the day after casting, the cubes are demoulded and stored in a water bath at 20±2°C. At an age of 7 days, the cubes are stored in a climate chamber at 20±2°C and 60±20% R.H. At an age of 21±2 days, a 50 mm thick slice is cut out of each cube so that one cut surface is obtained from the center of the cube. It is recommended that at least 4 such specimens are used.

After cutting, the 50mm slices are stored for 7 days at 20±2°C and 65±5% R.H. in the climate chamber (the climate in the climate chamber shall be such that the rate of evaporation from a free water surface is 45±15 g/m²/hour). During this time, a 3 mm rubber sheet is glued on to all specimen surfaces except the test surface, figure A1-1.

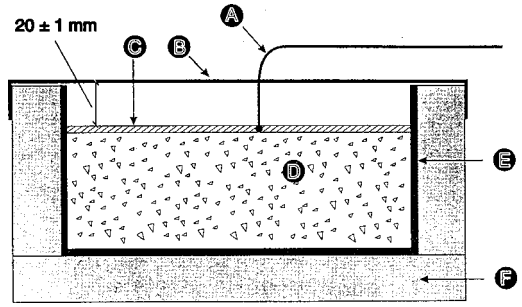

A: Thermoelement
B: Evaporation protection
C: Salt solution
D: Specimen
E: Rubber sheet
F: Heat insulation

Figure A1-1: Specimen prepared for testing according to SS 13 72 44.

After the 7 day storage in the climate chamber, tap water (at +20±2°C) is poured onto the test surface to a depth of 3 mm. Testing begins 27±2 hours later.

Before testing, the specimen is heat insulated with 20± mm polystyrerene, figure A1-1. The tap water is removed and salt solution (to a depth of 3 mm) is applied to the test surface no more than 15 minutes before the specimens are placed in the freezing chamber. A tight plastic foil lid is applied as a protection against evaporation. Hereafter, the specimens are repeatedly

frozen and thawed. The temperature in the salt solution shall fall within the shaded area in figure A1-2. The time of T>0°C shall be 7-9 hours.

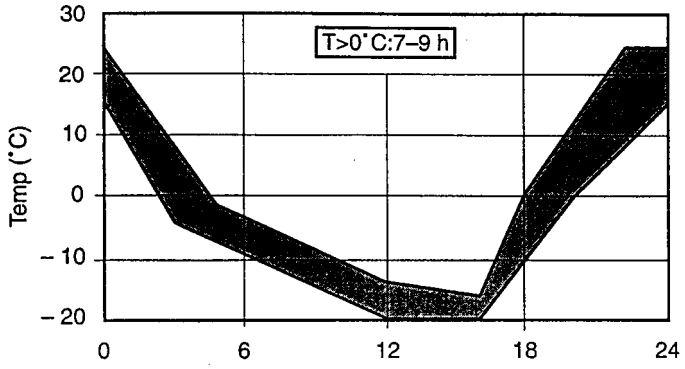

Figure A1-2: 24 hour temperature cycle for SS 13 72 44. Temperature of salt solution shall fall within shaded area.

Scaled off material is collected and dried after 7, 14, 28, 42 and 56 frost cycles. On each occasion, new salt solution is applied to the test surface.

The following acceptance criteria are recommended:

SFS resistance	Demands
Very high	The accumulated scaling after 56 cycles must not exceed 0.1 kg/m² for any of the tested specimens.
High	The average accumulated scaling after 56 cycles must not exceed 0.5 kg/m² and $m_{56}/m_{28}<2$.
Acceptable	The average accumulated scaling after 56 cycles must not exceed 1.0 kg/m² and $m_{56}/m_{28}<2$.
Non acceptable	(any other case)

m_{56} = average accumulated scaling after 56 cycles, [kg/m²]

CDF - (Capillary suction of Deicing solution and Freeze thaw test)

Source: Materials and Structures, 1995, **28**, pp 175-182

The method prescribes different specimens for different types of test (pre-testing, testing of concrete structure surface, testing precast concrete elements). Here, only the test method for pre-testing of concrete is considered.

The concrete to be tested is cast in 150 mm cubes. A teflon disc is mounted vertically in the center of the cubes. The surface to be tested is that facing the teflon disc. After 24±2 h of curing the specimens are demoulded and stored for 6 days (until the age of 7 days) in tap water at 20±2°C. If strength development of the specimens is low the curing in the mould can be increased. The storage in tap water is then decreased by the same amount.) At least 5 specimens, with a total area of 0.08m² is recommended.

The test consists of three steps: the dry storage, the presaturation by capillary suction and the freeze-thaw cycles.

The concrete specimens are stored in the climate chamber (20°C, 65 R.H.) for surface drying for 21 days. In the climate chamber the evaporation from a free water surface shall be 45±15 g/m²/hour.

Between 7 and 2 days before presaturation, the specimens are sealed on their lateral surfaces.

The specimens are placed on spacers in a special container and test liquid is filled into the container as shown in figure A1-3. This period of capillary suction shall be 7 days and the temperature shall be 20±2°C.

After this presaturation, the container is moved to a freezer, figures A1-3 and A1-5. A temperature cycle as shown in figure A1-6 is applied. The temperature must not deviate from the prescribed temperature curve by more than 0.5°C at the minimum temperature and by no more than ±1°C at any other time.

Surface scaling is measured while temperature is above 15°C. An ultrasonic bath is used for removing any loosely adhering material at the specimen surface. The scaled off material is dried at 110±5°C for 24 h, cooled at 20±2°C/60±5%R.H. for 1 hour and then weighed.

28 temperature cycles are run. The acceptance criterion is recommended to be 1500 g/m².

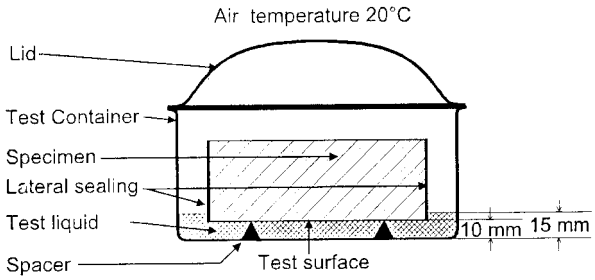

Figure A1-3: Setup for capillary suction of test liquid.

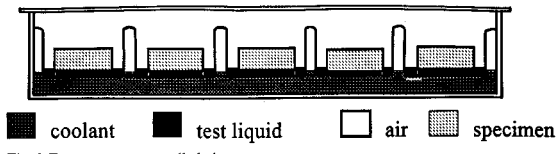

Figure A1-3: 5 specimens placed in the freezer.

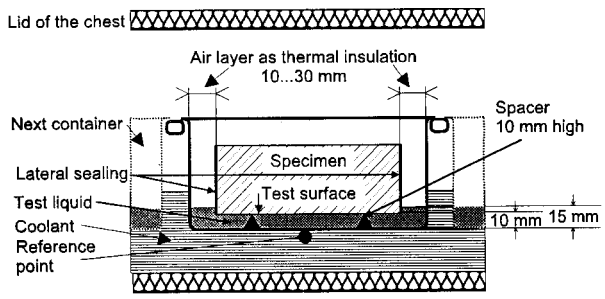

Figure A1-3: Setup for freeze-thaw testing.

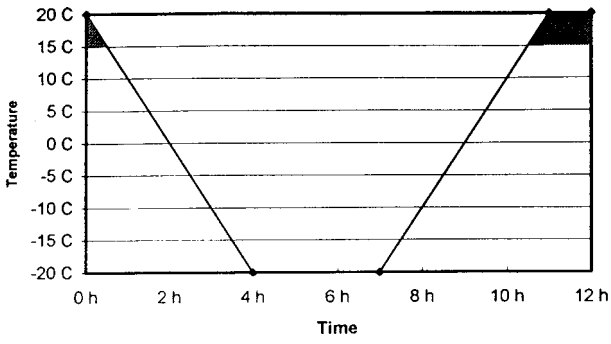

Figure A1-3: Temperature cycle for the CDF method.

ASTM C672-92: Standard Test Method for Scaling Resistance of Concrete Surfaces Exposed to Deicing Chemicals

Source: 1996 Annual Book of ASTM Standards, Volume 04.02: Concrete and Aggregates, ASTM, PA, USA:

Specimens shall have a surface of at least 0.046 m^2 and be at least 75 mm in depth. At least two specimens shall be used. Specimens shall be mixed according to ASTM C192. After the surface is finished, a dike is placed along the perimeter of the top surface of the specimen. The specimens are covered with a polyethylene sheet immediately after finishing. Specimens are demoulded after 20-24 hours and placed in a climate chamber at 23±1.7°C and R.H.≥95% (according to ASTM C511). At the age of 14 days, the specimens are stored in air for 14 days at 23±1.7°C and 45-55% R.H.

After pre-storage, a solution of calcium chloride is applied to a depth of 6 mm to the specimen surface. The concentration of the solution shall be such that 100 ml of solution contains 4 g of anhydrous calcium chloride.

The specimens are placed in a freezing environment for 16-18 hours. The temperature chamber shall be capable of cooling the specimens to -17.8±2.8°C within 16-18 hours. Hereafter, the specimens are placed in laboratory air at 23±1.7°C and at a relative humidity of 45 to 55% for 6 to 8 hours. Water shall be added between freezing cycles to maintain depth of solution. At the end of every 5 cycles, the specimen surface is flushed off thoroughly and a visual inspection is made. New solution is applied and the test is continued. It is recommended that at least 50 frost cycles be undertaken.

The final report is based on the visual rating. The condition of the specimen surfcae is rated according to the following scale:
0 No scaling
1 Very slight scaling (max. 3.2 mm depth, no coarse aggregate visible)
2 Slight to moderate scaling
3 Moderate scaling (some coarse aggregate visible)
4 Moderate to severe scaling
5 Severe scaling (coarse aggregate visible over entire surface)

GENERAL APPENDIX 2:

ANLÄGGNINGSCEMENT

Source: Cementa AB, Sweden (producer)
Average results from analyses during 1997

Chemical analysis, average values

CaO	65.5	%
SiO_2	22.7	%
Al_2O_3	3.56	%
Fe_2O_3	4.32	%
K_2O	0.57	%
Na_2O	0.05	%
MgO	0.45	%
SO_3	2.07	%
Cl	0.02	%
Ignition loss	0.45	%
Rest:	0.04	%
CO_2	-	
Chrome reduction	27	mg/kg

Clinker components (Bogue)

C_3S	55.7	%
C_2S	22.8	%
C_3A	2.1	%
C_4AF	13.1	%

Grain size distribution

125 µm	99.9	%
63	97.8	%
32	74.7	%
15	47.1	%
8	31.9	%
4	20.9	%
2	13.0	%
1	5.9	%

Density	3209	kg/m^3
Specific surface	304	m^2/kg

References

A 1943 Arnfelt, H: ”Damage on Concrete Pavements by Wintertime Salt Treatment” Meddelande 66, Statens Väginstitut, Stockholm 1943 (In Swedish)

A 1967 Anderson, D. M: ”The Interface Between Ice and Silicate Surfaces”, J. Colloid and Interface Science 25, pp 174-191, 1967

A 1972 Ahlgren, L: ”Moisture Fixation in Porous Building Materials”, Report 36, Division of Building Technology, The Lund Institute of Technology, Lund, Sweden, 1972

A 1990 Atkins, P.W: ”Physical Chemistry, 4th ed.”, Oxford University Press

An 1990 Adamson, A.W: ”Physical Chemistry of Surfaces, 5th ed.”, John Wiley&Sons, 1990

B 1974 Beaudoin, J.J, MacInnis, C: ”The mechanism of Frost Damage in Hardened Cement Paste”, Cement and Concrete Research, vol 4, pp. 139-147, 1974

B 1975 Browne, F. P, Cady, P.D: ”Deicer Scaling Mechanisms in Concrete”, in ”*Durability of Concrete”* ACI SP 47, 1975, pp 101-119

B 1976 Braun, C.V Jr, Drost-Hansen, W: ”A DSC Study of the Heat Capacity of Vicinal Water in Porous Materials”, Colloid and Interface Science, Vol. 3, M. Kerker Ed., Academic Press, New York 1976

B 1977 Brun, M, Lallemand, A, Quinson, J-F, Eyraud, C: ”A New Mthod for the Simultaneous Determination of the Size and the Shape of Pores: The Thermoporometry”, Themochimica Acta, 21, pp 59-88, 1977

B 1979 Björkman, B, Fredriksson, T: ”Effect of w/c Ratio, Air Content, Curing Technique and Age on the Resistance of Concrete to Salt Frost Attack”, TRITA-BYMA-1979:8 E, Royal Institute of Technology, Stockholm, 1979 (in Swedish)

B 1980 Bager, D.H, Sellevold, E.J: ”Ice formation in Hardened Cement Paste–II. Steam-Cured Pastes with Variable Moisture Content”, Durability of Building Materials and Components, ASTM STP 691, P.J Sereda and G.G. Litvan, Eds., American Society for Testing and Materials, 1980, pp 439-454.

B 1982 ”Betonghandboken, Material”, Eds. G. Möller, N. Petersons, P. Samuelsson, Svensk Byggtjänst, 1982 (in Swedish)

B 1987 Binda, L, Baronio, G: ”Mechanism of Masonry Decay Due to Salt Crystallization”, Durability of Building Materials, 4, pp 227-2240, 1987

B 1988 Beddoe, R.E, Setzer, M.J: ”A Low Temperature DSC Investigation of Hardened Cement Paste Subjected to Chloride Action”, Cement and Concrete Research. Vol 18, pp.249-256. 1988

B1 1986 Bager, D.H, Sellevold, E.J: ”Ice formation in Hardened Cement Paste, Part 1 – Room Temperature Cured Pastes with Variable Moisture Content”, Cem. Con. Res. Vol. 16, pp 709-720, 1986.

B2 1986 Bager, D.H, Sellevold, E.J: ”Ice formation in Hardened Cement Paste, Part 2 – Drying and Resaturation on room temperature cured pastes”, Cem. Con. Res. Vol. 16, pp 835-844, 1986.

C 1944 Collins, A.R: ”The Destruction of Concrete by Frost”, J. Inst. Civ. Eng, 23, 1944

C 1945 Collins, A.R: ”Discussion of a paper by T.C. Powers: A Working Hypothesis for Further Studies of Frost Resistance of Concrete”, Journal of the American Concrete Institute, Supplement, November 1945

C 1956 Copeland, L.E: ”Specific Volume of Evaporable Water in Hardened Portland Cement Pastes”, Proc. Am. Conc. Inst. 52, pp 863-874, 1956, research and Develop. Lab. Portland Cement Assoc. Bull. No. 75

C 1960 Copeland, L.E, Kantro, D.L, Verbeck, G: ”Chemistry of Hydration of Portland Cement”, 4th International Symposium on the Chemistry of Cement, Washington D.C, 1960, paper IV-3.

C 1963 Cordon, W.A, Merrill, D: ”Requirements fro Freezing and Thawing Durability for Concrete”, Proc. ASTM, V. 63, 1963 (pp 1026-1036)

C 1969 Cady, P. D:”Mechanisms of Frost Action in Concrete Aggregates”, Journal of Materials, vol 4, no 2, June 1969

C 1995 Carlsson, T: ”Effects of the air void system on the properties of plaster and mortar”, Lund Institute of Technology, Div. of Building Materials, Report TVBM-3066, 1995 (In Swedish)

D 1966 Defay, R, Prigogine, I, Bellemans, A: ”Surface Tension and Adsorption”, Trans. By Everett, D.H, Longmans, Green&Co Ltd, 1966

D-H 1967 Drost-Hansen, W: ”The Water-Ice Interface as seen from the Liquid Side”, J. Colloid and Interface Science 25, pp 131-160, 1967

E 1961 Everett, D.H: ”The Thermodynamics of Frost Damage to Porous Solids”, Trans. Faraday Soc, 57, 1961.

E 1990 Etzler, F.M, Conners, J.J: ”Temperature Dependence of the Heat Capacity of Water in Small Pores”, Langmuir, vol 6, No. 7, 1990, pp 1250-1253

E 1991 Etzler, F.M, Conners, J.J: ”Structural Transitions in Vicinal Water: Pore Size and Temperature Dependence of the Heat Capacity of Water in Small Pores”, Langmuir, vol 7, No. 10, 1991, pp 2293-2297

F 1970 Fletcher, N.H: ”The Chemical Physics of Ice”, Cambridge University Press, 1970

F 1972 Fagerlund, G: ”Critical Degrees of Saturation at Freezing of Porous and Brittle Materials”, The Lund Institute of Technology, Division of Building Technology, Report 42, 1972

F 1973 Fagerlund, G: ”Methods of Characterization of Pore Structure”, Lund Institute of Technology, Division of Building Materials, Report 41, 1973

F 1973b Fagerlund, G: ”Non-Freezable Water Contents of Porous Building Materials”, Lund Institute of Technology, Division of Building Materials, Report 42, 1974

F 1977 Fagerlund, G: ”The Critical Degree of Saturation Method of Assessing the Freeze/Thaw Resistance of Concrete”, Swedish Cement and Concrete Research Institute at the Institute of Technology, Stockholm, Report 6:77, 1977

F 1982 Fagerlund, G: ”The Influence of Slag Cement on the Frost Resistance of the Hardened Concrete”, Swedish Cement and Concrete Institute, Report 1:82, Stockholm 1982

F 1986 Fagerlund, G: ”The Critical Size in Connection with Freezing of Porous Materials”, CM Rapport T 86039, Cementa AB, Sweden, 1986

F 1988 Foy, C, Pigeon, M, Banthia, N: ”Freeze-Thaw Durability and Deicer Salt Scaling Resistance of a 0.25 Water-Cement Ratio Concrete”, Cement and Concrete Research, vol. 18, 1988, pp. 604-614

F 1990 Fagerlund, G: ”Air-Pore Instability and Its Effect on the Concrete Properties”, Nordic Concrete Research, Nr 9, Oslo, 1990

F 1991 Fagerlund, G: ”Studies of the Scaling, the Water Uptake and the Dilation of Mortar Specimens Exposed to Freezing and Thawing in NaCl Solutions”, in ”*Freeze-Thaw and De-Icing Resistance of Concrete*”, RILEM Committee TC-117 FDC meeting in Lund, June, 1991, Lund Institute of Technology, Div. Building Materials, report TVBM-3048, pp 36-66

F 1993 Fagerlund, G: ”The Critical Spacing Factor”, Lund Institute of Technology, Div. Building Materials, report TVBM-7058, 1993

F 1993b Fagerlund, G: ”The Long Time Water Absorption in the Air-Pore Structure of Concrete” , Lund Institute of Technology, Div. Building Materials, report TVBM-3051, 1993

F 1994 Fagerlund, G: ”Predicting the Service Life of Concrete Exposed to Frost Action through a Modelling of the Water Absorption Process in the Air-Pore System”, Lund Institute of Technology, Div. Building Materials, report TVBM-7085, 1994

F 1996 Fagerlund, G: ”The Required Air Content in Concrete”, Contribution to the workshop on ”Mass-Energy transfer and Deterioration of Building Components”, Paris, January 1995

G 1977 Greenspan, L: ”Humidity Fixed Points of Binary Saturated Aqueous Solutions”, Journal of Research of the Bureau of Standards, vol. 81A, No. 1, 1977

G 1996 of Geiker, M, Thaulow, N: ”Ingress of Moisture due to Freeze/Thaw Exposure”, in ”Frost Resistance Building Materials”, Ed. S. Lindmark, Report TVBM-3072, Lund Institute of Technology, Div. Building Materials, 1996

H 1960 Helmuth, R.A: ”Capillary Size Restrictions on Ice Formation in Hardened Portland Cement Pastes”, 4th International Symposium on the Chemistry of Cement, Washington D.C., 1960.

H 1961 Helmuth, R.A: ”Dimensional Changes of Hardened Portland Cement Pastes Caused by Temperature Changes” Highway Research Board, Proc. 60, 1961

H 1963 Hansen: ”Crystal Growth as a Source of Expansion in Portland-cement Concrete”, ASTM Proc. Vol 63, 1963.

H 1964 Haynes, J. M: ”Frost Action as a Capillary Effect”, Brit. Cer. Soc. Trans. Vol 83, No 11, Nov 1964.

H 1967 Hoekstra, P, Miller, R.D: ”On the Mobility of Water Molecules in the Transition Layer Between Ice and a Solid Surface”, J. Colloid and Interface Science 25, pp 166-173, 1967

H 1968 Haynes, J.M: ”Thermodynamics of Freezing in Porous Solids”, in ”Low Temperature Biology of Foodstuffs”, Eds. J. Hawthorn and E.J. Rolfe, Pergamon Press, London, 1968

H 1974 Hobbs, P. V: ”Ice Physics”, Oxford University Press, 1974

H 1980 Harnik, A.B, Meier, U, Rösli, A: ”Combined Influence of Freezing and Deicing Salt on Concrete – Physical Aspects” Durability of Building Materials and Components, ASTM STP 691, P.J. Sereda and G.G. Litvan, Eds. American Society for Testing and Materials, pp. 474-484, 1980.

H 1990 Handbook of Chemistry and Physics, 70th Ed. CRC Press, Florida, 1989-1990.

H 1991 Hallet, B, Walder, J.S, Stubbs, C.W: ”Weathering by Segregation Ice Growth in Microcracks at Sustained Subzero Temperatures: Verification from an Experimental Study Using Acoustic Emissions”, Permafrost and Periglacial Processes, Vol 2: 283-300, 1991

H 1993 Hedenblad, G: ”Moisture Permeability of Mature Concrete, Cement Mortar and Cement Paste”, Lund Institute of Technology, Div. of Building Materials, Report TVBM-1014, 1993

H 1994 Hedenblad, G, Janz, M: Effect of Alkali on the Measured Relative Humidity in Concrete. *Report TVBM-3057*, Lund Institute of Technology, Div. of Building Materials, 1994.

H 1996 Hedenblad, G: ”Materialdata för fukttransportberäkningar”, T19:1996, Byggforskningsrådet, Stockholm (Materialdata for calculations on moisture transport, in Swedish)

H2 1960 Helmuth, R.A: Discussion on a paper by Nerenst, 4th International Symposium on the Chemistry of Cement, Washington D.C., 1960, pp 829-833.

Ht 1964 Hesstvedt, E: ”The Interfacial Energy Ice/Water”, Norges Geotekniska Institutt, Publikasjon nr. 56, Oslo, 1964

I 1970 Ivey, D. L, Torrans, P.H: ”Air void Systems in Ready-Mixed Cocncrete” J. Materials 5 1970:2

J 1993 Janssen, D.J, Snyder, M.B: ”Mass loss experience with ASTM C666: With and Without Deicing Salt”, in International Workshop on the Resistance of Concrete to Scaling due to Freezing in the Presence of Deicing Salts, Centre de Recherche Interuniversitaire sur le Beton, Université de Sherbrooke - Université Laval, Quebec, August 1993, pp 137-151

J 1995 Jacobsen, S: ”Scaling and Crackingin Unsealed Freeze/Thaw Testing of Portland Cement and Silica Fume Concretes”, Thesis, Report 1995:101, Norwegian Institute of Technology, Trondheim, 1995

K 1981 Kobayashi, M, Nakakuro, E, Kodama, K, Negami, S: ”Frost Resistance of Super plasticised Concrete”, ACI SP 68, pp 269-282, 1981

K 1986 Kropp, J: ”Struktur und Eigenschaften Karbonatisierter Betonrandzonen”, Bautenschutz-Bausanierung, heft 2, Juni 1986

K 1997 Kaufmann, J, Studer, W: ”Length Changes of Concrete Specimen During Frost Deicing Salt Resistance Test”, in *Frost Resistance of Concrete*, Setzer, M.J, Auberg, R, Eds, E&FN Spon, London, 1997

L 1972 Litvan, G.G: ”Phase Transition of Adsorbates: IV, mechanism of Frost Action in Hardened Cement Paste”, J. American Ceramic Society, Vol. 55, No.1, 1972

L 1973 Litvan, G.G: ”Frost Action in Cement Paste”, Materials and Structures, No. 34, July-August 1973.

L 1974 Litvan, G.G: ”Frost Action in Cement in the Presence of De-Icers”, VI International Congress on the Chemistry of Cement, Moscow, Sept. 1974

L 1979 Low, P.F: ”Nature and Properties of Water in Montmorillonite-Water Systems”, Soil Sci. Soc. Am. J. 43:651-658.

L 1980 Litvan, G.G: ”Freeze-thaw durability of porous building materials”, Durability of Building Materials and Components, ASTM STP 691, P.J. Sereda and G.G. Litvan, Eds. American Society for Testing and Materials, 1980, pp. 455-463.

L 1991 Löfgren, M, deSharengrad, P: ”Salt-Frost Durability of air free cement paste”, Lund Institute of Technology, Div. Building Materials, Report TVBM-5021, 1991 (In Swedish)

L 1995 Laidler, K.J, Meiser, J.H: ”Physical Chemistry, 2nd ed.”, Houghton Mifflin Company, Boston

Lk 1991 Lindmark, S: ”Salt frost resistance and air void system characteristics of high performance concrete”, Diploma work, Lund Institute of Technology, Div. of Building Materials, Report TVBM-5020, 1991 (In Swedish)

M 1979 MacInnis, C, Whiting, J.D: ”The Frost Resistance of Concrete Subjected to a Deicing Agent”, Cem. Conc. Res. Vol. 9, pp. 325-336, 1979

M 1980 MacInnis, C, Nathawad, Y.R: ”The Effects of a Deicing Agent on the Absorption and Permeability of Various Concretes” Durability of Building Materials and Components, ASTM STP 691, P.J. Sereda and G.G. Litvan, Eds. American Society for Testing and Materials, 1980, pp. 485-496.

M 1987 Malhotra, M.V, Painter, K.A, Bilodeau, A: ”Mechanical Properties and Freezing and Thawing resistance of High-Strength Concrete Incorporating Silica Fume”, ASTM Cement, Concrete and Aggregates, 1987:2, vol. 9

M 1990 Malmström, K: ”Effect of Type of Cement on the Frost Resistance of Concrete”, Swedish National Testing Institute, Report 1990:07 (In Swedish)

M 1995 Matala, S: ”Effect of carbonation on the pore structure of granulated blast furnace slag concrete”, Helsinki University of Technology, Faculty of Civil Engineering and Surveying, Concerete Technology, Report 6.

Md 1994 Marchand, J, Sellevold, E.J, Pigeon, M: ”The Deicer Salt Scaling Deterioration of Concrete - An Overview”, American Concrete Institute, SP 145-1

Md 1995 Marchand, J, Pleau, R, Gagné, R: ”Deterioration of Concrete Due to Freezing and Thawing” in Materials Science of Concrete IV. Jan Skalny, Sidney Mindess, Eds. 1995.

N 1977 Nilsson, L-O: ”Moisture Problems at Concrete Floors”, Lund Institute of Technology, Div. of Building Materials, Report TVBM-3002, 1977 (In Swedish)

N 1991 Nielsen, C B: ”Salts in Porous Building Materials”, Technical Report 243/91, Building Materials Laboratory, The Techical University of Denmark, 1991

N 1996 Nilsson, L-O, Poulsen, E, Sandberg, P, Sørensen, H.E, Klinghoffer, O: ”HETEK Chloride Penetration into Concrete, State-of-the-Art”, Report No. 53, 1996, The Road Directorate, Copenhagen, Denmark

O 1981 Okada, E, Hisaka, M, Kazama, Y, Hattori, K: ”Freeze-Thaw Resistance of Superplasticized Concretes”, American Concrete Institute, SP 68, 1981, pp. 215-231

P 1945 Powers, T.C: ”A Working Hypothesis for Further Studies of Frost Resistance of Concrete”, Journal of the American Concrete Institute, Vol. 16, No. 4, Feb. 1945

P 1948 Powers, T.C, Brownyard, T.L: ”Studies of the Physical Properties of Hardened Portland Cement Paste”, Research Laboratories of the Portland Cement Association, Bull. 22, 1948.

P 1949 Powers, T.C: ”The Air Requirement of Frost-Resistant Concrete”, Proceedings, Highway Research Board 29, PCA Bull. 33, 1949

P 1953 Powers, T.C, Helmuth, R.A: ”Theory of Volume Changes in Hardened Portland-Cement Paste during Freezing”, Proceedings, Highway Research Board 32, PCA Bull 46, 1953.

P 1954 Powers, T.C, Copeland, L.E, Hayes, J.C, Mann,H.M 1954: ”Permeability of Portland Cement Paste”, Proc.Am. Concrete Inst. 51

P 1959 Powers, T.C, Copeland, L.E, Mann, H.M: ”Capillary Continuity or Discontinuity in Cement Paste”, J. PCA Research and Development Laboratories, vol 1, no. 2, 38-48, May 1959

P 1960 Powers, T.C: ”Physical Properties of Cement Paste”, 4th International Symposium on the Chemistry of Cement, Washington D.C, 1960

P 1963 Pruppacher, H.R: ”Some Relations between the Super Cooling and the Structure of Aqueous Solutions”, Jour. Chem. Phys, Vol 39, No. 6, 1963

P 1965 Powers, T.C: ”The Mechanisms of Frost Action in Concrete”, in Stanton Walker Lecture Series on the Materials Science, Lecture no 3, November 1965

P 1974 Pearson, R.T, Derbyshire, W: ”NMR Studies of Water Adsorbed on a Number of Silica Surfaces”, J. Coll. Interf. Sci. Vol 46, No. 2, Feb. 1974

P 1975 Powers, T.C: ”Freezing Effects in Concrete”, in ”*Durability of Concrete”*, ACI SP-47, 1975, pp 1-11

P 1984 Petersson, P-E: ”Inverkan av Salthaltiga Miljöer på Betongs Frostbeständighet”, Statens Provningsanstalt, Rapport SP-RAPP 1984:34, Sweden, 1984 (In Swedish)

P 1989 Penttala, V.E: ”Effects of Microporosity on the Compression Strength and Freezing Durability of High-Strength Concretes”, Mag. Concrete Research, 41, No. 148, sept. 1989, pp. 171-181

P 1991 Petterson, O: ”The Chemical Effects on Cement Mortar of Solutions of Calcium Magnesium Acetate and oOther Deicing Salts”, TVBM-3045, Division of Building Materials, Lund Institute of Technology, 1991

P 1994 Petersson, P-E: ”Influence of Minimum Temperatures on the Scaling Resistance of Concrete”, Swedish National Testing and Research Institute, SP Report 1994:22, Sweden, 1994

P 1995 Petersson, P-E: ”Scaling Resistance of Concrete - Field Exposure Tests”, Swedish National Testing and Research Institute, SP Report 1995:73, Sweden, 1995, In Swedish, Summary in English

Pn 1994 Pigeon, M: ”Frost Resistance, A Critical Look”, in ACI SP 144-7, 1994

Pü 1996 Pühringer, J: ”Deterioration of Materials by Hydraulic Pressure in Salt Water Systems - An outline Model”, Proc. 8th Intl. Congr. On Deterioration and Conservation of Stone, Berlin, 1996

R 1980 Rösli, A, Harnik, A.B: ”Improving the Durability of Concrete to Freezing and Deicing Salts” Durability of Building Materials and Components, ASTM STP 691, P.J. Sereda and G.G. Litvan, Eds. American Society for Testing and Materials, 1980, pp. 464-473.

R 1985 ”Instructional Modules in Cement Science”, Ed. Roy, D.M, Journal of Materials Education, Materials Education Council, Materials Research laboratory, University Park, Pennsylvania State University, PA 16802, 1985

R 1995 Rilem Committee TC-117: ”Draft Recommendations for Test Methods for the Freeze-Thaw Resistance of Concrete, Slab Test and Cube Test.” Materialds and Structures vol. 28 ,pp 366-371, 1995

S 1960 Scheidegger, A.E: ”The Physics of Flow through porous Media”, University of Toronto Press, 2nd ed., 1960

S 1993 Setzer, M.J: ”On the Abnormal Freezing of Pore Water and Testing on Freeze-Thaw and Deicing Salt Resistance”, in International Workshop on the Resistance of Concrete to Scaling due to Freezing in the Presence of Deicing Salts, Centre de Recherche Interuniversitaire sur le Beton, Université de Sherbrooke - Université Laval, Quebec, August 1993, pp 1-20

Sc 1984 Saucier, K.L: ” High-Strength Concrete for Peacekeeper Facilities”, Misc. Paper SL-84-3, Waterways Experiment Station, Vicksburg, MS, 1984

Sd 1976 Sellevold, E.J, Radjy, F: ”Low Temperature Dynamic Mechanical Response of Porous Vycor Glass as a Function of Moisture Content”, Journal of Materials Science 11, pp 1927-1938, 1976

Sd 1980 Water- le Sage de Fontenay, C, Sellevold, E.J: ”Ice formation in Hardened Cement Paste – 1. Mature Saturated Pastes”, Durability of Building Materials and Components, ASTM STP 691, P.J Sereda and G.G. Litvan, Eds., American Society for Testing and Materials, 1980, pp 425-438.

Sd 1988 Sellevold, E.J: ”Betongens funksjonsdyktighet, Delrapport nr 27”, SINTEF Rapport STF65 A88090, Trondheim, 1988 (In Norwegian)

Sd 1991 Sellevold, E J, Farstad, T: Frost/Salt-testing of concrete: Effect of test parameters and concrete moisture history. *Report TVBM-3048, pp 83-100.* RILEM Committee TC-117 FDC meeting in Lund 1991. Lund Institute of Technology, Div. Of Building Materials, 1991.

Sd 1993 Sellevold, E.J, Jacobsen, S, Bakke, J.A: ”High-Strength Concrete without Air Entrainment: Effect of Rapid Temperature Cycling Above and Below 0°C”, in International Workshop on the Resistance of Concrete to Scaling due to Freezing in the Presence of Deicing Salts, Centre de Recherche Interuniversitaire sur le Beton, Université de Sherbrooke - Université Laval, Quebec, August 1993, pp 153–164

Sk 1994 Stark, J, Ludwig, H-M: ”The Influence of the Water Quality on the Frost Resistance of Concrete”, RILEM TC-117 meeting, Trondheim, Norway, June 1994

Sk 1997 Stark, J, Ludwig, H-M: ”Freeze-Deicing Salt Resistance of Concretes Containing Cement Rich in Slag”, in ”Frost Resistance of Concrete”, Eds. Setzer and Auberg, Proc. International RILEM Workshop, University of Essen, Sept. 1997, pp 123-138

St 1997 Stark, J, Stürmer, S: ”Investigation of Compatibility of Cements with Several Salts”, paper 4iv031, Proc. 10th International Congress on the Chemistry of Cement, Gothenburg, 1997

Sn 1983 Sørensen, E.V: ”Freezing and Thawing Resistance of Condensed Silica Fume (Microsilica) Concrete Exposed to Deicing Chemicals”, American Concrete Institute SP 79, 1983, pp 709-718

Sr 1991 Studer, W: ”Experiences with the Critical Degree of Saturation Method to measure frost Resistance of Concrete”, in ”*Freeze-Thaw and De-Icing Resistance of Concrete*”, RILEM Committee TC-117 FDC meeting in Lund, June, 1991, Lund Institute of Technology, Div. Building Materials, report TVBM-3048, pp 131-135

Sr 1993 Studer, W: ”Internal Comparative Tests on Frost-Deicing-Salt Resistance”, in International Workshop on the Resistance of Concrete to Scaling due to Freezing in the Presence of Deicing Salts, Centre de Recherche Interuniversitaire sur le Beton, Université de Sherbrooke - Université Laval, Quebec, August 1993, pp 175-187

Sr 1994 Studer, W: ”Comparative Temperature Measurements for Different Freeze-Thaw and Deicing-Salt Tests”, Test Report Nr. 4117/3E, EMPA Dübendorf, Switzerland, 1994

Sw 1992 Shaw, D J: ”Introduction to Colloid and Surface Chemistry”, 4th Ed, Butterworth-Heinemann, Oxford, 1992.

Sy 1965 Snyder, M.J: ”Protective Coatings to Prevent Deterioration of Concrete by deicing Chemicals”, National Cooperative Highway research Program Report 16, Highway Research Board of the Division of Engineering and Industrial Reserach, National Academy of Sciences - National Research Council, 1965

T 1930 Taber, S: ”Mechanics of Frost Heaving”, Journal of Geology, 38, 1930, pp. 303-317.

T 1945 Terzaghi, R.D, McHenry, D, Brewer, H.W: ”Discussion of a paper by T.C. Powers: A Working Hypothesis for Further Studies of Frost Resistance of Concrete”, Journal of the American Concrete Institute, Supplement November 1945

T 1990 Takagi, S: ”Approximate Thermodynamics of the Liquid-like Layer on an Ice Sphere Based on an Interpretation of the Wetting parameter”, J. Coll. Interf. Sci. Vol 137, No. 2 , July 1990.

T 1996 Tang, L: ”Chloride Ion Transport in Concrete - Measurement and Prediction”, Publication P-96:6, Chalmers University of Technology, Dep. Building Materials, Gothenburg, 1996

Tr 1990 Taylor, H.F.W: ”Cement Chemistry”, Academic Press Ltd, 1990

V 1939 Volmer, M:”Kinetik der Phasenbildung”, Dresden and Lepzig: Steinkopff.

W 1954 Whiteside, T.M, Sweet, H.S: ”Effect of Mortar Saturation in Concrete Freezing and Thawing Tests” Highway Res. Board.30 (1950) pp 204-216.

V 1957 Verbeck, G.J, Klieger, P: ”Studies of ”Salt” Scaling of Concrete” Highway Research Bulletin, Bull. 150, Washington D.C, 1957
W 1964 Watson, A: ”The Mechanism of Frost Action on Bricks”, Brit. Cer. Soc, Trans. Vol 63, no 11, 1964
V 1969 Vuorinen, J: ”On the freezable Water in Concrete”, Communication, RILEM Symposium on the Durability of Concrete, Prague, sept. 1969
W 1970 Winslow, Diamond 1970: ”A Mercury Porosimetry Study of the Evolution of Porosity in Portland Cement Paste”, J. Materials 5, 1970
W 1996 Wadsö, I, Wadsö, L: ”A New Method for Determination of Vapour Sorption Isotherms Using a Twin Double Microcalorimeter”, Thermochimica Acta 271, 1996, pp 179-187
W 1997 Wadsö, I, Wadsö, L: ”A Second Generation Twin Double Microcalorimeter”, Journal of Thermal Analysis, vol 49, 1997, pp 1045-1052
Y 1997 Yang, Q, Wu, X, Huang, S: ”Concrete Deterioration due to Physical Attack by Salt Crystallisation”, paper 4iv032, Proc. 10th International Congress on the Chemistry of Cement, Gothenburg, 1997

Indirect references
(Referred to by Authors in the literature references)

A 1965 Anderson, D.M, Hoekstra, P: ”Migration of interlamellar water during freezing and thawing of Wyoming Bentonite”, Soil Sci. Soc. Am. Proc. 29, 498, 1965
B 1962 Barnes, G.T, Z. Angew. Math. Phys. 13, 533, 1962
Bl 1977 Bonzel, J, Siebel, E: ”Neuere Untersuchungen über derFrost-Salzwiderstand von Beton”, Betontechnischer Berischte, Düsseldorf, 1977
C 1985 Christenson, H.K, J. Colloid Interface Sci. 104, 234, 1985
D 1965 Dunn, J.R, Hudec, P.P: ”The Influence of Clay on Water and Ice in Rock Pores”, Physical Research Report RR 65-5, New York State Department of Public Works, 1965
G 1944 Gonnerman, H.F: ”Tests of Concrete Containing Air-Entraining Portland Cements or Air-entraining Materials Added to Batch at Mixer”, Proc. Am. Conc. Inst. Vol 40, p 477, Portland Cement Association, Bull 13, 1944 (in [P 1949])
G 1976 Grudemo, Å: ”Determination of Desorption Isotherms for Cement Paste”, Personal communication
H 1957 Hartmann, E: ”Effect of Frost and De-Icing Salts on Concrete with and Without Air Entraining Agents”, Zement-Kalk-Gips, vol 10, 1957, pp 265-281, 314-323 (In German)
L 1966 Lindenmeyer, C.S, Chalmers, B: ”Growth Rates of Ice Dendrites in Aqueous Solutions”, J. Chem. Phys. 45, 2807-8, 1966
L 1993 Lagerblad, B, Utkin, P: ”Silica Granulates in Concrete - Dispersion and Durability Aspects”, CBI Report 3:93, Swedish Cement and Concrete Institute, Stockholm, 1993
M 1952 Mason (Hobbs om ytenergi)
M 1953 McDonald (Hobbs om ytenergi)
P 1967a Pruppacher, H.R:”Growth Modes of Ice Crystals in Supercooled water and Aqueous Solutions”, J. Glaciol. 6, 651-62, 1967
P 1967b Pruppacher, H.R:”On the Growth of Ice in Aqueous Solutions contained in Capillaries”, Z. Naturforsch. 22a, 895-901, 1967
W 1955 Wheeler, A: ”Reaction Rates and Selectivity in Catalyst Pores”, Catalysis Part II, Ed. P H Emmett Rheinhold Publ. Corp. NY 1955, pp 105-165